



HAL
open science

Novel generation of tungsten-based catalysts grafted on oxides for propylene production

Etienne Mazoyer

► **To cite this version:**

Etienne Mazoyer. Novel generation of tungsten-based catalysts grafted on oxides for propylene production. Catalysis. Université Claude Bernard - Lyon I, 2010. English. NNT : 2010LYO10169 . tel-01214316

HAL Id: tel-01214316

<https://theses.hal.science/tel-01214316>

Submitted on 12 Oct 2015

HAL is a multi-disciplinary open access archive for the deposit and dissemination of scientific research documents, whether they are published or not. The documents may come from teaching and research institutions in France or abroad, or from public or private research centers.

L'archive ouverte pluridisciplinaire **HAL**, est destinée au dépôt et à la diffusion de documents scientifiques de niveau recherche, publiés ou non, émanant des établissements d'enseignement et de recherche français ou étrangers, des laboratoires publics ou privés.

THESE

Présentée

devant l'**UNIVERSITE CLAUDE BERNARD - LYON 1**
ECOLE DOCTORALE DE CHIMIE
SPECIALITE CHIMIE

Pour l'obtention du

DIPLOME DE DOCTORAT

(arrêté du 7 août 2006)

présentée et soutenue le

11 octobre 2010

par

Etienne MAZOYER

**Nouvelle génération de catalyseurs a base de tungstène supporté sur oxydes
pour la production du propylène.**

Jury :

M. Jean-Marie BASSET
M. Jean-François CARPENTIER
M. Régis GAUVIN
M. Klaus KÖHLER
M. Marc LEMAIRE
M. Christopher NICHOLAS
M. Mostafa TAOUFIK

Rapporteurs :

M. Jean-François CARPENTIER
M. Klaus KÖHLER

UNIVERSITE CLAUDE BERNARD - LYON 1

Président de l'Université

Vice-président du Conseil Scientifique
Vice-président du Conseil d'Administration
Vice-président du Conseil des Etudes et de la Vie
Universitaire
Secrétaire Général

M. le Professeur L. Collet

M. le Professeur J-F. Mornex
M. le Professeur G. Annat
M. le Professeur D. Simon

M. G. Gay

COMPOSANTES SANTE

Faculté de Médecine Lyon Est – Claude Bernard
Faculté de Médecine Lyon Sud – Charles Mérieux
UFR d'Odontologie
Institut des Sciences Pharmaceutiques et Biologiques
Institut des Sciences et Techniques de Réadaptation
Département de Biologie Humaine

Directeur : M. le Professeur J. Etienne
Directeur : M. le Professeur F-N. Gilly
Directeur : M. le Professeur D. Bourgeois
Directeur : M. le Professeur F. Locher
Directeur : M. le Professeur Y. Matillon
Directeur : M. le Professeur P. Farge

COMPOSANTES ET DEPARTEMENTS DE SCIENCES ET TECHNOLOGIE

Faculté des Sciences et Technologies
Département Biologie
Département Chimie Biochimie
Département GEP
Département Informatique
Département Mathématiques
Département Mécanique
Département Physique
Département Sciences de la Terre
UFR Sciences et Techniques des Activités Physiques et
Sportives
Observatoire de Lyon
Ecole Polytechnique Universitaire de Lyon 1
Institut Universitaire de Technologie de Lyon 1
Institut de Science Financière et d'Assurance
Institut Universitaire de Formation des Maîtres

Directeur : M. le Professeur F. Gieres
Directeur : M. le Professeur C. Gautier
Directeur : Mme le Professeur H. Parrot
Directeur : M. N. Siauve
Directeur : M. le Professeur S. Akkouche
Directeur : M. le Professeur A. Goldman
Directeur : M. le Professeur H. Ben Hadid
Directeur : Mme S. Fleck
Directeur : M. le Professeur P. Hantzpergue

Directeur : M. C. Collignon
Directeur : M. B. Guiderdoni
Directeur : M. le Professeur J. Lieto
Directeur : M. le Professeur C. Coulet
Directeur : M. le Professeur J-C. Augros
Directeur : M R. Bernard

Acknowledgement

None of the work contained in this thesis would have been possible without the tight collaboration between UOP LCC and the LCOMS. I would like to acknowledge Prof. Jean-Marie Basset who welcomed me in his dynamic team. I would also thank him for giving me the opportunity to work in a very interesting and promising subject. I am very thankful to Dr. Paul Barger, Dr. Christopher Nicholas and Dr. James Rekoske for their constant interest in the progresses of my work and UOP LCC for the funding.

I am very thankful to Dr. Mostafa Taoufik for his supervision and guidance along these three years. His passionate interest for chemistry has been an inexhaustible source of inspiration and an indispensable input to the project.

I am also very grateful to Prof. Jean-François Carpentier and Prof. Klaus Köhler for accepting to evaluate this work.

I am filled with gratitude to all those who contributed, directly or indirectly, to the advancement of this research; Dr. Nicolas Merle for his teaching of technical skills; Dr. Régis Gauvin and Dr. Laurent Delevoye for the fruitful collaboration; Dr Jérémie Pelletier for all its useful comments; Olivier Boyron for his help in polymers characterization; all the students and members of the LCOMS and LCPP, all the members of UCBL, ESCPE Lyon and UCCS Lille, who had provided excellent expertise in their respective fields.

All thoughts go to my family for their constant encouragement and specifically to Angelique. I would also like to take this opportunity to show my gratitude to all the people who offered support and friendship during the last three years.

Remerciements

Ces travaux de thèse ont été rendus possibles grâce à l'étroite collaboration entre la société UOP LCC et le LCOMS. Je tiens particulièrement à remercier le Prof. Jean-Marie Basset de m'avoir accueilli dans son équipe très dynamique. Je le remercie également de m'avoir accordé sa confiance et donné l'opportunité de travailler sur ce sujet aussi intéressant que prometteur. Je tiens à remercier vivement le Dr. Paul Barger, le Dr. Christopher Nicholas et le Dr. James Rekoske de leur intérêt constant pour mes travaux ainsi que UOP LCC pour son soutien financier.

J'adresse tout mes remerciements au Dr. Mostafa Taoufik pour la supervision de ce travail durant ces trois années. Son intérêt passionné pour la chimie pour la chimie a constitué une source d'inspiration intarissable pour toute cette thèse.

Que le Prof. Jean-François Carpentier et le Prof. Klaus Köhler soient remerciés d'avoir accepté d'évaluer ce travail.

Je suis reconnaissant à tout ceux qui ont participé de près ou de loin à l'avancement de ces recherches ; le Dr. Nicolas Merle pour m'avoir appris, entre autre, les techniques de la chimie organométallique de surface ; les Dr. Régis Gauvin et Dr. Laurent Delevoye pour leur fructueuse collaboration ; le Dr. Jeremie Peletier pour ces commentaires judicieux ; Olivier Boyron pour son aide dans la caractérisation des polymères ; tous les étudiants et permanents du LCOMS et du LCPP, les membres de l'UCBL, de l'ESCPE Lyon et de l'UCCS Lille, qui m'ont apporté leur expertise dans leurs domaines respectifs.

Toutes mes pensées vont à ma famille pour leurs encouragements constants et spécialement à Angélique. J'aimerais enfin remercier chaleureusement tous mes amis qui m'ont soutenu (et supporté !) pendant ces trois dernières années.

Abbreviations

Δ	Thermal treatment
δ	Chemical shift
$\delta_{(AB)}$	Deformation frequencies of A-B bond
$\nu_{(AB)}$	Stretching frequencies of A-B Bond
Å	Angström
Barg	Bar gauge
BET	Brunauer, Emmett, Teller
ⁱ Bu	<i>isobutyl</i> group CH ₂ -CH-(CH ₂) ₂
^t Bu	<i>tertiobutyl</i> group CH ₂ -CH-(CH ₂) ₂
C _n =	n carbon olefin
CP	Cross-Polarization
DMF	N,N-dimethylformamide
DRIFT	Diffuse Reflectance Infrared Fourier Transform
DSC	Differential Scanning Calorimetry
DTG	Differential Thermogravimetry
Et	Ethyl group
EWG	Electron Withdrawing Group
EXAFS	Extended X-Ray Absorption Fine Structure
GC	Gas Chromatography
HDPE	High Density Poly Ethylene
HETCOR	HETeronuclear CORelation
HPDEC	High Power DECoupling
IR	InfraRed
^x J _{AB}	Scalar coupling between A and B nuclei separate by x bond
LDPE	Low Density PolyEthylene
MAS	Magic Angle Spinning
Me	Methyl group
NMR	Nuclear Magnetic Resonance
PE	PolyEthylene
POSS	Polyhedral Oligomeric Silsequioxane
Pural	Aluminum Magnesium Hydroxyde
R	Substrate to catalyst ratio
SiAl	Silica-alumina
SOMC	Surface OrganoMetallic Chemistry
TEM	Transmission Electronic Microscopy
TGA	Thermo Gravimetric Analysis
THF	Tetrahydrofuran
TMS	Tetramethylsilane
TON	Turnover Number
VHSV	Volume Hourly Space Velocity (volumetric flow.catalyst volume ⁻¹)
XRD	X-Ray diffraction

Nomenclature

$A_xO_{y-(z)}$	Oxyde partially dehydroxylated at $z^\circ\text{C}$
1	Molecular complex
1/A_xO_{y-(z)}	Molecular complex grafted on solid
1a	Surface species of molecular complex grafted on solid

Contents

Introduction	11
Chapter 1: Metathesis for propylene production and Surface organometallic chemistry of tungsten	13
Chapter 2: Characterizations of the tungsten hydride supported catalyst	59
Chapter 3: Catalytic activity of WH/Al₂O₃ for direct conversion of ethylene to propylene	93
Chapter 4: Well-defined aluminum alkyl and hydride grafted on γ-Al₂O₃ – role in deactivation of WH/Al₂O₃	129
Chapter 5: Production of propylene from light olefins using the WH/Al₂O₃ catalyst	155
Chapter 6: Well-defined surface models of active sites of WO₃/SiO₂ and WH/Al₂O₃ catalysts	187
General Conclusion	239
Appendix A	247
Appendix B	259
Appendix C	251

Introduction

The target of this PhD thesis is the preparation of well-defined supported tungsten catalyst for the production of propylene. It is thus focused on the characterization of catalytic systems and on reactions allowing propylene from light olefins by metathesis. It is divided in six chapters.

Chapter 1 draws up the generalities for propylene production and particularly the olefin metathesis reaction. Then, the state of the art in tungsten surface organometallic chemistry, the existing catalytic systems, the reactions they perform and their mechanisms will be described. After this bibliographic study the goals and the strategy employed for the subject is presented.

Chapter 2 is devoted to the preparation and characterizations of tungsten hydride supported on alumina. The support, the carbynic precursor and the tungsten hydride have been studied.

Chapter 3 discloses a complete mechanistic study of the direct conversion of ethylene to propylene reaction using supported tungsten hydride as a catalyst.

Chapter 4 releases the preparation of supported aluminum species. Their reactivity toward ethylene was then investigated to test their influence in the catalytic activity of tungsten hydride supported on alumina.

Chapter 5 reveals the unprecedented activity of the tungsten hydride for the production of propylene from ethylene and/or butenes.

Chapter 6 finally presents the preparation of new model tungsten catalysts supported on silica bearing an oxo ligand.

A general conclusion sums up the whole results and considers the study perspectives.

Chapter 1

Metathesis for propylene production

and

**Surface Organometallic Chemistry of
tungsten**

1. Metathesis for propylene production.....	15
1.1. Propylene a key intermediary in chemical industry	15
1.2. Routes to propylene	17
1.2.1. Traditional routes: byproduct technologies	17
• Steam cracking.....	18
• Fluid Catalytic Cracking.....	18
• Alternative feedstock	18
1.2.2. Recent advances: on purpose technologies	19
• Propane dehydrogenation	19
• Olefin metathesis	20
1.3. Generalities about olefin metathesis.....	21
1.3.1. History and mechanism	21
1.3.2. Catalysts for olefin metathesis.....	23
1.3.3. Tungsten oxide on silica (WO ₃ /SiO ₂) catalyst	25
2. Surface Organometallic chemistry of tungsten.....	27
2.1. Introduction	27
2.2. Surface tungsten complexes	28
2.2.1. Surface properties	28
• Specificity of Silica.....	29
• Specificity of Alumina.....	30
2.2.2. Preparation and characterizations of supported tungsten complexes	32
• Oxide-supported tungsten carbyne species.....	32
• Oxide supported tungsten carbene	37
• Oxide supported tungsten hydride	39
2.3. Catalytic activity	41
2.3.1. Alkyne metathesis	41
2.3.2. Olefin metathesis	42
2.3.3. Non-oxidative coupling of methane, linear and branched alkane metathesis	44
• Non-oxidative coupling of methane	44
• Alkanes metathesis	46
3. Conclusion	50
4. Reference and Notes	52

This bibliographic study is divided in two main parts. The first one is devoted to the generalities about propylene and its commercial production routes, where olefin metathesis is in development. The basic principles of olefin metathesis will then be discussed. After that the WO_3/SiO_2 system will be described, as it is the mostly used olefin metathesis catalyst. The second part focuses on the several tungsten species obtained by surface organometallic chemistry with emphasis being put on their complete characterization. Their singular catalytic performance will be presented through a structure-reactivity relationship approach. A brief conclusion will finally indicate the strategy used for this thesis.

1. Metathesis for propylene production

1.1. Propylene a key intermediary in chemical industry

Propylene, [115-07-1], $\text{CH}_3\text{-CH}=\text{CH}_2$, is one of the principal light olefins. It is mainly obtained as a by-product of ethylene (*vide infra*) and is a starting material of many significant processes. It was first used for isopropanol synthesis, by combination with water using sulfuric acid or heterogeneous acid catalyst.¹ Until 1965, it was far less used than ethylene, which demand increase constantly and has led to the building of new production units. As a result, propylene became readily available, leading to the development of new applications. Propylene is now used for the synthesis of numerous products, e.g. polypropylene, acrylonitrile, propylene oxide, cumene and acetone (Scheme 1.1). The demand for propylene for production of polypropylene was 17% in 1970 and 64% in 2004 (Figure 1.1).² This growing of the demand of polypropylene, replacement of the metal in automotive applications is a major contribution to the global increase of propylene demand. This demand is in constant evolution for all part of the world with the rate of 5% per year (Figure 1.2).³

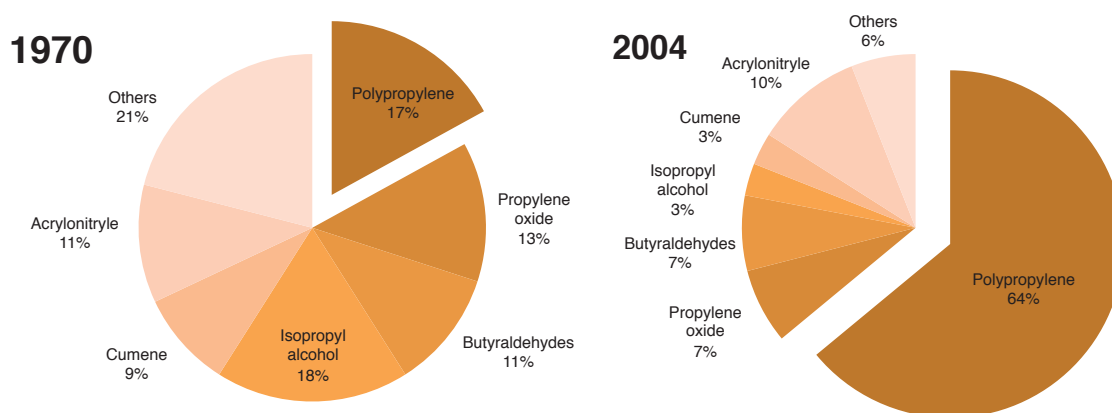
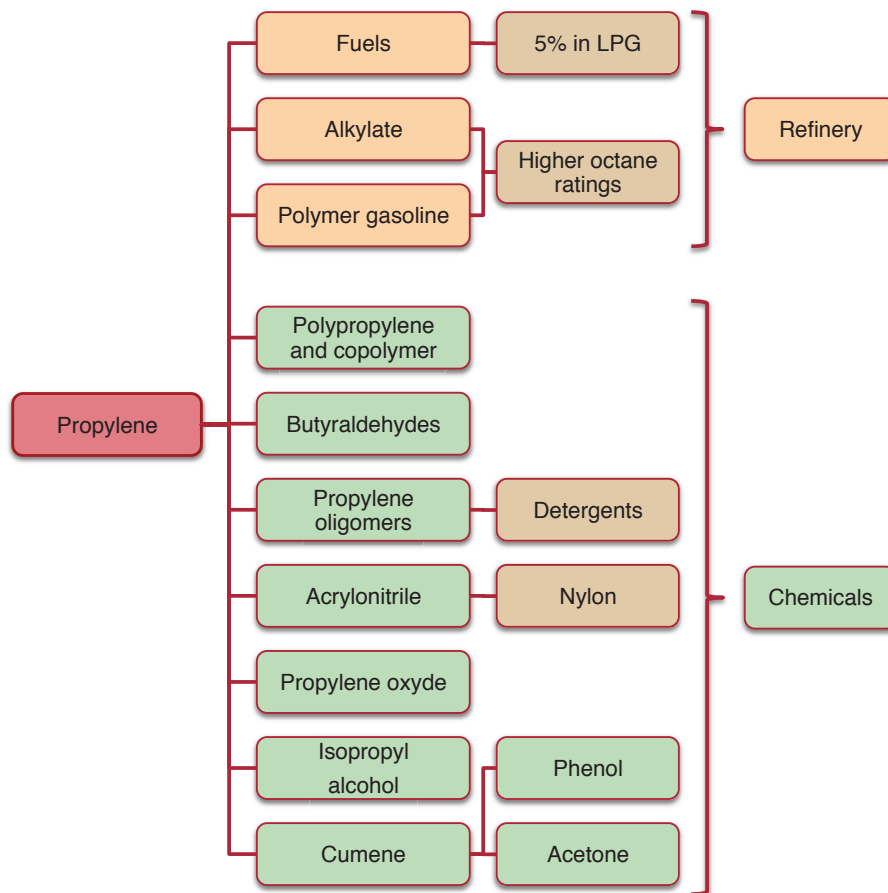


Figure 1.1 Evolution of the propylene demand for chemicals between 1970 and 2004 ²



Scheme 1.1 Propylene as starting material for refinery products and chemicals

Since 1992, although the overall demand for ethylene is greater than that for propylene, the rate of growth for propylene has outpaced that for ethylene. For instance, in the US the propylene/ethylene (P/E) demand ratio has increased from 0.43 in 1992 to 0.54 in 2004. A similar phenomenon is seen to an even greater extent in Western Europe and Asia-Pacific, where the P/E demand ratio is 0.77. In 2002, worldwide production for chemical use amounted to 60.10^6 t and was valued at roughly $\$25.10^9$. Consumption is outpacing production. The supply-side shortage in the United States has so far been accommodated by increasing imported materials. However, dedicated units may be needed to fill demand.⁴

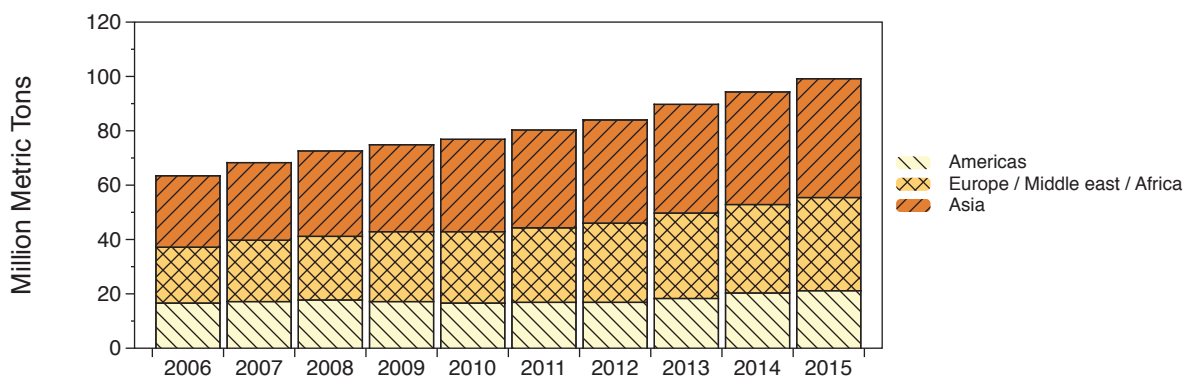
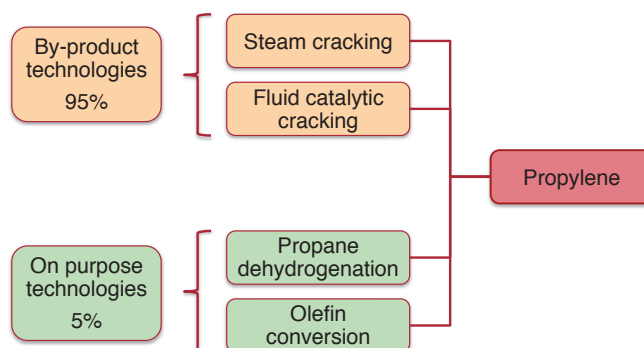


Figure 1.2 Global propylene consumption and prevision by regions ³

1.2. Routes to propylene

Propylene can be produced by two different paths: by-product technologies or on purpose technology (Scheme 1.2). In the former, which account for most of production, propylene is a by-product, *i.e.* the production units are not devoted to the production of propylene itself. In the later, propylene is specifically targeted, but that remains the minor path. This section briefly describes the technologies used for the propylene production and the recent advances that have been obtained for the two paths, in order to enhance the P/E ratio or to produce propylene from alternative feedstock.



Scheme 1.2 Commercial routes to propylene ⁵

1.2.1. Traditional routes: byproduct technologies

Although propylene is a major feedstock in industrial chemistry, it is mostly produced as a byproduct of ethylene by steam cracking and in refinery process (product from fluid catalytic cracking). Steam cracking supplies major part of the chemical industry consumption, whereas refineries only supplies between 20-40%. Most of the propylene produced in refineries is consumed in in-house, non-chemical applications, such as gasoline production (alkylate or polymer gasoline), liquefied petroleum gas production (LPG) or as heating gas.⁶

- Steam cracking

Steam cracking is the principal industrial process used to produce light olefins, *e.g.* ethylene or propylene, from heavier feedstock such as naphtha (C5 to C12 hydrocarbon mixture constituting between 15 and 30%_wt of crude oil).⁷ In this process, the hydrocarbon feed is mixed with steam and reacted at high temperature (from 750 to 950°C) with a very short residence time (0.1 to 0.6 s). Steam is used to minimize the side reaction of coke formation. The formation of light olefins occurs via a free radical mechanism. This complex mechanism explains the wide range of product of this process. Indeed, numerous reactions, *e.g.* H abstraction or addition, radical isomerization or decomposition, occur during the propagation step.^{8,9} Moreover, the nature of the feedstock has a strong influence on the selectivity. Indeed with complex feedstock, up to 2000 reaction may occur simultaneously. The steam cracker can be operated in different condition, by varying pressure or oil to steam ratio. These parameters can be adjusted to afford higher P/E ratio.

- Fluid Catalytic Cracking

Fluid catalytic cracking (FCC) is the central technology in modern refining.^{10,11} This process upgrade heavy gas oil (the hydrocarbon portion with molecular weight from 200 to 600 or higher) to higher valued gasoline. The total amount of propylene produced depends on the mix of these processes and the specific refinery product slate. For example, in the USA, refiners have maximized gasoline production. This results in a higher level of propylene production than in Europe, where proportionally more heating oil is produced. In FCC, partially vaporized gas oil is contacted with catalyst. Contact time varies from 5 s to 2 min; pressure usually is in the range of 2.5 to 4 atm, depending on the design of the unit and reaction temperatures are 450 to 580°C. The catalyst employed in FCC has known several significant evolutions. Indeed, during the 60's the replacement of the amorphous silica-alumina catalyst by zeolite Y improve the gasoline selectivity of the process. Then, in the 80's the use of ZSM-5 additives boosts the propylene yield. In 2004, Davison Catalyst starts the commercialization of Apex[®] additives and claiming they allow a 15% selectivity in propylene.

- Alternative feedstock

In order to reduce the dependence to oil, processes that produce light olefins from alternative recourses, *i.e.* coal, natural gas or even biomass, have been developed. An innovative process, namely MTO (Methanol To Olefin) that affords light olefins (*i.e.* ethylene, propylene and butenes) from methanol has been developed by UOP and HYDRO. This process is claimed to provide a broad range of P/E ratio (from 0.77 to 1.33) that can be adjust

according market demands.¹² It uses a molecular silico-aluminophosphate synthetic molecular sieve based catalyst and methanol as a feedstock. The main challenge of this method is the purification of the product obtained, due to the presence of oxygen in the methanol, to match polymer grade standards. Methanol can be obtained from alternative natural resources such as coal and natural gas, *via* syngas (CO/H₂), or even biomass. Hence, it provides a new access to plastic materials such as polyethylene and polypropylene, without recourse to oil. This process is actually tested in Belgium, coupled with the Total petrochemicals' olefin cracking process (OCP), which converts the butenes and higher olefins produced by MTO to ethylene and propylene.¹³

Different routes, using the cracking method and focused on alternative feedstock are in development. Indeed, the direct conversion of ethanol to propylene over acidic catalyst has been patented by Toyota Motor Company.¹⁴ The inventors claim very high selectivity in propylene (80-90%). A patent describing the use of SAPO-34 (a silico-aluminophosphate zeolite) to convert ethanol/methanol mixture to propylene have also been filled by China Petroleum & Chemical and Shanghai Research Institute of Petrochemical Technology.¹⁵ Nevertheless in that case the P/E ratios are similar to the ratio obtained for the MTO process. These companies also filled a patent¹⁶ wherein methyl chloride is reacted at high temperature over silico-aluminophosphate zeolite catalyst leading to a propylene ethylene mixture and HCl, contrary to MTO that afford H₂O. These HCl may be oxidized to Cl₂ which will be recycle for the synthesis of methyl chloride from methane avoiding thus the natural gas reforming to syngas and the subsequent methanol synthesis.

1.2.2. Recent advances: on purpose technologies

The expansion of propylene consumption has enhanced the demand of on-purpose processes, *i.e.* processes devoted to the production of propylene only. Indeed, they are now economically relevant. Different processes have been developed and some of them are currently running. Outside cracking, propylene can be obtained by propane dehydrogenation or by olefin conversion.

- Propane dehydrogenation

Propane dehydrogenation is an endothermic equilibrium reaction that can be catalyzed using heavy or noble metals. Operating at higher temperature and low pressure increases the propylene yield. With too high temperature, the selectivity moves towards coke formation. As a result, the reaction is usually performed between 500 and 700°C at atmospheric pressure. A number of processes are commercially available, among them Oleflex (UOP

LCC), Catofin (ABB Lummus) or STAR (Phillips Petroleum), they differ in the nature of the catalyst, the operation and regeneration conditions.

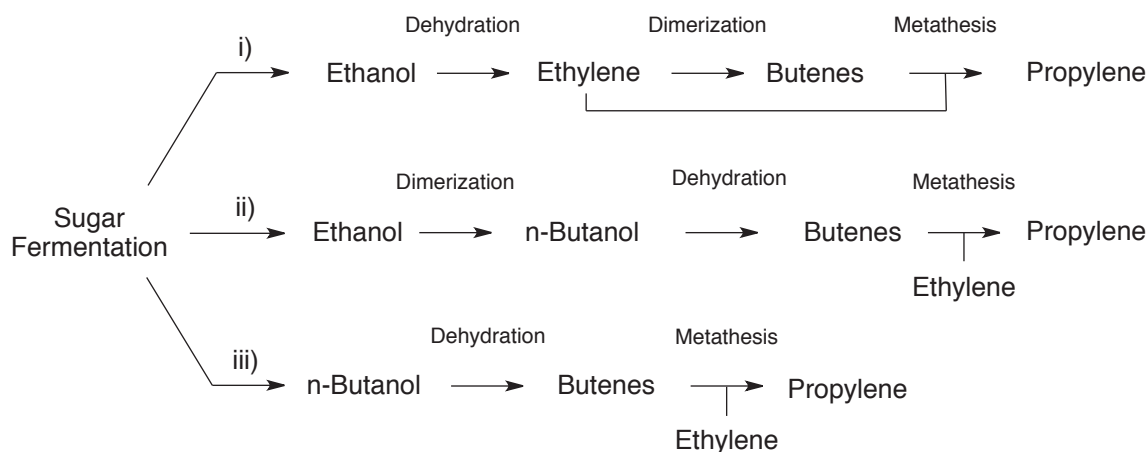
- Olefin metathesis

Propylene can be produced by olefin metathesis. The Olefin Conversion Technology (OCT) provided by ABB Lummus enhances the amount of propylene produced by naphtha steam cracker units. This process converts the raw C₂ and C₄ feedstock of the steam cracker to propylene. The C₄ raw feedstock contains both 1-butene and 2-butenes. The reaction occurs over a mixture of WO₃/SiO₂ and MgO at a temperature higher than 260°C and a pressure of 30-35 bar. The 1-butene of the feed is isomerized to 2-butene, over a MgO catalyst, while the original 2-butene is consumed by the cross-metathesis with ethylene.¹⁷

Another process based on metathesis has been conjointly developed and tested by IFP and the Chinese Petrol Corporation (Taiwan), namely the Meta-4 process. This process uses a Re₂O₇/Al₂O₃ catalyst to convert ethylene and 2-butene at 35°C and 60 bar.^{18,19} This technology is not yet commercialized, probably due to the high cost of the catalyst and the necessity of very pure feedstock (high sensibility of the catalyst toward polar functions).²⁰

The use of olefin metathesis has also been investigated using alternative feedstock. For example, Mitsui Chemicals of Japan has filed a patent application²¹ that describes three methods for producing biomass-derived propylene (see Scheme 1.3). All start by using alcohol (*i.e.* ethanol or butanol) obtained by selective sugar fermentation: i) dehydrating ethanol to ethylene, dimerizing the produced ethylene to butenes and finally cross-metathesis of both materials to give propylene; ii) making the butenes, not by dimerizing ethylene, but instead dimerizing ethanol to n-butanol and then dehydrating the n-butanol to n-butenes and then metathesizing the ethylene and butenes to give propylene; iii) production of n-butanol and then dehydrating to n-butenes and cross-metathesis with ethylene.

None of these steps are novel; in fact, it is believed that Brazilian petrochemical major Braskem has made biopropylene in commercial development quantities by a similar approach.²² The Mitsui patent application is focused on means of removing impurities from the bio-feedstocks, to preclude poisoning of the notoriously sensitive metathesis catalysts.



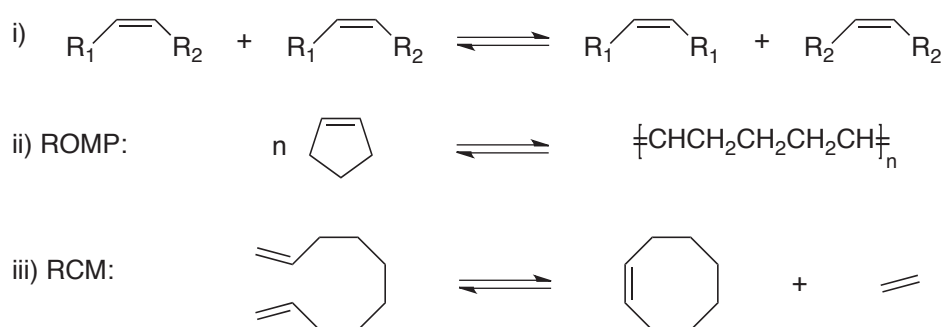
Scheme 1.3 Reactions proposed by Mitsui Chemicals' patent to produce propylene from biomass.

1.3. Generalities about olefin metathesis

In this thesis, the use of olefin metathesis to provide propylene from light olefin such as ethylene and/or butenes will be investigated. Therefore, in this subsection, the metathesis reaction is presented.

1.3.1. History and mechanism

Olefin metathesis consists in the exchange, usually catalyzed by transition metals, of alkylidene fragments between two olefins. It can be categorized in three types of reactions (Scheme 1.4): i) exchange between two olefins (self-metathesis and cross-metathesis), ii) ring opening metathesis polymerization (ROMP) and iii) ring closing metathesis (RCM) of a diene.

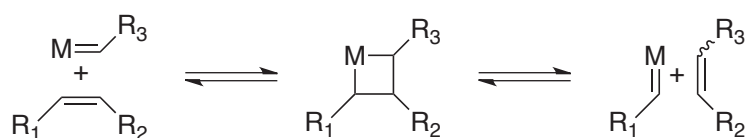


Scheme 1.4 Metathesis reactions can be categorized in three main types: i) exchange, ii) ROMP, iii) RCM

This reaction is catalyzed by homogeneous or heterogeneous systems involving a transition metal. These systems are mostly based on Mo, Ru, W or Re chlorides or oxides, generally combined with a co-catalyst or a promoter.

In the 60's Banks *et al.* have first reported an olefin disproportionation reaction.²³ Several processes were developed to allow the conversion of propylene to ethylene and 2-butene, as at that time the demand was stronger for ethylene than for propylene. The term “olefin metathesis” has been later introduced by Calderon *et al.*²⁴

The main concerns were then, the role of the catalyst and the mechanism of the reaction. Calderon *et al.* demonstrated that C=C bonds involved in the reaction are the olefinic ones and not those of the substituents.²⁴ The complete mechanism has been revealed by Hérisson and Chauvin in 1971.²⁵ The key element of this mechanism is a metallocarbene species that react with an olefin to form a metallacyclobutane. The former evolve to give a new olefin and a new metallocarbene (Scheme 1.5).



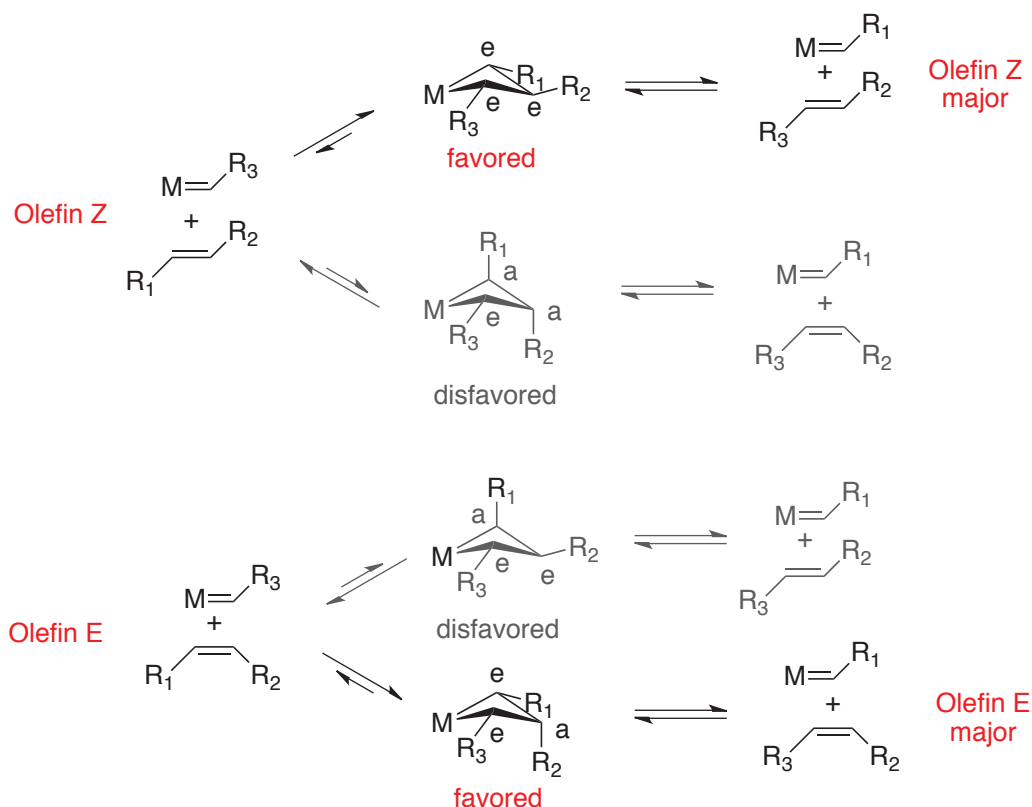
Scheme 1.5 Chauvin's mechanism for olefin metathesis

As this mechanism involves equilibrated reactions, the metallacyclobutane can afford new products (productive metathesis) or regenerate the reagents. Degenerative metathesis occurs when the metallacyclobutane decomposes only in products identical to the reagents ($R_1 = R_3$). The degenerative metathesis may be responsible of a slower kinetic rate of the reaction, *e.g.* when the productive path is less favored than the degenerative path.

This metallacyclobutane mechanism has been extensively examined, for instance, Katz *et al.* confirmed it by kinetics studies.²⁶ Then, homogeneous organometallic species, bearing a carbene ligand not substituted with heteroatoms, in the coordination sphere of the metal have been synthesized.²⁷⁻³⁰ These species have shown a good activity in olefin metathesis supporting the hypothesis of the need of a metallocarbene to perform this reaction. Finally, the synthesis of metallacyclobutanes has brought a supplementary proof for this mechanism in homogeneous catalysis.³¹

The olefin metathesis is an equilibrated reaction. Indeed, the number and the nature of products' bonds are generally the same that the reagents' (except for the strained cyclic or highly substituted olefins). The reaction is thus quasi-isenthalpic. An interesting effect of this characteristic is the quasi-athermicity of the reaction. Entropic factor dictates the reactivity leading to a statistic distribution of product and reagent. For instance, 2-pentene metathesis at 298 K leads, at thermodynamic equilibrium, to a mixture of 2-pentenes/butenes/hexenes in a ratio close to 2/1/1. This behavior is not observed in the case of

highly substituted olefins. Indeed, isobutene metathesis reaches only 3% conversion at 298 K ($\Delta G^\circ = + 17.3 \text{ kJ.mol}^{-1}$).



Scheme 1.6 Formation of favored and disfavored metallacyclobutanes explaining the E/Z selectivity before reaching thermodynamic equilibrium^{32,33}

In the case of acyclic olefins, when a mixture of E/Z diastereoisomers is obtained, the ratio obtained at the equilibrium is imposed by thermodynamics. Nevertheless, if the thermodynamic equilibrium is not reached (*i.e.* in the beginning of the reaction (batch) or at short contact time (continuous flow)), a singular stereoselectivity may be observed. In these conditions, the E/Z ratio is governed by the nature of the catalyst and the substrate and can be explained by Chauvin's mechanism. Thus, outside of thermodynamic equilibrium, a Z olefin (respectively E) gives a Z olefin (respectively E). This can be interpreted by the formation of favored or disfavored metallacyclobutane intermediaries. The (1,3) equatorial (e) disubstituted metallacyclobutanes are the most stable followed by the (1,2) equatorial (e) disubstituted ones (Scheme 1.6).^{32,33}

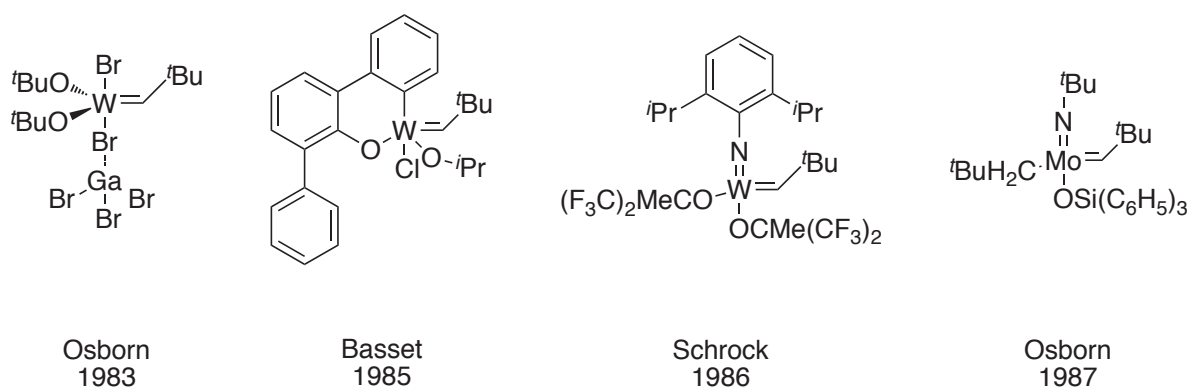
1.3.2. Catalysts for olefin metathesis

The catalytic systems for olefin metathesis include generally a metal center drawn from the group IV to VIII. These catalysts may be homogeneous or heterogeneous. Herein are

presented homogeneous catalysts based on several metals (*i.e.* Mo, W, Re or Ru), whereas the presentation of heterogeneous systems will focus on WO_3/SiO_2 as this thesis is related to its chemistry.

The first catalyst used for cyclic and acyclic olefin metathesis has been described by Banks and Bailey.²³ It is composed of $\text{WCl}_6/\text{EtAlCl}_2/\text{EtOH}$. The olefin metathesis catalysts developed after were Zeigler-Natta type system. They were composed of an inorganic transition metal complex and an alkylating agent. In some case, a promoter (*e.g.* O_2 or an alcohol), is also added to enhance the catalytic activity. The alkylation agent can also be replaced by photochemical activation. In spite of numerous related systems developed, the nature of the active species is not well understood yet.

The proposition of Chauvin that the active species must be a metallocarbene (*vide supra*) has been pivotal. Afterwards, the investigations were focused on the synthesis of this active species. The first metallocarbene prepared were electrophilic carbene (Fischer's carbene), and therefore inactive in olefin metathesis.³⁴ Nevertheless, Katz *et al.* described^{35,36} the first use of a electrophilic carbene, $[(\text{CO})_5\text{W}=\text{C}(\text{C}_6\text{H}_5)_2]$,²⁷ for olefin metathesis, that is active without co-catalyst at room temperature. Selected catalysts obtained using metallocarbene are summarized on Scheme 1.7.³⁷⁻⁴⁰



Scheme 1.7 d^0 carbenic complexes active in olefin metathesis

The coordination sphere of all these complexes has been optimized regarding steric and electronic parameters. For instance using electro withdrawing groups (EWG) as ligand weaken the electron density around the metal center. It is believed to favor the approach of the olefin toward the metal and thus the formation of the metallacyclobutane.

Ruthenium-based catalysts have then been documented with Ru IV (d^4) based systems showing a high activity for olefin metathesis.⁴¹⁻⁴⁴ Examination of the structure-reactivity relationship of these catalysts has disclosed a completely different behavior than for the d^0 electrophilic early transition metal complexes. In the case of ruthenium, the

more σ -donating the ligand, the higher the activity observed in olefin metathesis.⁴² The molybdenum and ruthenium catalysts are currently commercially available. Those based on molybdenum are more active than those based on ruthenium, but the latter are more tolerant toward polar functions and are not air-sensitive. This latter property makes the ruthenium used in industrial scale, especially in pharmaceutical applications.⁴⁵

1.3.3. Tungsten oxide on silica (WO_3/SiO_2) catalyst

Tungsten has provided more heterogeneous catalysts for olefin metathesis than all other metals combined (*e.g.* Re, Mo). Many studies have discussed the catalyst systems themselves in an attempt to elucidate the nature of the active species and its mode of formation.³¹ Herein is presented the WO_3/SiO_2 system which is the most commonly used among tungsten based catalysis. Tungsten oxide on silica appears to be particularly desirable because of its high resistance to common poisons such as air and water, and its low coke formation.^{46,47}

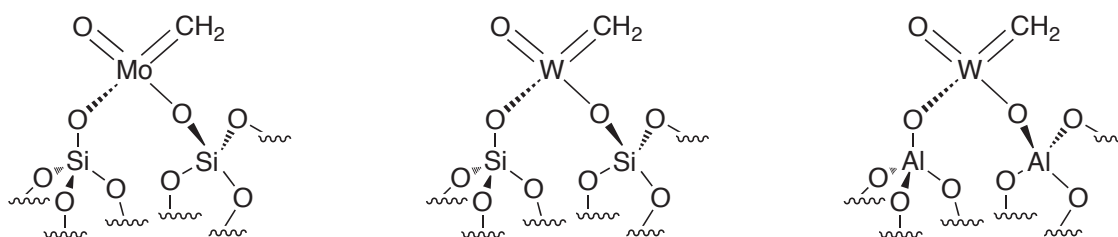
It is often prepared by incipient wetness impregnation of ammonium metatungstate-hydrate solution on silica. This method is convenient but lead to non-uniform deposition of the impregnated material on the support.⁴⁸ The catalyst is then generally activated in dry air at 550°C. When the tungsten loading exceeds 10%_{wt}, WO_3 crystallites are observed on XRD spectra and RAMAN spectroscopy.⁴⁹

The heterogeneity of surface species present at the surface has been evidenced by mass transfer limitations of the catalyst. This observed interphase mass transfer effects, although unexpected via calculations,⁵⁰ are explainable by assuming that a small number of very active sites are widely separated and, hence, the reaction is limited by site localized diffusional effects.⁵¹

This catalyst also exhibits a significant feature: during the initial contacting of freshly activated tungsten oxide on silica catalyst with propylene there exists a steady increase in catalyst activity.⁵² Depending on process conditions, this initiation step may last up to 24 h. At the end of this step the catalyst achieves a stable steady-state activity. This period of increasing activity is known as “break-in”.^{48,53} This phenomenon has been attributed to the formation of steady-state active sites, *i.e.* tungsten centers with the appropriate oxidation number. Indeed, the duration of the break-in can be greatly shortened by pretreating the catalyst with hydrogen or carbon monoxide⁵² or by activating at temperatures above 630°C.⁵⁴ This reduction of the tungsten from WO_3 to $WO_{2.9}$ is observed by a characteristic change of color from yellow to blue⁵⁵ and accompanied by a slight loss of oxygen in the catalyst.⁵⁶ This loss of oxygen is also observed by formation of traces of

acetone and acetaldehyde when propylene is contacted to freshly activated WO_3/SiO_2 . The formation of these products probably occurs in two steps: i) reduction of the tungsten centre yielding acetone and tungsten oxide and ii) formation of a tungsten carbene and acetaldehyde.⁵⁷ The nature of the active site is still a matter of debate but it seems clear that WO_3 crystallites are not involved in the catalytic cycle.⁵⁸ The catalytic activity is thus attributed to isolated tungsten surface species bearing a carbenic ligand.

It is interesting to compare WO_3/SiO_2 with its group VI counterpart $\text{MoO}_3/\text{SiO}_2$. Shelimov *et al.* have described the preparation of highly active isolated Mo species on silica by treatment of Mo(IV) with cyclopropane lead to a Mo(VI) bearing two siloxy, an oxo and a carbene ligand (Scheme 1.8 left).⁵⁹ Moreover, Grünert *et al.* have proposed a structure for the active isolated sites of $\text{WO}_3/\text{Al}_2\text{O}_3$ catalyst, which consist of a W(VI) bearing two aluminoxy, an oxo and a carbene ligand (Scheme 1.8 left).⁶⁰ It can be postulated that the isolated active species of the WO_3/SiO_2 catalyst may thus have similar structure (Scheme 1.8 centre).



Scheme 1.8 left: Isolated molybdenum species described by Shelimov *et al.*⁵⁹; centre: Postulated active sites of the WO_3/SiO_2 catalyst; right: Isolated tungsten species of $\text{WO}_3/\text{Al}_2\text{O}_3$ described by Grünert *et al.*⁶⁰

The main drawback of these heterogeneous systems is the low concentration of isolated active species. The preparation of tungsten isolated active species by Surface Organometallic Chemistry can be the best method to increase the activity and selectivity of these catalysts. In this thesis the preparation of well-defined heterogeneous tungsten catalyst will be presented. The structure-reactivity relationship of the active species will be emphasized.

2. Surface Organometallic chemistry of tungsten

2.1. Introduction

Employing Tungsten for Surface Organometallic Chemistry (SOMC) has allowed, for the past decade, the access to unprecedented performances for the catalytic transformation of hydrocarbons. By changing the ligands and the nature of the support, novel catalysts were prepared and characterised with significant insights about the organometallic active species and their reactivity being gained. These progresses, although still restrained to the laboratory scale, can potentially affect several main processes involved in the petrochemical industry.

The use of inorganic carriers based on metal oxides such as silica, alumina or silica-alumina has been extensively investigated to generate heterogeneous catalysts with many early transition metals (*e.g.* Ti,⁶¹⁻⁶⁵ Zr,⁶⁶⁻⁸⁶ Hf,⁸⁷⁻⁹³ Ta,^{76,81,94-115} etc). A few conclusions, regardless the metal involved, can be drawn on the impact of the support. When considering the surface as ligands, these systems can be assimilated as polynuclear catalysts in which one ligand (*i.e.* the particules of inorganic carrier) hosts several metals. This is believed to prevent the metal to react with one another thus reducing *in fine* to the deactivation of the catalyst. It is noteworthy that the nature of the support affects tremendously the metal reactivity. For example, chemisorption of [Zr(CH₂tBu)₄] on alumina provides an efficient olefin polymerization catalyst,⁸⁴ while its silica counterpart is inactive under the same conditions. The support employed controls over prominent parameters of the grafted species such as its distribution, its amount, its oxophilicity, its ionic character and its polarity among others.

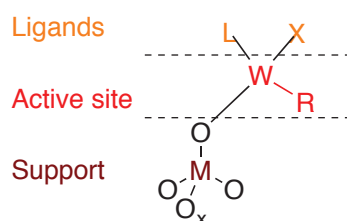
Supported systems such as those obtained by SOMC are notoriously difficult to characterize, but the last decade have seen an important improvement of the tools available to access their molecular structure. Techniques such as IR spectroscopy, mass balance and elemental analysis have long proved their capacity to access overall properties and stoichiometry of grafted species. However, removing the uncertainty around the coordination sphere of the metal remains challenging, hence encouraging the development of new analytical means. For instance spectroscopic techniques such as SSNMR, EXAFS or even Raman spectroscopy have more recently demonstrated their ability to access the intimate structure of tungsten species obtained by SOMC. In addition, the use of soluble molecular analogues (*i.e.* polyoligomeric silsesquioxane (POSS-OH)^{85,86} or (tBuO)₃Si-OH) and of theoretical models¹¹⁶ have also allowed to gain an understanding more complete and accurate. The potential contribution of these analytical techniques can be briefly

and non-exhaustively summarized. SSNMR spectrometry is highly relevant to characterizing grafted organometallic species with several ^{13}C SSNMR and other experiments dedicated to observe the carbon and the hydrogen directly bound to the metal and more: intermediaries ligands complexes. EXAFS permit to know the coordination sphere (*i.e.* number of atoms and distance) of heavy elements such as transition metal. Raman spectroscopy can also allow to observe vibrations, usually elusive, of metal-oxide bonding.

Herein will be summarized exclusively the well-characterised W complexes grafted to the surface that are relevant to heterogeneous catalysis. For clarity purpose, the discussion is divided in two parts the preparation of the tungsten surface complexes (section 2.2) and their catalytic performance (section 2.3).

2.2. Surface tungsten complexes

In all the W-grafted complexes discussed there, the ligands can be deconstructed similarly in regard to their role in catalysis (Scheme 1.9). For instance, carbyne, carbene or hydride moieties intervene directly in the catalytic process and command over the catalytical performance. In contrast, the remaining ligands serve supplementary purposes that can be conveniently distinguished; the surface (silica, silica/alumina, alumina) maintains the metal by one or more bonds to a carrier while the spectator ligands (*viz.* imido, aryloxy, amido) tune indirectly the active site. For the sake of clarity, the examination of these systems will begin by a concise description of the support with a comparative account of their properties will be given. Secondly, a selection of various W-complexes will be outlined by categorizing the reactive ligands and reporting the relevant examples in term of characterization.



Scheme 1.9 Deconstruction of the grafted complexes: support, active site and ancillary ligands

2.2.1. Surface properties

Several types of inorganic carriers based on metal oxide have been employed to graft tungsten complexes. However, silica, silica-alumina and alumina have all been involved in the formation of the most significant surface complexes in regards of the wealth of their characterization and their prime involvement in catalytic processes. A discussion of their

common properties prior to that of their differences, namely, the type and the reactivity of their hydroxyl, seems judicious.

For all compounds obtained by SOMC, the surface area is a parameter determinant over the total amount of metal potentially immobilizable. This is largely controlled the type of materials employed with two mains options available: non-porous or porous. Both consist in spheroid particles of variable diameters, but porous materials contain controlled-size pores that extend significantly the surface area compared to their non-porous counterparts. It has also been recognized that non porous materials present a few advantages such as their readily availability, their convenient handling and their optimal geometry for the characterization of single site species. Furthermore, the utilization of porous material currently knows great interest but will not be discussed herein. Another common feature to these surfaces is the dehydroxylation treatment that can control the hydroxyl groups distribution. Submitting the carrier to a given temperature under high vacuum induces the elimination of water from the surface and narrows selectively the OH population.

- Specificity of Silica

Silica has been extensively employed as an inorganic carrier for the grafting of transition metals drawn from group IV to X. Fumed silica is made of spherical particles of diameters between 5 to 50 μm . For instance, specific surface areas are dependent of the type of silica employed and are typically comprised between 50 and 200 $\text{m}^2\cdot\text{g}^{-1}$ for fumed silica. Regardless the type of silica employed, siloxane and silanol are the two main functionalities with the latter being found almost exclusively at the surface. In the bulk, silica is constituted of tetrahedral SiO_4 units that are generally inaccessible and inert to metal reagents. At the surface, the silanols, due to their higher reactivity, are available to immobilise the metal by forming up to three siloxy groups. As the siloxy substituents modify the structure and properties of grafted early transition metals, thus commanding over their reactivity, the type and the distribution of silanol existing at the surface are determinant. These parameters can be controlled by the temperature of the dehydroxylation treatment (*vide supra*). The type (*viz* geminal, vicinal and isolated) of silanol and their relative proportion at a given temperature can be conveniently determined by combining IR spectroscopy (Figure 1.3)¹¹⁷ and reactivity studies.

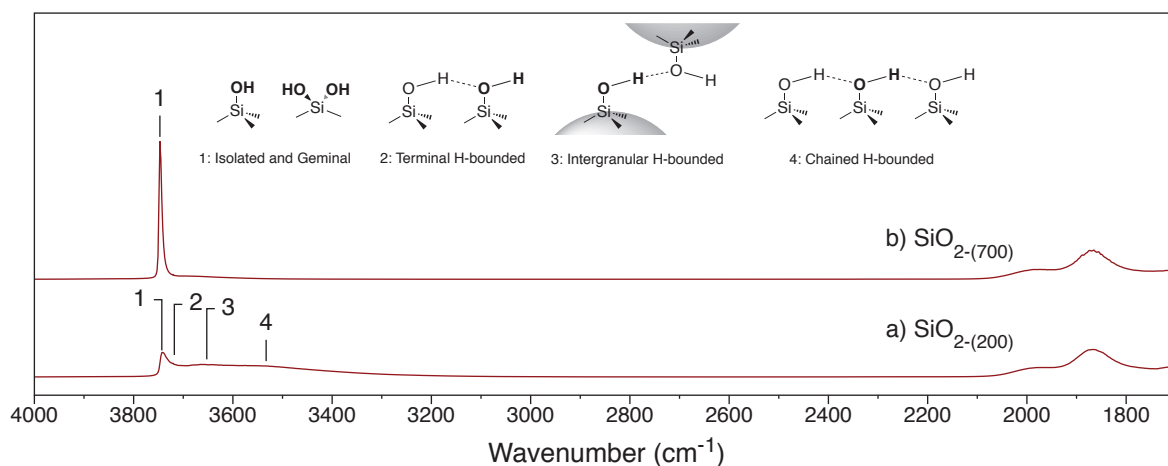


Figure 1.3 Diffuse reflectance infrared spectra of silica dehydroxylated at a) 200°C and b) 700°C and interpretation according reference 117

It appears that vicinal and geminal silanols are removed by increasing dehydroxylation temperature. For instance, hydroxyl rich silica surfaces of Degussa Aerosil® (0.86 OH.g⁻¹) displaying mostly vicinal and geminal OH with smaller amount of isolated ones are obtained when dehydroxylated at 200-300°C. At 700°C, this treatment affords almost only isolated silanol (0.26 mmol OH.g⁻¹) separated by an average of ca. 13Å.¹¹⁸

Silica-alumina has been used as a support for W-SOMC. Its structure is very close from Silica but allows the formation of species impossible on silica avoiding sintering effects (*vide infra*). Therefore, silica-alumina should be considered as modified silica as silanol are exclusively observed on the surface.^{119,120} Both Si-O-Si and Al-O-Si bridges can be found in the bulk; the loading of alumina, and the preparative methods, can be directly correlated with this two groups ratio. Two preparative methods are commonly employed: co-hydrolysis of silica and alumina and the silication of alumina. The silica-alumina has interesting Brønsted acid character.

- Specificity of Alumina

Transition aluminas have been extensively investigated as an inorganic carrier and exhibit significant differences with silica. Among them, γ -alumina is one of the most used in industrial processes due to its high mechanical stability (in large fixed bed reactor the bottom catalyst may carry more than 10 metric tons) and its interesting acidic behavior. The γ -alumina is obtained by heating bohemite above 500°C. This treatment gives a material with specific surface around 200 m².g⁻¹, less acidic than η -alumina where surface plane 110 is predominant.^{121,122} It is made of aluminoxane in the bulk and displays only aluminols at the surface. However, in many aspects, its chemistry is more complicated than either silica or silica/alumina.

Indeed γ -alumina, like η -alumina, is a spinels compound: Al atoms from the bulk are either tetrahedral or octahedral. At the surface, aluminols and aluminium possessing a Lewis acid character or aluminol possessing weak Brønsted acid character are both present.

The combination of all these factors generates a distribution of types of site available for the grafting of metals. Consequently, the deep structure of alumina is still a debated matter with recent progress coming from model provided by theoretical chemistry aiming to provide models in line with experimental data.

The modelisation proposed by Knözinger,¹²³ and more recently by Sautet,¹²⁴ have been explaining the IR spectra of γ -Alumina (Figure 1.4). Notably, the bands observed have been correlated to the interaction between the hydroxyl and the geometry of the aluminums beside.

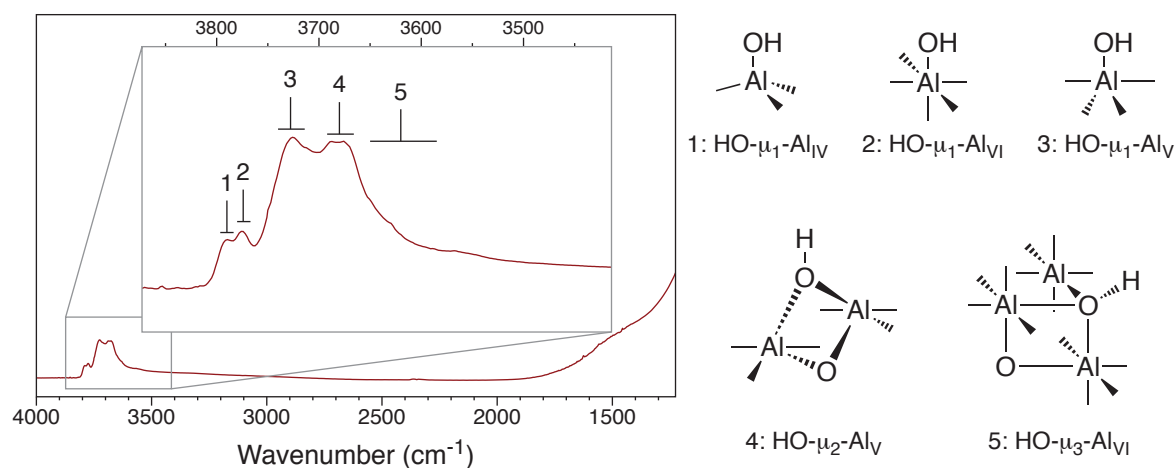


Figure 1.4 Diffuse reflectance infrared spectra of γ -alumina dehydroxylated at 500°C and interpretation according reference 124

The utilization of silica and silica-alumina dehydroxylated at different temperature as a supports in SOMC, leads to well defined structures, as only one type of silanol is involved in the grafting reaction. In contrary, the use of alumina affords more complex structures, as the reactivity of the different aluminol toward organometallic species is variable. Moreover, the acidic character of alumina may lead to the formation of cationic species in unpredictable proportions.^{103,125} Theoretical calculations are therefore very profitable to understand these surface species.¹¹⁶

2.2.2. Preparation and characterizations of supported tungsten complexes

In the following section, the synthesis and the characterizations of selected tungsten-based species obtained by SOMC will be expounded. The discussion will be organized as follows: i) Oxide-supported tungsten carbyne species, ii) Oxide-supported tungsten carbene species and iii) Oxide-supported tungsten hydride species

For all surface species the range of analytical techniques usually relevant was employed: IR spectroscopy, DRIFT, SSNMR, mass balance, gas evolution measurement and elemental analysis. Besides, EXAFS, Raman spectroscopy and high-resolution SSNMR spectroscopy (HETCOR, J-resolved 2D SSNMR) will receive particular attention for they had decisively contributed to the identification of the coordination sphere of the grafted tungsten.

Finally, the chemistries of oxide-supported have been closely entangled and directly related to that of their soluble counterparts. When necessary, comparison between the two will be made to account the observations gathered from the grafted species.

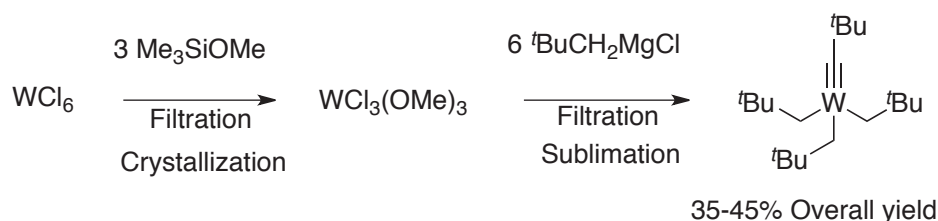
- Oxide-supported tungsten carbyne species

Oxide-supported tungsten carbyne species have found a key employment as catalytic components for the metathesis of alkynes. High oxidation state tungsten alkyldynes have been initially reported by Schrock in 1978 with the preparation of $[W(\equiv C^tBu)(CH_2^tBu)_3]$.¹²⁶ Due, in part, to their high reactivity, a rich chemistry has since been elaborated.^{127,128} Schrock has developed latter $[W(\equiv C^tBu)(O^tBu)_3]$, which is the most extensively used catalyst in alkyne metathesis. Nevertheless, a recurring problem hindering these systems is the rapid deactivation that can occur by the mean of either formation of W-metallacyclopentadienyl or through a bimolecular dimerization resulting to a $W\equiv W$ triple bond.^{129,130} The heterogenisation of W-carbyne species can be suggested in response of the latter (*vide supra*).

The first significant advance in the area of W-based SOMC was the synthesis and the characterization of $[(\equiv SiO)W(\equiv C^tBu)(CH_2^tBu)_2]$. The results obtained were later transposed to silica/alumina and alumina.

To obtain $[(\equiv SiO)W(\equiv C^tBu)(CH_2^tBu)_2]$, the W precursor is reacted with silica to result in at least one of the neopentyl group being displaced by the silanol moieties. Although different synthetic methods are available, the most efficient preparation of $[W(\equiv C^tBu)(CH_2^tBu)_3]$ begins with displacing three chlorines in WCl_6 to afford $[W(OMe)_3Cl_3]$ that is then alkylated by tBuCH_2MgCl (Scheme 1.10).¹³¹ As with other

highly electrophilic metals (*e.g.* Ta, etc) W alkyl complexes are prone to α -elimination causing *in fine* the rearrangement of the coordination sphere. In the present case, the W-carbyne species is the sole product while $[\text{W}(\text{CH}_2\text{tBu})_6]$ cannot be observed. Hence, this suggests that the electron-deficient tungsten atom undergoes two eliminations by forming 'agostic' bonds with hydrogens in the α -positions; at the beginning, by one neopentyl ligand, and following elimination of one neopentane, on the corresponding the alkylidyne complex formed.¹²⁷



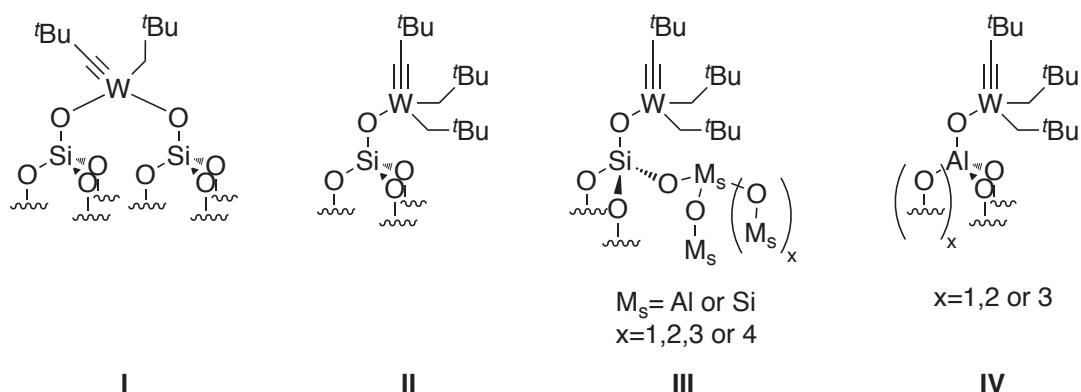
Scheme 1.10 Synthesis of $[\text{W}(\equiv\text{C}^t\text{Bu})(\text{CH}_2^t\text{Bu})_3]$

Weiss *et al.* initially completed the grafting on silica of $[\text{W}(\equiv\text{C}^t\text{Bu})(\text{CH}_2^t\text{Bu})_3]$ but wrongly recognized a W-carbene surface species, $[(\equiv\text{SiO})\text{W}(=\text{CH}^t\text{Bu})(\text{CH}_2^t\text{Bu})_3]$ of the Schrock-type resulting from the carbyne ligand with silanol of silica.¹³² Since, this reaction have been reproduced in the laboratory with both $\text{SiO}_2-(200)$ and $\text{SiO}_2-(700)$, to afford two species **I** and **II**, respectively.¹³³ At that stage, the identification of the ligands nature (carbene *vs* carbyne) was inconclusive. Submitting ^{13}C enriched **I** and **II** to ^{13}C SSNMR, 2D ^1H - ^{13}C HETCOR and J resolved 2D SSNMR undoubtedly disproved the presence of carbyne while confirming that of a neopentylidyne and neopentyl ligands. In the ^{13}C spectra, two signals at 95 ppm and 318 ppm, can be attributed to the methylene of a neopentyl, and to the carbyne of a neopentylidene, respectively. Besides, the J-resolved 2D SSNMR spectra of **I** and **II**, contains a triplet (CH_2^tBu , $^1J_{\text{C-H}} = 110$ Hz) at 95 ppm assigned to the methylene carbon of the neopentyl fragment but no signal consistent with a carbene moieties. The low $^1J_{\text{CH}}$ value for the methylene is indicative of a weak agostic interaction of these protons with the metal center.

Regardless the silica employed, the metal, assumed to keep its (VI) oxidation state, is coordinated to four ligands with one neopentylidene moities. The three remaining ligands depend on the silica employed with the $\text{SiO}_2-(200)$ being bipodal (**I**) and the $\text{SiO}_2-(700)$ monopodal (**II**) with the neopentyl ligands filling (Scheme 1.11).

The mechanism of the grafting has not been fully demonstrated, indeed it can occurs either i) by reaction of the carbyne ligand with silanol followed by α -H abstraction with

evolution of neopentane or ii) by σ -bond metathesis between O-H bond of a surface silanol and W-C bond of a neopentyl ligand.



Scheme 1.11 Different structures proposed for surface species obtained by grafting $[\text{W}(\equiv\text{C}^t\text{Bu})(\text{CH}_2^t\text{Bu})_3]$ on oxides

On silica-alumina dehydroxylated at 500°C ($\text{SiAl}_{(500)}$), $[\text{W}(\equiv\text{C}^t\text{Bu})(\text{CH}_2^t\text{Bu})_3]$ reacts with OH groups to give selectively a monografted $[(\equiv\text{SiO})\text{W}(\equiv\text{C}^t\text{Bu})(\text{CH}_2^t\text{Bu})_2]$ (**III**). Moreover, the ^1H and ^{13}C solid-state NMR spectra of this solid display the same signals as those observed for (**II**).¹³⁴

The alumina equivalent $[(\text{Al}_s\text{O})\text{W}(\equiv\text{C}^t\text{Bu})(\text{CH}_2^t\text{Bu})_2]$ (**IV**) can be obtained by treatment of γ -alumina dehydroxylated at 500°C by $[\text{W}(\equiv\text{C}^t\text{Bu})(\text{CH}_2^t\text{Bu})_3]$. Due to the more complicated surface of alumina (*vide supra*), understanding the structure of **IV** required to confront extensive characterizations (mass balance analysis, IR spectroscopy, NMR spectroscopy and EXAFS) and density functional theory calculations. The evolution of 1 equiv of $^t\text{BuCH}_3$ per grafted W and the disappearance of the highest $\nu(\text{OH})$ band, while the lowest are left unreacted, suggest that **IV** is a monopodal species mostly coordinated to a tetrahedral aluminum. It should be noted that this selectivity of grafting is specific to $[\text{W}(\equiv\text{C}^t\text{Bu})(\text{CH}_2^t\text{Bu})_3]$. In contrast, the grafting of $[\text{Zr}(\text{CH}_2^t\text{Bu})_4]$ on similar alumina consumes all present isolated hydroxyl and gives $\{[(\text{Al}_s\text{O})_2\text{Zr}(\text{CH}_2^t\text{Bu})]^+[(^t\text{BuCH}_2)(\text{Al}_s)]^-\}$, a bisgrafted cationic complex as major surface species. The difference of reactivity demonstrated by these two complexes has been investigated by DFT calculation. According to them, the reaction of the Zr precursors is far more exothermic than its W counterpart, which possesses a much higher activation barrier (E_a) $81 \text{ kJ}\cdot\text{mol}^{-1}$. In addition, the rigidity imparted to the complex by the carbyne hinders the coming of the complex close to some type of the aluminol. As a result, the first step consists in the electrophilic cleavage of the W- CH_2^tBu bond preferentially on HO-Al_{IV} ($\Delta rE = -150 \text{ kJ}\cdot\text{mol}^{-1}$) to form a neutral surface species: $[(\text{Al}_s\text{O})\text{W}(\equiv\text{C}^t\text{Bu})(\text{CH}_2^t\text{Bu})_2]$ (**IV**).⁷⁹

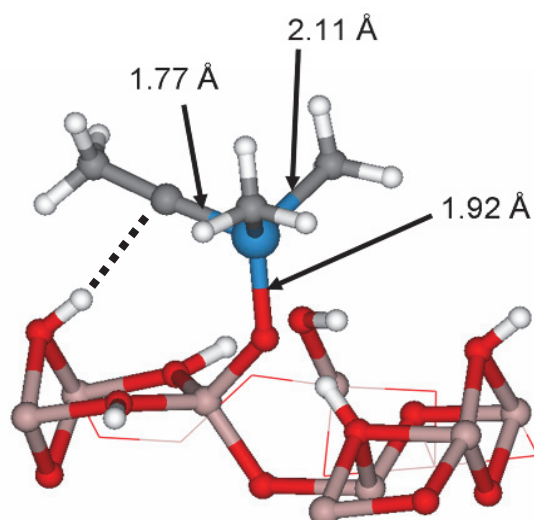
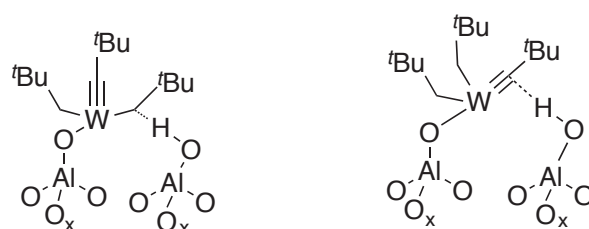


Figure 1.5 Structure of $[(\text{Al}_5\text{O})\text{W}(\equiv\text{C}^t\text{Bu})(\text{CH}_2^t\text{Bu})_2]$ (**IV**) obtained by DFT Calculations.⁷⁹

EXAFS experiments shows that (**IV**) may be the major surface species with the following features: i) about one carbon (1.773 Å) and one oxygen (1.862 Å) atom, the distances of which are consistent with a carbynic carbon atom and σ -bonded OAls, respectively; ii) two carbon atom neighbors at a greater distance (2.110 Å) assigned to two neopentyl ligands; iii) two carbon atoms at 3.314 Å, assigned to the two quaternary carbon atoms of the neopentyl ligands; and iv) a carbon atom at 3.323 Å, corresponding to the quaternary carbon atoms of the neopentylidyne ligand.^{135,136}

The solid state ^{13}C -CP-MAS NMR spectrum of $[\text{W}(\equiv\text{C}^t\text{Bu})(\text{CH}_2^t\text{Bu})_3]$ grafted on alumina reveals a broad signal from 50 to 110 ppm. This complexity is explained by theoretical calculation as an interaction between carbynic and methylenic carbons of the carbyne and neopentyl ligand respectively with unreacted aluminols (Scheme 1.12).

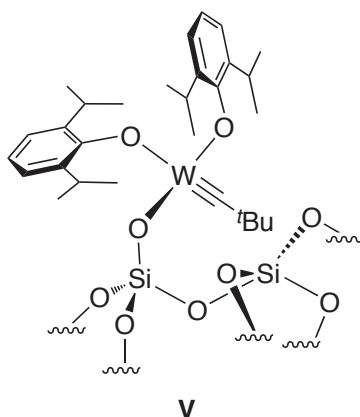


Scheme 1.12 Interactions proposed by Joubert *et al.* to explain the complexity of ^{13}C -CP-MAS NMR spectrum of $[\text{W}(\equiv\text{C}^t\text{Bu})(\text{CH}_2^t\text{Bu})_3]$ grafted on alumina⁷⁹

The preparation of tungsten-based complexes by SOMC related to **I** and **II** was undertaken by replacing the neopentyl ligands with spectator aryloxy groups. Related soluble analogues have been reported by Schrock with the view to examine the modification caused to the steric and electronic parameters of the metal centre. A precursor $[\text{W}(\equiv\text{C}-$

$t\text{Bu}(\text{CH}_2-t\text{Bu})(\text{OAr})_2$ ($\text{Ar} = 2,6\text{-}i\text{Pr}_2\text{C}_6\text{H}_3$) was prepared by a similar pathway as that used for the preparation of $[\text{W}(\equiv\text{C}-t\text{Bu})(\text{CH}_2-t\text{Bu})_3]$: WCl_6 is derivatised to produce $\text{W}(\text{OAr})_3\text{Cl}_3$ that is then alkylated by 4 equivalent $t\text{BuCH}_2\text{MgCl}$ to lead to the target.¹³⁷

$[\text{W}(\equiv\text{C}-t\text{Bu})(\text{CH}_2-t\text{Bu})(\text{OAr})_2]$ was grafted on $\text{SiO}_2\text{-}(700)$ to lead to **V**. All characterisations: IR spectroscopy, solid-state NMR spectroscopy (^1H SSNMR, ^{13}C CP-MAS) and mass balance analysis were consistent with a monopodal $[(\equiv\text{Si}-\text{O})\text{W}(\equiv\text{C}-t\text{Bu})(\text{OAr})_2]$ (Scheme 1.13).



Scheme 1.13 Proposed structure for the surface species **V**, obtained by grafting of $[\text{W}(\equiv\text{C}-t\text{Bu})(\text{CH}_2-t\text{Bu})(\text{OAr})_2]$ on $\text{SiO}_2\text{-}(700)$

The ^{13}C CP-MAS spectrum of this species shows seven resolved peaks, which can be assigned to the aromatic carbons, the isopropyl groups and the carbynic $t\text{Bu}$ moiety. Unfortunately, it has not been possible to detect the resonance of the carbynic atom (a resonance should be expected at *ca.* 300 ppm), probably due to the fact that i) it is not surrounded by proton and ii) the signal is probably relatively broad due to the interaction with the metal. However the observation of the signal at 51 ppm and the absence of any signal of a methylenic carbon (like in **I**) at *ca.* 74 ppm support the above proposed structure.¹³⁸

Gauvin *et al.* have developed an alternative to the direct grafting of the organometallic complex by immobilising dimeric metal compounds on the surface prior to its alkylation. Tungsten dimeric derivatives of the $d^3\text{-}d^3$ type involved in metal-to-metal triple bonding are convenient precursors and have found applications in numerous fields, such as in materials, organometallic synthesis, and in catalysis. One of the most versatile entries into this class of compounds relies on the substitution of amido ligands of the $\text{W}_2(\text{NR}_2)_6$ species through protonolysis or halogenation.¹³⁹ The immobilization of such key compounds onto an inorganic support to generate heterogeneous dinuclear amido de-

rivatives is therefore of great interest capable to act as precursor to form supported carbene bis amido tungsten after treatment with an internal alkyne.¹⁴⁰

The investigation of this grafting of such compounds is complicated by the absence of bonding between the metal and element easily observable such as ¹³C or ¹H in NMR spectrometry or even in IR spectroscopy do not allow us to access direct information about the coordination modes of the metals. By contrast, observing the low frequency region (200-600 cm⁻¹) by Raman spectroscopy permitted to confirm the immobilisation of W₂(NR₂)₆ on SiO₂₋₍₇₀₀₎. The modification of the symmetry and the vibration modes involving tungsten centre such as stretching of W≡W observed at 328 cm⁻¹ can attest that the dimeric W is attached to the surface.

- Oxide supported tungsten carbene

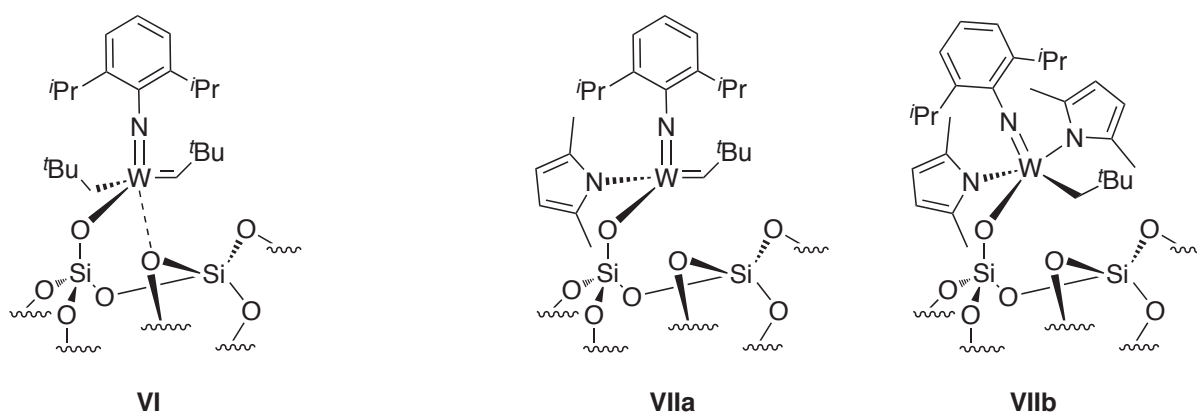
Most silica supported metallocarbene complexes of tungsten VI have been obtained by grafting their molecular equivalents developed by Schrock *et al.*¹⁴¹ on silica, and more specifically SiO₂₋₍₇₀₀₎. They are typically tetra-coordinated and have a d⁰ configuration and they can be described with the following general formula [W(=NR₁)(=CHR₂)(X)₂] (R₁ = R₂ = alkyl or aryl, X = neopentyl or pyrrolyl). These complexes can be grafted on the surface OH group of silica through different possible competitive ways. Therefore, the nature of surface species are typically investigated as follows: i) monitoring the ligands exchange before and after grafting by combining labelling studies (¹³C labelled or different types of ligands) and solid state NMR spectroscopy, and ii) using soluble molecular models of silica, based on molecular silanols, *i.e.* polyoligomeric silsesquioxane (POSS-OH) or (tBuO)₃Si-OH, to obtain mechanistic insight through monitoring the reaction of molecular silanols by solution NMR.

During the grafting of [W=N(2,6-ⁱPrC₆H₃)(CH₂^tBu)₂(=CH^tBu)] on SiO₂₋₍₇₀₀₎, as observed on the immobilisation of their carbyne counterparts, one of the alkyl ligand of the W precursors can be easily displaced by one of the surface silanol, affording VI [(≡SiO)W=N(2,6-ⁱPrC₆H₃)(=CH^tBu)(CH₂^tBu)].¹⁴² IR and mass balance analysis undoubtedly prove the immobilisation of the complex, the presence of the carbene ligands could only be confirmed by using a W analogue of VI in which 100% of the carbon directly attached to W have been labelled with ¹³C. Its CP-MAS ¹³C NMR spectrum revealed two intense signals at 60 and 255 ppm, attributed to the methylene and the carbene carbons, respectively.

The same organometallic starting compound reacts with [(C₅H₉)₇Si₇O₁₂SiOH] (POSS-OH) to give [((C₅H₉)₇Si₇O₁₂SiO)W=N(2,6-ⁱPrC₆H₃)(=CH^tBu)(CH₂^tBu)], which

shows similar spectroscopic properties to the silica-grafted moiety. In particular, the syn conformation is assigned to both the surface and the molecular siloxy W(VI) species based on the low $^1J_{\text{CH}}$ coupling constants for the alkylidene signals in the NMR spectra ($^1J_{\text{CH}} = 107$ Hz for ^{13}C solution spectra of the silasesquioxanes vs. $^1J_{\text{CH}} = 107$ Hz for J -resolved 2D ^1H - ^{13}C HETCOR solid-state NMR spectrum of the ^{13}C labeled silica grafted compound).

The structural assignment for **VI** is also supported by the EXAFS data, which are in agreement with a W atom bound to one nitrogen at 1.734(7) Å, a bond length consistent with an imido ligand, two carbons at 1.873 and 2.16(2) Å, consistent with neopentylidene and neopentyl ligands, respectively, and one oxygen at 1.95(3) Å, consistent with a siloxy substituent. Moreover, an oxygen atom from a siloxane bridge is close enough (*i.e.* 2.43(1) Å) to the metal for allowing interaction.



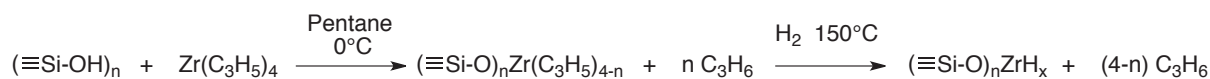
Scheme 1.14 Structures proposed for surface species **VII** and **VIII**

More recently the replacement of the pending alkyl by amido ligands, (2,5- $\text{Me}_2\text{NC}_4\text{H}_2$), which is readily achieved by grafting bis(amido) complex on silica ($[\text{W}\equiv\text{N}(2,6\text{-}^i\text{PrC}_6\text{H}_3)(=\text{CH}^t\text{Bu})(2,5\text{-}\text{Me}_2\text{NC}_4\text{H}_2)_2]$) has been reported. The grafting of 2,5-dimethylpyrrolyl compounds is more complex yielding the expected monosiloxy alkylidene surface complex as the major products, $[(\equiv\text{SiO})\text{W}(\equiv\text{NAr})(=\text{CH}^t\text{Bu})(2,5\text{-}\text{Me}_2\text{NC}_4\text{H}_2)]$ **VIIa**, along with a surface complex resulting from the protonation of the alkylidene ligand in place of the silanolysis of the W-N bond, $[(\equiv\text{SiO})\text{W}(\equiv\text{NAr})(\text{CH}_2^t\text{Bu})(2,5\text{-}\text{Me}_2\text{NC}_4\text{H}_2)_2]$ **VIIb**.¹⁴³ It demonstrates that the addition of heteroelements in the coordination sphere of the homogeneous precursor impacts the selectivity of grafting reaction.

- Oxide supported tungsten hydride

The preparation of oxide supported tungsten complexes is generally operated by reaction of a surface OH group with a W-C bound of the relative molecular precursor. A similar method has been undertaken to prepare supported tungsten hydride by grafting of molecular tungsten hydride complexes such as $\text{WH}_6(\text{PR}_3)_3$. Nevertheless, this route is not convenient due to the weak reactivity of W-H bound toward water and therefore toward surface OH groups.¹⁴⁴

In the 70's Zakharov *et al.* initiate a new method for the preparation of zirconium hydrides supported on silica by the reaction of corresponding organometallic perhydrocarbyl compounds with partially dehydroxylated silica followed by reduction of the surface complexes thus formed at 150°C under H_2 (Scheme 1.15).¹⁴⁵ In the 80's they developed titanium and hafnium hydrides using the same methodology.¹⁴⁶ In the 90's, Vidal *et al.* have extended these investigations to group V, describing silica supported tantalum trisulfide.⁹⁶

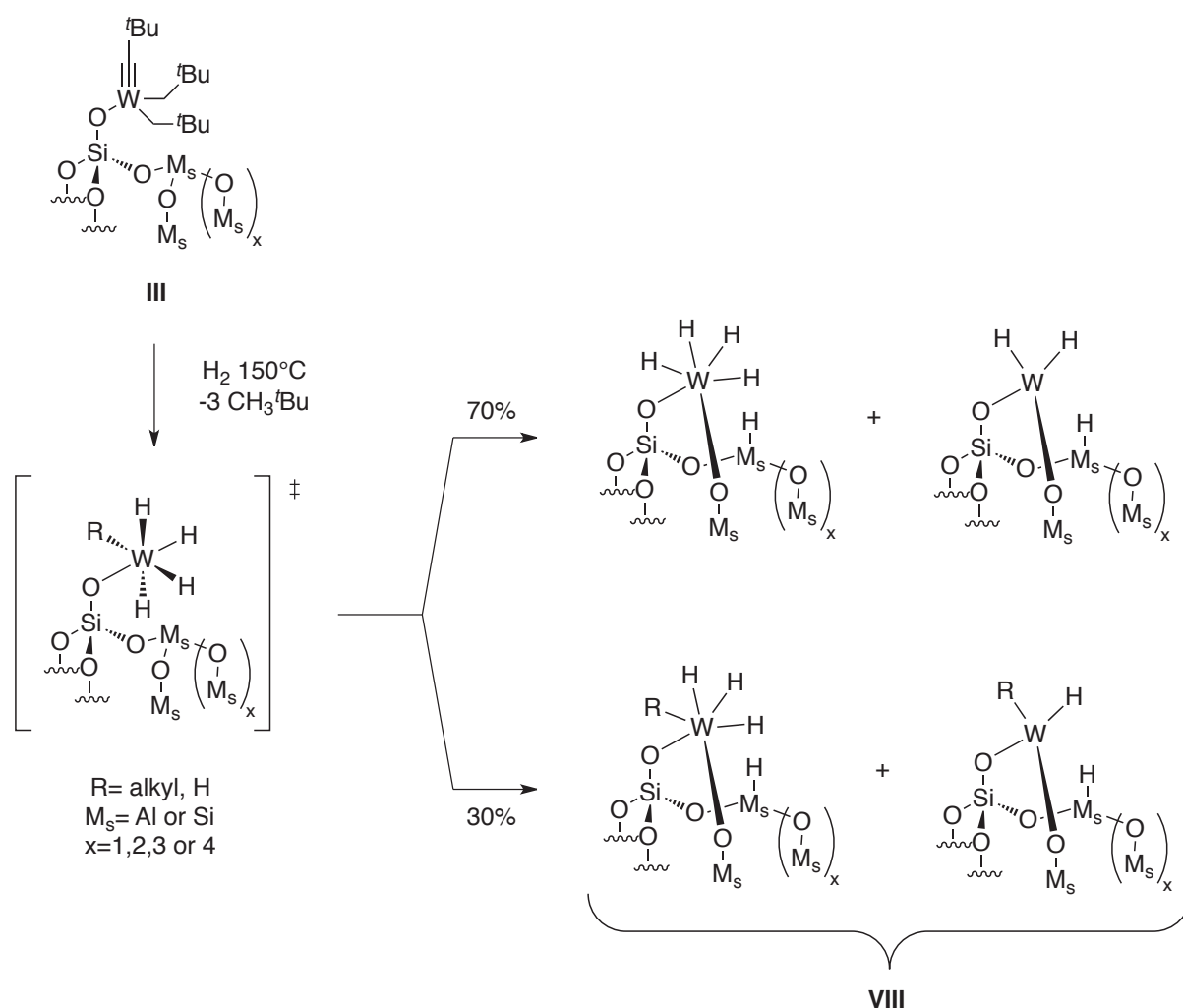


Scheme 1.15 Preparation of surface zirconium hydride described by Zakharov *et al.*¹⁴⁵

In the light of these results, the development of this methodology for group VI metals has been envisaged by hydrogenolysis of the corresponding supported organometallic precursor such as **I**, **II**, **III**, or **IV**. Nevertheless, the energy of W-W and W-O bound are relatively close (675 and 666 $\text{kJ}\cdot\text{mol}^{-1}$ respectively)¹⁴⁷ let think that the stabilization of tungsten hydrides on oxides surface may be disfavored, letting the formation of tungsten particles by sintering. In the case of group V, the difference of energy between the metal-metal and metal-oxygen bounds is wide enough to avoid sintering (*e.g.* Ta-Ta: $390\pm 96 \text{ kJ}\cdot\text{mol}^{-1}$ and Ta-O: $799\pm 13 \text{ kJ}\cdot\text{mol}^{-1}$).^{148,149}

Therefore, the treatment of **I** and **II** (supported on $\text{SiO}_{2-(200)}$ and $\text{SiO}_{2-(700)}$) at 150°C for 15h, under H_2 leads to partial or total sintering of the tungsten surface species. The formation of small particles (10 to 20 Å) has been evidenced by TEM, CO adsorption and by resurgence of the Si-OH signal on the infrared spectrum.¹⁵⁰ In sharp contrast, the similar treatment of **III** and **IV** (supported on $\text{SiAl}_{(500)}$ and $\text{Al}_2\text{O}_{3-(500)}$), generate the corresponding hydrides, **VI** and **IX**, without sintering. This difference of reactivity highlights the significant role of the support in the stability of species obtained by SOMC. It seems that the presence of aluminum atoms at the surface of the support (*i.e.* silica-alumina or alumina) prevents the migration of tungsten atoms.

However the structures of the resulting tungsten hydride are quite complex. In the case of silica-alumina supported species, **VIII**, the structure presented on Scheme 1.16 has been proposed based on the chemical reactivity, spectroscopic evidences and analogy with other oxide supported metal hydrides.¹³⁴ The tungsten hydrides have been characterized by IR spectroscopy ($\nu_{(WH)}$ at 1980–1800 cm^{-1}) and ^1H Solid-state NMR spectroscopy (6.6, 11.5 and 19.5 ppm) which were a first indication that several tungsten hydride species existed on the surface. The assignments have been confirmed by reversible exchange with D_2 . The formation of Si-H and Al-H suggest the reaction of tungsten hydride intermediates with adjacent bridges (Si-O- M_s , $M_s = \text{Si}$ or Al) according to the same mechanism observed for group IV and V metals.



Scheme 1.16 Proposed structures for tungsten hydrides supported on silica-alumina **VIII**¹³⁴

In the case of alumina, the spectroscopic data are less complex than for the silica-alumina species **IX**.^{135,136} ^1H Solid-state NMR spectroscopy shows a weak signal 10.1 ppm that can be attributed to a W-H. Furthermore, IR spectroscopy of this reaction per-

mitted the observation of the qualitative consumption of the alkyl bands simultaneously to the appearance of two large bands at 1903 and 1804 cm^{-1} ascribed to W-H. Submitting the sample to D_2 under the same condition results in the presence of W-D due to exchange reaction consistently with two corresponding signals at 1388 and 1293 cm^{-1} . Further characterization of this surface species will be presented in Chapter 2 of this thesis.

2.3. Catalytic activity

The SOMC of tungsten has led to the preparation of a wide range of surface species bearing several ligands. This section will consider the singular catalytic activity of these compounds, and will be divided in three main parts: i) Alkyne metathesis, ii) Olefin metathesis and iii) Non-oxidative coupling of methane, linear and branched alkane metathesis

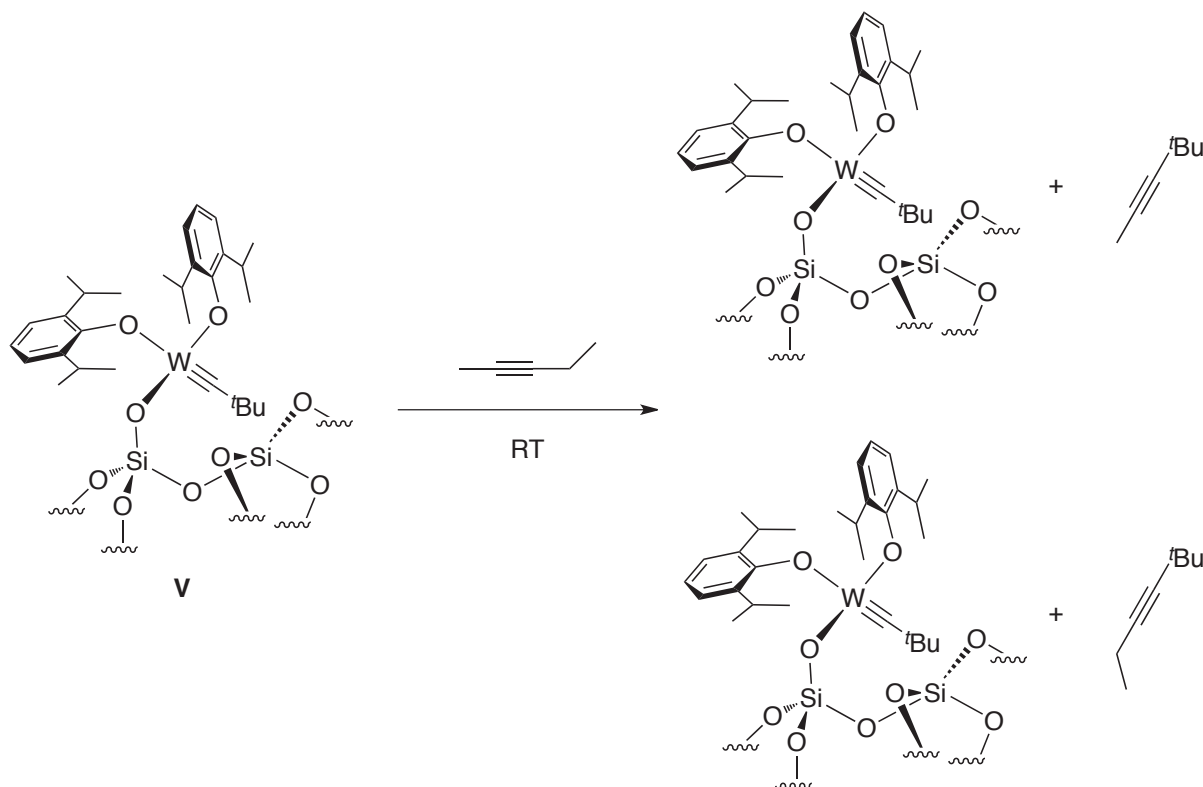
2.3.1. Alkyne metathesis

Olefin metathesis is now routinely used in organic synthesis.¹⁵¹⁻¹⁵³ Some recent and elegant applications are the synthesis of macrocycles by ring closing metathesis of a diene.¹⁵⁴ However, olefin metathesis meets some limitations as it gives mixtures of E and Z isomers, thus decreasing its potential as a highly stereoselective synthetic method. An approach to overcome this difficulty may be found with alkyne metathesis.¹⁵⁵ Indeed, the newly formed C=C bond could then be stereo-selectively reduced to either E or Z, C=C isomers, or converted to another functionality. Up to now, several alkyne metathesis catalysts are known.^{155,156} To avoid deactivation by bimolecular dimerization reaction,^{129,130} Moore *et al.* reported the grafting reaction of the molybdenum complex $[\text{Mo}(\equiv\text{C}^t\text{Bu})(\text{NAr}^t\text{Bu})_3]$ on amorphous silica pretreated at 400°C under dry O_2 , the purpose being to induce minimal changes in the electronic structure of the complex and to reduce its mobility.¹⁵⁷ This catalyst showed a high catalytic activity and a good stability.

Using the similar hypothesis, the different tungsten-carbyne surface species presented in last subsection have been identified as potential catalyst for this reaction. Nevertheless, **II** displays only a stoichiometric activity in alkyne metathesis, probably due to the formation of a biscarbene species by α -H abstraction inactive in this reaction. The modification of the metal coordination sphere by replacing the two neopentyl moieties by ancillary ligands as in surface species **V** may prevent this phenomenon.¹³⁸

Thus, the reaction of **V** with an excess of pent-2-yne was performed in a batch reactor at room temperature. After reaction 0.65 equiv. per tungsten of a 1/1 mixture of 4,4-dimethylpent-2-yne ($\text{Me}-\text{C}\equiv\text{C}-^t\text{Bu}$) and 2,2-dimethylhex-3-yne ($\text{Et}-\text{C}\equiv\text{C}-^t\text{Bu}$) had evolved (Scheme 1.17). These products arise from the interaction between pent-2-yne and the car-

byne ligand, namely the initiation step for alkyne metathesis. The 1/1 ratio is consistent with a comparable stability of both possible metallacyclobutadiene intermediates,²⁶ which is not influenced by 1,2- or 1,3-interactions due to the planarity of the cycle, at the difference of olefin metathesis.¹⁵⁸



Scheme 1.17 Stoichiometric reactivity of **V** toward pent-2-yne at room temperature¹³⁸

However, at 80°C the reaction of **V** with an excess of pent-2-yne (61 equiv. per W atom) forms a mixture of but-2-yne and hex-3-yne in a 1/1 ratio (Scheme 1.18). The initial turnover frequency was 0.32 mol.mol_W⁻¹.min⁻¹. Interestingly, no oligomerization of the alkyne substrate or of the reaction products was evidenced either by GC after extraction of the solid or via the mass balance. This behavior is different from that of similar homogeneous catalysts for which formation of heavy products is problematic.¹³⁷



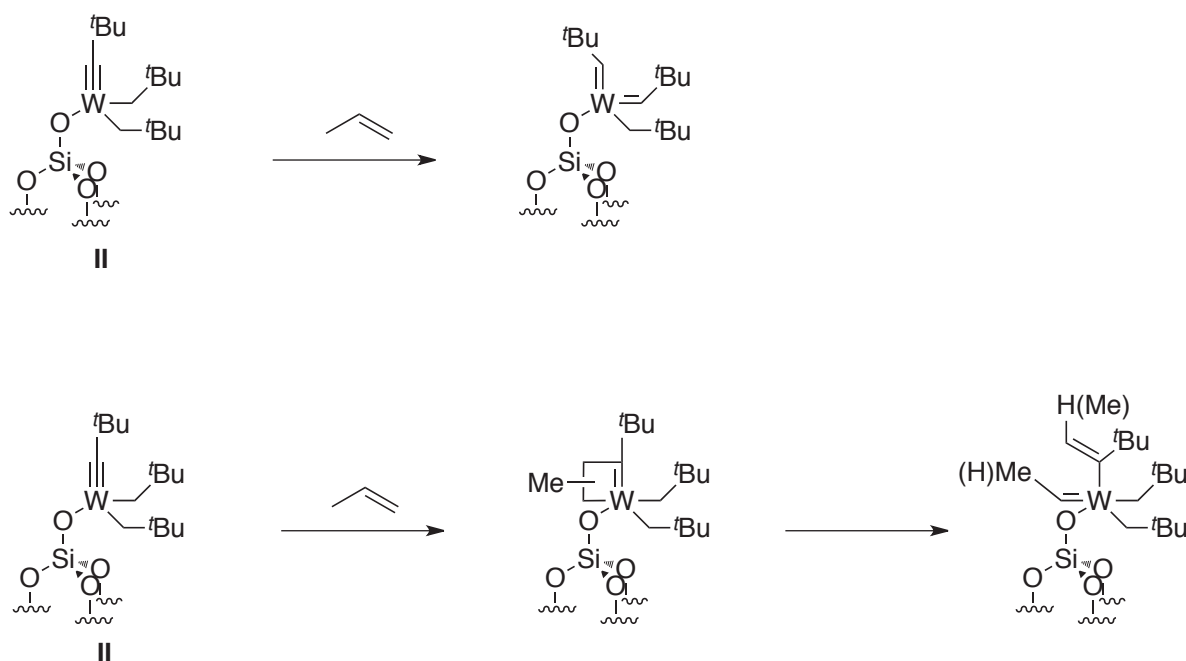
Scheme 1.18 Pent-2-yne metathesis reaction

2.3.2. Olefin metathesis

Olefin metathesis has a crucial role in the chemical industry and academic. While the petrochemical industry has used this technology for forty years, it has gained even more im-

portance in the recent years with the increasing world demand in propylene (*vide supra*). The development of supported catalysts that are easily recyclable and have durable lifetime is thus primordial. SOMC has allowed preparing tungsten species with well-defined coordination sphere, affording a rational approach of the development of heterogeneous catalysts. Several species described in subsection 2.2, *i.e.* **II**, **VI** and **VII**, have been tested for propylene metathesis in continuous flow reactor at room temperature.

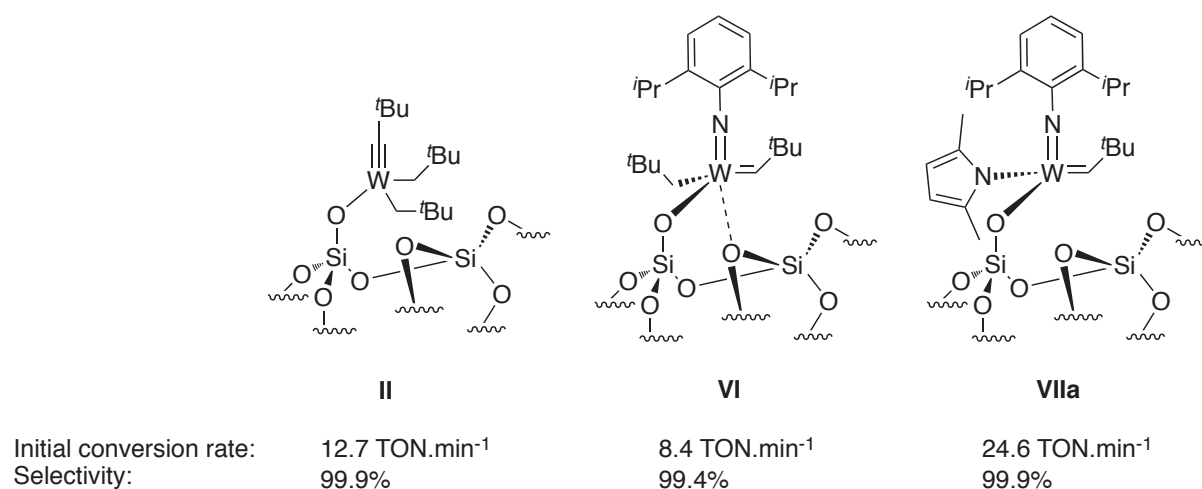
Despite the absence of alkylidene ligand, **II** exhibits a high activity with an initial rate of 12.7 TON.min⁻¹ and a selectivity of 99.9% in metathesis products.¹³³ Therefore, this system can be used as a precursor for olefin metathesis and the carbene ligand is probably generated *in situ* after coordination of olefin either by α -H abstraction from an alkyl ligand leading to a bis-alkylidene surface species¹⁵⁹ or by direct metathesis of an olefin with an alkylidyne, which creates in turn a propagating ligand (Scheme 1.19).



Scheme 1.19 Possible formation of the carbene from the alkylidyne ligand¹³³

In the same conditions, the corresponding tungsten carbene species bearing an imido ligand, **VI**, gives an initial rate of 8.4 TON.min⁻¹ and a selectivity of 99.4%.¹³³ The replacement of the alkyl by a pyrrolyl ligand to form the isoelectronic species namely **VII**, dramatically increases the performances of the catalyst, with an initial rate of 24.6 TON.min⁻¹ and a selectivity of 99.9%.¹⁴³ DFT calculations on the metathesis, the deactivation, and the byproduct formation pathways for the imido tungsten species **VI** and **VII** give a rational for the role of pyrrolyl ligand.¹⁶⁰ The greatest benefit of substituting the ancillary alkyl by a pyrrolyl ligand, is in fact not to improve the efficiency of the cata-

lytic cycle of olefin metathesis, but to shut down deactivation and byproduct formation pathways. Pyrrolyl ligand, and more generally ligands having metal-bound-atoms more electronegative than carbon, disfavors mostly the two first steps (α -H abstraction at the metallacyclobutane and subsequent insertion of an ethene in the M-H bond) of the deactivation channel. The **VII** catalyst is thus highly efficient because pyrrolyl ligand is optimal: (i) it is still a better electron donor than the siloxy group, thus, favoring the metathesis pathway (dissymmetry at the metal center); and (ii) the nitrogen of the pyrrolyl ligand is more electronegative than the carbon of the alkyl group, thus, specifically disfavoring the decomposition of the metallacyclobutane intermediate via α -H abstraction.



Scheme 1.20 Propylene metathesis catalyst precursors and their performances

2.3.3. Non-oxidative coupling of methane, linear and branched alkane metathesis

- Non-oxidative coupling of methane

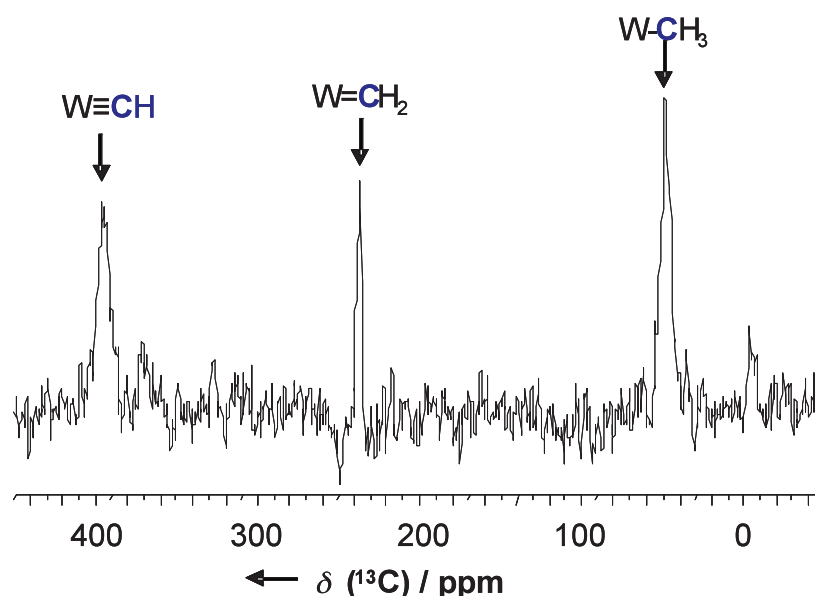
Methane, which is the main component of natural gas, represents an important reserve of fossil carbon. Transformation of natural gas into higher hydrocarbons remains an important economical target and a huge scientific challenge.¹⁶¹⁻¹⁶³ Contrary to the other existing method to convert methane into higher hydrocarbon, namely Fisher-Tropsch synthesis and oxidative coupling of methane, the direct non-oxidative coupling of methane (NOCM) into ethane and hydrogen avoid without production of carbon oxides.

Various attempts to accomplish the NOCM reaction (Scheme 1.21) used classical and ill-defined heterogeneous catalysts, *i.e.* supported metal particles.^{164,165} The use of well-defined supported tantalum hydride as catalyst to perform NOCM has also been reported.¹¹⁴

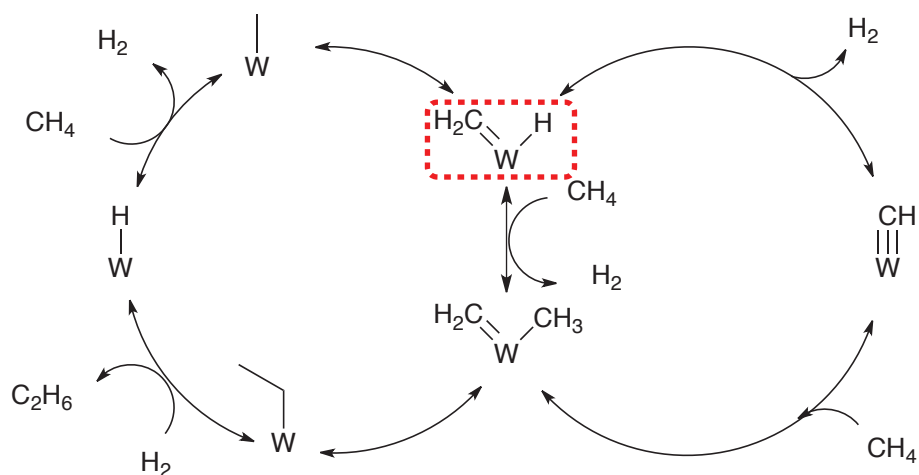


Scheme 1.21 NOCM reaction

It has been recently shown that tungsten hydride supported on silica-alumina or alumina, **VIII** and **IX**, catalyze the coupling of methane at 350°C, 50 bar in a classical fixed-bed reactor.¹⁶⁶ After an induction period due to modification of the coordination sphere of the metal under methane, the activity remains constant after the initial state (conversion = 0.2%). Ethane is formed selectively (>99% among hydrocarbons) along with an equimolar amount of H₂). When the maximum conversion is reached, a stable steady state is observed, showing an essential improvement compared to the tantalum hydride, which suffers from deactivation.

Figure 1.6 ¹³C CP MAS NMR spectrum of **VIII** obtained after ¹³CH₄ activation at 150°C

The mechanism of the reaction has been proposed according solid-state NMR characterisation of the catalyst (**VIII**) after reaction with ¹³CH₄. ¹³C CP- MAS and 2D ¹H-¹³C HETCOR NMR spectrum reveals three peaks with chemical shifts compatible with tungsten methyl (48 ppm), methylidene (237 ppm), and methylidyne (395 ppm) ligands (Figure 1.6). These observations indicate that the methyl species formed after activation of CH₄ onto **VIII**, leads to a partial evolution to a mixture of unsaturated surface species such as [W=CH₂] and [W≡CH] probably by subsequent α-H elimination and α-H abstraction, respectively (Scheme 1.22).^{114,167,168}



Scheme 1.22 Proposed mechanism for the NOCM reaction catalyzed by supported tungsten hydride

The postulated mechanism involves the formation of tungsten-methylene-hydride as the key intermediate (Scheme 1.22). The following step is C-H bond activation on the hydride via σ -bond metathesis with the formation of a tungsten-methyl-methylidene. A *cis* migration of the methyl to the methylidene occurs, affording the formation of the C-C bond as already observed on a corresponding tantalum complex.¹⁶⁹ Then, the cleavage of the resulting tungsten-ethyl by hydrogen would take place.

These dual properties of the active site, *i.e.* tungsten carbene and hydride, afford the occurrence of two noticeable elementary steps on the same metal center: i) C-H bond activation and ii) carbene insertion. While during NOCM reaction catalyzed by supported metal particles, these elementary steps involves two adjacent metal atoms.^{164,165,170-172}

- Alkanes metathesis

The catalytic activation of alkanes remains one of the most important challenges in chemistry in view of their inertness and considerable application potential.^{173,174} In the 70's, Hughes and Burnet have evidenced a catalytic reaction, named disproportionation of alkanes, which directly transforms butane, at 399°C and 62.2 bar, into its lower and higher homologues.¹⁷⁵ The catalytic system used in the conversion of butane was based on the succession of reactions: i) dehydrogenation of butane in butenes, ii) butenes metathesis allowing the formation of higher and lower olefins and iii) their hydrogenation in the corresponding olefins. To achieve these reactions, they used a Pt/Li based dehydrogenation-hydrogenation catalyst supported on alumina and WO_3/SiO_2 as olefin metathesis catalyst mixed together. These mixed catalysts are inoperative for ethane formal disproportionation because of degenerated ethylene metathesis.

In 1997, Vidal *et al.* used a tantalum hydride supported on silica as a catalyst for alkanes disproportionation at low temperature, *i.e.* 150°C, and atmospheric pressure.⁹⁶ They introduce the term “alkanes metathesis” in analogy with olefin metathesis. This was the first description of a single site system affording this reaction. The authors have proposed a mechanism where σ -bond metathesis is the only elementary step, due the highly electrophilic character of the silica-supported tantalum-alkyl species, which involve a four-centered transition state with the presence of an sp^3 carbon in the middle of the metallocycle.⁹⁶ The cumulated TON of this system remains modest but corresponds to the productive reaction, whereas degenerate processes also take place as evidenced in the case of ^{13}C mono-labeled ethane.⁹⁸ It was then evidenced that the precursor of silica supported tantalum hydrides, namely $[(\equiv SiO)Ta(=CH^tBu)(CH_2^tBu)_2]$, was also active for propane metathesis.¹⁰¹

In light of these results, the activities of supported tungsten species for alkanes metathesis have been investigated. Tungsten carbyne species supported on silica (**II**), silica-alumina (**III**) and alumina (**IV**) have been tested for propane metathesis in batch reactor at 150°C (Table 1.1).¹³⁴⁻¹³⁶ **III** and **IV** are active catalyst precursor for the metathesis of propane. Their initial rate is 0.7 TON.h⁻¹ and 1.8 TON.h⁻¹ respectively, while the corresponding silica-supported system, **II**, is inactive even if its NMR spectroscopic features are identical to these of **III**, and somewhat different from these of **IV**. It confirms the essential role of the support in catalytic activity of the metal centre, and particularly the beneficial influence of aluminum. The comparison of the activity of **III** and **IV** with $[(\equiv SiO)Ta(=CH^tBu)(CH_2^tBu)_2]$, reveals that the cumulated TONs after 120 are similar, whereas the initial rate for tantalum complex is higher with 3.0 TON.h⁻¹, which indicates that the tungsten catalysts are less prone to deactivation.

Table 1.1 Activity of tungsten surface species in propane metathesis at 150°C in batch reactor

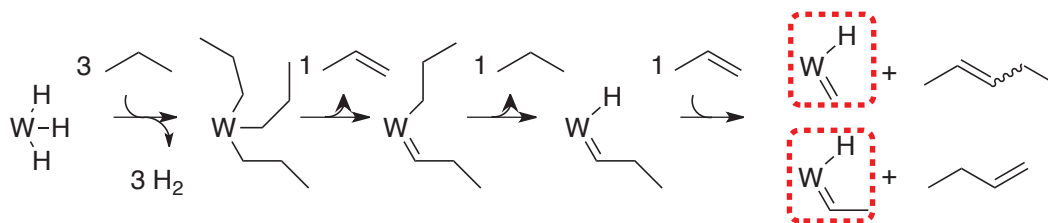
Pre-catalysts	Initial rate ^[a]	TON at 120 h	Product selectivity ^[b]				
			Methane	Ethane	Butanes ^[c]	Pentanes ^[d]	Hexanes ^[e]
$[(\equiv SiO)Ta(=CH^tBu)(CH_2^tBu)_2]_{SiO_2}$	3.0	35	12.8	47.7	22.8/10.4	3.5/2.5	0.9
$[(\equiv SiO)W(\equiv C^tBu)(CH_2^tBu)_2]_{SiO_2}$ II	-	0	-	-	-	-	-
$[(\equiv SiO)W(\equiv C^tBu)(CH_2^tBu)_2]_{SiAl}$ III	0.7	29	1.6	61.7	25.7/3.4	5.5/1.3	0.8
$[(Al_3O)W(\equiv CtBu)(CH_2^tBu)_2]_{Al_2O_3}$ IV	1.8	28	2.7	65.4	20.7/2.9	5.3/1.5	1.5
TaH/SiO ₂₋₍₇₀₀₎	2.5	60	10	46.0	30.6/6.0	4.8/2.2	0.4
WH/SiAl ₍₅₀₀₎ VII	8.5	123	1.9	58.0	28.9/3.2	5.2/1.4	1.4
WH/Al ₂ O ₃₋₍₅₀₀₎ IX	8.5	121	2.4	57.3	28.9/3.7	5.0/1.3	1.4

[a] TON.h⁻¹ [b] The selectivities are defined as the amount of product *i* over the total amount of product [c] C₄/*i*C₄ [d] C₅/*i*C₅ [e] Selectivity for the sum of all the C₆ isomers

The tungsten hydrides supported on silica-alumina (**VIII**) and alumina (**IX**) have then been tested for propane metathesis in the same reaction conditions (Table 1.1). Notably, **VIII** and **IX** give better results with initial rate of $8.5 \text{ TON}\cdot\text{h}^{-1}$ and *ca.* 125 TON at 120 h. In addition to this higher activity, hydride systems, contrary to perhydrocarbyl precursors, can be regenerated by treatment under H_2 .¹⁷⁶

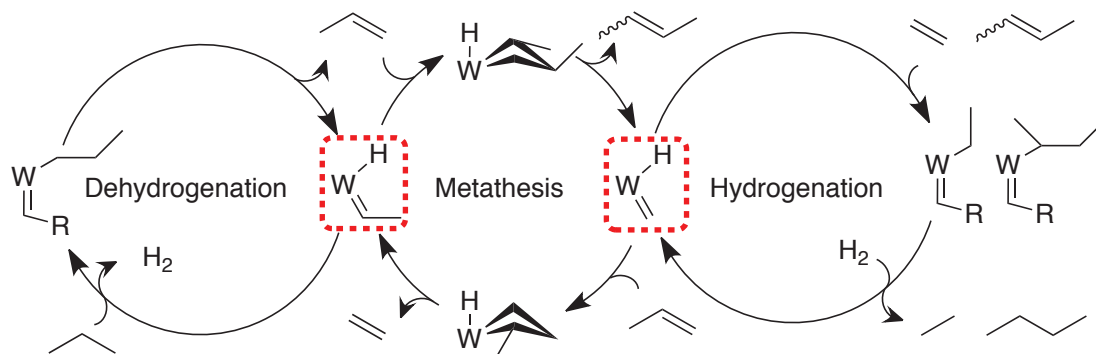
The comparison with the tantalum-based systems supposes that the tungsten hydride catalysts are more active and as for perhydrocarbyl species the deactivation is slower. Moreover, tungsten based catalysts lead to a narrowed distribution in the product selectivity. Indeed, the methane selectivity after 120 h is less than 3% for tungsten based catalysts, when it was *ca.* 10% for the tantalum ones, which is consistent with greater hydrogenolysis capability of tantalum. This significant improvement in activity probably reflects the difference between the intrinsic properties of tungsten and those of tantalum. Interestingly, in olefin metathesis, it is known that tungsten based are much better than tantalum based homogeneous systems, due to the instability of tantalacyclobutanes.^{177,178} In addition high ratio of linear to branched products is observed and the selectivities for higher homologues are as follows $\text{C}_{n+1} > \text{C}_{n+2} \gg \text{C}_{n+3}$. These selectivities are similar to those generally described in olefin metathesis, where 1,3-disubstituted metallacyclobutane intermediates are favored toward 1,2-disubstituted ones.³² These data have suggested to revisit the σ -bond metathesis based mechanism proposed earlier.^{76,96,98,101} Therefore, kinetic studies under dynamic conditions have identified olefins and hydrogen as primary product of the reaction for tantalum and tungsten based catalysts.^{107,135,136} It confirms that alkane metathesis mechanism involves elementary steps related to that of olefin metathesis.

For the tungsten hydride supported on alumina the initiation steps of alkane metathesis has been proposed by C-H bond activation of three alkanes to lead to trisalkyl tungsten intermediate. This intermediate can undergo an α -H abstraction to form an alkyl-alkylidene tungsten surface species, which further leads to the carbene-hydride by β -H elimination (Scheme 1.23).



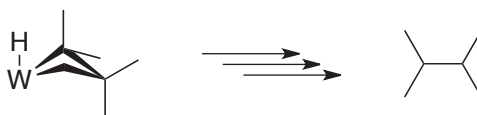
Scheme 1.23 proposed initiation step for propane metathesis catalyzed by tungsten hydrides

This tungsten carbene-hydride is the key intermediate of the mechanism (Scheme 1.24). This tungsten-hydride can operate either dehydrogenation of propane to propylene by σ -bond metathesis followed by β -elimination or perform the reverse reaction, *i.e.* hydrogenation by olefin insertion followed by cleavage of the tungsten alkyl by hydrogen. Concomitantly the tungsten-carbene can form metallacyclobutane with the propylene to form either 2-butenes or ethylene *via* the classical Chauvin mechanism.²⁵



Scheme 1.24 Proposed mechanism for propane metathesis on supported W hydrides for the production of linear products

It has to be noted that, while the silica supported tantalum hydride transforms isobutane classically into propane and 2-methyl propane by transfer of one carbon, tungsten hydride supported on alumina, **IX**, convert isobutane with an unusual selectivity into 2,3-dimethylbutane (41.7%) and ethane (41.3%).¹⁷⁹ This reaction is the first example of the transfer of two carbons in alkane metathesis. Hence, for this reaction the selectivities of higher homologues are quite different from those obtained in metathesis of linear alkanes (*vide supra*) and can be ordered as follows: $C_{n+2} \gg C_{n+1} > C_{n+3}$. The mechanism proposed for this reaction is similar to the mechanism of propane metathesis (Scheme 1.24). Yet again a tungsten carbene-hydride is the key species of the mechanism. Nevertheless, the main difference in the mechanism of isobutane conversion is the sterical crowding of the metallacyclobutane, which presents 1,2-gem-dimethyl substituents (Scheme 1.25).¹⁷⁹



Scheme 1.25 Metallacyclobutane intermediate proposed for the for isobutane metathesis¹⁷⁹

Interestingly, as in NOCM, the key intermediate is a tungsten carbene-hydride. Moreover this active species displays dual functionality: i) tungsten hydride afford dehydrogenation of alkanes or hydrogenation of olefins and ii) tungsten carbene is involved in olefin metathesis reaction.

3. Conclusion

Propylene is a key intermediates in chemical industry especially for the production of polypropylene. The increasing of propylene demand favors the expansion of new technologies for its synthesis. While the traditional routes produces propylene as a by-product, the main developments are yet focused on “on purpose” processes. Among them, olefin metathesis is a promising tool. Nevertheless, while numerous homogeneous and heterogeneous catalytic systems has been investigated in academia, WO_3/SiO_2 remains the major catalyst employed at the industrial scale for production of propylene by ethylene/2-butene cross-metathesis. The active site of this catalyst is still not well understood, which prevent rational development to improve its activity.

The use of surface organometallic chemistry (SOMC) has afford to produce well-defined surface tungsten species, which are highly active catalysts, or precatalysts for different reactions such as alkyne, olefin and alkane metathesis or non-oxydative coupling of methane. Among this surface species, tungsten hydrides have attracted the attention due to their potential regeneration under H_2 stream.

These supported tungsten hydrides are precursor of carbene-hydride species that gives singular reactivity to the tungsten centre. The hydride ligand affords: C-H activation, alkane dehydrogenation and olefin hydrogenation, while the carbene instigates: olefin metathesis or carbene insertion. These remarkable properties have been extended to the transformation of olefins and particularly propylene production. The supported tungsten hydrides have been evidenced as catalyst for the unusual direct conversion of ethylene to propylene.¹⁸⁰ It has been proposed that the hydride ligand may induce dimerization and isomerization reactions.

This PhD work has thus been organized as follows. Chapter 2 is devoted to the preparation and characterizations of tungsten hydride supported on alumina. The complex alumina properties have been studied and structural identifications of the carbynic precursor and of the tungsten hydride have been deepened.

Chapter 3 discloses a complete mechanistic study of the direct conversion of ethylene to propylene using supported tungsten hydride as a catalyst confirming the results proposed earlier.¹⁸⁰ The optimization of reaction parameters has been undertaken. A particular attention has been given to the determination of the deactivation mechanism according the characterizations presented in Chapter 2. Different methods will also be attempted to regenerate the catalyst.

Chapter 4 releases the preparation of isolated supported aluminum alkyl and hydride, which presence has been spotted at the surface of tungsten hydride catalyst in Chapter 2. Their reactivity toward ethylene was then investigated to test their influence in the catalytic activity and deactivation mechanism of tungsten hydride supported on alumina.

Chapter 5 reveals the activity of supported tungsten hydride for the production of propylene from light olefins, taking advantage of singular reactivity of the tungsten carbene-hydride active site and avoiding the deactivation observed in Chapter 3.

Chapter 6 finally presents the preparation of new model tungsten catalysts supported on silica. The preparation of first supported tungsten oxo derivatives using SOMC methodology will be tackled in order to obtain models of the active sites of WO_3/SiO_2 and tungsten hydride supported on alumina. A deep structure-reactivity relationship study confirms the mechanism and the deactivation pathway presented in Chapter 3.

4. Reference and Notes

- (1) Logsdon, J. E. and Loke, R. A. In *Kirk-Othmer Encyclopedia of Chemical Technology*; John Wiley & Sons, Inc., 2000.
- (2) *Propylene Refineries*, Nexant ChemSystems PERP report; 2005.
- (3) *Propylene Technology: The next generation*, Nexant ChemSystems PERP report; 2009.
- (4) Calamur, C. N. and Carrera, C. M. In *Kirk-Othmer Encyclopedia of Chemical Technology: Propylene*; John Wiley & Sons, Inc., 2005; p. 1-25.
- (5) *Alternative routes to propylene*, Nexant ChemSystems PERP report; 2010.
- (6) Eisele, P. and Killpack, R. In *Ullmann's Encyclopedia of Industrial Chemistry*; John Wiley & Sons, Inc., 2000.
- (7) Sundaram, K. M.; Shreehan, M. M.; and Olsewski, E. F. In *Kirk-Othmer Encyclopedia of Chemical Technology: Ethylene*; John Wiley & Sons, Inc., 2001; p. 593-632.
- (8) Rice, F. O. *Journal of the American Chemical Society*. 1931, *53*, 1959-1972.
- (9) Rice, F. O. *Journal of the American Chemical Society*. 1933, *55*, 3035-3040.
- (10) Venuto, P. B. and Habib, E. T. *Fluid catalytic cracking with zeolite catalysts*, M. Dekker: New York; 1979.
- (11) Wilson, J. W. *Fluid catalytic cracking technology and operations*, Tulsa, Okla. : PenWell; 1997.
- (12) <http://www.uop.com/objects/MTO.pdf>.
- (13) http://www.totalpetrochemicals.com/media/104_brochure_mto_fr.pdf.
- (14) *EP 1976813*. 2008.
- (15) Xie, Z.; Qi, G.; Zhang, H.; and Zhong, S. *WO 2008095417*. 2008.
- (16) Qi, G.; Xi, Z.; Zhong, S.; Xin, X.; and Wang, H. *US 2008188701*. 2008.
- (17) Mol, J. C. *Journal of Molecular Catalysis A: Chemical*. 2004, *213*, 39-45.
- (18) Amigues, P.; Chauvin, Y.; Commereuc, D.; Lai, C. C.; Liu, Y. H.; and Pan, J. M. *Hydrocarbon Process*. 1990, *69*, 79.
- (19) Cosyns, J.; Chodorge, J.; Commereuc, D.; and Torck, B. *Hydrocarbon Process*. 1998, *77*, 61.
- (20) Mol, J. C. *Catalysis Today*. 1999, *51*, 289-299.
- (21) Takai, T.; Mochizuki, D.; and Umeno, M. *EP 1953129*. 2008.
- (22) *Braskem press release* : http://www.braskem.com.br/site/portal_braskem/en/sala_de_imprensa/sala_de_imprensa_detalhes_9529.aspx. 2009.
- (23) Banks, R. L. and Bailey, G. C. *I&EC Product Research and Development*. 1964, *3*, 170-173.
- (24) Calderon, N.; Chen, H. Y.; and Scott, K. W. *Tetrahedron Letters*. 1967, *8*, 3327 - 3329.
- (25) Hérisson, J. L. and Chauvin, Y. *Makromol. Chem*. 1971, *141*, 161-176.
- (26) Katz, T. J. and McGinnis, J. *Journal of the American Chemical Society*. 1975, *97*, 1592-1594.
- (27) Casey, C. P. and Burkhardt, T. J. *Journal of the American Chemical Society*. 1973, *95*, 5833-5834.
- (28) Schrock, R. R. *Journal of the American Chemical Society*. 1974, *96*, 6796-6797.
- (29) Schrock, R. R. *Journal of the American Chemical Society*. 1975, *97*, 6577-6578.
- (30) Guggenberger, L. J. and Schrock, R. R. *Journal of the American Chemical Society*. 1975, *97*, 6578-6579.

- (31) Ivin, K. J. and Mol, J. C. *Olefin metathesis and metathesis polymerization*, Academic Press: San Diego ;; 1997.
- (32) Bilhou, J. L.; Basset, J. M.; Mutin, R.; and Graydon, W. F. *Journal of the American Chemical Society*. 1977, *99*, 4083-4090.
- (33) Leconte, M. and Basset, J. M. *Journal of the American Chemical Society*. 1979, *101*, 7296-7302.
- (34) Fischer, E. O. and Maasböl, A. *Angewandte Chemie International Edition in English*. 1964, *3*, 580-581.
- (35) McGinnis, J.; Katz, T. J.; and Hurwitz, S. *Journal of the American Chemical Society*. 1976, *98*, 605-606.
- (36) Katz, T. J.; McGinnis, J.; and Altus, C. *Journal of the American Chemical Society*. 1976, *98*, 606-608.
- (37) Kress, J. and Osborn, J. A. *Journal of the American Chemical Society*. 1983, *105*, 6346-6347.
- (38) Quignard, F.; Leconte, M.; and Basset, J. M. *Journal of the Chemical Society, Chemical Communications*. 1985, *1985*, 1816-1817.
- (39) Schaverien, C. J.; Dewan, J. C.; and Schrock, R. R. *Journal of the American Chemical Society*. 1986, *108*, 2771-2773.
- (40) Ehrenfeld, D.; Kress, J.; Moore, B. D.; Osborn, J. A.; and Schoettel, G. *Journal of the Chemical Society, Chemical Communications*. 1987, *1987*, 129-131.
- (41) Nguyen, S. T.; Johnson, L. K.; Grubbs, R. H.; and Ziller, J. W. *Journal of the American Chemical Society*. 1992, *114*, 3974-3975.
- (42) Demonceau, A.; Stumpf, A. W.; Saive, E.; and Noels, A. F. *Macromolecules*. 1997, *30*, 3127-3136.
- (43) Weskamp, T.; Schattenmann, W. C.; Spiegler, M.; and Herrmann, W. A. *Angewandte Chemie International Edition*. 1998, *37*, 2490-2493.
- (44) Furstner, A.; Liebl, M.; Lehmann, C. W.; Picquet, M.; Kunz, R.; Bruneau, C.; Touchard, D.; and Dixneuf, P. H. *Chemistry - A European Journal*. 2000, *6*, 1847-1857.
- (45) Grubbs, R. H. *Handbook of metathesis*, Wiley-VCH : Weinheim; 2003.
- (46) Heckelsberg, L. F.; Banks, R. L.; and Bailey, G. C. *Ind. Eng. Chem. Prod. Res. Dev.* 1968, *7*, 29-31.
- (47) Banks, R. L. and Heckelsberg, L. F. *Product R&D*. 1975, *14*, 33-36.
- (48) Wills, G. B.; Fathikalajahi, J.; Gangwal, S. K.; and Tang, S. *Rec. Trav. Chim. Pays-Bas*. 1977, *96*, M110-M114.
- (49) Kerkhof, F. P. J. M.; Thomas, R.; and Moulijn, J. A. *Recl. Trav. Chim. Pay. B*. 1977, *96*, M134-M135.
- (50) Moffat, A. J.; Johnson, M. M.; and Clark, A. *Journal of Catalysis*. 1970, *18*, 345 - 348.
- (51) Moffat, A. J.; Clark, A.; and Johnson, M. M. *Journal of Catalysis*. 1971, *22*, 379 - 388.
- (52) Luckner, R. C. and Wills, G. B. *Journal of Catalysis*. 1973, *28*, 83 - 91.
- (53) Gangwal, S. K.; Fathi-kalajahi, J.; and Wills, G. B. *Product R&D*. 1977, *16*, 237-241.
- (54) Andreini, A. and Mol, J. C. *Journal of Colloid and Interface Science*. 1981, *84*, 57 - 65.
- (55) Penrice, P. W. In *Kirk-Othmer Encyclopedia of Chemical Technology: Tungsten compounds*; John Wiley & Sons, Inc., 2010.
- (56) Choung, S. J. and Weller, S. W. *Industrial & Engineering Chemistry Process Design and Development*. 1983, *22*, 662-665.
- (57) Basrur, A. G.; Patwardhan, S. R.; and Was, S. N. *Journal of Catalysis*. 1991, *127*, 86 - 95.
- (58) Spamer, A.; Dube, T. I.; Moodley, D. J.; van Schalkwyk, C.; and Botha, J. M. *Applied Catalysis a-General*. 2003, *255*, 153-167.

- (59) Shelimov, B. N.; Elev, I. V.; and Kazansky, V. B. *Journal of Molecular Catalysis*. 1988, *46*, 187 - 200.
- (60) Grünert, W.; Feldhaus, R.; Anders, K.; Shpiro, E. S.; and Minachev, K. M. *Journal of Catalysis*. 1989, *120*, 444-456.
- (61) Rosier, C.; Nicolai, G. P.; and Basset, J. -M. *Journal of the American Chemical Society*. 1997, *119*, 12408-12409.
- (62) Saint-Arroman, R. P.; Basset, J. -M.; Lefebvre, F.; and Didillon, B. *Applied Catalysis A: General*. 2005, *290*, 181 - 190.
- (63) Wang, X.; Lian, W.; Fu, X.; Basset, J. -M.; and Lefebvre, F. *Journal of Catalysis*. 2006, *238*, 13 - 20.
- (64) Bini, F.; Rosier, C.; Saint-Arroman, R. P.; Neumann, E.; Dablemont, C.; de Mallmann, A.; Lefebvre, F.; Nicolai, G. P.; Basset, J. -M.; Crocker, M.; and Buijink, J. -K. *Organometallics*. 2006, *25*, 3743-3760.
- (65) Larabi, C.; Merle, N.; Norsic, S.; Taoufik, M.; Baudouin, A.; Lucas, C.; Thivolle-Cazat, J.; de Mallmann, A.; and Basset, J. -M. *Organometallics*. 2009, *28*, 5647-5655.
- (66) Lecuyer, C.; Quignard, F.; Choplin, A.; Olivier, D.; and Basset, J. M. *Angewandte Chemie International Edition in English*. 1991, *30*, 1660-1661.
- (67) Quignard, F.; Choplin, A.; and Basset, J. M. *Journal of the Chemical Society, Chemical Communications*. 1991, *1991*, 1589-1590.
- (68) Nicolai, G. P. and Basset, J. -M. *Applied Catalysis A: General*. 1996, *146*, 145 - 156.
- (69) Corker, J.; Lefebvre, F.; Evans, J.; Lécuyer, C.; Dufaud, V.; Quignard, F.; Choplin, A.; and Basset, J. M. *Science*. 1996, *271*, 966.
- (70) Wang, X. X.; Lefebvre, F.; Patarin, J.; and Basset, J. -M. *Microporous and Mesoporous Materials*. 2001, *42*, 269 - 276.
- (71) Millot, N.; Santini, C. C.; Baudouin, A.; and Basset, J. M. *Chemical Communications*. 2003, *2003*, 2034-2035.
- (72) Nicholas, C. P.; Ahn, H. S.; and Marks, T. J. *J. Am. Chem. Soc.* 2003, *125*, 4325-4331.
- (73) Adachi, M.; Nédez, C.; Wang, X. X.; Bayard, F.; Dufaud, V.; Lefebvre, F.; and Basset, J. -M. *Journal of Molecular Catalysis A: Chemical*. 2003, *204-205*, 443 - 455.
- (74) Wang, X. -X.; Veyre, L.; Lefebvre, F.; Patarin, J.; and Basset, J. -M. *Microporous and Mesoporous Materials*. 2003, *66*, 169 - 179.
- (75) Thieuleux, C.; Quadrelli, E. A.; Basset, J. M.; Döbler, J.; and Sauer, J. *Chem Commun (Camb)*. 2004, 1729-31.
- (76) Thieuleux, C.; Copéret, C.; Dufaud, V.; Marangelli, C.; Kuntz, E.; and Basset, J. M. *Journal of Molecular Catalysis A: Chemical*. 2004, *213*, 47 - 57.
- (77) Rataboul, F.; Baudouin, A.; Thieuleux, C.; Veyre, L.; Copéret, C.; Thivolle-Cazat, J.; Basset, J. -M.; Lesage, A.; and Emsley, L. *Journal of the American Chemical Society*. 2004, *126*, 12541-12550.
- (78) Millot, N.; Soignier, S.; Santini, C. C.; Baudouin, A.; and Basset, J. M. *J Am Chem Soc*. 2006, *128*, 9361-70.
- (79) Joubert, J.; Delbecq, F.; Sautet, P.; Roux, E. L.; Taoufik, M.; Thieuleux, C.; Blanc, F.; Coperet, C.; Thivolle-Cazat, J.; and Basset, J. M. *J. Am. Chem. Soc.* 2006, *128*, 9157-9169.
- (80) Thieuleux, C.; Maraval, A.; Veyre, L.; Copéret, C.; Soulivong, D.; Basset, J. M.; and Sunley, G. J. *Angew Chem Int Ed Engl*. 2007, *46*, 2288-90.
- (81) Rataboul, F.; Copéret, C.; Lefort, L.; de Mallmann, A.; Thivolle-Cazat, J.; and Basset, J. M. *Dalton Trans*. 2007, 923-7.

- (82) Guillemot, G.; Thieuleux, C.; Copéret, C.; Soulivong, D.; Spitzmesser, S.; and Basset, J. M. *Dalton Trans.* 2007, 4589-93.
- (83) Riollet, V.; Taoufik, M.; Basset, J. -M.; and Lefebvre, F. *Journal of Organometallic Chemistry.* 2007, 692, 4193 - 4195.
- (84) Joubert, J.; Delbecq, F.; Thieuleux, C.; Taoufik, M.; Blanc, F.; Copéret, C.; Thivolle-Cazat, J.; Basset, J. -M.; and Sautet, P. *Organometallics.* 2007, 26, 3329-3335.
- (85) Salinier, V.; Corker, J. M.; Lefebvre, F.; Bayard, F.; Dufaud, V.; and Basset, J. M. *Advanced synthesis & catalysis.* 2009, 351, 2155-2167.
- (86) Salinier, V.; Niccolai, G.; Dufaud, V.; and Basset, J. -M. *Advanced Synthesis & Catalysis.* 2009, 351, 2168-2177.
- (87) Dornelas, L.; Reyes, S.; Quignard, F.; Choplin, A.; and Basset, J. M. *Chemistry letters.* 1993, 1931-1934.
- (88) Tosin, G.; Santini, C. C.; Taoufik, M.; and Basset, J. M. *Actualité Chimique.* 2005, 34-36.
- (89) Tosin, G.; Santini, C. C.; Taoufik, M.; Mallmann, A. D.; and Basset, J. -M. *Organometallics.* 2006, 25, 3324-3335.
- (90) Tosin, G.; Santini, C. C.; Baudouin, A.; De Mallmann, A.; Fiddy, S.; Dablemont, C.; and Basset, J. -M. *Organometallics.* 2007, 26, 4118-4127.
- (91) Tosin, G.; Santini, C. C.; and Basset, J. M. *Topics in catalysis.* 2009, 52, 1203-1210.
- (92) Tosin, G.; Delgado, M.; Baudouin, A.; Santini, C. C.; Bayard, F.; and Basset, J. -M. *Organometallics.* 2010, 29, 1312-1322.
- (93) Delgado, M. *PhD Thesis.* 2010.
- (94) Vidal, V.; Théolier, A.; Thivolle-Cazat, J.; and Basset, J. M. *Journal of the Chemical Society, Chemical Communications.* 1995, 1995, 991-992.
- (95) Vidal, V.; Theolier, A.; Thivolle-Cazat, J.; Basset, J. -M.; and Corker, J. *Journal of the American Chemical Society.* 1996, 118, 4595-4602.
- (96) Vidal, V.; Theolier, A.; Thivolle-Cazat, J.; and Basset, J. M. *Science.* 1997, 276, 99-102.
- (97) Meunier, D.; Piechaczyk, A.; de Mallmann, A.; and Basset, J. M. *Angewandte Chemie International Edition.* 1999, 38, 3540-3542.
- (98) Maury, O.; Lefort, L.; Vidal, V.; Thivolle-Cazat, J.; and Basset, J. M. *Angewandte Chemie International Edition.* 1999, 38, 1952-1955.
- (99) Chabanas, M.; Vidal, V.; Copéret, C.; Thivolle-Cazat, J.; and Basset, J. -M. *Angewandte Chemie International Edition.* 2000, 39, 1962-1965.
- (100) Lefort, L.; Chabanas, M.; Maury, O.; Meunier, D.; Copéret, C.; Thivolle-Cazat, J.; and Basset, J. -M. *Journal of Organometallic Chemistry.* 2000, 593-594, 96 - 100.
- (101) Coperet, C.; Maury, O.; Thivolle-Cazat, J.; and Basset, J. M. *Angewandte Chemie.* 2001, 113, 2393-2395.
- (102) Taoufik, M.; de Mallmann, A.; Prouzet, E.; Saggio, G.; Thivolle-Cazat, J.; and Basset, J. -M. *Organometallics.* 2001, 20, 5518-5521.
- (103) Ahn, H. and Marks, T. J. *Journal of the American Chemical Society.* 2002, 124, 7103-7110.
- (104) Saggio, G.; de Mallmann, A.; Maunders, B.; Taoufik, M.; Thivolle-Cazat, J.; and Basset, J. -M. *Organometallics.* 2002, 21, 5167-5171.
- (105) Rataboul, F.; Chabanas, M.; de Mallmann, A.; Copéret, C.; Thivolle-Cazat, J.; and Basset, J. -M. *Chemistry - A European Journal.* 2003, 9, 1426-1434.

- (106) Taoufik, M.; Schwab, E.; Schultz, M.; Vanoppen, D.; Walter, M.; Thivolle-Cazat, J.; and Basset, J. M. *Chemical Communications*. 2004, 1434-5.
- (107) Basset, J. M.; Coperet, C.; Lefort, L.; Maunders, B. M.; Maury, O.; Le Roux, E.; Saggio, G.; Soignier, S.; Soulivong, D.; Sunley, G. J.; Taoufik, M.; and Thivolle-Cazat, J. *Journal of the American Chemical Society*. 2005, 127, 8604-8605.
- (108) Thivolle-Cazat, J.; Coperet, C.; Soignier, S.; Taoufik, M.; and Basset, J. M. In *NATO Science Series II: Mathematics, Physics and Chemistry vol. 191*; 2005; p. 107-123.
- (109) Soignier, S.; Taoufik, M.; Le Roux, E.; Saggio, G.; Dablemont, C.; Baudouin, A.; Lefebvre, F.; de Mallmann, A.; Thivolle-Cazat, J.; Basset, J. -M.; Sunley, G.; and Maunders, B. M. *Organometallics*. 2006, 25, 1569-1577.
- (110) Taoufik, M.; Roux, E.; Thivolle-Cazat, J.; Copéret, C.; Basset, J. -M.; Maunders, B.; and Sunley, G. *Topics in Catalysis*. 2006, 40, 65-70.
- (111) Avenier, P.; Lesage, A.; Taoufik, M.; Baudouin, A.; De Mallmann, A.; Fiddy, S.; Vautier, M.; Veyre, L.; Basset, J. -M.; Emsley, L.; and Quadrelli, E. A. *Journal of the American Chemical Society*. 2007, 129, 176-186.
- (112) Avenier, P.; Taoufik, M.; Lesage, A.; Solans-Monfort, X.; Baudouin, A.; de Mallmann, A.; Veyre, L.; Basset, J. M.; Eisenstein, O.; Emsley, L.; and Quadrelli, E. A. *Science*. 2007, 317, 1056-1060.
- (113) Saint-Arroman, R. P.; Didillon, B.; de Mallmann, A.; Basset, J. M.; and Lefebvre, F. *Applied Catalysis A: General*. 2008, 337, 78 - 85.
- (114) Soulivong, D.; Norsic, S.; Taoufik, M.; Coperet, C.; Thivolle-Cazat, J.; Chakka, S.; and Basset, J. -M. *Journal of the American Chemical Society*. 2008, 130, 5044-5045.
- (115) Avenier, P.; Solans-Monfort, X.; Veyre, L.; Renili, F.; Basset, J. -M.; Eisenstein, O.; Taoufik, M.; and Quadrelli, E. A. *Topics in catalysis*. 2009, 52, 1482-1491.
- (116) Sautet, P. and Delbecq, F. *Chemical Reviews*. 2009, 110, 1788-1806.
- (117) Lataste, E.; Demourgues, A.; Leclerc, H.; Goupil, J. M.; Vimont, A.; Durand, E.; Labrugère, C.; Benalla, H.; and Tressaud, A. *The Journal of Physical Chemistry C*. 2008, 112, 10943-10951.
- (118) Millot, N.; Santini, C. C.; Lefebvre, F.; and Basset, J. M. *Comptes Rendus Chimie*. 2004, 7, 725-736.
- (119) Peri, J. B. *Journal of Catalysis*. 1976, 41, 227 - 239.
- (120) Bronnimann, C. E.; Chuang, I. S.; Hawkins, B. L.; and Maciel, G. E. *Journal of the American Chemical Society*. 1987, 109, 1562-1564.
- (121) Beaufils, J. P. and Barbaux, Y. *Journal de Chimie Physique et de Physico-Chimie Biologique*. 1981, 78, 347-352.
- (122) Nortier, P.; Fourre, P.; Saad, A. B.; Saur, O.; and Lavalley, J. C. *Applied Catalysis*. 1990, 61, 141-160.
- (123) Knözinger, H. and Ratnasamy, P. *Catalysis Reviews-Science and Engineering*. 1978, 17, 31-70.
- (124) Digne, M.; Sautet, P.; Raybaud, P.; Euzen, P.; and Toulhoat, H. *Journal of Catalysis*. 2002, 211, 1-5.
- (125) Jezequel, M.; Dufaud, V.; Ruiz-Garcia, M. J.; Carrillo-Hermosilla, F.; Neugebauer, U.; Niccolai, G. P.; Lefebvre, F.; Bayard, F.; Corker, J.; Fiddy, S.; Evans, J.; Broyer, J. -P.; Malinge, J.; and Basset, J. -M. *Journal of the American Chemical Society*. 2001, 123, 3520-3540.
- (126) Clark, D. N. and Schrock, R. R. *Journal of the American Chemical Society*. 1978, 100, 6774-6776.
- (127) Schrock, R. R. *Accounts of Chemical Research*. 1986, 19, 342-348.
- (128) Schrock, R. R. In *Carbene chemistry*; Bertrand, G., Ed.; Marcel Dekker: New York, N.Y. , 2002; p. 205-230.

- (129) Chisholm, M. H.; Folting, K.; Hoffman, D. M.; and Huffman, J. C. *Journal of the American Chemical Society*. 1984, *106*, 6794-6805.
- (130) Chisholm, M. H.; Conroy, B. K.; Eichhorn, B. W.; Folting, K.; Hoffman, D. M.; Huffman, J. C.; and Marchant, N. S. *Polyhedron*. 1987, *6*, 783 - 792.
- (131) Schrock, R. R.; Clark, D. N.; Sancho, J.; Wengrovius, J. H.; Rocklage, S. M.; and Pedersen, S. F. *Organometallics*. 1982, *1*, 1645-1651.
- (132) Weiss, K. and Lössel, G. *Angewandte Chemie International Edition in English*. 1989, *28*, 62-64.
- (133) Le Roux, E.; Taoufik, M.; Chabanas, M.; Alcor, D.; Baudouin, A.; Coperet, C.; Thivolle-Cazat, J.; Basset, J. M.; Lesage, A.; Hediger, S.; and Emsley, L. *Organometallics*. 2005, *24*, 4274-4279.
- (134) Le Roux, E.; Taoufik, M.; Baudouin, A.; Copèret, C.; Thivolle-Cazat, J.; Basset, J. -M.; Maunders, B. M.; and Sunley, G. J. *Advanced Synthesis & Catalysis*. 2007, *349*, 231-237.
- (135) Le Roux, E.; Taoufik, M.; Copèret, C.; de Mallmann, A.; Thivolle-Cazat, J.; Basset, J. -M.; Maunders, B. M.; and Sunley, G. J. *Angewandte Chemie*. 2005, *117*, 6913-6916.
- (136) Le Roux, E.; Taoufik, M.; Copèret, C.; de Mallmann, A.; Thivolle-Cazat, J.; Basset, J. -M.; Maunders, B. M.; and Sunley, G. J. *Angewandte Chemie International Edition*. 2005, *44*, 6755-6758.
- (137) Tonzetich, Z. J.; Lam, Y. C.; Muller, P.; and Schrock, R. R. *Organometallics*. 2007, *26*, 475-477.
- (138) Merle, N.; Taoufik, M.; Nayer, M.; Baudouin, A.; Roux, E. L.; Gauvin, R. M.; Lefebvre, F.; Thivolle-Cazat, J.; and Basset, J. -M. *Journal of Organometallic Chemistry*. 2008, *693*, 1733-1737.
- (139) Chisholm, M. H. and Cotton, F. A. *Accounts of Chemical Research*. 1978, *11*, 356-362.
- (140) Gauvin, R. M.; Coutelier, O.; Berrier, E.; Mortreux, A.; Delevoye, L.; Paul, J. F.; Mamède, A. S.; and Payen, E. *Dalton Trans.* 2007, 3127-30.
- (141) Schrock, R. R. *Chem Rev.* 2009, *109*, 3211-26.
- (142) Rhers, B.; Salameh, A.; Baudouin, A.; Quadrelli, E. A.; Taoufik, M.; Coperet, C.; Lefebvre, F.; Basset, J. -M.; Solans-Monfort, X.; Eisenstein, O.; Lukens, W. W.; Lopez, L. P. H.; Sinha, A.; and Schrock, R. R. *Organometallics*. 2006, *25*, 3554-3557.
- (143) Blanc, F.; Berthoud, R.; Copèret, C.; Lesage, A.; Emsley, L.; Singh, R.; Kreickmann, T.; and Schrock, R. R. *Proceedings of the National Academy of Sciences*. 2008, *105*, 12123-12127.
- (144) Michos, D.; Luo, X. L.; Faller, J. W.; and Crabtree, R. H. *Inorganic Chemistry*. 1993, *32*, 1370-1375.
- (145) Zakharov, V. A.; Dudchenko, V. K.; Paukshtis, E. A.; Karakchiev, L. G.; and Yermakov, Y. I. *Journal of Molecular Catalysis*. 1977, *2*, 421 - 435.
- (146) Zakharov, V. A. and Ryndin, Y. A. *Journal of Molecular Catalysis*. 1989, *56*, 183 - 193.
- (147) Luo, Y. -R. *Comprehensive handbook of chemical bond energies*, CRC Press: Boca Raton; 2007.
- (148) Morse, M. D. *Chemical Reviews*. 1986, *86*, 1049-1109.
- (149) Simoes, J. A. M. and Beauchamp, J. L. *Chemical Reviews*. 1990, *90*, 629-688.
- (150) Le Roux, E. *PhD Thesis*. 2004.
- (151) Chauvin, Y. *Angewandte Chemie-International Edition*. 2006, *45*, 3740-3747.
- (152) Grubbs, R. H. *Angewandte Chemie International Edition*. 2006, *45*, 3760-5.
- (153) Schrock, R. R. *Angewandte Chemie-International Edition*. 2006, *45*, 3748-3759.
- (154) Furstner, A. *Angewandte Chemie International Edition*. 2000, *39*, 3012-3043.
- (155) Zhang, W. and Moore, J. S. *Advanced Synthesis & Catalysis*. 2007, *349*, 93-120.
- (156) Coutelier, O. and Mortreux, A. *Advanced Synthesis & Catalysis*. 2006, *348*, 2038-2042.
- (157) Weissman, H.; Plunkett, K. N.; and Moore, J. S. *Angew Chem Int Ed Engl*. 2006, *45*, 585-8.

- (158) Couturier, J. L.; Paillet, C.; Leconte, M.; Basset, J. M.; and Weiss, K. *Angewandte Chemie International Edition in English*. 1992, *31*, 628-631.
- (159) Morton, L. A.; Zhang, X. -H.; Wang, R.; Lin, Z.; Wu, Y. -D.; and Xue, Z. -L. *Journal of the American Chemical Society*. 2004, *126*, 10208-10209.
- (160) Solans-Monfort, X.; Coperet, C.; and Eisenstein, O. *Journal of the American Chemical Society*. 2010, *132*, 7750-7757.
- (161) Crabtree, R. H. *Chemical Reviews*. 1995, *95*, 987-1007.
- (162) Lunsford, J. H. *Catalysis Today*. 2000, *63*, 165 - 174.
- (163) Blanksby, S. J. and Ellison, G. B. *Accounts of Chemical Research*. 2003, *36*, 255-263.
- (164) Kurosaka, T.; Matsushashi, H.; and Arata, K. *Journal of Catalysis*. 1998, *179*, 28 - 35.
- (165) Pareja, P.; Mercy, M.; Gachon, J. -C.; Amariglio, A.; and Amariglio, H. *Industrial & Engineering Chemistry Research*. 1999, *38*, 1163-1165.
- (166) Szeto, K. C.; Norsic, S.; Hardou, L.; Le Roux, E.; Chakka, S.; Thivolle-Cazat, J.; Baudouin, A.; Papaioannou, C.; Basset, J. M.; and Taoufik, M. *Chem Commun (Camb)*. 2010, *46*, 3985-7.
- (167) Schrock, R. R.; Shih, K. -Y.; Dobbs, D. A.; and Davis, W. M. *Journal of the American Chemical Society*. 1995, *117*, 6609-6610.
- (168) Schrock, R. R.; Seidel, S. W.; Mosch-Zanetti, N. C.; Dobbs, D. A.; Shih, K. -Y.; and Davis, W. M. *Organometallics*. 1997, *16*, 5195-5208.
- (169) Parkin, G.; Bunel, E.; Burger, B. J.; Trimmer, M. S.; Asselt, A. V.; and Bercaw, J. E. *Journal of Molecular Catalysis*. 1987, *41*, 21 - 39.
- (170) Koerts, T. and van Santen, R. A. *J Chem Soc , Chem Commun*. 1991, 1281-1283.
- (171) Belgued, M.; Pareja, P.; Amariglio, A.; and Amariglio, H. *Nature*. 1991, *35*, 789-790.
- (172) Koerts, T. and Santen, R. A. V. *Studies in Surface Science and Catalysis*. 1993, *75*, 1065 - 1078.
- (173) Hill, C. L. . *Activation and functionalization of alkanes*, Wiley: New York; 1989.
- (174) Crabtree, R. H. *Journal of Organometallic Chemistry*. 2004, *689*, 4083 - 4091.
- (175) Burnett, R. L. and Hughes, T. R. *Journal of Catalysis*. 1973, *31*, 55 - 64.
- (176) Coperet, C.; Basset, J. M.; Thivolle Cazat, J.; Daravong, S.; and Taoufik, M. *WO 2004089541*. 2004.
- (177) Wallace, K. C.; Liu, A. H.; Dewan, J. C.; and Schrock, R. R. *Journal of the American Chemical Society*. 1988, *110*, 4964-4977.
- (178) Schrock, R. R. *Chemical Reviews*. 2002, *102*, 145-180.
- (179) Merle, N.; Stoffelbach, F.; Taoufik, M.; Le Roux, E.; Thivolle-Cazat, J.; and Basset, J. M. *Chem Commun (Camb)*. 2009, 2523-5.
- (180) Taoufik, M.; LeRoux, E.; Thivolle-Cazat, J.; and Basset, J. -M. *Angewandte Chemie International Edition*. 2007, *46*, 7202-7205.

Chapter 2

Characterizations of the tungsten hydride supported catalyst

1. Introduction	61
2. Results and discussions	63
2.1. Characterizations of the catalyst support.....	63
• Preparation	64
• Influence of the pretreatment temperature on the of Al ₂ O ₃ (RP) properties.....	64
2.2. Characterizations of the [W(=C^tBu)(CH₂^tBu)₃] supported on Al₂O₃₋₍₅₀₀₎ (RP)	68
2.2.1. IR spectroscopy	69
2.2.2. Mass balance analysis.....	70
2.2.3. Solid-state NMR spectroscopy	71
2.2.4. 100% ¹³ C labeled NMR	71
2.3. Characterizations of the tungsten hydride on Al₂O₃₋₍₅₀₀₎ (RP)	75
2.3.1. Preparation.....	75
2.3.2. IR Spectroscopy.....	75
2.3.3. D ₂ exchange.....	76
2.3.4. Theoretical calculations.....	77
2.3.5. RAMAN spectroscopy	78
2.3.6. ¹ H NMR and ¹ H NMR spetroscopy after D2 exchange.....	79
2.3.7. Multiple Quanta NMR Spectroscopy	80
2.3.8. Steoichiometric reactivity with methane.....	82
2.3.9. Transmission Electron Microscopy (TEM).....	83
2.3.10. Extended X-Ray Adsorption Fine Structure Spectroscopy (EXAFS).....	83
2.4. Conclusion.....	84
3. Experimental section	85
3.1. General procedures.....	85
3.2. Pyridine adsorption on alumina monitored by IR spectroscopy	87
3.3. Synthesis of 99% ¹³C-labeled ^tBu*CH₂Cl.....	87
3.4. Monitoring the synthesis of 1/Al₂O₃₋₍₅₀₀₎ by IR spectroscopy	88
3.5. Preparation of 1/Al₂O₃₋₍₅₀₀₎ (RP)	88
3.6. Extended X-ray Absorption Fine Structure Spectroscopy (EXAFS).....	89
3.7. Monitoring the treatment of 1/Al₂O₃₋₍₅₀₀₎ (RP) under H₂ by IR spectroscopy	89
3.8. Treatment of 1/Al₂O₃₋₍₅₀₀₎ (RP) under H₂	90
3.9. Reaction of WH/Al₂O₃₋₍₅₀₀₎ (RP) with D₂	90
3.10. Hydrolysis of WH/Al₂O₃₋₍₅₀₀₎ (RP).....	90
3.11. Activation of methane on WH/Al₂O₃₋₍₅₀₀₎ (RP) in continuous flow reactor.....	90
4. Reference and Notes	90

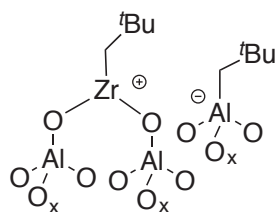
1. Introduction

In surface organometallic chemistry, a fundamental understanding of the chemisorptive interaction and reaction of organometallic complex with the oxide surface is crucial to produce well-defined metallic species. The cationic or neutral character of the surface species is a key aspect of its catalytic properties, not easily accessible by classical characterizations techniques. The choice of the oxide support plays a critical role. After years of research, it has been shown that silica could be used as a tunable solid ligand, and the chemistry is now understood at a molecular level.¹ Typically one can generate either monosiloxy, bisiloxy, and even in some cases trisiloxy surface complexes. These systems have been characterized by several methods (elemental analysis, IR spectroscopy, Solid-state NMR spectroscopy, and EXAFS), and they have been used as catalyst precursors in several reactions (hydrogenation, polymerization, depolymerization, olefin metathesis, oxidation, and alkane metathesis). Typically, the siloxy substituent of the surface activates the metal center by generating more electrophilic metal centers, but in some instances, it is necessary to use other supports such as alumina to obtain a gain in reactivity. Several hydrogenation, metathesis, and polymerization supported catalysts have been prepared, for which the alumina support is critical to obtain catalytic activity. For example, chemisorption of $[\text{Zr}(\text{CH}_2^t\text{Bu})_4]$ on alumina provides an efficient olefin polymerization catalyst, while when supported on silica it is inactive.²⁻⁴ Alumina has a richer chemistry than silica since it combines a variety of hydroxyl groups, with several modes of coordination, with a Lewis acid character on the aluminum. Various types of aluminum atoms are potentially present on the surface, from tri- to pentacoordinated, originating from the tetrahedral or octahedral cations of bulk γ -alumina.⁵ The role of the aluminum Lewis centers for the chemisorptive interaction of the metal-organic complex and more generally the specificity of alumina for this process is still unclear. In some cases the formation of partially or fully cationic species has been proposed based on NMR spectroscopy and theoretical calculations.^{2-4, 6-9}

Recently Delgado *et al.* have described the reactivity of hafnium complex, $[\text{Hf}(\text{CH}_2^t\text{Bu})_4]$, with $\gamma\text{-Al}_2\text{O}_{3-(500)}$.¹⁰ This reaction provides several surface species: a neutral monoaluminoxy, $[(\text{Al}_s\text{O})\text{Hf}(\text{CH}_2^t\text{Bu})_3]$, a neutral bisaluminoxy $[(\text{Al}_s\text{O})_2\text{Hf}(\text{CH}_2^t\text{Bu})_2]$ and a cationic bisaluminoxy $[(\text{Al}_s\text{O})(\text{Al}_s\text{O})(\text{Al}-\text{O}-\text{Al})\text{Hf}(\text{CH}_2^t\text{Bu})]^+ [\text{BuCH}_2\text{Al}_s]^-$ species. The cationic species is formed by transfer of a neopentyl fragment on Lewis acidic site of alumina giving $^t\text{BuCH}_2\text{Al}_s$. The treatment of these species under H_2 at 150°C provides a mixture of a neutral, $[(\text{Al}_s\text{O})_3\text{HfH}]$, and a cationic mono hafnium hydride, $[(\text{Al}_s\text{O})(\text{Al}_s\text{O})\text{Hf}(\text{H})]^+[(\text{CH}_2^t\text{Bu})\text{Al}_s]^-$. In this study, theoretical calculations were very helpful to interpret the spectroscopic characterizations of all these species. These catalysts

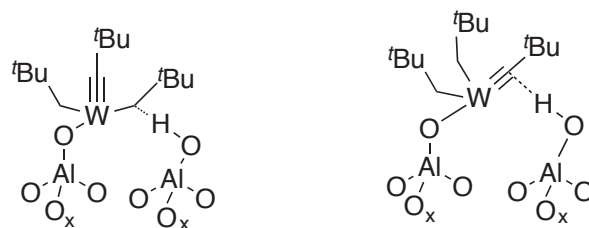
have shown high activity, without co-catalyst, for olefin polymerization, due to the cationic species present at the surface. Marks *et al.* have reported the reactivity of $[\text{Cp}^*\text{TaMe}_4]$ with the surface of dehydroxylated $\gamma\text{-Al}_2\text{O}_3$.⁹ In that case also, the transfer of a methyl group on Lewis acidic site to form cationic species $[\text{Cp}^*\text{TaMe}_3]^+[\text{MeAl}_5]^-$, via pathways analog to those established for group IV organometallic and actinides complex, has been evidenced.

Group IV and group V organometallic complexes react with dehydroxylated Al_2O_3 to form cationic species. One can wonder if group VI complex, *i.e.* $[\text{W}(\equiv\text{C}^t\text{Bu})(\text{CH}_2^t\text{Bu})_3]$, **1**, react toward $\gamma\text{-Al}_2\text{O}_3\text{-(500)}$ to give cationic species? Joubert *et al.* have evidenced using DFT approach, that this reaction give selectively a monografted neutral surface complex $[(\text{Al}_5\text{O})\text{W}(\equiv\text{C}^t\text{Bu})(\text{CH}_2^t\text{Bu})_2]$. The calculation show that the reaction between **1** and surface hydroxyl, is less exothermic and has a considerably higher activation barrier than the one of $[\text{Zr}(\text{CH}_2^t\text{Bu})_4]$, which chemisorption on $\text{Al}_2\text{O}_3\text{-(500)}$ afford mainly cationic species (Scheme 2.1). The authors claim that the transfer of an alkyl group onto adjacent aluminum centre is disfavored, and hence cationic species are not formed. They interpret the complexity of the experimental NMR and IR data^{11,12} by interaction between some ligands of this monoaluminoxy surface complex and remaining surface hydroxyls.¹³



Scheme 2.1 Proposed cationic surface species obtained by chemisorption of $[\text{Zr}(\text{CH}_2^t\text{Bu})_4]$ on $\text{Al}_2\text{O}_3\text{-(500)}$ ¹⁴

Nevertheless, some uncertainties subsist on the interpretation of the NMR spectra of this tungsten surface species. Therefore the proposed interactions between surface hydroxyl and tungsten carbene and alkyl (Scheme 2.2) are not possible as they will certainly evolve to the formation of bis aluminoxy species by addition or σ -bond metathesis of the hydroxyl group to the very reactive carbene or tungsten neopentyl fragment respectively. The interaction between surface hydroxyl and alkyl fragment observed on the IR spectrum, is only due well-known Wan-der-Valls interactions between surface hydroxyl and less reactive methyl of the neopentyl fragments far from the electron deficient tungsten centre ($12 e^-$ complex).¹⁵ The examples of organometallic complexes grafted on dehydroxylated oxides, shows that these weak interactions do not affect the NMR spectrum.¹



Scheme 2.2 Interaction between surface hydroxyl and $[(\text{Al}_5\text{O})\text{W}(\equiv\text{C}^t\text{Bu})(\text{CH}_2^t\text{Bu})_2]$ surface complex proposed by Joubert *et al.*¹³

In this thesis the catalytic activity of supported tungsten hydrides obtained by treatment under H_2 of the perydrocarbyl tungsten **1** supported on alumina will be studied for the production of propylene from ethylene and/or butenes. It is indispensable to perform further investigations of the catalyst structure, in order to spot the formation of eventual cationic species that may have singular reactivity toward olefins. Indeed, a good description of the catalyst is needed to understand correctly the catalytic activity, mechanism, and deactivation process.

This chapter presents characterizations of this tungsten system. First, the support used for grafting, *i.e.* Al_2O_3 , has been studied and particularly the influence of the pretreatment temperature on its properties. Then, the structure of $[\text{W}(\equiv\text{C}^t\text{Bu})(\text{CH}_2^t\text{Bu})_3]$, **1**, grafted on alumina dehydroxylated at 500°C has been examined. The preparation and characterizations of the hydride obtained from this surface species is finally presented.

2. Results and discussions

2.1. Characterizations of the catalyst support

Different oxides have been studied before being used as a support for the tungsten catalyst. Hence, different aluminas have been expected as potential support for the catalyst. The nature of their crystalline phase, their pretreatment temperatures and the use of metal doping elements have been studied for the preparation catalyst. Moreover silica-alumina and alumina-magnesium oxide have also been studied for their specific acido-basic character (see Chapter 1). Previous work realized on the immobilization of **1**, on Al_2O_3 have been performed using *AEROXIDE*[®] *Alu C* purchased from Evonik. Nevertheless, after analysis by XRD, this alumina was identified as a mixture of γ - and δ - phase. As γ - Al_2O_3 was intensively studied by experimental and theoretical approach (see Chapter 1), and to avoid eventual problems of characterization, it was decided to use an alumina with supposed single γ -phase. In this paragraph, only the characterizations of Alumina E7102 from Rhone-Poulenc, referred to as Al_2O_3 (RP), support are presented. The characterizations of

the others supports as well as the obtaining of tungsten hydride on these support are presented in Appendix A.

- Preparation

The Al₂O₃ (RP) is formed of extrudates, they were crushed in a mortar and sieved (40-60 mesh) to limit eventual mass transfers limitation during catalytic tests. The resulting powder was calcinated at 500°C under dry air for 15h. It was then hydrated with a vapor pressure of degassed water at 100°C for 1h prior to treatment under high vacuum (10⁻⁵ Torr) at the desired temperature, *i.e.* dehydroxylation, for 15h. The resulting material will be referred to as Al₂O₃-(dehydroxylation temperature) (RP).

These materials were characterized using IR spectroscopy, ¹H and ²⁷Al solid-state NMR, XRD, elemental analysis and the specific surface was determined using BET adsorption.

- Influence of the pretreatment temperature on the of Al₂O₃ (RP) properties

The influence of the temperature on Al₂O₃ (RP) has been fully studied and is presented in this paragraph. First, Solid state N.M.R. was performed on Al₂O₃ (RP) dehydroxylated at 300°C, 500°C and 800°C (Figure 2.1).

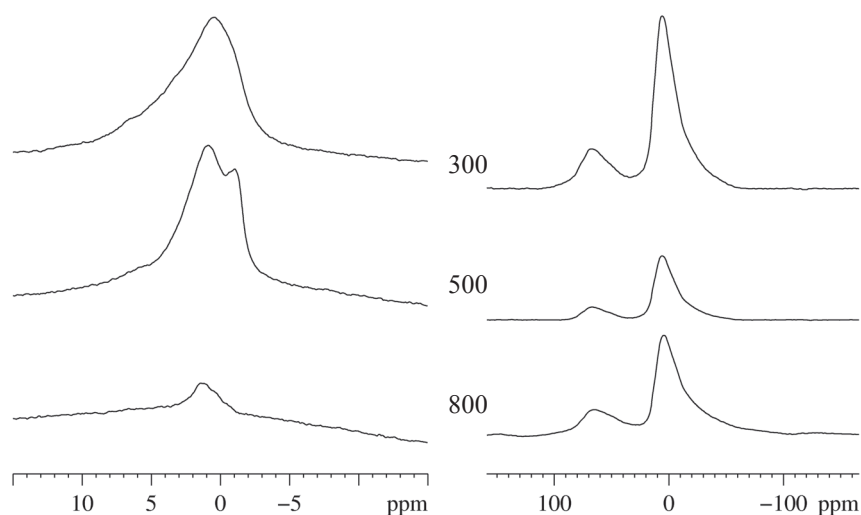


Figure 2.1 ¹H (left) and ²⁷Al (right) N.M.R. spectra of Al₂O₃ (RP) dehydroxylated at 300°C (top), 500°C (middle) and 800°C (bottom)

¹H N.M.R. spectra of Al₂O₃ (RP) dehydroxylated at 300°C, 500°C and 800°C (Figure 2.1, left) show the presence of three types of proton at the surface of the alumina, which is in agreement with literature data.¹⁶ At low field, around 4.3 ppm, the signal cor-

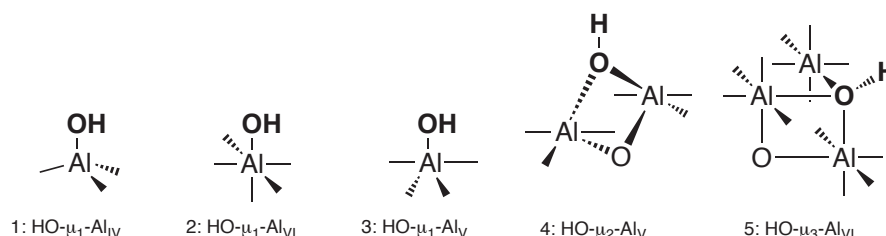
responds to proton of bonded OH. This bridged OH is present only on $\text{Al}_2\text{O}_3\text{-(300)}$ and no longer persists for higher dehydroxylation temperature. Around 2.0 ppm, the signal is attributed to proton of terminal OH groups bonded at two (μ_2) or three (μ_3) Al. At higher field, around 0.1 ppm the signal corresponds to proton of terminal OH groups bonded to one (μ_1) Al. As expected, both signals decrease in intensity with dehydroxylation temperature. Quantitative ^1H NMR study, using the method described by Millot et al.,¹⁷ provides the OH density at the surface of Alumina for each dehydroxylation temperature (Table 2.1). As expected, the higher the dehydroxylation temperature, the lower the OH density is observed. At 800°C the OH density is extremely low with only 21 $\mu\text{mol.g}^{-1}$.

Table 2.1 Surface OH density for Al_2O_3 (RP) dehydroxylated at 300°C, 400°C, 500°C and 800°C determined by ^1H NMR.

Al_2O_3 dehydroxylation temperature (°C)	300	400	500	800
OH density ($\mu\text{mol.g}^{-1}$) $\pm 10\%$	1300	1200	660	21

The ^{27}Al N.M.R. spectra of Al_2O_3 (RP) dehydroxylated at 300°C, 500°C and 800°C (Figure 2.1, right) are very similar. Two peaks are observed, assigned to Al from the bulk. The first one, at 62 ppm, is attributed to tetrahedral Al and the second one, at 4 ppm, corresponds to octahedral Al as described for $\gamma\text{-Al}_2\text{O}_3$.¹⁸ These data do not bring information about the surface Al. Nevertheless, they show that the dehydroxylation process does not impact bulk structure of the alumina.

The dehydroxylation temperature has a strong influence on the number of surface OH groups. This influence has been evocated on silica in Chapter 1. It was also discussed that the easiest way to characterize the nature of these different OH groups (Scheme 2.3) is the IR spectroscopy. Indeed, Knözinger and Sautet have made deep studies on the assignment of surface OH of alumina in IR.^{5,19}



Scheme 2.3 Different hydroxyl groups at the surface of alumina

IR spectra (Figure 2.2) in the $\nu_{(\text{OH})}$ region of $\text{Al}_2\text{O}_3\text{-(300)}$ -(500) and -(800) (RP) show the presence of three types of OH groups. Two absorption bands at highest frequencies, in the

region $3800\text{-}3775\text{ cm}^{-1}$, correspond to terminal groups (μ_1) attached to Al_{IV} and Al_{VI} . Bands in the region $3730\text{-}3745\text{ cm}^{-1}$ are attributed to a (μ_2) OH coordinated to Al_{V} and Al_{IV} . Bands in the region $3710\text{-}3690\text{ cm}^{-1}$ correspond to a (μ_3) OH attached to three Al sites. In conclusion, the OH stretching frequency depend on the number of Al neighbors in the first coordination sphere of the oxygen atom and on the coordination number of Al itself. These experimental data are in good agreement with Digne theoretical calculations for $\gamma\text{-Al}_2\text{O}_3$.⁵ The three types of OH groups are present on each Al_2O_3 (RP). The intensity of all these bands decreases with dehydroxylation temperature. On the Al_2O_3 (300) (RP) other stretching bands remain at lower frequencies ($<3600\text{ cm}^{-1}$) corresponding to H bonded OH groups. These bridged OH disappeared at higher dehydroxylation temperatures.

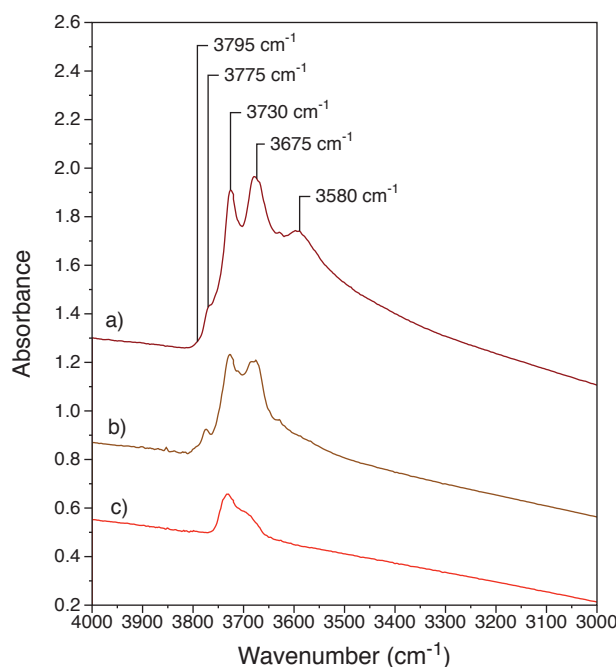


Figure 2.2 IR spectra (transmission) of the same 30 mg pellet of Al_2O_3 (D) dehydroxylated at a) 300°C ; b) 500°C and c) 800°C

The influence of dehydroxylation temperature on the Lewis acidic character was then studied using pyridine as a molecular probe. Indeed, pyridine is known to adsorb on oxides *via* Brønsted or Lewis acid sites (Scheme 2.4).²⁰⁻²³ The hydrogen bonded pyridine is desorbed over 100°C .

Table 2.2 B.E.T. measurement for Al₂O₃ (RP) dehydroxylated at 300°C, 400°C, 500°C and 800°C

Al ₂ O ₃ dehydroxylation temperature (°C)	300	400	500	800
Specific surface (m ² .g ⁻¹) ±10%	203	205	200	195

Finally, in order to be sure that pretreatment do not modify crystalline phase of alumina, XRD was performed on Al₂O₃ (RP) before calcination, and compared to alumina dehydroxylated at 500°C.

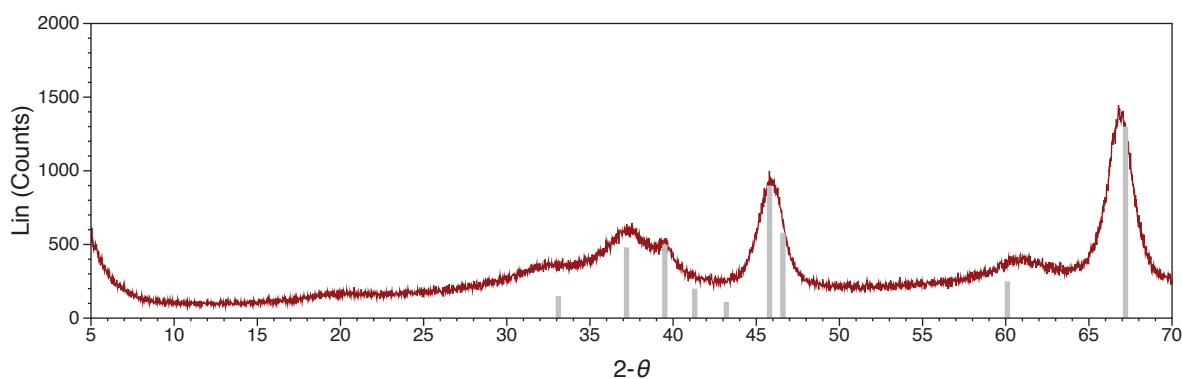
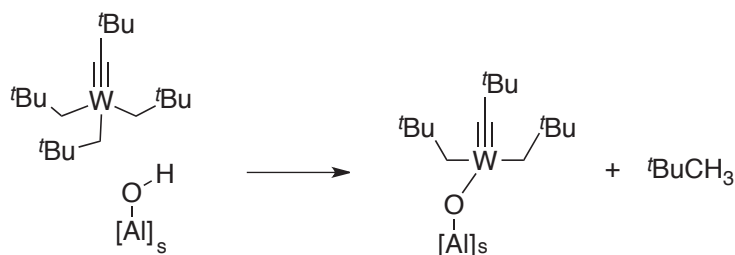


Figure 2.4 DRX spectrum of Al₂O₃ (RP) after calcination and dehydroxylation at 500°C (grey bars: ICDD Ref γ -Al₂O₃ PDF# 00-047-1308)

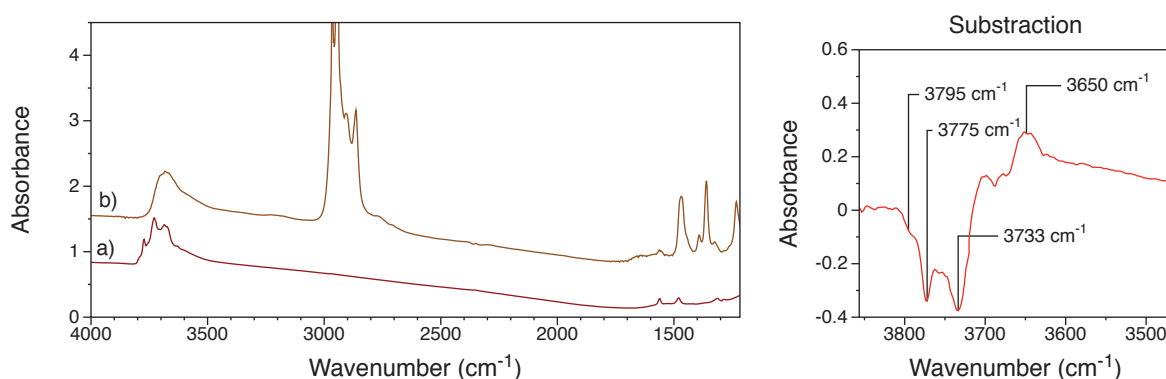
The same spectra were obtained before and after calcination, showing that the pretreatment does not change the nature of the crystalline phase of the support. Figure 2.4 presents the XRD spectrum of Al₂O₃₋₍₅₀₀₎ (RP), by comparison with the reference, it is clear that this is a γ -Al₂O₃. This alumina was chosen for this reason.

2.2. Characterizations of the [W(=C^tBu)(CH₂^tBu)₃] supported on Al₂O₃₋₍₅₀₀₎ (RP)

The γ -Al₂O₃ dehydroxylated at 500°C was chosen as support for the characterization of the tungsten complex. Indeed, it is one of the most employed in similar studies, due to its simpler reactivity than Al₂O₃₋₍₃₀₀₎ and Al₂O₃₋₍₈₀₀₎. The first presents water molecules at its surface, which can react with the molecular precursor.²⁵ The second bears a very few surface OH (see Table 2.1) and show very strained aluminoxanes bridge, these later may thus be opened by the molecular precursor and lead to mixture of surface species.⁸ On Al₂O₃₋₍₅₀₀₎, only protonolysis is expected (Scheme 2.5).

Scheme 2.5 Grafting of **1** by protonolysis reaction

2.2.1. IR spectroscopy

Figure 2.5 left: IR spectra of a) $\text{Al}_2\text{O}_{3-(500)}$ (RP) and b) **1**/ $\text{Al}_2\text{O}_{3-(500)}$ (RP); right: subtraction of the two spectra in the $\nu(\text{OH})$ region.

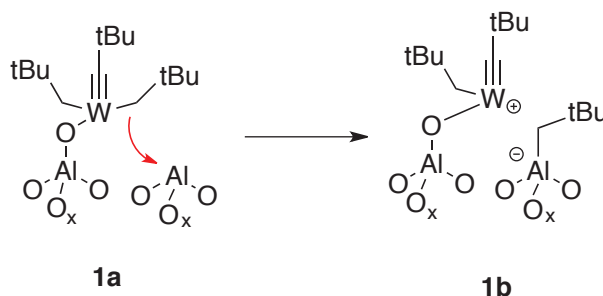
Upon sublimation of an excess of **1**, $[\text{W}(=\text{C}^t\text{Bu})(\text{CH}_2^t\text{Bu})_3]$, the alumina disk partially dehydroxylated at 500 °C ($\text{Al}_2\text{O}_{3-(500)}$ (RP)) turns brown and yields the solid **1**/ $\text{Al}_2\text{O}_{3-(500)}$ (RP). The IR spectrum of $\text{Al}_2\text{O}_{3-(500)}$ (RP) displays the five bands at 3795, 3775, 3733, 3650 and 3600 cm^{-1} (Figure 2.5) corresponding to the $\nu(\text{OH})$ vibrations of different types of surface hydroxyls (*vide supra*). Upon sublimation of **1**, the $\nu(\text{OH})$ vibrations at 3795, 3776 and 3730 cm^{-1} (assigned to $\text{HO}-\mu_1-\text{Al}_{\text{IV}}$, $\text{HO}-\mu_1-\text{Al}_{\text{VI}}$ and $\text{HO}-\mu_1-\text{Al}_{\text{V}}$ respectively) totally disappeared and the band at 3675 cm^{-1} (assigned to $\text{HO}-\mu_2-\text{Al}_{\text{VI}}$) is untouched, while some OH appear as a broad band centered at 3650 cm^{-1} resulting from interaction with alkyl ligands.¹⁵ Moreover, the characteristic bands in the 3000-2700 cm^{-1} and 1500-1300 cm^{-1} regions associated with the $\nu(\text{CH})$ and $\delta(\text{CH})$ of the perhydrocarbyl ligands around W also appear.

2.2.2. Mass balance analysis

A mixture of **1**, $[\text{W}(\equiv\text{C}^t\text{Bu})(\text{CH}_2^t\text{Bu})_3]$ (311 mg, 660 μmol) and $\text{Al}_2\text{O}_{3-(500)}$ (RP) (2 g) was stirred at 66 °C for 4 h under argon atmosphere. All volatile compounds were condensed into another reactor (of known volume) in order to quantify neopentane evolved during the grafting. Pentane (10 mL) was introduced into the reactor by distillation, and the solid was washed three times with pentane via filtration-condensation cycles. After evaporation of the solvent, the resulting brown powder was dried under vacuum.

Elemental analysis shows the presence of W to the extent of 5.5%_{wt}, which corresponds to 289 $\mu\text{mol}_\text{W}\cdot\text{g}^{-1}$, confirming that a partial consumption of surface hydroxyls (46%, of the 660 $\mu\text{mol}_\text{W}\cdot\text{g}^{-1}$ on $\text{Al}_2\text{O}_{3-(500)}$ (RP)). Moreover, 14.5 C/W are found by elemental analysis. And during grafting 327 $\mu\text{mol}_{t\text{BuCH}_3}\cdot\text{g}^{-1}$ have evolved, which correspond to 1.1 $t\text{BuCH}_3/\text{W}$. Upon treatment of **1**/ $\text{Al}_2\text{O}_{3-(500)}$ (RP) with an excess of H_2 at 150°C for 15h, the evolution of a mixture of methane and ethane (*ca.* 20:1) corresponding to 670 $\mu\text{mol}_{t\text{BuCH}_3}\cdot\text{g}^{-1}$ and 2.3 $t\text{BuCH}_3$ per grafted tungsten are observed. Elemental analysis after hydrogenolysis shows the presence of 2.5 carbons per grafted tungsten, showing that *ca.* 0.5 neopentyl per grafted tungsten remains at the surface of the material. This remaining neopentyl fragment was confirmed by hydrolysis experiments.

Overall, the data are consistent with the formation of a monopodal surface complex by protonolysis with surface hydroxyl, accompanied with the evolution of one neopentane per tungsten. The presence of carbon remaining at surface after treatment under H_2 at 150°C, demonstrate the presence of a non-hydrogenolyzable carbon species. It can be postulated that this remaining carbon is probably bonded to an aluminum centre resulting from neopentyl transfer on Lewis acidic site of the Alumina (Figure 2.5), as described in group IV or V systems (*vide supra*).



Scheme 2.6 Formation of cationic species by neopentyl transfer on acidic sites of Al_2O_3 .

Advanced solid-state NMR spectroscopy will be essential to confirm the structure of the surface complex.

2.2.3. Solid-state NMR spectroscopy

The solid-state MAS ^1H NMR spectrum of $1/\text{Al}_2\text{O}_3\text{-(500)}$ (**RP**) (Figure 2.6 left) exhibits only one broad signal at 1.0 ppm, tentatively assigned to the perhydrocarbyl ligand resonances, and particularly to the methyl and methylene of the neopentyl-like ligands. The solid-state CP/MAS ^{13}C NMR spectrum of solid $1/\text{Al}_2\text{O}_3\text{-(500)}$ (**RP**) (Figure 2.6 right) shows an intense peak at 32 ppm assigned to the methyl of the ^tBu fragments and a broad, albeit weak, signal at 85 ppm, which can tentatively be assigned to the methylene carbons of the neopentyl fragment (CH_2^tBu). The signal related to carbene is not observed.

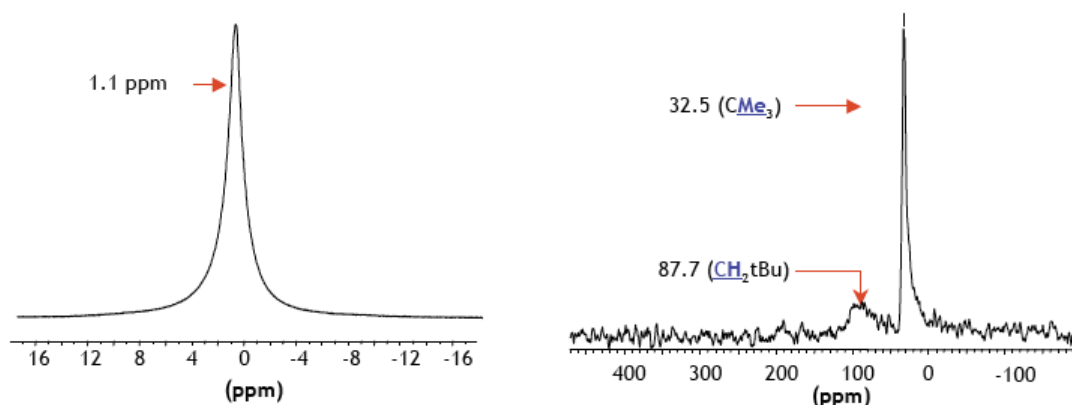
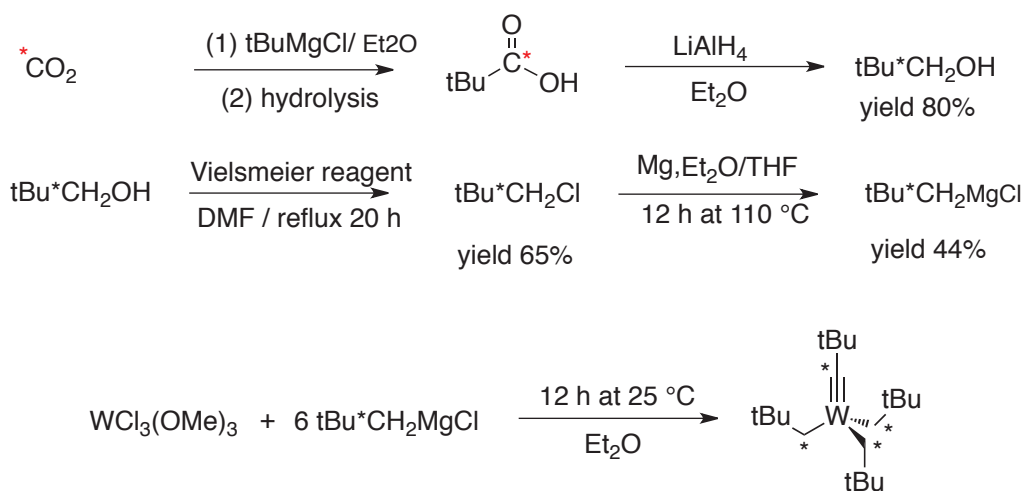


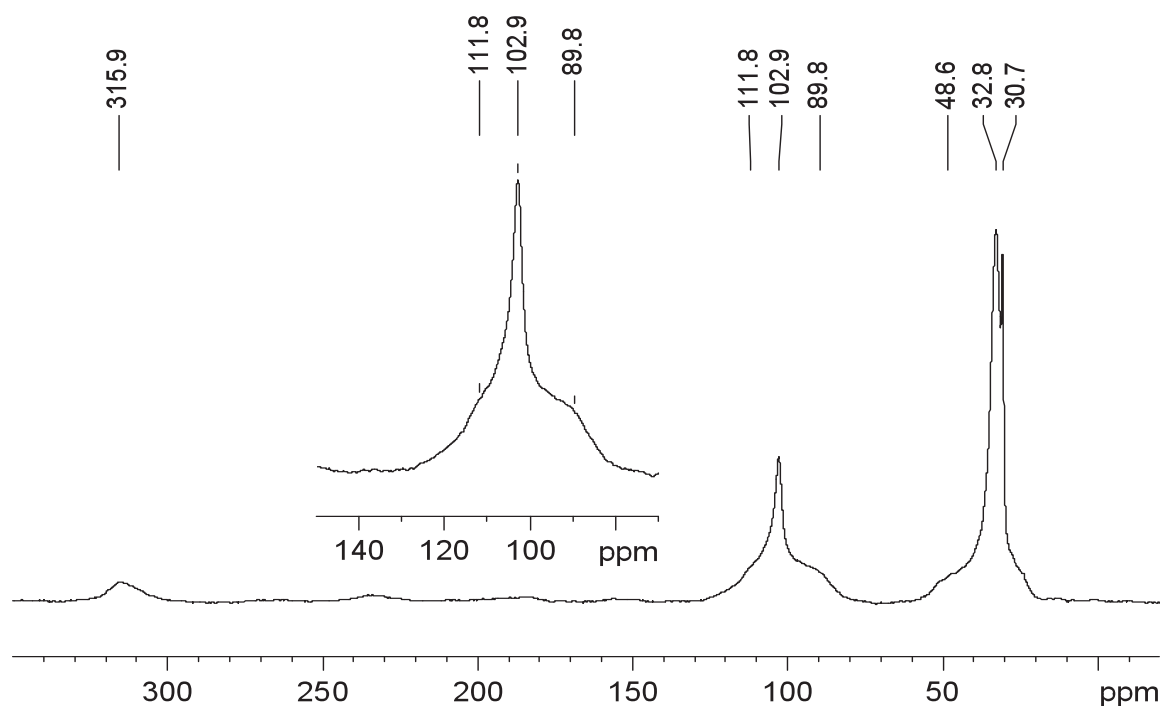
Figure 2.6 solid-state NMR spectra of $1/\text{Al}_2\text{O}_3\text{-(500)}$ (**RP**): left ^1H -MAS; right ^{13}C CP-MAS

2.2.4. 100% ^{13}C labeled NMR

Generally, α -carbons (such as carbenic and carbynic carbons but also methylenic ones) are difficult to observe under these conditions (*i.e.* diluted systems). In order to improve the signal-to-noise ratio, the corresponding ^{13}C enriched complex,^{7,9,26,27} $1^*/\text{Al}_2\text{O}_3\text{-(500)}$ (**RP**), 99 % enriched on the α -position was prepared starting from 99% ^{13}C -labeled $^*\text{CO}_2$ and using the following reaction sequence : reaction of $^t\text{BuMgCl}$ with $^*\text{CO}_2$ to form $^t\text{Bu}^*\text{COOH}$, followed by a reduction with LiAlH_4 to yield to the corresponding alcohol. Nucleophilic substitution with the Vilsmeier reagent $[\text{ClCH}=\text{N}(\text{CH}_3)_2]$ ^{28,29} gave 2,2-dimethylchloropropane, 99% ^{13}C enriched in the α -position. It was then transformed into the corresponding Grignard reagent. Its reaction with $\text{WCl}_3(\text{OMe})_3$ gave 1^* in which the carbons directly bonded to W were ^{13}C -enriched to the extent of 99%. The molecular complex 1^* was finally grafted on $\text{Al}_2\text{O}_3\text{-(500)}$ (**RP**) to yield $1^*/\text{Al}_2\text{O}_3\text{-(500)}$ (**RP**).

Figure 2.7 Preparation of the 99% ^{13}C labeled $[\text{W}(\equiv\text{C}^*\text{Bu})(^*\text{CH}_2^*\text{Bu})_3]$

Using labelled $\mathbf{1^*}/\text{Al}_2\text{O}_{3-(500)}$ (**RP**), the spectrum displays the following features (Figure 2.8): a broad and weak signal at 316 ppm, a broad intense signal at 103 ppm along with a shoulder at 90 and 112 ppm, broad signal around 48 ppm, and a signal at 32 ppm and a thin signal at 30 ppm.

Figure 2.8 solid-state ^{13}C HP-DEC NMR spectra of $\mathbf{1^*}/\text{Al}_2\text{O}_{2-(500)}$ (**RP**)

By comparison with the ^{13}C N.M.R. spectrum of the corresponding silica supported W complex,³⁰ it is clear that the carbyne ligand was left intact during grafting as evidenced by the peak at 315 and 49 ppm assigned, respectively, to the carbynic carbon ($\equiv\text{C}^*\text{Bu}$) and the quaternary carbon of the ^tBu directly attached to this carbon ($\equiv\text{C}\text{CMe}_3$).

Nonetheless, several species are possibly present as evidenced by the broadness of the resonance at 316 ppm. Several peaks around 103 ppm are attributed to different types of methylene carbon ($\underline{\text{C}}\text{H}_2^t\text{Bu}$) from neutral and cationic species, which is shifted slightly downfield as might be expected for a formally “cation-like” complex.⁶ Similarly, different peaks around 32 ppm are attributed to different ^tBu groups. The deconvolution of these signals, shows a signal at 26 ppm in addition to the signal at 32 and 30 ppm (Figure 2.9). The thin signal at 30 and the shoulder at 26 ppm have to be noticed. Indeed, these two signals, are still present on the ^{13}C NMR spectrum of $\mathbf{1}^*/\text{Al}_2\text{O}_3\text{-(500)}$ (**RP**) after the treatment at 150°C . On this spectrum, the intense signal at 26 ppm may be attributed to ^{13}C labeled (99%) carbon of $\text{Al}-\underline{\text{C}}\text{H}_2^t\text{Bu}$, whereas the signal at 30 ppm is due to terminal methyl of neopentyl bonded to aluminum, $\text{Al}-\text{CH}_2(\underline{\text{C}}\text{H}_3)_3$.

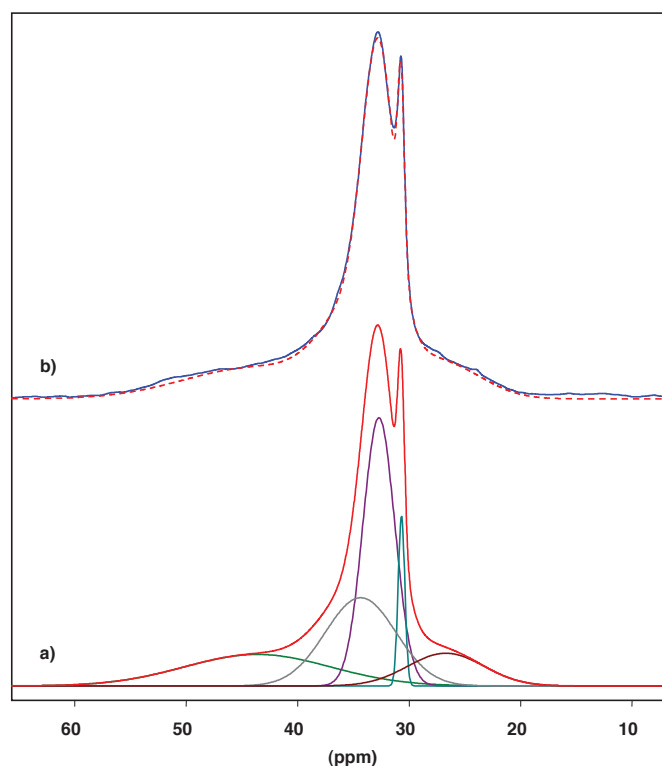
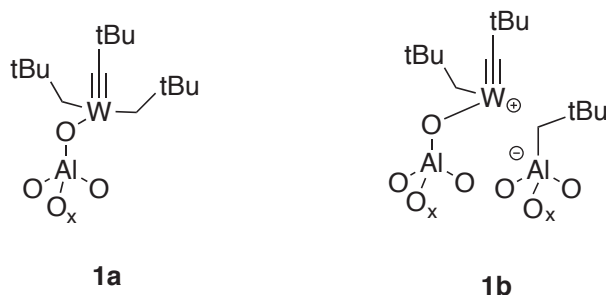
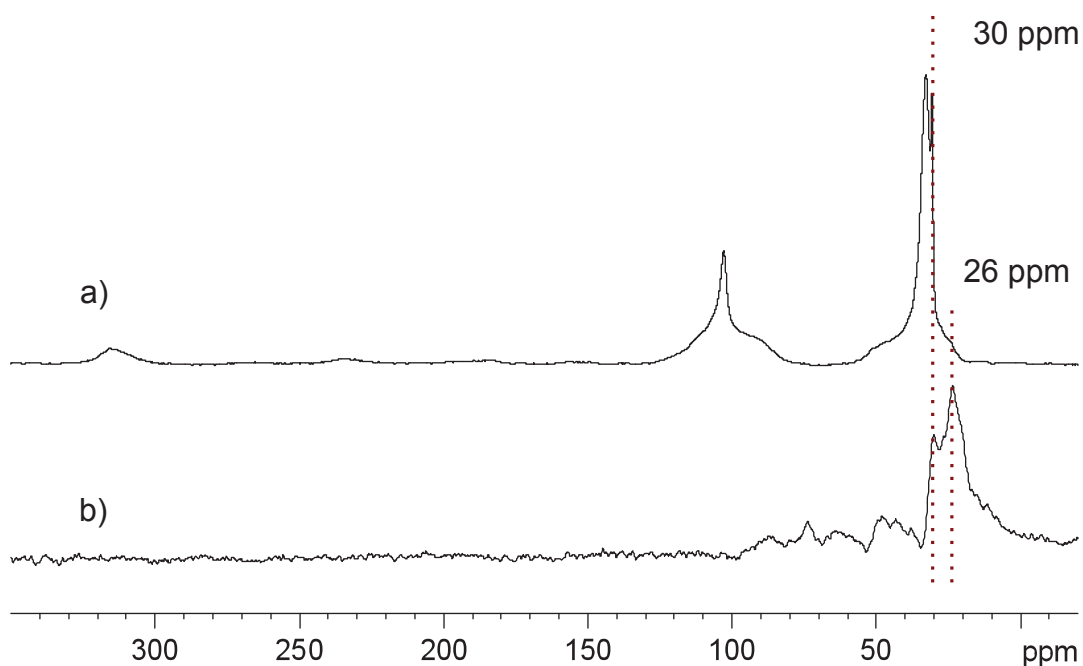


Figure 2.9 Deconvolution, using DMFIT, of the ^{13}C HP-DEC NMR spectrum of $\mathbf{1}^*/\text{Al}_2\text{O}_2\text{-(500)}$ (**RP**) in the 20-60 ppm range a) five different peaks have been obtained, in red the fit obtained b) plain line experimental spectra, tick line fit obtained

Scheme 2.7 Proposed structure for the different surface species of $1/\text{Al}_2\text{O}_{3-(500)}$ (RP)

Similarly to Zr, Hf and Ta chemistry, where partial transfer of alkyl group is observed and confirmed by NMR spectroscopy and theoretical calculation, the grafting of tungsten on alumina lead to a mixture of neutral and cationic surface species. Regarding the mass balance analysis, during the grafting reaction and the treatment under H_2 , the surface species are consist on a mixture of neutral, **1a**, and cationic species, **1b**, in an approximate 1:1 ratio (Scheme 2.7).

Figure 2.10 ^{13}C HPDEC N.M.R. spectrum of 99% ^{13}C -labeled complex $1^*/\text{Al}_2\text{O}_{3-(500)}$ a) before and b) after treatment under H_2 at 150°C

2.3. Characterizations of the tungsten hydride on $\text{Al}_2\text{O}_{3-(500)}$ (RP)

In this subsection, the treatment of $1/\text{Al}_2\text{O}_{3-(500)}$ (RP) under H_2 at 150°C will be studied in detail. The supported tungsten hydrides species, obtained by hydrogenolysis of the neutral (**1a**) and cationic (**1b**) species will be characterized by IR, ^1H , ^{13}C and DQ solid-state NMR and Raman spectroscopies, TEM, theoretical calculations and EXFAS.

2.3.1. Preparation

The previous solid, $1/\text{Al}_2\text{O}_{3-(500)}$ (RP), was heated in static reactor, at 150°C in the presence of a large excess of dry H_2 (550 Torr). After 15 h, the gaseous products were quantified by GC, and the resulting solids were obtained after evacuating the gas phase for 15 min.

2.3.2. IR Spectroscopy

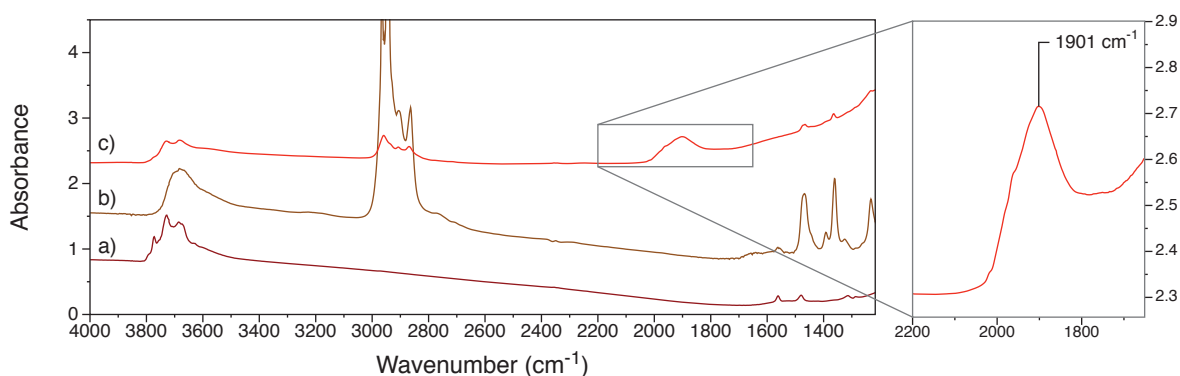
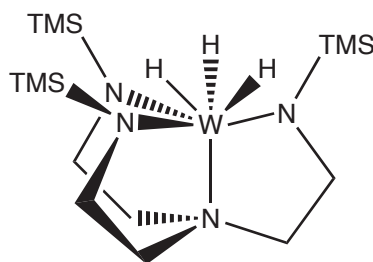


Figure 2.11 left: IR spectra of a) $\text{Al}_2\text{O}_{3-(500)}$ (RP), b) $1/\text{Al}_2\text{O}_{3-(500)}$ (RP) and c) $\text{WH}/\text{Al}_2\text{O}_{3-(500)}$ (RP); right: zoom on the W-H region.

When $1/\text{Al}_2\text{O}_{3-(500)}$ (RP), is heated under H_2 for 15 h at 150°C , the pale yellow solid turns brown and leads to the solid $\text{WH}/\text{Al}_2\text{O}_{3-(500)}$ (RP) (Figure 2.11). Monitoring by IR spectroscopy (spectrum c) shows the disappearance of 95% of the bands associated with $\nu_{(\text{C-H})}$ and $\delta_{(\text{C-H})}$. Some OH groups reappear at 3775 cm^{-1} and some still remain at 3650 cm^{-1} . Note that during the treatment under H_2 , the IR region corresponding to the hydroxyl groups ($\text{Al}_s\text{-OH}$) is greatly perturbed. While, it is clear that some of hydroxyls previously in interaction with alkyl ligands are transformed into isolated hydroxyls, this observation probably shows that surface restructuring has occurred, and that some hydroxyl groups have reacted with some W species. Additionally, a large broad band appears at 1901 cm^{-1} in the M-H region (Figure 2.11). This value is in good agreement with the molecular tung-

sten trishydride described by Dobbs *et al.*³¹ (Structure in Scheme 2.8) with two bands attributed to W-H at 1903 and 1887 cm^{-1}



Scheme 2.8 Structure of the tungsten trishydride isolated by Dobbs *et al.*

2.3.3. D_2 exchange

When the solid **WH/Al₂O₃₋₍₅₀₀₎ (RP)** is treated with D_2 at 80°C for 1 h, affording **WD/Al₂O₃₋₍₅₀₀₎ (RP)**, the intensity of $\nu_{(WH)}$ band at 1901 cm^{-1} decrease, at the same time, weak $\nu_{(WD)}$ vibrations can be observed at 1388 cm^{-1} , while expected at 1365 cm^{-1} (Figure 2.12). Additionally, after treatment under D_2 , a band at 1897 cm^{-1} , not exchanged under these conditions, can be assigned to Al-H. It has to be noted that Al-H band is usually observed when preparing metal hydride from perhydrocarbyl precursor grafted on alumina: [Ta(=C^tBu)(CH₂^tBu)₃]/Al₂O₃₋₍₅₀₀₎³² (1930 cm^{-1}) or [Hf(CH₂^tBu)₃]/Al₂O₃₋₍₅₀₀₎¹⁰ (1915 to 1960 cm^{-1}) or when contacting H₂ with dehydroxylated alumina (1866 and 1902 cm^{-1}).²⁵ When **WD/Al₂O₃₋₍₅₀₀₎ (RP)** is treated at 80°C under H₂ the spectroscopic features of the resulting material are identical to those of **WH/Al₂O₃₋₍₅₀₀₎ (RP)**.

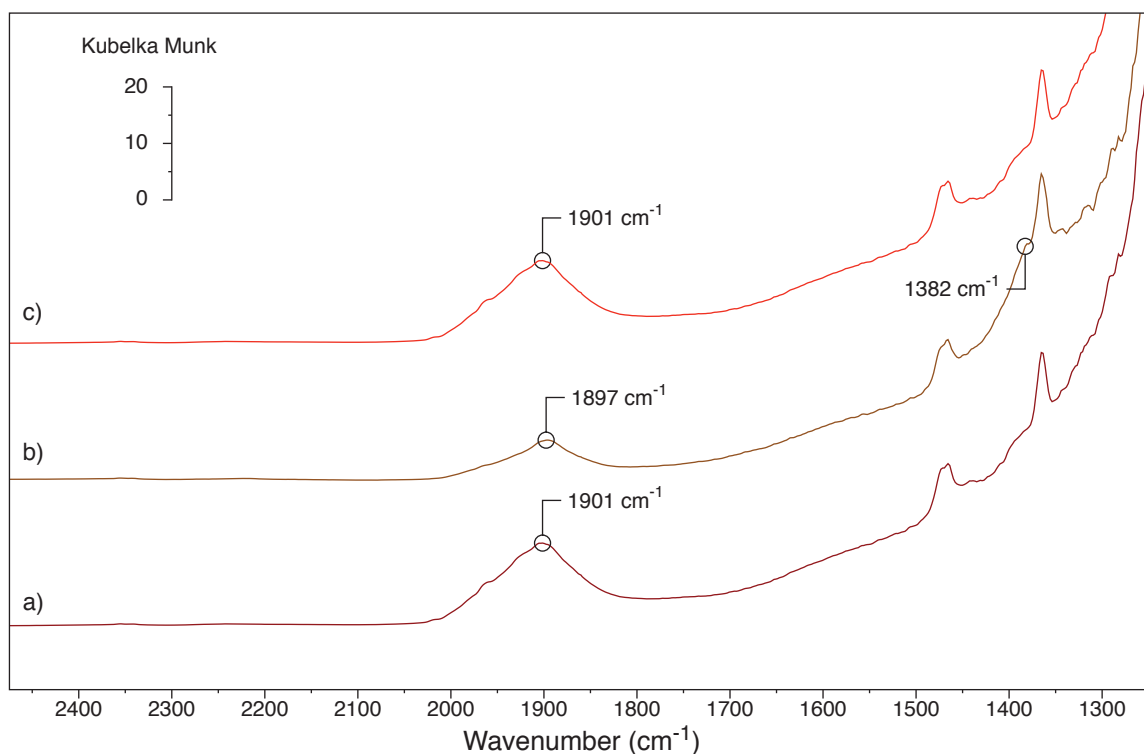
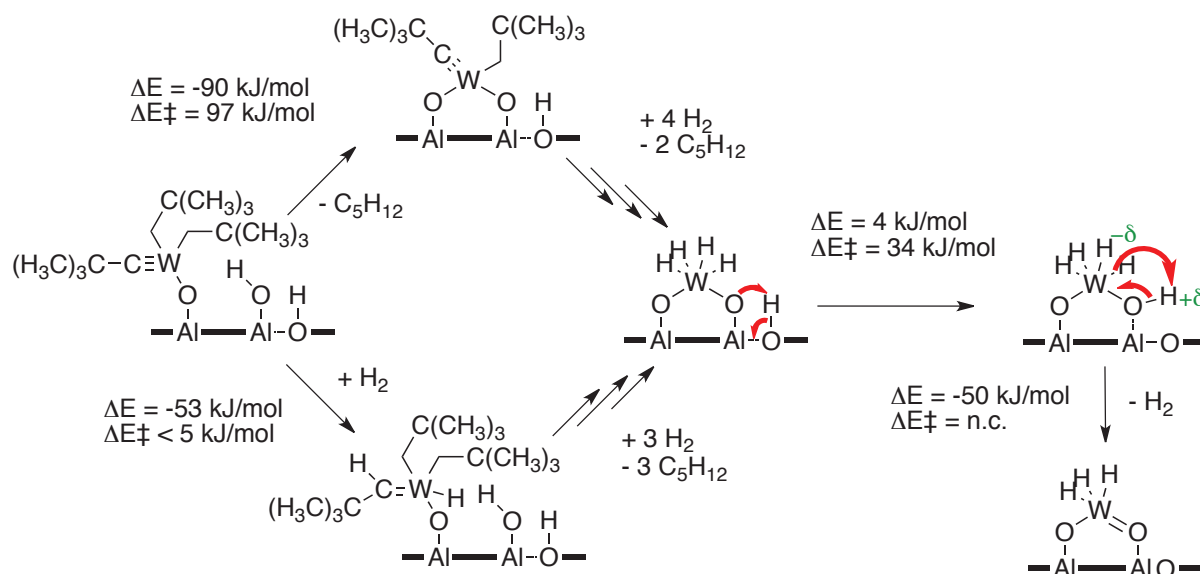


Figure 2.12 Diffuse reflectance infrared spectra of: a) **WH/Al₂O₃-(500) (RP)**; b) after treatment at 80°C with D₂ (**WD/Al₂O₃-(500) (RP)**) and c) after a final treatment at 80°C with H₂.

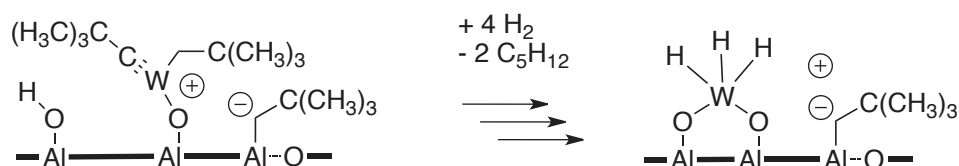
2.3.4. Theoretical calculations

Sautet *et al.* have performed DFT calculation to understand the mechanism of formation of a tungsten hydride from **1a**. The expected mechanism is presented on Scheme 2.9 with the ΔE value calculated for each species. These calculations show that the formation of a tungsten hydride is favored. The first reaction step may be the reaction with a neighbor hydroxyl to form a bipodal transition species. This exothermic reaction ($\Delta E = -90 \text{ kJ.mol}^{-1}$) is confirmed by IR spectroscopy, which as evidenced perturbation of $\nu_{(\text{O-H})}$ signals (Figure 2.11). The resulting species is later hydrogenolysed. The reaction between an aluminosy ligand and an adjacent hydroxyl group by prototropy of the oxygen bond to tungsten followed by an hydrogen elimination will form an oxo ligand in interaction with a surface aluminum affording a stable surface species ($\Delta E = -50 \text{ kJ.mol}^{-1}$).



Scheme 2.9 Theoretical calculation of the expected mechanism of formation of supported tungsten hydride from neutral surface species. (Sautet *et al.*; unpublished results)

At that time no calculation have been performed on the cationic surface species **1b**. Nevertheless, the same mechanism should be considered. First the reaction with a neighbor hydroxyl to form a bipodal transition species and the hydrogenolysis of tungsten ligand may leading to a cationic tungsten hydride species (see Scheme 2.10), letting the Al-CH₂^tBu untouched as the Al-C bond is known to be hydrogenolyzed under sever conditions only.³³ The reactivity of grafted alkyl aluminum toward hydrogenolysis is known to occurs only over 250°C (see Chapter 4).



Scheme 2.10 Formation of a cationic supported tungsten hydride from cationic surface species.

2.3.5. RAMAN spectroscopy

To confirm the presence of an oxo ligand in the coordination sphere of the tungsten, Raman spectrometry was performed on **WH/Al₂O₃-(500) (RP)** (Figure 2.13). As Al₂O₃ does not give any signal in Raman spectrometry, all the signals were attributed to tungsten species.

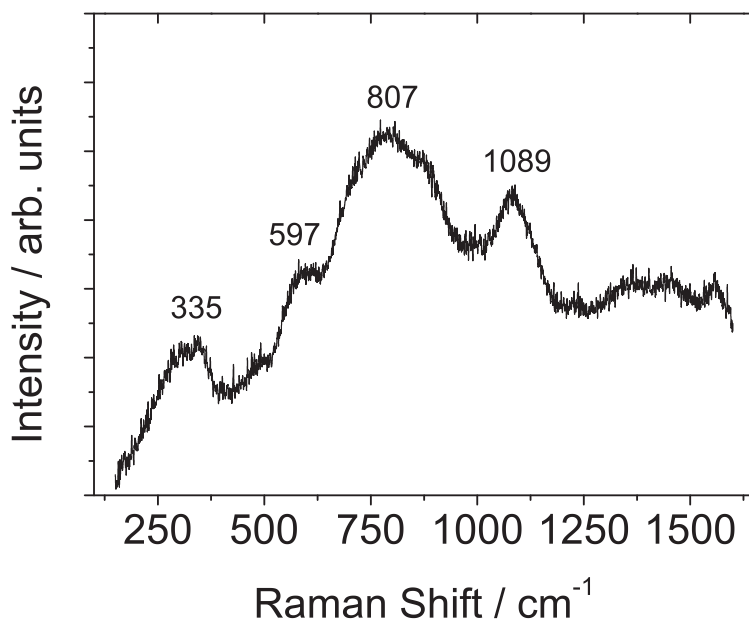


Figure 2.13 Raman spectrum of **WH/Al₂O₃-(500) (RP)**

The observed bands are very broad, showing, as expected by heterogeneity of alumina surface, a distribution of structures of surface species. The broad signal around 800 cm^{-1} may be assigned to Al-O-W modes. The bands at 335 and 1089 cm^{-1} , are assigned, respectively to bending and symmetric stretching mode of the W=O. These values are high for a W=O, which are reported to be at 300 cm^{-1} (bending) and 1020 cm^{-1} (symmetric stretching) for surface tungsten oxo species on Al₂O₃.³⁴ The coordination of the oxo ligand proposed by theoretical calculation may induce this shift of the signal. Theoretical investigations about Raman shift may explain this high value. No signal assignable to W-O-W, characteristic of WO₃ crystalline particles are observed. Finally, no signals imputable to WH or OH are detected.

2.3.6. ¹H NMR and ¹H NMR spectroscopy after D₂ exchange

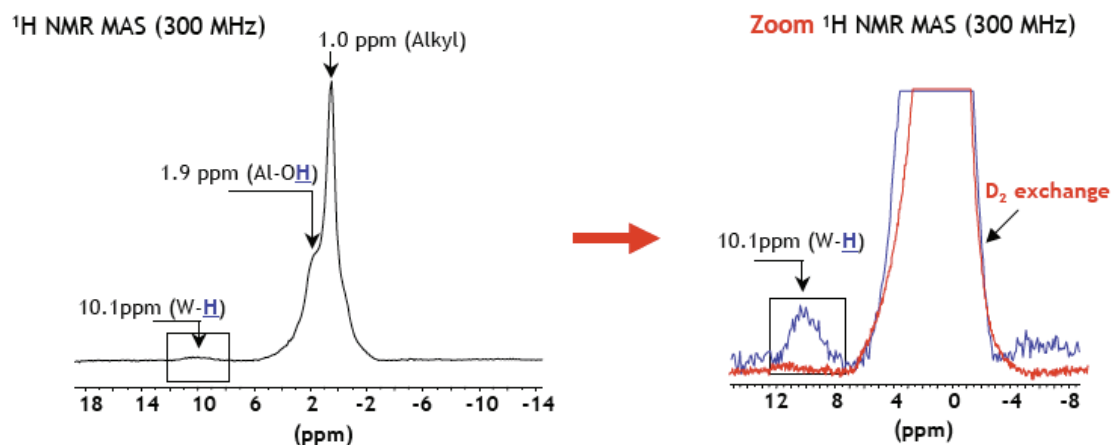


Figure 2.14 Solid state ^1H -MAS NMR spectra of **WH/Al₂O₃₋₍₅₀₀₎ (RP)** left comparison with **WD/Al₂O₃₋₍₅₀₀₎ (RP)**. The ^1H MAS NMR spectrum (Figure 2.14) of the solid **WH/Al₂O₃₋₍₅₀₀₎ (RP)** exhibits two intense signals at 1.9 and 1.0 ppm, which are, respectively, characteristic of residual hydroxyl groups and neopentyl fragments (see ^{13}C NMR spectrum in Figure 2.10). Moreover, there is a weak broad signal at 10.1 ppm, which disappears when **WH/Al₂O₃₋₍₅₀₀₎ (RP)** is contacted with D_2 at 80°C for 1h (**WD/Al₂O₃₋₍₅₀₀₎ (RP)**). This value is in agreement with the ^1H NMR of the tungsten trishydride isolated by Dobbs *et al.* (*vide supra*) reported to give a signal at 10.01 ppm. The broadness of the signal can be explained by the $^1J_{\text{W-H}}$ coupling and eventually the distribution of products regarding their close environment. In contrast to IR spectroscopy, the ^1H MAS NMR spectrum of the surface species does not show a resonance indicating the presence of Al-H species (ca. 3.3 ppm, see Chapter 4), probably due to the broadness of the signal induced by the quadrupolar moment of trigonal Al centers and their low concentration at the surface.

2.3.7. Multiple Quanta NMR Spectroscopy

To further assign these various signals, 2D multiple-quantum (MQ) proton spectroscopy under magic angle spinning (MAS) was applied.³⁵⁻³⁸ To probe structural information inherent to proton-proton dipolar couplings, the ^1H DQ MAS spectrum was recorded for **WH/Al₂O₃₋₍₅₀₀₎ (RP)** at a MAS frequency of ca. 10 kHz (Figure 2.15). In this experiment, the evolution of the DQ coherence created between a pair of dipolar-coupled protons is observed during the indirect detection time t_1 . The DQ frequency in the ω_1 dimension corresponds to the sum of the two single quantum frequencies of the two coupled protons and correlates in the ω_2 dimension with the two corresponding proton resonances. Therefore, the observation of a DQ cross-peak implies a close proximity between the two protons involved in this correlation.

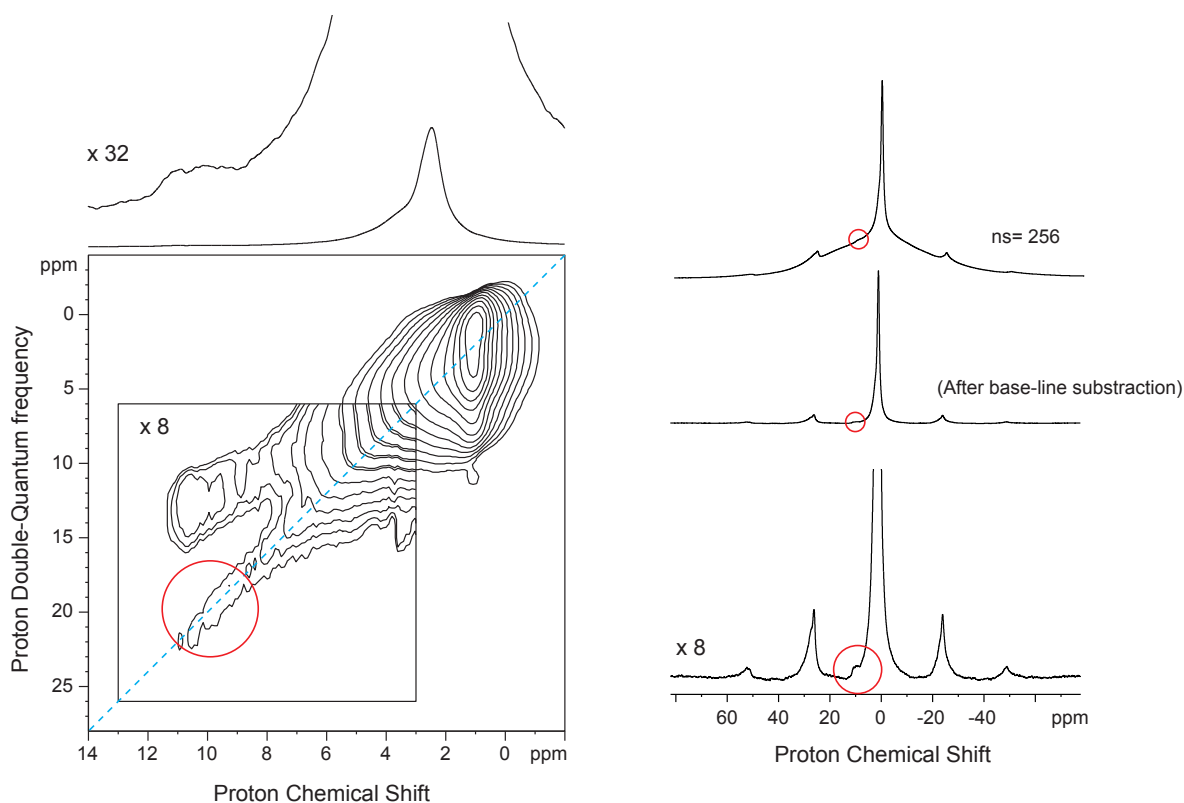


Figure 2.15 left: DQ Solid state ^1H -MAS NMR spectra of **WH/Al₂O₃-(500) (RP)**

Autocorrelation peaks are observed on the diagonal of the 2D spectrum (Figure 2.15), in particular for the alkyl protons at 0.9 ppm (ca. 2 ppm in the ω_1 dimension, for CH_z , with $z=2, 3$). A weak auto-correlation peak is also observed for a proton resonance at ca. 10.1 ppm (ca. 20 ppm in the ω_1 dimension), which unambiguously demonstrate that the tungsten bears almost two hydride, as was found previously in the case of zirconium and titanium surface organometallic chemistry, where $[(\equiv\text{SiO})_2\text{ZrH}_2]$ or $[(\equiv\text{SiO})(\text{MsO})\text{TiH}_2]$ species were similarly characterized.^{39,40}

In order to demonstrate the presence of three hydride on the tungsten, Triple Quantum experiment has been performed, but unfortunately no exploitable signal were obtained. This is probably due to the broadness of the tungsten hydride signal at 10.1 ppm and to the complexity of alumina supported hydride structures, as observed for zirconium, hafnium and tantalum (*vide supra*).

2.3.8. Stoichiometric reactivity with methane

Regarding the complexity of the characterization of these surface hydrides, stoichiometric reactivity study has been undertaken to confirm the tris-hydride structure given by theoretical calculations.

Methane activation on 500mg of **WH/Al₂O₃-(500) (RP)** was studied in continuous flow reactor at 50 barg starting from 25°C to 350°C. The evolution of hydrogen vs. time was monitored by on-line GC analysis. The instant and cumulated evolution of hydrogen vs. time on stream has been plotted. The evolution of hydrogen is observed during a period of 1000 min, the cumulated hydrogen evolution corresponds to 2 H₂ per W (Figure 2.1). The hydrogen evolution could arise from two sources: i) formation of tungsten monohydride by liberation of one H₂ per W from the presumed tungsten trihydride species, as demonstrated by the high evolution of hydrogen before 300 min and similarly to [(≡SiO)₂TaH₃]⁴¹ ii) consecutive C-H bond activation of methane, releasing one H₂ per W and formation of tungsten IV methyl surface species (Scheme 2.11). These results are consistent with trishydride structure proposed by theoretical calculation and IR spectroscopy.

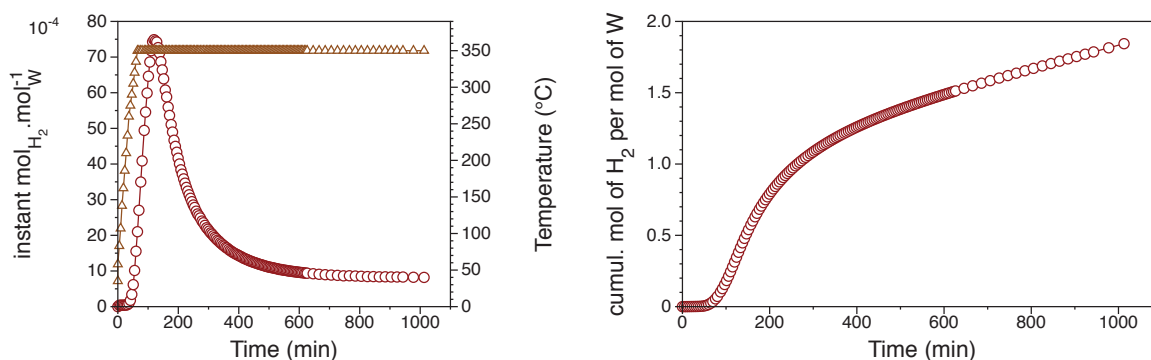
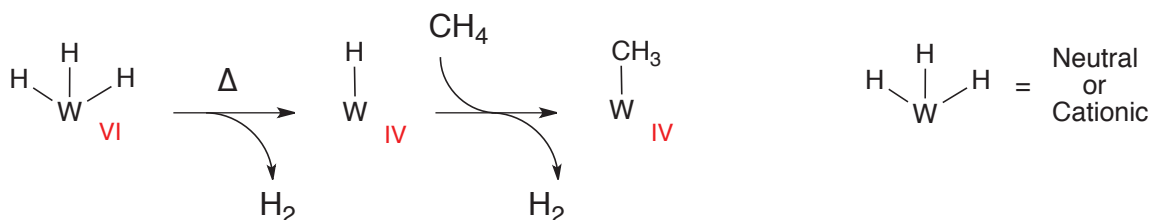


Figure 2.16 Instant (left) and cumulated (right) hydrogen evolution during activation of methane on **WH/Al₂O₃-(500) (RP)**



Scheme 2.11 Methane activation on **WH/Al₂O₃-(500) (RP)**

2.3.9. Transmission Electron Microscopy (TEM)

When the tungsten perhydrocarbyl complex grafted on $\text{SiO}_{2-(700)}$ is treated under H_2 at 150°C a sintering of tungsten is evidenced by the resurgence of SiOH signals on IR spectrum and formation of tungsten particles on TEM images. The observation of **WH/Al₂O₃₋₍₅₀₀₎ (RP)** by TEM did not reveal the presence of any particles. Nevertheless the contrast for TEM on Al_2O_3 is known to be quite low. EXAFS has thus been performed to prove the absence of tungsten particles.

2.3.10. Extended X-Ray Adsorption Fine Structure Spectroscopy (EXAFS)

Regarding all the characterizations of **WH/Al₂O₃₋₍₅₀₀₎ (RP)**, and particularly ^{13}C NMR spectroscopy and mass balance analysis (presented in subsections 2.2.2 and 2.2.4), a mixture of two major surface species can be proposed: a neutral, and a cationic tungsten hydride. The characterization of **WH/Al₂O₃₋₍₅₀₀₎ (RP)** by analysis of the W L_{III}-edge Extended X-Ray Adsorption Fine Structure Spectroscopy (EXAFS) data confirms several features of these surface species (Figure 2.17 and Table 2.3). The difficulty to establish a good fit ($\rho = 6.0\%$), compared to well-defined species of tungsten alkyl supported on silica (see Chapter 6), corroborates the presence of a mixture of surface species. Due to this mixture of surface species, the EXAFS data have to be considered with caution.

Nevertheless, the results exclude tungsten-tungsten contributions, ruling out the formation of particles, and point out the presence of 0.5(2) oxygen neighbor at short distances (1.74(3) Å), which can be attributed to W=O species, as obtained by theoretical calculations and Raman spectroscopy.

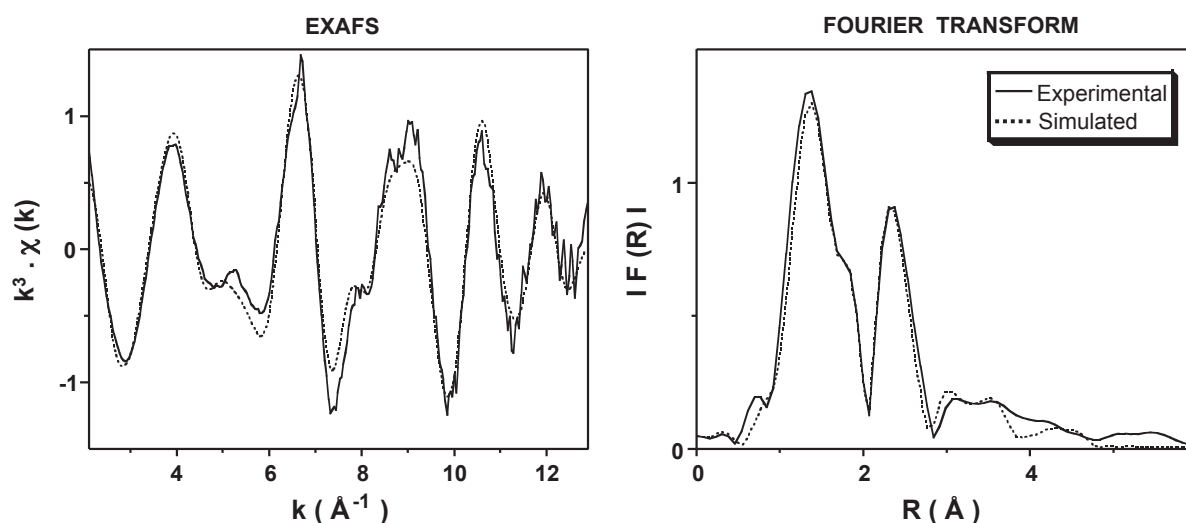


Figure 2.17 W L_{III}-edge k^3 -weighted EXAFS (left) and Fourier transform (right) of **WH/Al₂O₃₋₍₅₀₀₎ (RP)**. Dashed lines: experimental, solid lines: spherical wave theory.

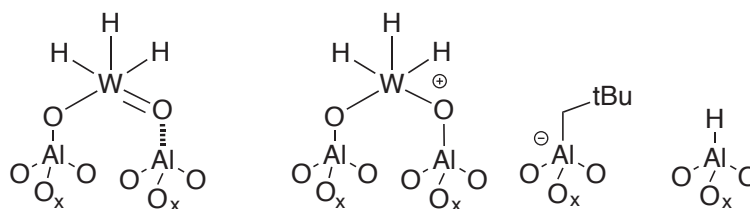
Table 2.3 EXAFS data for **WH/Al₂O₃₋₍₅₀₀₎ (RP)** errors between parentheses; fit residue: $\rho = 6.0\%$

Type of neighbour	Number of neighbours	Distance (Å)	σ^2 (Å ²)
W=O	0.5(2)	1.74(3)	0.001(1)
W-O	0.6(2)	1.87(3)	0.001(1)
W-C	1.1(6)	2.16(3)	0.006(4)
W--O	1.0(3)	2.72(2)	0.002(1)
W--O	1.8(13)	3.17(9)	0.04(4)

2.4. Conclusion

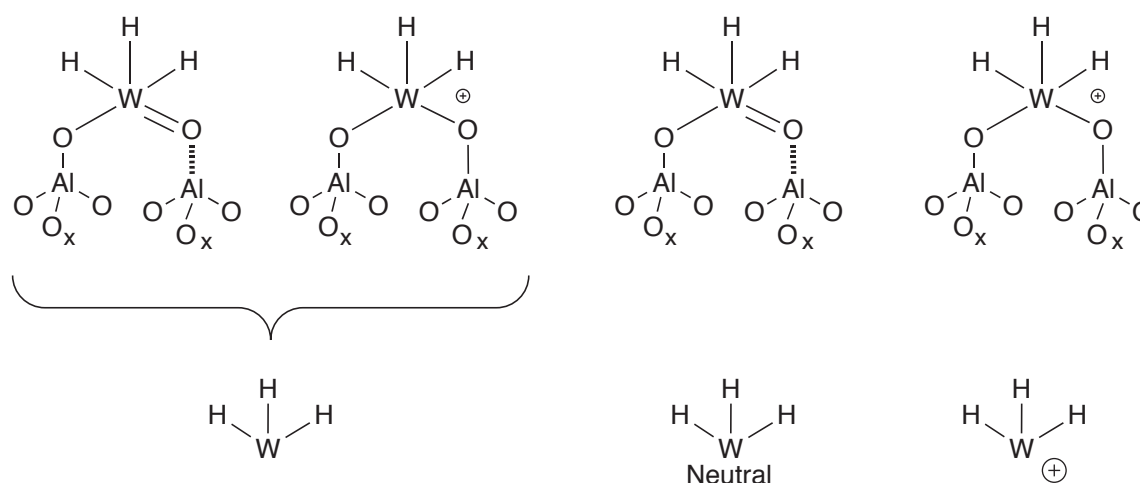
The grafting of $[W(\equiv C^tBu)(CH_2^tBu)_3]$, **1**, on $Al_2O_{3-(500)}$ (RP) leads to **1/Al₂O₃₋₍₅₀₀₎ (RP)**, which surface exhibits a mixture of neutral and cationic species respectively **1a** and **1b**. This later results from a transfer of a neopentyl ligand to an acidic aluminum atom. The structure of these species have been determined using IR spectroscopy, mass balance analysis of grafting and treatment under H₂ at 150°C, and ¹³C solid-state NMR spectroscopy. The formation of the cationic species, **1b**, is in agreement with the reactivity of group IV, group V and actinides organometallic complexes on alumina but contradict theoretical calculations results of Joubert *et al.*¹³

The treatment of **1/Al₂O₃₋₍₅₀₀₎ (RP)** under H₂ at 150°C afford **WH/Al₂O₃₋₍₅₀₀₎ (RP)** with evolution of a methane:ethane mixture corresponding to 2.5 Np/W and letting 0.5 Np/W at the surface. The characterizations and calculations made on this product prove the presence of different surface species (Scheme 2.12). Indeed, a neutral tungsten oxo tris-hydride is formed from **1a**. The opening of strained aluminoxane bridges during the treatment at 150°C or the activation of H₂ on default of alumina surface may also creates surface **Al-H**. The cationic species **1b** is hydrogenated at 150°C but its anionic **Al-CH₂^tBu** counterparts is conserved during this treatment. The complexity of the system as not allowed a rigorous determination of the relative amount of each species. A complete study using DFT calculation is necessary to completely solve such a complex systems, the presence of a cationic species.

Scheme 2.12 Proposed surface species of **WH/Al₂O₃₋₍₅₀₀₎ (RP)**

The next chapters are devoted to the role of each species in catalytic activities. Hence on Chapter 3 the activity of **WH/Al₂O₃₋₍₅₀₀₎ (RP)** for the direct conversion of ethylene to propylene will be studied. The catalytic mechanism and the deactivation mechanism will be studied regarding the characterizations obtained here. Chapter 4 will focus on the preparation of well-defined **Al-alkyl** and **Al-H** supported on Alumina and presents their activity toward ethylene. Chapter 5 will pay attention to the use of olefins feedstock different than ethylene for the propylene production. On Chapter 6, the preparation of new tungsten supported model catalyst will be presented. A structure-reactivity relationship study of these model complexes to better understand the active site of **WH/Al₂O₃₋₍₅₀₀₎**.

For the sake of clarity, in the following chapters, the neutral and cationic tungsten tris-hydride site will be presented as in Scheme 2.13 when their reactivity is similar. When their reactivity will differ, the neutral or cationic character will be clearly indicated.



Scheme 2.13 Simplified representation of the neutral and cationic tungsten tris-hydride adopted for the following chapters

3. Experimental section

3.1. General procedures

All experiments were carried out by using standard Schlenk and glove-box techniques. Solvents were purified and dried according to standard procedures.⁴² The trichlorotrimethoxytungsten was prepared from WCl_6 (99 %, Strem, used as received) and methoxytrimethylsilane (99 %, Aldrich, $CH_3OSi(CH_3)_3$ was distilled over sodium and stored over 3 Å molecular sieves) according to published procedure.⁴³ 1,2-dibromoethane (99%, Aldrich), benzyl alcohol (99%, Aldrich), p-xylene (99%, Aldrich), 2-2'-biquinoline (98%, Lancaster), $tBuMgCl$ (2M solution in Et_2O , Aldrich), $LiAlH_4$ (95%, Aldrich, stored under argon), $MgSO_4$ (Laurylab), $NaHCO_3$ (Prolabo), Vielsmeier reagent (95%, Aldrich,

stored under argon), and isotopic labeled CO₂ (99% ¹³C, Cambridge Isotope Laboratories, Inc.) were used as received. Methane (N50, Air liquide), H₂ and D₂ (N30, Air liquide) were purified over R3-11 BASF/MS4Å catalysts. Pyridine (Aldrich, 99%) was dried on solid KOH and distilled under argon, degassed and stored over 3Å molecular sieves. Aqueous solution of HCl and H₂SO₄ were prepared from a concentrated HCl solution (37 %wt, Aldrich) and H₂SO₄ solution (36 %wt, Aldrich) respectively. ^tBuCH₂MgCl or 99% ¹³C-labeled ^tBu*CH₂MgCl was prepared from ^tBuCH₂Cl (98 %, Aldrich, used as received) or 99% ¹³C-labeled ^tBu*CH₂ (synthesis is described in detail below) respectively and Mg turnings (Lancaster) using 1,2-dibromoethane as activator. Concentration of the resulting solution was titrated using benzyl alcohol solution in p-xylene and 2-2'-biquinoline as indicator. [W(≡C^tBu)(CH₂^tBu)₃], **1**, was prepared according literature procedures.^{44,45} 99% ¹³C-labeled [W(≡*C^tBu)(*CH₂^tBu)₃], **1***, was prepared according the same procedures but using 99% ¹³C-labeled ^tBu*CH₂MgCl as alkylation agent. Alumina E7102 from Rhone-Poulenc extrudates were crushed in a mortar and sieved (40-60 mesh). The resulting powder was calcinated at 500°C under dry air for 15h. It was then hydrated with a vapor pressure of degassed water at 100°C for 1h prior to treatment under high vacuum (10⁻⁵ Torr) at the desired temperature, for 15h. Gas-phase analyses were performed on a Hewlett-Packard 5890 series II gas chromatograph equipped with a flame ionisation detector and an Al₂O₃/KCl on fused silica column (50 m X 0.32 mm). Elemental analyses were performed at the CNRS Central Analysis Department of Solaize (metal analysis) or in the LSEO (Dijon, for C, H analysis). IR spectra were recorded on a Nicolet 5700 FT-IR spectrometer by using a IR cell equipped with CaF₂ window. Typically, 16 scans were accumulated for each spectrum (resolution 2 cm⁻¹). The nitrogen adsorption and desorption isotherms were measured at 77 K using micromeritics automated gas adsorption analyzer. Before the adsorption measurements, the samples were degassed under vacuum at 200°C for 12 hours. The surface area was calculated by Brunauer-Emmett-Teller (BET) mode. Confocal Raman spectra were acquired using the 488nm line of a Ar-ion laser (Melles Griot). The excitation beam was focused on the sample by a 50X long working distance microscope and the scattered light was analyzed by an air-cooled CCD (Labram HR, Horiba Jobin Yvon). The fluorescence was subtracted from the spectra for clarity. Solution NMR spectra were recorded on an Avance-300 Bruker spectrometer. All chemical shifts were measured relative to residual ¹H or ¹³C resonance in the deuterated solvent: C₆D₆, δ 7.15 ppm for ¹H, 128 ppm for ¹³C. All solid-state NMR spectra were recorded under MAS (νR = 10 kHz) on a Bruker Avance 500 spectrometer equipped with a standard 4-mm double-bearing probe head and operating at 500 and 125 MHz for ¹H and ¹³C respectively. The freshly prepared samples were introduced into the 4 mm zirconia rotor in a glove box

and tightly closed. Compressed air was used for both bearing and driving the rotors. Chemical shifts were given in ppm with respect to TMS as external reference for ^1H and ^{13}C NMR and $\text{Al}(\text{H}_2\text{O})_6^{3+}$ for ^{27}Al . Two-Dimensional Double-Quantum (DQ) Experiments were performed according to the following scheme: excitation of DQ coherences, t_1 evolution, reconversion into observable magnetization, Z-filter, and detection. Fourteen pC7 basic elements⁴⁶ were used for both excitation and reconversion steps, with 70 kHz rf field strength ($=7\omega_R$); the Z-filter delay was 200 μs . A total of 512 increments of 64 scans each was collected with 1.5 s recycle delay, which gave a total experiment time of 14 h. Determination of OH density was performed using ^1H solid-state NMR spectroscopy following the method described by Millot *et al.* using $\text{SiO}_2-(700)$ as reference.¹⁷ Deconvolution of NMR spectra was achieved using DMFIT#20100301.⁴⁷ Procedures related to Extended X-ray Absorption Fine Structure Spectroscopy (EXAFS) are described in detail below. XRD on powder have been realized at the Centre de Diffractométrie UCBL using a Bruker D8 Advance. Transmission electron microscopy (TEM) was recorded at the IRCÉLYON (Institut de Recherche Catalyse et Environnement de Lyon). Conventional transmission electron microscopy was performed using a JEOL 100 CX electron microscope. Samples were examined both dry and after dispersion in CH_2Cl_2 followed by solvent evaporation.

3.2. Pyridine adsorption on alumina monitored by IR spectroscopy

The alumina (RP) (40 ± 1 mg) was pressed into a 18 mm self-supporting pellet, adjusted in a sample holder, and introduced into a glass (quartz) reactor equipped with CaF_2 windows. The supports were calcined under air at 500°C , hydrated with a vapor pressure of degassed water at 100°C for 1h prior to treatment at the desired temperature. Under static vacuum, pyridine was adsorbed on $\text{Al}_2\text{O}_3-(300)$, $\text{Al}_2\text{O}_3-(300)$ and $\text{Al}_2\text{O}_3-(800)$ at room temperature. The reactor was then put under dynamic vacuum and heated to 100°C . IR spectrum was recorded after 2 hours.

3.3. Synthesis of 99% ^{13}C -labeled $^t\text{Bu}^*\text{CH}_2\text{Cl}$

99% ^{13}C -labeled $^*\text{CO}_2$ (2 L, 85 mmol) was added in a 1L round bottom flask to $^t\text{BuMgCl}$ (85 mmol) in frozen Et_2O (200 mL) by trapping using liquid N_2 bath. Acetone was added slowly to the liquid N_2 bath until the reaction media reach -77°C . After 1 h under constant stirring the solution was slowly warmed to RT while continuing stirring. The reaction media is hydrolyzed at -20°C using aqueous H_2SO_4 solution. The aqueous phase is then extracted 3 times with Et_2O . The organic phases are added, dried over MgSO_4 and concentrated. The concentration of the solution of $^t\text{Bu}^*\text{COOH}$ in Et_2O is determined by ^1H NMR, confirming a quantitative yield of the reaction. ^1H NMR (δ , 295 K, CD_2Cl_2 , 300 MHz)

10.71 (1 H, s, $(\text{CH}_3)_3\text{C}^*\text{COOH}$) 1.17 (9 H, d, $^3J_{\text{CH}} = 4.4$ Hz, $(\text{CH}_3)_3\text{C}^*\text{COOH}$); $^{13}\text{C}\{^1\text{H}\}$ NMR (δ , 295 K, CD_2Cl_2 , 75 MHz) 185.2 (s, $(\text{CH}_3)_3\text{C}^*\text{COOH}$) 38.4 (d, $^2J_{\text{CC}} = 55.8$ Hz, $(\text{CH}_3)_3\text{C}^*\text{COOH}$) 26.9 (s, $(\text{CH}_3)_3\text{C}^*\text{COOH}$) This $^t\text{Bu}^*\text{COOH}$ solution in Et_2O (85 mmol in Et_2O at 0.9M) was added dropwise to a suspension of LiAlH_4 (6.5 g, 170 mmol) in Et_2O (100 mL) at 0°C over 2 h while stirring. After addition the solution was slowly warmed to RT before being hydrolyzed with aqueous HCl solution at 0°C . The aqueous phase is then extracted 3 times with Et_2O . The organic phases are added, dried over MgSO_4 and concentrated. The concentration of the solution of $^t\text{Bu}^*\text{CH}_2\text{OH}$ in Et_2O is determined by ^1H NMR, confirming a quantitative yield of the reaction. ^1H NMR (δ , 295 K, CD_2Cl_2 , 300 MHz) 3.22 (2 H, d, $^1J_{\text{CH}} = 140$ Hz, $(\text{CH}_3)_3\text{C}^*\text{CH}_2\text{OH}$) 2.09 (1 H, s, $(\text{CH}_3)_3\text{C}^*\text{CH}_2\text{OH}$) 0.84 (9 H, d, $^3J_{\text{CH}} = 4.8$ Hz, $(\text{CH}_3)_3\text{C}^*\text{CH}_2\text{OH}$); $^{13}\text{C}\{^1\text{H}\}$ NMR (δ , 295 K, CD_2Cl_2 , 75 MHz) 73.3 (s, $(\text{CH}_3)_3\text{C}^*\text{CH}_2\text{OH}$) 32.4 (d, $^2J_{\text{CC}} = 37.7$ Hz, $(\text{CH}_3)_3\text{C}^*\text{CH}_2\text{OH}$) 26.0 (s, $(\text{CH}_3)_3\text{C}^*\text{CH}_2\text{OH}$) A part of the resulting $^t\text{Bu}^*\text{CH}_2\text{OH}$ solution (55 mmol in Et_2O at 5M) was diluted with DMF (10 mL) and added dropwise to a solution of Vilsmeier reagent [$\text{ClCH}=\text{N}(\text{CH}_3)_2$] (7.5 g, 55 mmol) in DMF (10 mL) over 1 h while stirring. After addition the solution was refluxed overnight. The product was purified by distillation affording 3.9 g of $^t\text{Bu}^*\text{CH}_2$ (65% yield). ^1H NMR (δ , 295 K, CD_2Cl_2 , 300 MHz) 3.22 (2 H, d, $^1J_{\text{CH}} = 150$ Hz, $(\text{CH}_3)_3\text{C}^*\text{CH}_2\text{Cl}$) 0.90 (9 H, d, $^3J_{\text{CH}} = 4.6$ Hz, $(\text{CH}_3)_3\text{C}^*\text{CH}_2\text{Cl}$) $^{13}\text{C}\{^1\text{H}\}$ NMR (δ , 295 K, CD_2Cl_2 , 75 MHz) 57.3 (s, $(\text{CH}_3)_3\text{C}^*\text{CH}_2\text{Cl}$) 36.6 (s, $(\text{CH}_3)_3\text{C}^*\text{CH}_2\text{Cl}$) 27.1 (s, $(\text{CH}_3)_3\text{C}^*\text{CH}_2\text{Cl}$)

3.4. Monitoring the synthesis of $1/\text{Al}_2\text{O}_{3-(500)}$ by IR spectroscopy

The oxide (40 mg) was pressed into an 18 mm self-supporting disk, adjusted in the sample holder, and put into a glass reactor equipped with CaF_2 windows. The supports were calcined under N_2/O_2 and partially dehydroxylated under vacuum at 500°C . The compound **1** was then sublimed under dynamic vacuum at 90°C onto the oxide disk, which typically turned yellow. The solid was then heated at 80°C for 2 h, and the excess of **1** was removed by reverse sublimation at 90°C and condensed into a tube cooled by liquid N_2 , which was then sealed off using a torch. An IR spectrum was recorded at each step.

3.5. Preparation of $1/\text{Al}_2\text{O}_{3-(500)}$ (RP)

A mixture of **1**, [$\text{W}(\equiv\text{C}^t\text{Bu})(\text{CH}_2^t\text{Bu})_3$] (311 mg, 660 μmol) and $\text{Al}_2\text{O}_{3-(500)}$ (RP) (2 g) was stirred at 66°C for 4 h under argon atmosphere. All volatile compounds were condensed into another reactor (of known volume) in order to quantify neopentane evolved during the grafting (654 μmol). Pentane (10 mL) was introduced into the reactor by distillation, and the solid was washed three times with pentane via filtration-condensation cycles. Af-

ter evaporation of the solvent, the resulting brown powder was dried under vacuum. Elemental analysis: W: 5.5%_{wt}, C: 5.2%_{wt}

3.6. Extended X-ray Absorption Fine Structure Spectroscopy (EXAFS)

X-ray absorption spectra were acquired at the SRS of the CCLRC in Daresbury (UK), using beam-line 9.3 (project # 50049), at room temperature at the tungsten L_{III} edge, with a double crystal Si(111) monochromator detuned 70% to reduce the higher harmonics of the beam. The spectra were recorded in the transmission mode between 10.05 and 11.45 keV. The supported W sample was packaged within a nitrogen filled dry box in a double air-tight sample holder equipped with kapton windows. This type of cell has already been used and proved to be very efficient for air-sensitive compounds. The spectra analyzed were the results of four such acquisitions and no evolution could be observed between the first and last acquisition. The data analyses were performed by standard procedures using in particular the program “Athena”⁴⁸ and the EXAFS fitting program “RoundMidnight”,^{49,50} from the “MAX” package. The program FEFF8 was used to calculate theoretical files for phases and amplitudes based on model clusters of atoms.⁵¹ The value of the scale factor, $S_0^2 = 0.98$, was determined from the spectrum of the reference compound, a benzene solution of W(≡C-*t*Bu)Np₃ (one carbon at 1.76(1) Å and three carbon atoms at 2.10(1) Å in the first coordination sphere). The refinements were performed by fitting the structural parameters N_i , R_i , σ_i and the energy shift, ΔE_0 (the same for all shells). The fit residue, ρ (%), was calculated by the following formula:

$$\rho = \frac{\sum_k [k^3 \chi_{\text{exp}}(k) - k^3 \chi_{\text{cal}}(k)]^2}{\sum_k [k^3 \chi_{\text{exp}}(k)]^2} \times 100$$

As recommended by the Standards and Criteria Committee of the International XAFS Society,⁵² the quality factor, $(\Delta\chi)^2/\nu$, where ν is the number of degrees of freedom in the signal, was also calculated and considered.

3.7. Monitoring the treatment of 1/Al₂O₃₋₍₅₀₀₎ (RP) under H₂ by IR spectroscopy

An excess of H₂ was added at room temperature in IR cell containing a self-supported disc of 1/Al₂O₃₋₍₅₀₀₎ (RP) prepared as described in subsection 3.5. The cell was heated at 150°C for 15h. The gaseous products were quantified by GC and IR spectra were recorded at each step.

3.8. Treatment of 1/Al₂O₃₋₍₅₀₀₎ (RP) under H₂

2g of 1/Al₂O₃₋₍₅₀₀₎ (RP) was heated at 150 °C in the presence of a large excess of anhydrous H₂ (550 torr) to afford WH/Al₂O₃₋₍₅₀₀₎ (RP). After 15 h, the gaseous products were quantified by GC: mixture of methane and ethane (*ca.* 20:1) corresponding to 1340 μmol of ^tBuCH₃. Elemental analysis W: 5.5%_{wt}, C: 0.9%_{wt}

3.9. Reaction of WH/Al₂O₃₋₍₅₀₀₎ (RP) with D₂

An excess of D₂ (600 Torr, 460 equiv.) was added at room temperature to 200 mg of WH/Al₂O₃₋₍₅₀₀₎ (RP). After a 1 h treatment at 80°C the reactor was evacuated. 150 mg of the resulting material, WD/Al₂O₃₋₍₅₀₀₎ (RP), was collected in the glove box for DRIFT and NMR characterizations. The remaining material was then treated 1h with an excess of H₂ at 80°C. The resulting material was analyzed by DRIFT spectroscopy.

3.10. Hydrolysis of WH/Al₂O₃₋₍₅₀₀₎ (RP)

100 mg of WH/Al₂O₃₋₍₅₀₀₎ (RP) was treated with an excess of H₂O in gas phase (17 Torr). After 1 hour the gaseous products were quantified by GC. The main hydrolysis product is neopentane (15 μmol).

3.11. Activation of methane on WH/Al₂O₃₋₍₅₀₀₎ (RP) in continuous flow reactor

In a glove box, WH/Al₂O₃₋₍₅₀₀₎ (RP) (375 mg; 5.5 wt% W) was loaded into a stainless steel half inch cylinder fixed-bed reactor. Methane was passed at 3 mL.min⁻¹ over the catalyst bed at 50 barg starting from 25°C to 350°C. Hydrocarbon products and hydrogen were analyzed online by GC (HP 8890 chromatograph fitted with an Al₂O₃/KCl 50 m x 0.32 mm capillary column, FID detector for hydrocarbons with a 3-m molecular sieve column and a catharometer for hydrogen). See description of the reactor in Appendix B and subsection 2.1 in Chapter 2

4. Reference and Notes

- (1) Basset, J. -M.; Psaro, R.; Roberto, D.; and Ugo, R. *Modern surface organometallic chemistry*, Basset, J. -M.; Psaro, R.; Roberto, D.; and Ugo, R., Ed.; Wiley-VCH ; 2009.
- (2) Tullock, C. W.; Mulhaupt, R.; and Ittel, S. D. *Die Makromolekulare Chemie, Rapid Communications*. 1989, 10, 19-23.
- (3) Tullock, C. W.; Tebbe, F. N.; Mulhaupt, R.; Ovenall, D. W.; Setterquist, R. A.; and Ittel, S. D. *Journal of Polymer Science Part A: Polymer Chemistry*. 1989, 27, 3063-3081.
- (4) Collette, J. W.; Tullock, C. W.; MacDonald, R. N.; Buck, W. H.; Su, A. C. L.; Harrell, J. R.; Mulhaupt, R.; and Anderson, B. C. *Macromolecules*. 1989, 22, 3851-3858.

- (5) Digne, M.; Sautet, P.; Raybaud, P.; Euzen, P.; and Toulhoat, H. *Journal of Catalysis*. 2002, *211*, 1-5.
- (6) Marks, T. J. *Accounts of Chemical Research*. 1992, *25*, 57-65.
- (7) Toscano, P. J. and Marks, T. J. *Organometallics*. 1986, *5*, 400-402.
- (8) Jezequel, M.; Dufaud, V.; Ruiz-Garcia, M. J.; Carrillo-Hermosilla, F.; Neugebauer, U.; Niccolai, G. P.; Lefebvre, F.; Bayard, F.; Corker, J.; Fiddy, S.; Evans, J.; Broyer, J. -P.; Malinge, J.; and Basset, J. -M. *Journal of the American Chemical Society*. 2001, *123*, 3520-3540.
- (9) Ahn, H. and Marks, T. J. *Journal of the American Chemical Society*. 2002, *124*, 7103-7110.
- (10) Delgado, M. *PhD Thesis*. 2010.
- (11) Le Roux, E.; Taoufik, M.; Copèret, C.; de Mallmann, A.; Thivolle-Cazat, J.; Basset, J. -M.; Maunders, B. M.; and Sunley, G. J. *Angewandte Chemie*. 2005, *117*, 6913-6916.
- (12) Le Roux, E.; Taoufik, M.; Copèret, C.; de Mallmann, A.; Thivolle-Cazat, J.; Basset, J. -M.; Maunders, B. M.; and Sunley, G. J. *Angewandte Chemie International Edition*. 2005, *44*, 6755-6758.
- (13) Joubert, J.; Delbecq, F.; Sautet, P.; Roux, E. L.; Taoufik, M.; Thieuleux, C.; Blanc, F.; Coperet, C.; Thivolle-Cazat, J.; and Basset, J. M. *J. Am. Chem. Soc.* 2006, *128*, 9157-9169.
- (14) Joubert, J.; Delbecq, F.; Thieuleux, C.; Taoufik, M.; Blanc, F.; Copèret, C.; Thivolle-Cazat, J.; Basset, J. -M.; and Sautet, P. *Organometallics*. 2007, *26*, 3329-3335.
- (15) Nedez, C.; Theolier, A.; Lefebvre, F.; Choplin, A.; Basset, J. M.; and Joly, J. F. *Journal of the American Chemical Society*. 1993, *115*, 722-729.
- (16) Deng, F.; Wang, G. X.; Du, Y. R.; Ye, C. H.; Kong, Y. H.; and Li, X. D. *Solid State Nuclear Magnetic Resonance*. 1997, *7*, 281-290.
- (17) Millot, N.; Santini, C. C.; Lefebvre, F.; and Basset, J. M. *Comptes Rendus Chimie*. 2004, *7*, 725-736.
- (18) McMillan, M.; Brinen, J. S.; and Haller, G. L. *Journal of Catalysis*. 1986, *97*, 243-247.
- (19) Knözinger, H. and Ratnasamy, P. *Catalysis Reviews-Science and Engineering*. 1978, *17*, 31-70.
- (20) Parry, E. P. *Journal of Catalysis*. 1963, *2*, 371 - 379.
- (21) Pichat, P.; Mathieu, M. V.; and Imelik, B. *Bulletin de la société chimique de france*. 1969, 2611.
- (22) Ertl, G.; Knözinger, H.; and Weitkamp, J. *Handbook of heterogeneous catalysis*, Ertl, G.; Knözinger, H.; and Weitkamp, J., Ed.; VCH: Weinheim; 1997.
- (23) Schekler-Nahama, F.; Clause, O.; Commereuc, D.; and Saussey, J. *Applied Catalysis A: General*. 1998, *167*, 237 - 245.
- (24) Ballinger, T. H. and Yates, J. T. *Langmuir*. 1991, *7*, 3041-3045.
- (25) Joubert, J.; Fleurat-Lessard, P.; Delbecq, F.; and Sautet, P. *The Journal of Physical Chemistry B*. 2006, *110*, 7392-7395.
- (26) Walter, T. H.; Thompson, A.; Keniry, M.; Shinoda, S.; Brown, T. L.; Gutowsky, H. S.; and Oldfield, E. *Journal of the American Chemical Society*. 1988, *110*, 1065-1068.
- (27) Finch, W. C.; Gillespie, R. D.; Hedden, D.; and Marks, T. J. *Journal of the American Chemical Society*. 1990, *112*, 6221-6232.
- (28) Bruno, J. W.; Smith, G. M.; Marks, T. J.; Fair, C. K.; Schultz, A. J.; and Williams, J. M. *Journal of the American Chemical Society*. 1986, *108*, 40-56.
- (29) Cheon, J.; Rogers, D. M.; and Girolami, G. S. *Journal of the American Chemical Society*. 1997, *119*, 6804-6813.
- (30) Le Roux, E.; Taoufik, M.; Chabanas, M.; Alcor, D.; Baudouin, A.; Coperet, C.; Thivolle-Cazat, J.; Basset, J. -M.; Lesage, A.; Hediger, S.; and Emsley, L. *Organometallics*. 2005, *24*, 4274-4279.

- (31) Dobbs, D. A.; Schrock, R. R.; and Davis, W. M. *Inorganica Chimica Acta*. 1997, 263, 171-180.
- (32) Le Roux, E. *PhD Thesis*. 2004.
- (33) Podall, H. E.; Petree, H. E.; and Zietz, J. R. *The Journal of Organic Chemistry*. 1959, 24, 1222-1226.
- (34) Kim, D. S.; Ostromecki, M.; and Wachs, I. E. *Journal of Molecular Catalysis a-Chemical*. 1996, 106, 93-102.
- (35) Geen, H.; Titman, J. J.; Gottwald, J.; and Spiess, H. W. *Chemical Physics Letters*. 1994, 227, 79-86.
- (36) Geen, H.; Titman, J. J.; Gottwald, J.; and Spiess, H. W. *Journal of Magnetic Resonance, Series A*. 1995, 114, 264-267.
- (37) Friedrich, U.; Schnell, I.; Demco, D. E.; and Spiess, H. W. *Chemical Physics Letters*. 1998, 285, 49-58.
- (38) Brown, S. P. and Spiess, H. W. *Chem. Rev.* 2001, 101, 4125-4156.
- (39) Rataboul, F.; Baudouin, A.; Thieuleux, C.; Veyre, L.; Coperet, C.; Thivolle-Cazat, J.; Basset, J. M.; Lesage, A.; and Emsley, L. *J. Am. Chem. Soc.* 2004, 126, 12541-12550.
- (40) Larabi, C.; Merle, N.; Norsic, S.; Taoufik, M.; Baudouin, A.; Lucas, C.; Thivolle-Cazat, J.; de Mallmann, A.; and Basset, J. -M. *Organometallics*. 2009, 28, 5647-5655.
- (41) Soulivong, D.; Norsic, S.; Taoufik, M.; Coperet, C.; Thivolle-Cazat, J.; Chakka, S.; and Basset, J. -M. *Journal of the American Chemical Society*. 2008, 130, 5044-5045.
- (42) Armarego, W. L. F. and Chai, C. L. L. *Purification of laboratory chemicals*, Butterworth Heinemann; 2009.
- (43) Handy, L. B.; Sharp, K. G.; and Brinckman, F. E. *Inorganic Chemistry*. 1972, 11, 523-531.
- (44) Clark, D. N. and Schrock, R. R. *Journal of the American Chemical Society*. 1978, 100, 6774-6776.
- (45) Schrock, R. R.; Clark, D. N.; Sancho, J.; Wengrovius, J. H.; Rocklage, S. M.; and Pedersen, S. F. *Organometallics*. 1982, 1, 1645-1651.
- (46) Hohwy, M.; Jakobsen, H. J.; Eden, M.; Levitt, M. H.; and Nielsen, N. C. *The Journal of Chemical Physics*. 1998, 108, 2686.
- (47) Massiot, D.; Fayon, F.; Capron, M.; King, I.; Le Calvé, S.; Alonso, B.; Durand, J. O.; Bujoli, B.; Gan, Z.; and Hoatson, G. *Magnetic Resonance in Chemistry*. 2002, 40.
- (48) Ravel, B. , and Newville, M. , *J. Synchrotron Rad.* 2005, 12, 537-541.
- (49) Michalovicz, A. In *Logiciels pour la Chimie*; S.F.C.: Paris, 1991; p. 102.
- (50) Michalovicz, A.; Moscovici, J.; Muller-Bouvet, D.; and Provost, K. *Journal of Physics: Conference Series*. 2009, 190, 012034.
- (51) Ankudinov, A. L.; Ravel, B.; Rehr, J. J.; and Conradson, S. D. *Phys. Rev. B*. 1998, 58, 7565.
- (52) *Reports of the Standards and Criteria Committee of the International XAFS Society*: http://ixs.iit.edu/subcommittee_reports/sc/. 2000.

Chapter 3

Catalytic activity of WH/Al₂O₃ for the direct conversion of ethylene to propylene

1. Introduction	95
2. Results and discussions	98
2.1. Description of the reactor.....	98
2.2. Direct conversion of ethylene to propylene of over WH/Al₂O₃₋₍₅₀₀₎	99
2.3. Determination of the reaction mechanism.....	99
2.3.1. Determination of the initiation step.....	100
2.3.2. Influence of the initial step on conversion	100
2.3.3. Study of the early stages of catalysis.....	102
2.3.4. Contact time study.....	103
2.3.5. Introduction of 1-butene.....	106
2.3.6. Proposed mechanism.....	107
2.4. Optimization of the catalytic performances	108
2.4.1. Influence of the nature of the support.....	108
2.4.1. Influence of the support pretreatment temperature	110
2.5. Influence of the reaction temperature.....	111
2.5.1. Catalytic tests.....	112
2.5.2. Study of the carbonaceous deposits on the catalyst in function of the temperature of reaction	115
2.6. Characterizations of the aged catalyst, study of the deactivation mechanism	117
2.6.1. Drift and NMR spectroscopies studies	117
2.6.2. TGA and DSC study.....	119
2.6.3. Proposed deactivation mechanism	121
2.7. Attempts of regeneration of the catalyst	122
2.7.1. Regeneration after catalysis.....	123
2.7.2. “On-stream” regeneration.....	124
2.8. Conclusion.....	126
3. Experimental section	127
4. Reference and Notes	127

1. Introduction

The production of propylene has received growing attention in recent years due to its increasing demand.¹ Propylene is mainly produced as a by-product of ethylene,² as discussed in chapter 1. A new process that allows the conversion of ethylene to propylene will be economically relevant. The preparation of the supported tungsten hydride presented in Chapter 2 affords a catalyst with a singular coordination sphere that performs unprecedented reactions such as alkane metathesis³ or methane non-oxidative coupling.⁴ The mechanism of these reactions involves a carbene alkylidene and a carbene hydride species. This chapter will focus on the obtention of propylene from ethylene alone using this supported tungsten hydride.



Scheme 3.1 Reaction of direct conversion of ethylene to propylene

The conversion of three molecules of ethylene to two moles of propylene, as presented in Scheme 3.1, is highly thermodynamically favored. Below 900 K the standard Gibbs free enthalpy is negative, affording a large conversion of ethylene at equilibrium. Moreover, under 600 K the conversion of ethylene is complete at the equilibrium (Figure 3.1).

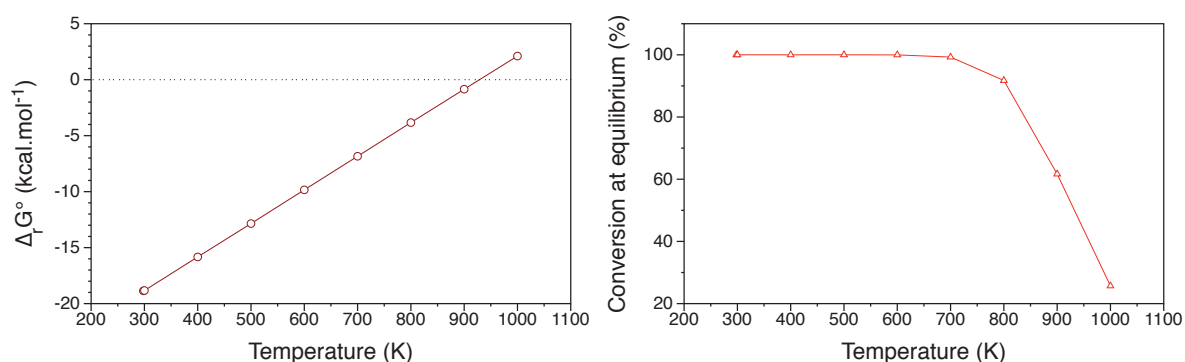
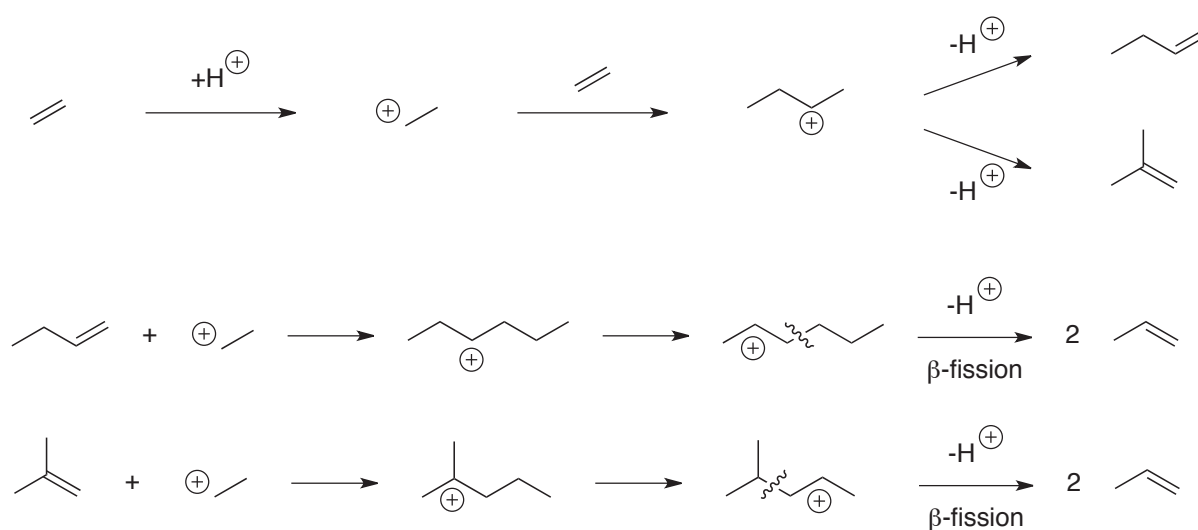


Figure 3.1 Thermodynamics' data for the ethylene to propylene reaction: left: $\Delta_r G^\circ$ vs. temperature; right conversion at equilibrium vs. temperature. Data calculated from tables⁵

A few examples of the direct transformation of ethylene into propylene have been reported. For instance, a deficiency of ethylene formation compared to butenes has been observed during the metathesis of propylene catalyzed by $[\text{Mo}(\text{CO})_6]/\text{Al}_2\text{O}_3$ and attributed to the direct transformation of ethylene into propylene.⁶ This reaction has also been observed, with a short lifetime, during Fischer–Tropsch synthesis in the presence of small iron nanoclusters formed by the thermal decomposition of $[\text{HFe}_3(\text{CO})_{11}]/\text{MgO}$.⁷ This reaction has also been reported to proceed with catalysts based on europium or ytterbium de-

posited on coal in combination with titanium compounds (TiCl_4 , $\text{Ti}(\text{OiPr})_4$)⁸ as well as with WO_3 on various oxides⁹ MO_x/SiO_2 ¹⁰ or Ru/SiO_2 catalysts.¹¹ However, the catalytic performances of all these systems were either not quantified or proved to be very low as they were only observed in closed recirculation systems.

A significant example of direct conversion of ethylene to propylene in terms of selectivity and productivity is reported using Zeolites.¹² The proposed mechanism of formation of propylene from ethylene over acidic catalyst implies the trimerization of ethylene. The cracking of the formed hexenes leads to propylene (Scheme 3.2).



Scheme 3.2 Mechanism proposed by Oikawa *et al.* for the conversion of ethylene to propylene over acidic catalyst

During their investigation Oikawa *et al.* shed light upon the importance of the pore size and the acidity of the catalyst to obtain a good selectivity and conversion respectively. They have identified SAPO-34 as the most efficient catalyst for direct ethylene to propylene conversion. Its pore size is similar to the kinetic diameter of the propylene, giving thus a good selectivity in this molecule, and its acid strength is intermediate, affording the best conversion rate. When the reaction is performed at 450°C , after 1 hour on stream, they obtain a propylene production rate of $7.00 \text{ mmol}_{\text{C}_3\text{H}_6} \cdot \text{g}^{-1} \cdot \text{h}^{-1}$ (79% selectivity) is obtained. Unfortunately, for the sake of comparison, no longer times on stream are mentioned.

Another example of direct conversion of ethylene to propylene has been described using nickel catalyst supported on mesoporous silica.^{13,14} In that example the catalyst shows a constant activity at 400°C , during 10 hours on stream, with a propylene production of $1.85 \text{ mmol}_{\text{C}_3\text{H}_6} \cdot \text{g}^{-1} \cdot \text{h}^{-1}$ and a selectivity of 49 %. The explanation was given by a mechanism, in which ethylene dimerization on Ni sites afford 1-butene that can be iso-

merized to 2-butene on acidic sites. 2-butene is supposed to react via cross-metathesis reaction with non-reacted ethylene. Ivamoto claims that Ni(I) are able to perform metathesis reaction by the formation of a nickel carbene (Ni(III)) intermediate. The large pore size of MCM-41 is the major argument presented to exclude an acidic mechanism such as this presented for SAPO-34. Nevertheless, after calcination of impregnated nickel nitrate, it can be agreed that the surface of the catalyst will exhibit silicates with non-negligible acidity and the high temperature of reaction do not exclude cracking of higher olefin to provide propylene as observed by Oikawa *et al.*

Finally, tungsten hydrides supported on alumina prepared by SOMC have shown outstanding activities for this reaction. Nevertheless, after this high initial activity, a fast deactivation of the catalyst is observed.¹⁵ In Chapter 2, the preparation of **WH/Al₂O₃-(500)** has been described. According NMR, IR, RAMAN spectroscopies, mass balance analysis, DFT calculations and EXAFS, it can be assumed that two different tungsten hydride species are present at the surface of this catalyst, *i.e.* a neutral oxoaluminoxo tungsten trishydride and a cationic bisaluminoxo trishydride, along with aluminum surface species, *i.e.* Al-Np and Al-H. These different species may have a different role in the catalytic activity, particularly the cationic tungsten species, highly electrophilic, should react singularly with ethylene. The presence of this different species raises three questions: i) What is the role of these different species in term of activity and mechanism? ii) Is the cationic tungsten species involved in the high initial activity? iii) What is the role of each surface species in the deactivation process?

In this chapter the performance of supported tungsten hydride for this reaction will be presented in details. It will be focused on determination of the reaction mechanism, optimization of parameters in order to increase the activity and determination of the deactivation pathway. The next chapters will be devoted to the role of the different species present at the surface of **WH/Al₂O₃-(500)** in its catalytic activity.

2. Results and discussions

2.1. Description of the reactor

The catalytic studies were performed in a stainless-steel microreactor (see Schematic representation in Appendix 3) from PID Eng&Tech. The reactor can be divided into three parts. The first one manages liquid and gas flow rates. The flow rate was controlled and monitored by a mass-flow controller for gases and by a piston pump for the liquids. A pressure regulator adjusted the reactor pressure. The second part is the reaction chamber that can be filled in a glove box, and its temperature controlled during the catalytic test. The reactor is tubular with a diameter of 1 cm and a length of 18 cm. Its volume can be varied by including stainless-steel inserts. The last part is monitoring of different parameters including pressure, flows, temperature that were monitored via indicators/regulators and a Labview interface. After release of the pressure (via a control pressure valve), the gases are also analyzed by online gas chromatography.

In this chapter, the direct conversion of ethylene to propylene is studied. For all experiments the test was carried out at atmospheric pressure. The temperature of the catalytic bed was adjusted to the desired value. Except for the contact time study, the mass of catalyst is adjusted such as the ethylene/tungsten ration reaches $R = 1.7 \text{ mol}_{\text{C}_2\text{H}_4} \cdot \text{mol}_{\text{W}}^{-1} \cdot \text{min}^{-1}$ with a flow rate of $4 \text{ mL} \cdot \text{min}^{-1}$ of ethylene. The standard reaction temperature is 150°C .

The ethylene conversion and selectivity were therefore calculated as follows:

$$\text{Conversion} = \frac{\text{mol of ethylene converted}}{\text{mol of ethylene introduced}}$$

$$\text{Selectivity}_i = \frac{\text{mol of product}_i \text{ formed}}{\text{mol of ethylene converted}}$$

The definition of the conversion is the number of moles of ethylene converted divided by the number of moles of ethylene introduced divided. The selectivity for a product i is equal to the number of mol of product i formed divided by the number of mol of ethylene converted.

2.2. Direct conversion of ethylene to propylene of over $\text{WH}/\text{Al}_2\text{O}_3-(500)$

The catalytic performances of $\text{WH}/\text{Al}_2\text{O}_3-(500)$, *i.e.* the catalyst prepared from γ -Alumina pretreated under *vacuum* at 500°C (see Chapter 2) have been tested for the direct conversion of ethylene to propylene. This will be the reference experiment for this chapter.

Propylene was obtained selectively (95%) by passing ethylene over $\text{WH}/\text{Al}_2\text{O}_3-(500)$ in a continuous-flow reactor ($P_{\text{C}_2\text{H}_4} = 1 \text{ bar}$, $T = 150^\circ\text{C}$, flow rate $4 \text{ mL}\cdot\text{min}^{-1}$ or volume hourly space velocity (VHSV) 400 h^{-1}). The reaction presents an initial steep maximal conversion rate of $0.6 \text{ mol}_{\text{C}_2\text{H}_4}\cdot\text{mol}_{\text{W}}^{-1}\cdot\text{min}^{-1}$ before reaching a pseudo plateau of $0.1 \text{ mol}_{\text{C}_2\text{H}_4}\cdot\text{mol}_{\text{W}}^{-1}\cdot\text{min}^{-1}$ with an overall TON of 930 after 120 h on stream. The selectivity for propylene increases rapidly up to a plateau at 92%, while that of butenes remains below 6.0%. Higher olefins are present in only trace amounts (less than 1.0 %). These results correspond to a productivity of $9.57 \text{ mmol}_{\text{C}_3\text{H}_6}\cdot\text{g}^{-1}\cdot\text{h}^{-1}$ at the maximum and $2.07 \text{ mol}_{\text{C}_3\text{H}_6}\cdot\text{g}^{-1}\cdot\text{h}^{-1}$ at pseudo plateau.

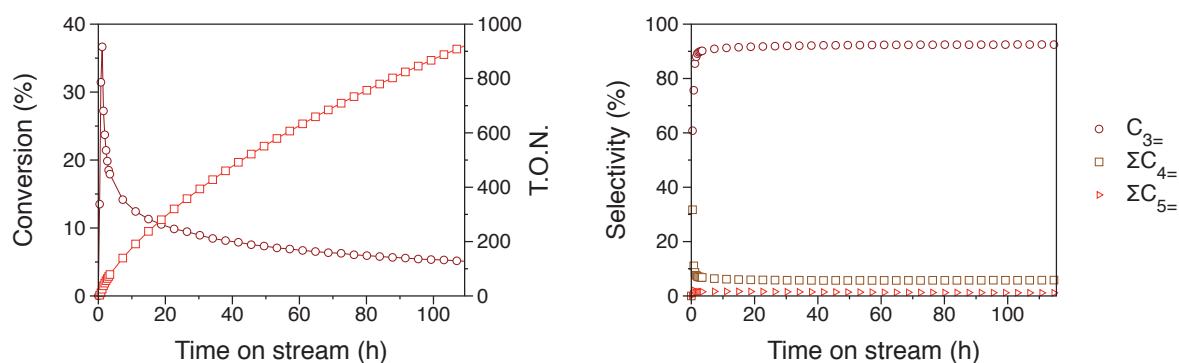


Figure 3.2 Conversion of ethylene (●), TON (□) and selectivity vs. time on stream

During the 10 first hours on stream, a fast deactivation rate of the catalyst is observed ($2.40\%\cdot\text{h}^{-1}$), before reaching a pseudo-plateau with a much lower deactivation rate ($0.05\%\cdot\text{h}^{-1}$). Despite this phenomenon, the selectivity is constant for all catalytic run. It should be presumed that two different sites are able to achieve the conversion of ethylene to propylene: the first one has an high production rate but deactivate quickly whereas the second one has a lower production rate and deactivate slowly. A study of the reaction mechanism, during the first hours and at pseudo steady state, will thus be performed.

2.3. Determination of the reaction mechanism

The complete mechanism of the direct conversion of ethylene to propylene was studied by identification of the products released in early stage of catalysts, influence of contact time and the introduction at pseudo steady state of supposed primary product in ethylene feed.

2.3.1. Determination of the initiation step

A short initiation period is observed in the early stage of catalysis, showing that the tungsten hydride is only the precatalyst of the direct conversion of ethylene to propylene. The initiation step was elucidated by identifying the products formed, in dynamic reactor, while heating to the reaction temperature of 150°C .

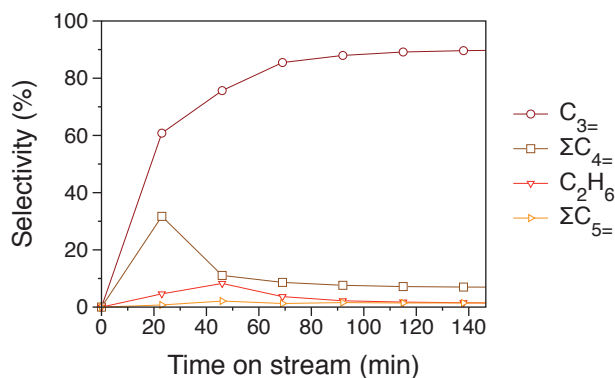
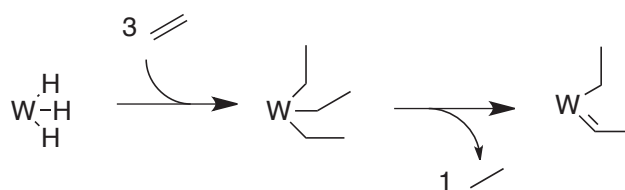


Figure 3.3 Selectivity of the ethylene to propylene reaction in the early stage of catalysis vs. time on stream

Interestingly a non-negligible amount of ethane is observed during the 100 first minutes of catalysis (Figure 3.3). About one equivalent of ethane is released per tungsten center after initial contact of $\text{WH}/\text{Al}_2\text{O}_3$ with ethylene. The reactivity of $\text{WH}/\text{Al}_2\text{O}_3\text{-(500)}$ toward ethylene in batch reactor has also confirmed this equimolar evolution of ethane. This finding suggests the formation of a surface tungsten ethyl-ethylidene species, $[\text{W}](\text{CH}_2\text{CH}_3)(=\text{CHCH}_3)$ from tungsten-triethyl $[\text{W}](\text{CH}_2\text{CH}_3)_3$, by the following elementary steps insertion of three molecules of ethylene in the trihydride, elimination of one ethane by α -H transfer to form a carbene (Scheme 3.3).¹⁵



Scheme 3.3 Formation of the active species

2.3.2. Influence of the initial step on conversion

When direct conversion of ethylene to propylene by $\text{WH}/\text{Al}_2\text{O}_3\text{-(500)}$ is performed in dynamic reactor, it can be noticed that the conversion is very high in the early stage of the catalysis. This high conversion may be explained by an high initial activity of the catalyst followed by a fast deactivation. The formation of the active species or ethylene adsorption

may also justify this high initial conversion. The mass balance of the reaction has to be studied in order to discriminate the causes of this phenomenon.

In this subsection, the mass balance during the reaction is studied using methane (considered as inert toward $\text{WH}/\text{Al}_2\text{O}_3\text{-}(500)$ in these conditions) as internal standard. The reaction has thus been performed in standard conditions but adding 10%± of methane in the ethylene feed. The ratios of ethylene that come in and out of the reactor toward methane have been plotted (Respectively $C_{2=\text{IN}}/\text{CH}_4$ and $C_{2=\text{OUT}}/\text{CH}_4$ on Figure 3.4). In the same way, the ratio of products (everything but ethylene) that comes out from the reactor has been plotted ($\text{Products}_{\text{OUT}}/\text{CH}_4$ on Figure 3.4). Finally, in order to check if the carbon balance is equilibrated, the sum of $C_{2=\text{OUT}}/\text{CH}_4$ and $\text{Products}_{\text{OUT}}/\text{CH}_4$ has been plotted ($(C_{2=\text{OUT}} + \text{Products}_{\text{OUT}})/\text{CH}_4$ on Figure 3.4). If the first plot, *i.e.* gases coming in the reactor, and the last plot, *i.e.* gases coming out of the reactor fits, hence the carbon balance is equilibrated (Eq.3.1).

$$\frac{C_{2=\text{IN}}}{\text{CH}_4} = \frac{C_{2=\text{OUT}}}{\text{CH}_4} + \frac{\text{Products}_{\text{OUT}}}{\text{CH}_4} \quad \text{Eq. 3.1}$$

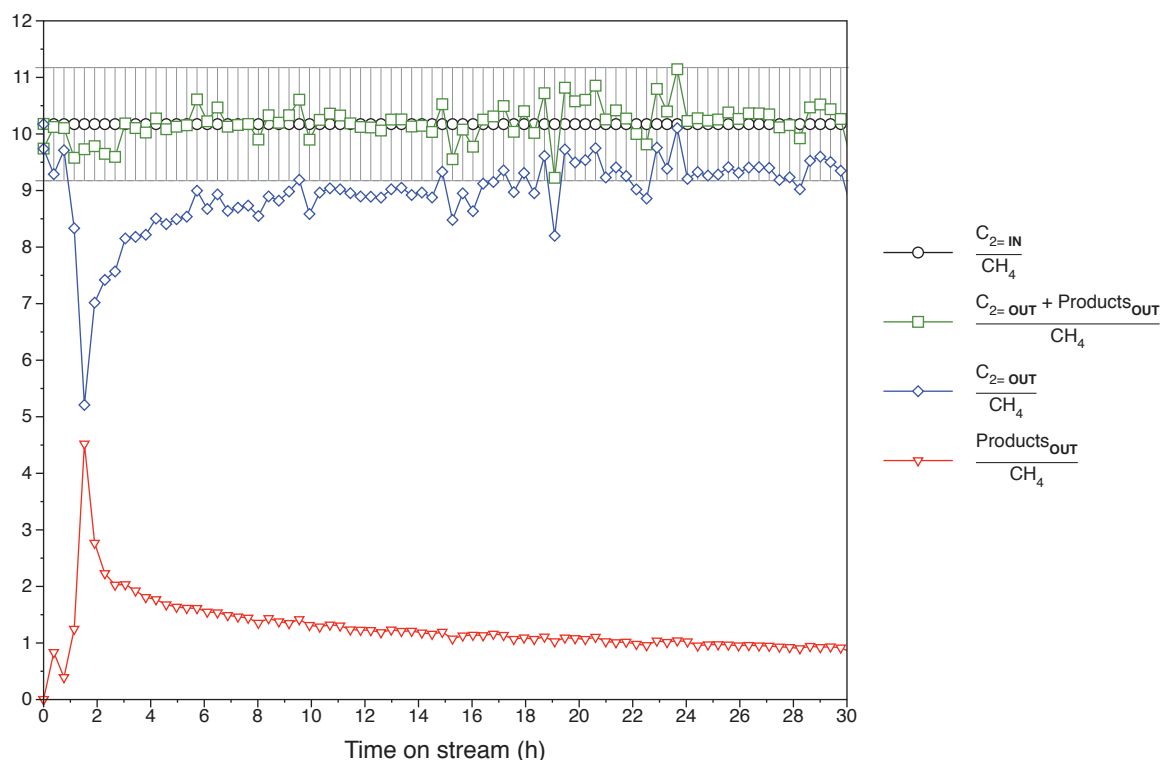


Figure 3.4 Carbon balance of the ethylene to propylene reaction vs. time on stream

Figure 3.4 shows that whatever the time on stream, the carbon balance is equilibrated, which implies that at each moment, the mass of gas going in and coming out of the reactor is equivalent, within experimental error ($\pm 10\%$), to the mass of ethylene coming in the reactor respecting Eq.3.1.

Therefore, for this experiment, 360 mg of 6%_wt W catalyst were used. Ethane is observed during one hour, after this time the activation is considered as completed. The mass of catalyst contains 0.12 mmol of tungsten. So it needs $3 \times 0.12 = 0.36$ mmol of Ethylene for the activation. The Ethylene flow rate during the reaction is $4 \text{ mL}\cdot\text{min}^{-1}$ corresponding to $0.16 \text{ mmol}\cdot\text{min}^{-1}$. During the activation phase of 100 min, 16 mmol (0.16×100) of ethylene pass through the catalytic bed. Thus the ratio of the ethylene consumed by the activation to the ethylene provided during the activation is less than 3% of the feed ($0.36 / 9.6 = 3,7\%$), which is less than the incertitude of the ratio of ethylene to methane.

Regarding these results it is clear that this high initial activity is due to the catalytic activity and neither to the formation of the active species nor to ethylene adsorption.

2.3.3. Study of the early stages of catalysis

A first insight into the mechanism of the direct conversion of ethylene to propylene is given by a careful study of the product selectivity at the early stage of the catalysis where the conversion of ethylene is extremely high for what is believed to be a multistep reaction, but where the formation of the active species is incomplete. Evolution of ethane shows that α -H abstraction leading to the carbenic species occurs only for the first 100 min. At short time on stream butene isomers appear in the gas phase (Figure 3.3). The initial 1-butene/trans-2-butene/cis-2-butene/isobutene isomeric distribution of 5.2 :1:2 :3.1 ($t = 20$ min) changed over time, tending to the ratio 1.1:3.2:1:0.7 (Figure 3.5). This ratio reveals a deficiency of 2-butenes and isobutene compared to the thermodynamic equilibrium values (1:8 :3.84 :29.6).⁵

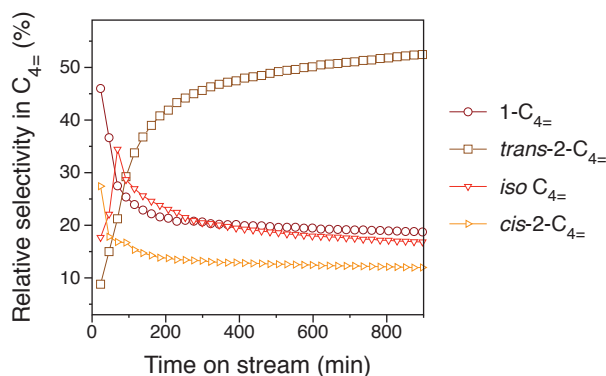
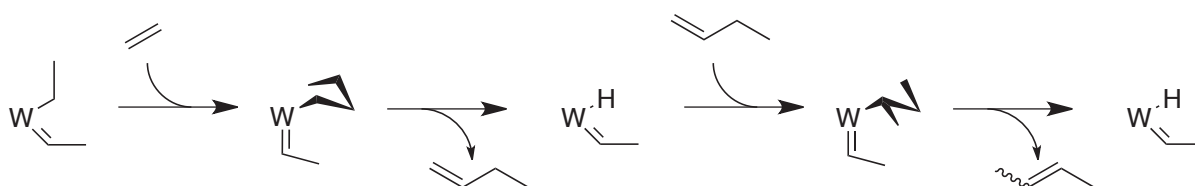


Figure 3.5 Relative selectivity of the butenes vs. time on stream

These results suggest that the primary step is the dimerization of ethylene to 1-butene is followed by a fast isomerization of 1-butene to cis- and trans-2-butenes. The newly formed catalyst $[W](CH_2CH_3)(=CHCH_3)$ can insert ethylene into the ethyl moiety to form an n-butyl species, which affords 1-butene by β -H elimination.¹⁶ Then cis- and trans-2-butenes are obtained after reinsertion of the newly formed 1-butene followed by a second β -H elimination of the sec-butyl species (Scheme 3.4) as proposed by Tolman for the isomerisation of 1-butene to 2-butene by nickel hydride.¹⁷



Scheme 3.4 Proposed mechanism for the formation of 1-butene and 2-butene.

After exposition of $WH/Al_2O_{3-(500)}$ to an excess of dry O_2 , in order to poison all the tungsten active site of the catalyst, isomerization of 1-butene was tested in continuous flow reactor in similar condition. No activity was observed, confirming that tungsten promotes the isomerization assuming that the oxygen treatment did not affect the isomerization activity of alumina.

2.3.4. Contact time study

In order to understand the propagation mechanism of this reaction, a complete contact time study was performed. The observation of the contact time ($VHSV^{-1}$) influence on the catalyst performances, *i.e.* conversion and selectivity, reveals two majors information on the catalytic process.^{18,19} First, if there is a linear dependence between conversion and contact time, that can be extrapolated to zero at zero contact time, it means that the catalytic process is not affected by mass transfer limitations. The observations can thus be interpreted regarding chemical steps: it is chemical regime. Then, the extrapolated selectivities at zero contact time allow a reliable determination of real primary products. Therefore the reduction of contact time decreases the period when reagents and active sites can interact, reducing *de facto* the formation of secondary products.

In subsection 2.2, it has been observed that the selectivity is constant with time on stream, whereas the deactivation rate is high in the early stage of the catalysis before reaching a pseudo-plateau. To determine if the mechanism of the reaction is the same dur-

ing this two period, contact time study was performed for different time on stream. Thus four experiments of 46h were carried out at different contact times (Table 3.1)

Table 3.1 Conditions for the four experimental runs, Pressure: 1 Bar, Temperature: 150 °C

Runs	1	2	3	4
VHSV (h^{-1})	463	928	1855	3800
VHSV ⁻¹ (min)	0.130	0.065	0.032	0.016

Plotting the conversion vs. inverse space velocity (Figure 3.6) confirms that the chemical regime is maintained, whatever the time on stream, in the range of VHSV studied. At each time on stream there is a strong linear dependence, which can be extrapolated to a zero conversion at infinite VHSV, between conversion and contact time.

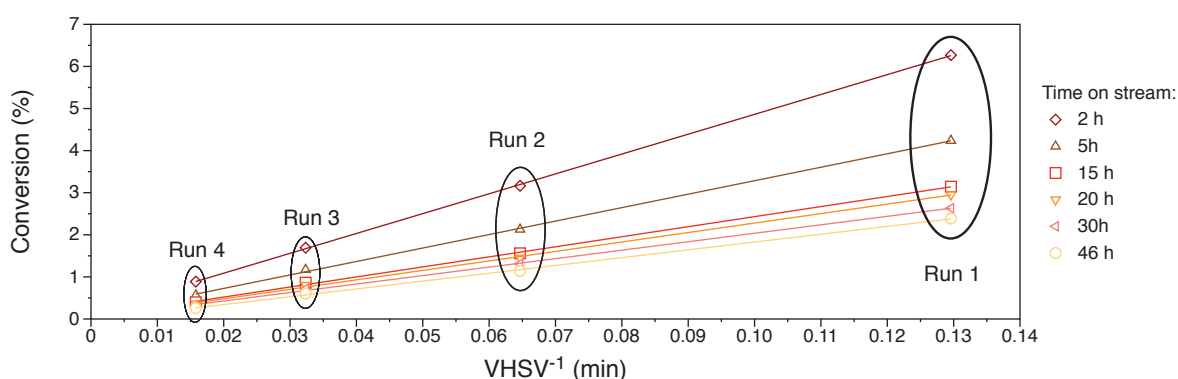


Figure 3.6 Conversion vs. inverse space velocity for 2 to 46 hours on stream with linear fits.

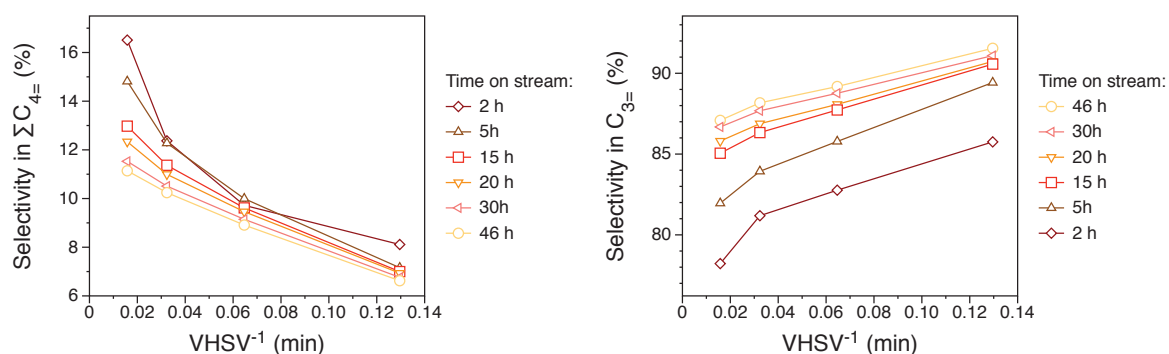


Figure 3.7 Selectivity in butenes (left) and propylene (right) at 150°C for different reaction time vs. inverse space velocity

Figure 3.7 indicates that butenes are primary products, since the selectivity intercept with the y-axis extrapolates to a non-zero value, and that propene is formed in a reaction that consumes butenes, since their curves are mirror images at any flow rate. Furthermore, according to Figure 3.8, the formation of 1-butene also appears to precede that of other butenes since it is the only one for which the selectivity increases with decreasing inverse

space velocity. It is notable that whatever the time on stream, the global selectivity and butenes partial selectivity *vs.* $VHSV^{-1}$ have the same profiles. Indeed, the mechanism of the conversion of ethylene to propylene stays the same regardless deactivation of the catalyst.

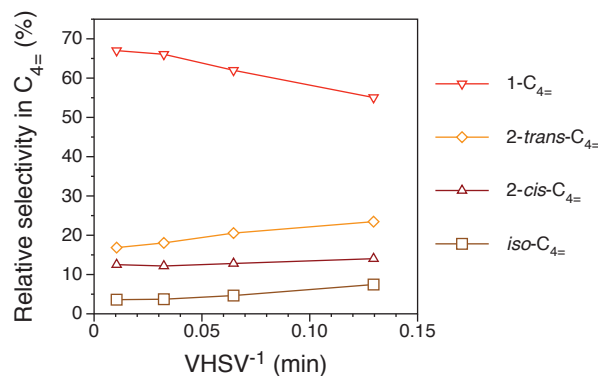


Figure 3.8 Relative selectivity of 1-butene, trans-2-butene, cis-2-butene and iso-butene at 150°C at 46 h on stream *vs.* inverse space velocity (the values for other time on steam have been omitted for clarity)

In chapter 5, a complete study will show that **WH/Al₂O₃** is a very active catalyst for olefin metathesis. These results thus strongly support the proposal that the first catalytic step of the reaction is ethylene dimerization to 1-butene (the alumina support alone was found to be inactive for this reaction) followed by isomerization to 2-butenes. Propylene is formed in a follow-up cross-metathesis of the resultant mixture of ethylene/2-butene, in agreement with the ability of **WH/Al₂O₃** to catalyze this reaction (see Chapter 5).

To corroborate this hypothesis a contact time study at lower temperature, *i.e.* 120°C has been performed. The dimerization and metathesis reaction kinetics do not have the same dependency on temperature. The influence of temperature on the selectivity of the reaction has been studied and will be discussed in subsection 2.5.1. It shows that higher selectivity in butenes are observed when lowering the reaction temperature. At 120°C the selectivity is thus even more influenced by contact time. Butenes selectivity clearly increases while contact time decreases (Figure 3.9 left). It is clearer at 120°C than at 150°C as these butenes are less consumed by the metathesis reaction which is less favored by the lower temperature (see subsection 2.5.1). At that temperature, it is also more obvious that 1-butene is a primary product whereas others butenes isomers are secondary products (Figure 3.9 right).

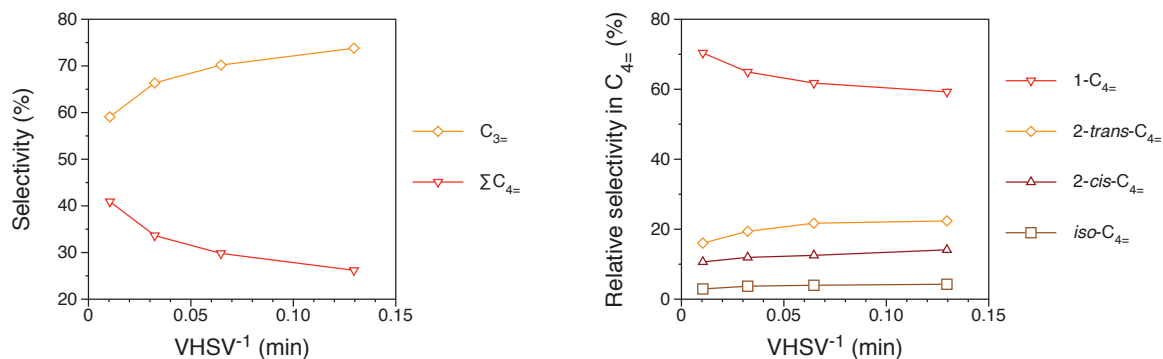


Figure 3.9 Selectivity in propylene (left) and butenes (right) at different reaction time vs. inverse space velocity

These results show that 1-butene is the primary product of the conversion of ethylene to propylene. Its formation occurs by ethylene dimerization. This formation is explained by the insertion of two ethylene molecules in the tungsten hydride bond followed by a β -H elimination retrieving the tungsten hydride. Regarding this results, the dimerization seems to be very slow, compared to other reaction occurring further, as it is very difficult to observe 100% selectivity in 1-butene.

2.3.5. Introduction of 1-butene

To confirm that 1-butene is a primary product in the conversion of ethylene to propylene, the effect of addition of 1-butene at the steady state was studied. So, the conversion of ethylene was run for a 70h experiment after that 1-butene was introduced in the ethylene feed, with increasing amounts from 5%_{vol} to 30%_{vol}.

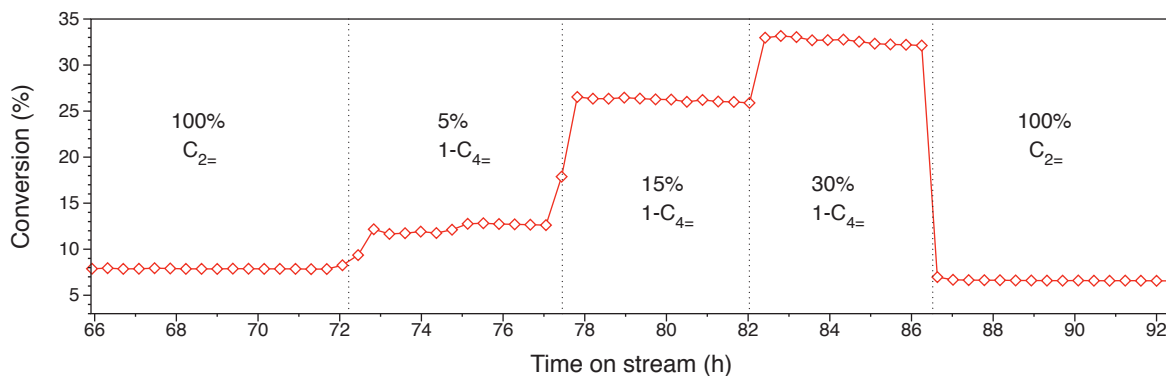


Figure 3.10 Conversion of ethylene vs. Time with a co-feed of 1-butene (percentage of 1-butene in the feed of ethylene)

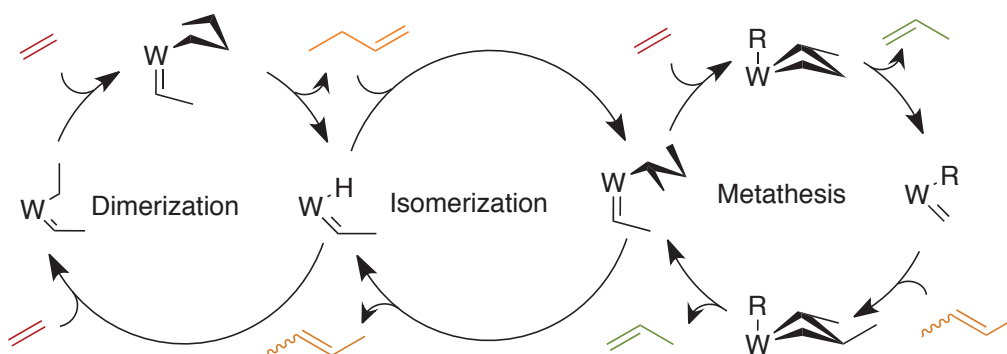
The introduction of 1-butene increases the conversion of ethylene without changing the selectivities. This raising is explained by an isomerization of this added 1-butene to 2-butene (cis or trans) and the cross-metathesis of this 2-butene with ethylene. From 0% to

15% of 1-butene in the ethylene feed, selectivity in pentenes, produced by cross-metathesis between 1-butene and butene-2 and in hexenes, produced by self-metathesis of 1-butene, remains constant. It shows a fast isomerization of 1-butene to 2-butene. It confirms that ethylene dimerization is the rate determining step of the mechanism.

This result shows that $\text{WH}/\text{Al}_2\text{O}_3\text{-(500)}$ catalyze the reaction of isomerization of 1-butene to 2-butene and ethylene/2-butene cross-metathesis. A study of all these reactions will be with more detail in Chapter 5.

2.3.6. Proposed mechanism

According to numerous examples,²⁰ olefin cross-metathesis is expected to be catalyzed by a tungsten-alkylidene species following a classical Chauvin mechanism.²¹ The same tungsten species is also involved in the observed ethylene dimerization reaction according to the classical Cosse-Arlman mechanism,^{22,23} which proceeds by a double ethylene insertion into the W-H bond of the tungsten ethylidene hydride; this latter species also catalyzes the isomerization of 1-butene into 2-butenes.



Scheme 3.5 Proposed mechanism for the direct conversion of ethylene to propylene

Thus, $[\text{W}](\text{CH}_2\text{CH}_3)(=\text{CHCH}_3)$, which bears both an alkyl and an alkylidene fragment, is able to catalyze the dimerization, isomerization, and metathesis of olefins on the same site. In other words, it behaves as a trifunctional catalyst. These multiple functionalities are observed in other reactions such as alkane metathesis.^{3,24}

2.4. Optimization of the catalytic performances

In order to increase the activity of the catalyst and decrease deactivation, the nature of the support and its pretreatment temperature have been investigated.

2.4.1. Influence of the nature of the support

As indicated in Chapter 2 and Appendix 1, the tungsten hydride was prepared on alumina (**WH/Al₂O₃-(500)**) but also on Aluminum Magnesium Hydroxyde (**WH/Pural₍₅₀₀₎**) and Silica-Alumina (**WH/SiAl₍₅₀₀₎**). SiAl and Pural have been chosen for their difference of acidity compared to Alumina. Therefore, this paragraph presents a study of the influence of the acidity of the supports for grafted tungsten hydride on catalytic performances in direct conversion of ethylene to propylene.

The results of the catalytic tests are shown in Figure 3.11. For **WH/Al₂O₃-(500)**, the maximum of conversion is ca. 35 % at 1.5 h on stream, and ca. 12 % at 15 h on stream. The cumulated T.O.N. is 230 at 15 h while the selectivity at 15 h is 92 % in propylene, 6 % in butenes and 2 % in heavier olefins.

Regarding the **WH/Pural₍₅₀₀₎**; it is noteworthy that, the conversion profile is drastically different than the conversion profile of the Al₂O₃ supported species. In the beginning of catalysis, the conversion of ethylene rises extremely rapidly, reaching a maximum superior to 80 % at 1 h on stream. At this maximum of conversion the selectivity in propylene has already reached 75% and stays constant with time on stream. Nevertheless, after this maximum, the conversion drops with the same velocity sinking to 14 % in 2 hours on stream. After 15 h on stream, this Pural supported hydride shows the lowest conversion rate, with 3 %. As the initial conversion is very high, the cumulated T.O.N. for this species is the highest for the 6 first hours, then, it is outclassed by the **WH/Al₂O₃-(500)** and reaches only 167 after 15 h on stream. The selectivity at 15 h is 75 % in propylene, 17 % in butenes and 8 % in heavier olefins.

WH/SiAl₍₅₀₀₎ reveals a conversion rate lower than **WH/Al₂O₃-(500)** even if its deactivation profile is similar. The maximum of conversion is ca. 27 % at 1.5 h on stream, and ca. 4 % at 15 h on stream. The cumulated T.O.N. is 100 at 15 h while the selectivity at 15 h is 89 % in propylene, 6 % in butenes and 5 % in heavier olefins.

It is interesting that for both of these Silica-alumina and Pural supported catalyst the selectivity in propylene is lower, and that formation of higher olefins is favoured. Regarding the tri-functional mechanism (*ie.* dimerization, isomerization and metathesis) this can

be explain that the ratio of the metathesis rate to dimerization rate is lower for **WH/Pural₍₅₀₀₎** and **WH/SiAl₍₅₀₀₎** than for **WH/Al₂O₃₋₍₅₀₀₎**. Moreover, these two catalysts deactivates faster than the Al₂O₃ supported one.

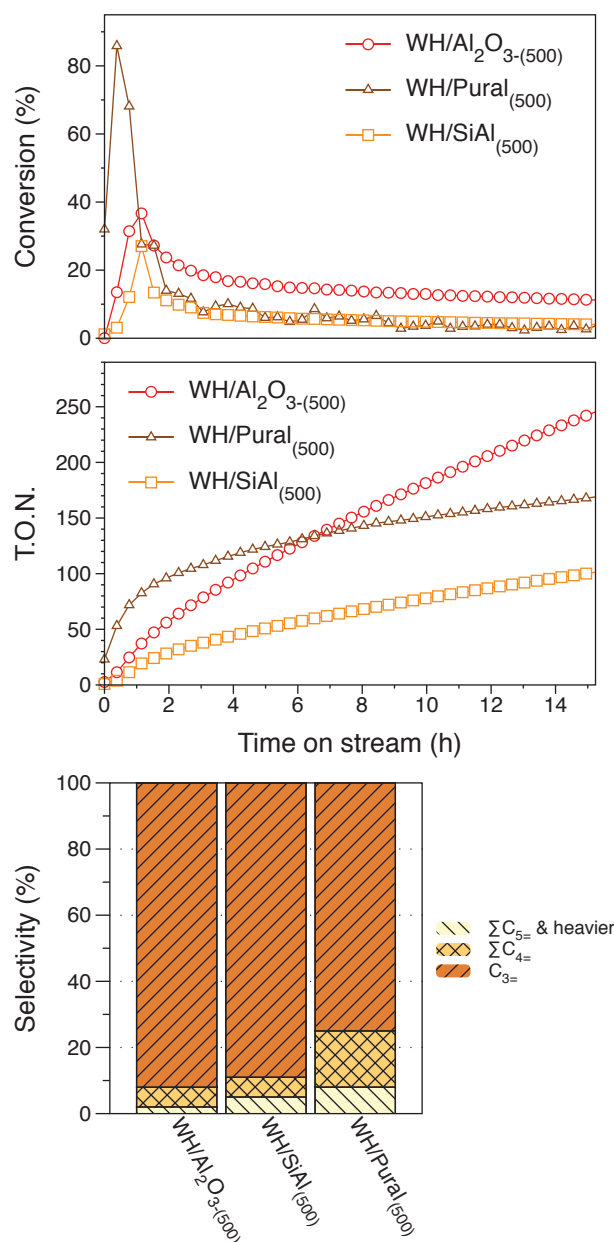


Figure 3.11 (Top) Conversion vs. Time on Stream; (Middle) Cumulated T.O.N.vs. Time on stream; (Bottom) Selectivity at pseudo steady state (15 h on stream) in propylene, butenes and heavier olefins for each support.

Finally, only one trend can be established between acidity of the support and activity of the grafted tungsten hydride. The optimal support stays the Al₂O₃, indeed the alkaline (*i.e.* Al₂O₃-MgO: Pural) or the acidic (*i.e.* Silica-Alumina: SiAl) supports gives catalyst exhibiting lower steady state conversion of ethylene and selectivity in propylene.

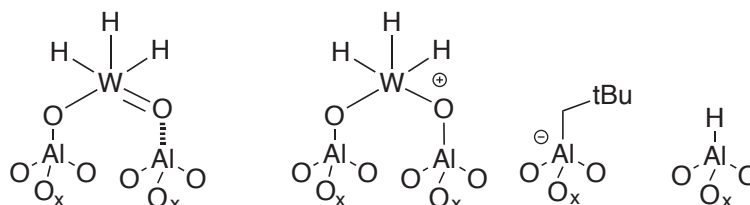
2.4.1. Influence of the support pretreatment temperature

In Appendix 1, the preparation of tungsten hydride supported on alumina dehydroxylated at different temperature (*i.e.* 300, 400, 500 and 800°C) is presented. All these catalysts have been tested for the direct conversion of ethylene to propylene.

The catalytic results are shown in Figure 3.12. For all the catalyst the conversion profile is similar, with an high initial conversion from 37% for **WH/Al₂O₃-(500)** to 47% for **WH/Al₂O₃-(300)** followed by a hyperbolic deactivation. It is noticeable that the higher the dehydroxylation temperature of the support, the faster the deactivations. The cumulated T.O.N. clearly shows that the activity of the catalyst is dependent of the support dehydroxylation temperature.

The selectivity in propylene is quite similar for **WH/Al₂O₃-(300)**, **WH/Al₂O₃-(400)** and **WH/Al₂O₃-(500)** reaching 92%, whereas it is only 55% for **WH/Al₂O₃-(800)**, where the formation of heavier olefins is observed.

This reactivity may be related to the structure of the catalyst. In chapter 2, it was concluded that the **WH/Al₂O₃-(500)** bears different surface species. It can thus be postulated that these different species are present at the surface of the catalyst whatever the pretreatment temperature. Nevertheless, their relative amount can vary with this dehydroxylation temperature. Taking into consideration that the number of Lewis acid site of the alumina increases with this pretreatment temperature,²⁵ it is reasonable to assume that the higher the dehydroxylation temperature, the more the alkyl transfers on the acidic aluminum proceed.^{26,27} Therefore **WH/Al₂O₃-(800)** should present more cationic species than **WH/Al₂O₃-(500)**. A high concentration in cationic species could thus explain the difference of selectivity observed, this cationic species favoring the formation of butenes and oligomers to the detriment of propylene. Noteworthy this catalyst grafted on Al₂O₃-(800) exhibits the fastest deactivation rate, the cationic tungsten species should be involved in the deactivation mechanism.



Scheme 3.6 Surface species of **WH/Al₂O₃-(500)**

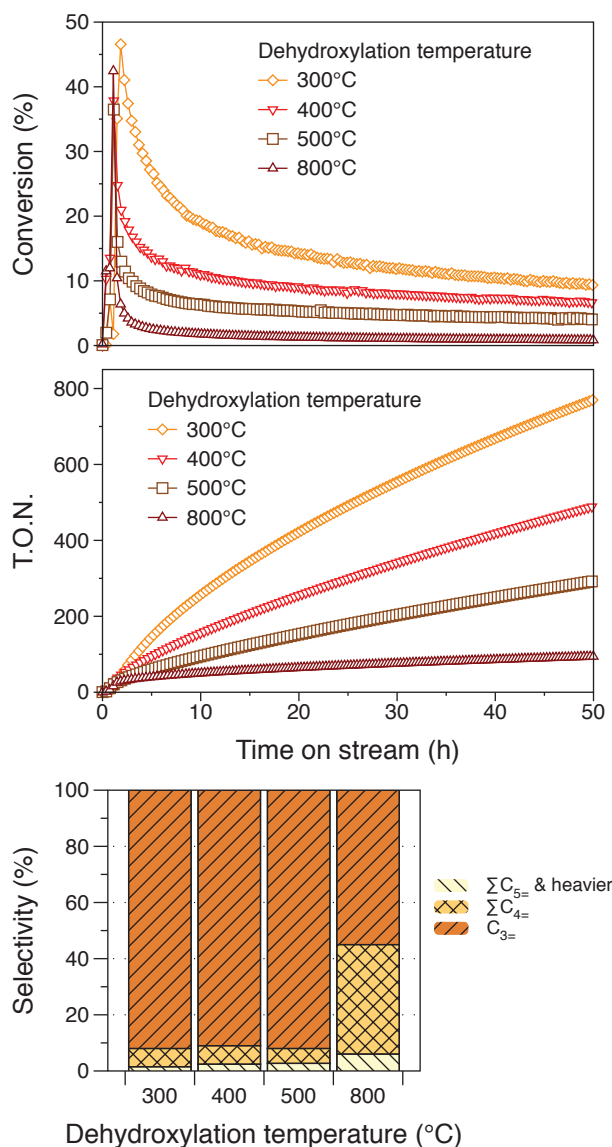


Figure 3.12 (Top) Conversion vs. Time on Stream; (Middle) Cumulated T.O.N. vs. Time on stream; (Bottom) Selectivity at pseudo steady state (30 h on stream) in propylene, butenes and heavier olefins for each dehydroxylation temperature.

2.5. Influence of the reaction temperature

The influence of the temperature on the activity and selectivity of the reaction of direct conversion of ethylene to propylene on $\text{WH}/\text{Al}_2\text{O}_{3-(500)}$ will be discussed in this subsection. The diminution of the reaction temperature may impact the dimerization and cross-metathesis rates, modifying thus selectivities and deactivation process. Four experiments have been performed with different reaction temperatures (*i.e.* 50°C, 100°C, 150°C and 200°C).

2.5.1. Catalytic tests

The results of the catalytic tests are shown in Figure 3.13 and Figure 3.14. For the experiment at 50°C the ethylene conversion reaches a maximum of 50 % whereas for the experiment at 100°C the maximum is 45 %. Both of these values are slightly superior to the 35 % observed at 150°C. On the other hand there is a more important decrease in the rate of conversion for the experiments at 50°C and 100°C compared to the experiment at 150°C. Thus after 24 h on stream the conversion is only 0.3% for the reaction at 50°C and 2% for the reaction at 100°C.

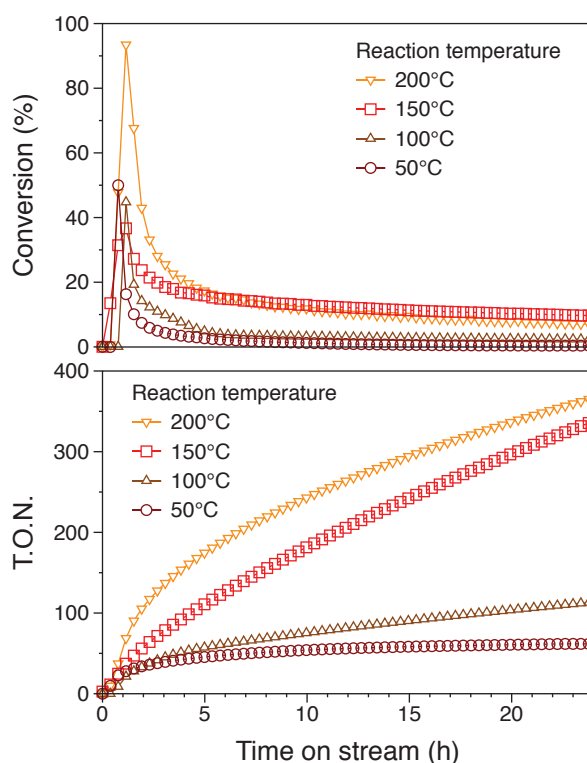


Figure 3.13 (Top) Conversion vs. Time on Stream; (Bottom) Cumulated T.O.N. vs. Time on stream for each reaction temperature.

Regarding the ethylene conversion, the experiment at 200°C shows a maximum of 93% after 1.5 h. The conversion rapidly drops and, after 7 h on stream, it is inferior to the conversion observed at 150°C.

The most interesting results concern the selectivity (Figure 3.14). After 15 h on stream, the selectivity of the experiment at 150°C and 200°C propylene is the major product with quite similar selectivity: 92% in propylene, 6% in butenes and 2% in heavier olefins at 150°C and 93% in propylene, 4% in butenes and 3% in heavier olefins at 200°C.

On the contrary for the experiments at 100°C and 50°C the major products are butenes, and the selectivity in propylene decreases with temperature: 55% in butenes, 39% in

propylene and 6% in heavier olefins at 100°C and 76% in butenes, 15% in propylene and 9% in heavier olefins at 50°C.

It can also be noted that, the relative selectivity of butenes is highly dependent of the temperature. Even at low temperatures (*i.e.* 50 and 100°C) the relative selectivity of 2-butenes (*i.e.* cis and trans) is superior to 80%. Thus the isomerization step of the mechanism is fast at low temperature. These results confirm the strong influence of temperature on reaction mechanism. The high selectivity in butenes at low temperature shows that below 150°C the dimerization is favored in comparison with metathesis reaction.

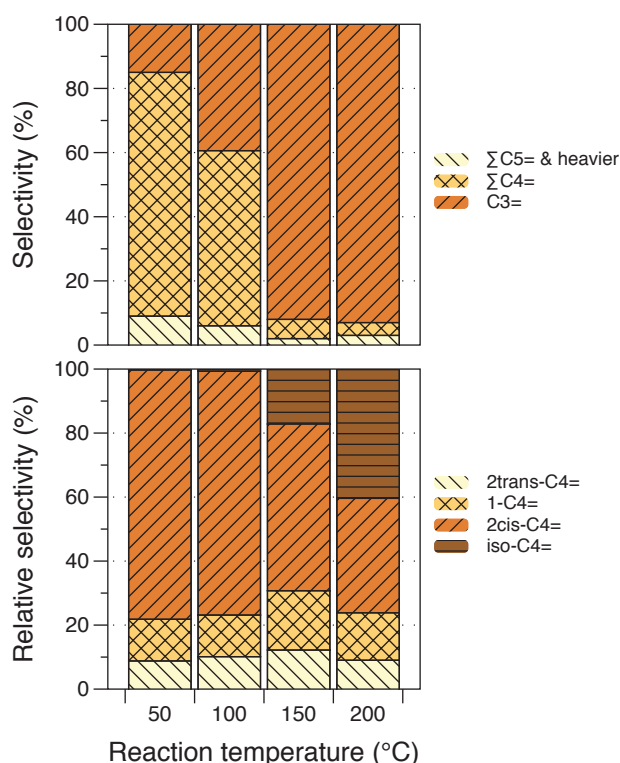
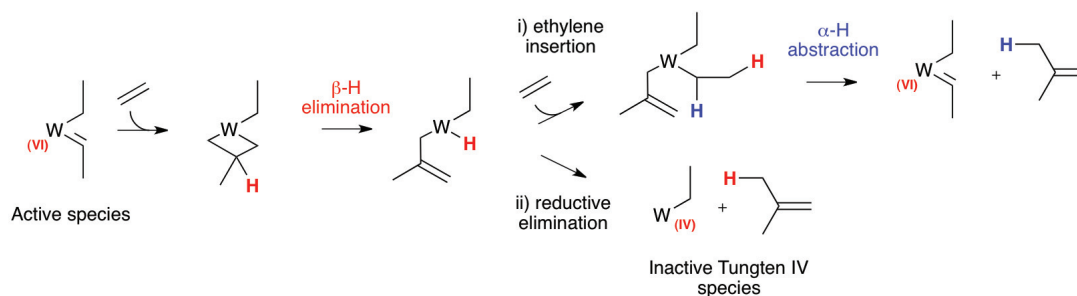


Figure 3.14 (Top) Selectivity at pseudo steady state (15 h on stream) in propylene, butenes and heavier olefins for each reaction temperature. (Bottom) Relative selectivity at pseudo steady state (15 h on stream) of the butene for each reaction temperature.

When the temperature increases, the 1-butene proportion stays constant but a significant increase of the isobutene proportion is observed. As presented on Scheme 3.7, the isobutene may have two origin: i) a “productive” path, where ethylene inserts in the alkyl-hydro-isobutenyltungsten species, then retrieves the active species by α -hydride abstraction; ii) a “destructive” path, eliminating the isobutenyl ligand and reducing the $W_{(VI)}$ to inactive $W_{(IV)}$ already described for group 6 metals.²⁸



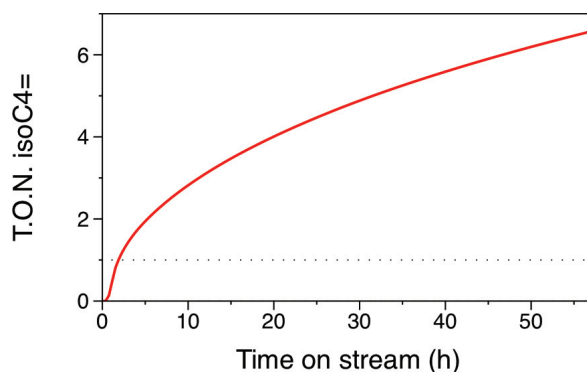
Scheme 3.7 Possible mechanisms for the formation of isobutene.

The production of isobutene has been studied for the 150°C experiment. The efficiency in isobutene has been calculated (Eq. 3.2). Using this efficiency formula, the $TON_{isoC4=}$ *i.e.* the number of mole of isobutene produced per number of mole of W was calculated (Eq. 3.3) and then the cumulated $TON_{isoC4=}$ was plotted *vs.* time on stream (Figure 3.15).

$$Eff_{isoC4=} (t) = Conversion(t) \times Selectivity_{isoC4=} (t) \quad (\text{Eq. 3.2})$$

$$TON_{isoC4=} (t) = R \times \frac{(Eff_{isoC4=} (t) + Eff_{isoC4=} (t-x))}{2} \times (t-x) \quad (\text{Eq. 3.3})$$

Figure 3.15 clearly shows that the production of isobutene is catalytic. Indeed, after 2 h on stream, the cumulated $TON_{isoC4=}$ exceed 1. Indeed path i) must occur during the reaction. Nevertheless, path ii) may occur simultaneously.

Figure 3.15 Cumulated TON for isobutene *vs.* time on stream for the reaction at 150°C

The isobutene formation by reduction of tungsten VI to tungsten IV may be the cause of deactivation of the active species; nevertheless, as its formation is catalytic, other mechanism may be involved in this deactivation.

2.5.2. Study of the carbonaceous deposits on the catalyst in function of the temperature of reaction

The deactivation process may not only be caused by the any changes in tungsten active species but also by the formation of carbonaceous species covering the catalyst. Therefore, the catalyst used in the experiments at 50°C, 100°C and 150°C have been studied after 24 h on stream. Thus, TGA and DSC have been performed on the used catalyst.

The TGA profiles, realized under air, of the catalysts after 24 h on stream at 50°C, 100°C and 150°C are presented on Figure 3.16, left. The differential thermo-gravimetric profiles, indicating the degradation temperature of the carbonaceous species present at the surface of the catalyst, have been plotted for each reaction temperature (Figure 3.16, right). The amount of carbonaceous deposits on the catalyst after 24h on stream, *i.e.* the weight loss at the end of the TGA experiment, has been plotted *vs.* the reaction temperature (Figure 3.17). Moreover, DSC profile for fusion and crystallization are presented (Figure 3.18 left and right, respectively).

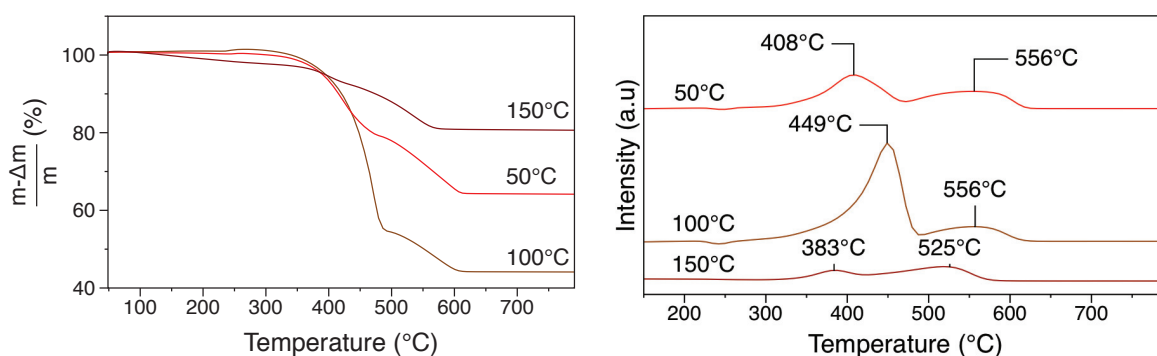


Figure 3.16 left: TGA profile of the catalyst after 24 h on stream at 50°C, 100°C and 150°C; right: Differential thermo-gravimetric profiles of the catalyst for each reaction temperature.

Figure 3.17 displays that whatever the reaction temperature, there is an important weight loss of the used catalyst. It clearly indicates that carbonaceous species are formed at the surface of the catalyst during reaction. It is noteworthy that the maximum amount of carbonaceous deposit is for the 100°C reaction with 57% of catalyst weight, followed by 36% at 50°C and 27% at 150°C. Thus lowering the working temperature favored the formation of surface carbonaceous species.

It is interesting to compare these results with the selectivity of at each reaction temperature on Figure 3.14 (top), where we can observe that the formation of heavier products (*e.g.* butenes, pentene at 85% in selectivity...) is favored at low temperature (*i.e.* $\leq 100^\circ\text{C}$).

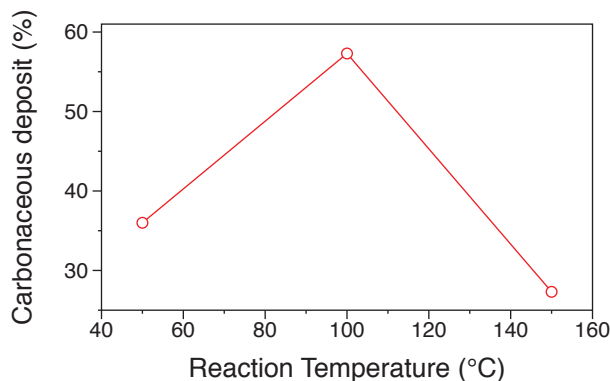


Figure 3.17 Amount of carbonaceous deposits on the catalyst after 24h on stream vs. reaction temperature

The differential thermo-gravimetric profiles on Figure 3.16 (right) show that no matter the reaction temperature two different weight losses are observed: a first between 383°C and 449°C and a second between 525°C and 556°C. Interestingly, the carbonaceous species formed at 50°C and 100°C burned at higher temperature than the species formed at 150°C.

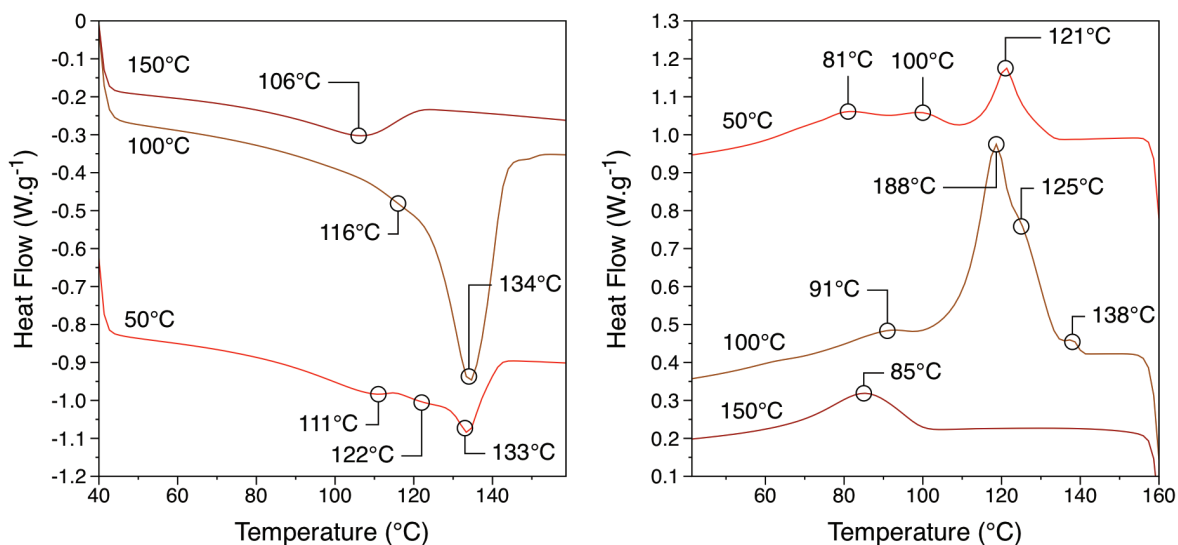


Figure 3.18 left: Fusion DSC profiles for each reaction temperature; right: Crystallization DSC profiles for each reaction temperature

DSC fusion profiles (Figure 3.18, left) reveals that at 50°C almost three different species are formed with melting points at 111°C, 122°C and 133°C. The different crystallizations temperature observed on Figure 3.18 (right) confirmed this multiple species.

The species formed at 100°C melt mostly at 134°C which is similar to the fusion temperature of linear HDPE. The crystallization profile shows the presence of almost four different types of carbonaceous deposits.

The DSC profiles for the catalyst which has been tested at 150°C are more simple, confirming the formation of only one species with a melting point of 106°C, corresponding to low density PE or heavy PE waxes (*i.e.* species containing more than 60 carbon atoms). The crystallization confirms the presence of a single type of carbonaceous deposit.

2.6. Characterizations of the aged catalyst, study of the deactivation mechanism

The support (*i.e.* nature, dehydroxylation temperature) and the reaction condition have shown an important influence on the selectivity and deactivation of the catalyst. Understanding the mechanism of deactivation may bring the key to regenerate our active species.

In order to better understand the mechanism of deactivation of the catalyst during the direct conversion of ethylene to propylene four experiments have been done in the same standard conditions with different running time (2 h, 24 h, 48 h and 264 h see Figure 3.19). At the end of each experiment, the catalyst was recovered in the glove box to be analyzed in inert conditions.

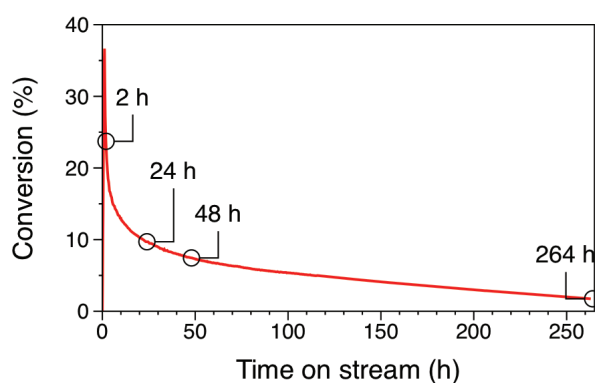


Figure 3.19 Conversion of ethylene vs. Time on stream for the ethylene to propylene reaction

2.6.1. Drift and NMR spectroscopies studies

The study of the catalyst along time on stream was first performed using DRIFT and NMR spectroscopies.

The DRIFT spectrum (Figure 3.20) of the fresh catalyst exhibits bands between 3500 and 3800 cm^{-1} corresponding to $\nu_{(\text{OH})}$, bands between 2750 and 3000 cm^{-1} corresponding with $\nu_{(\text{CH})}$ and bands 1360 and 1465 cm^{-1} corresponding to $\delta_{(\text{CH})}$. These can be attributed to the non hydrogenolysed species (Al-CH₂tBu). Finally the $\nu_{(\text{WH})}$ band is present at 1913 cm^{-1} .

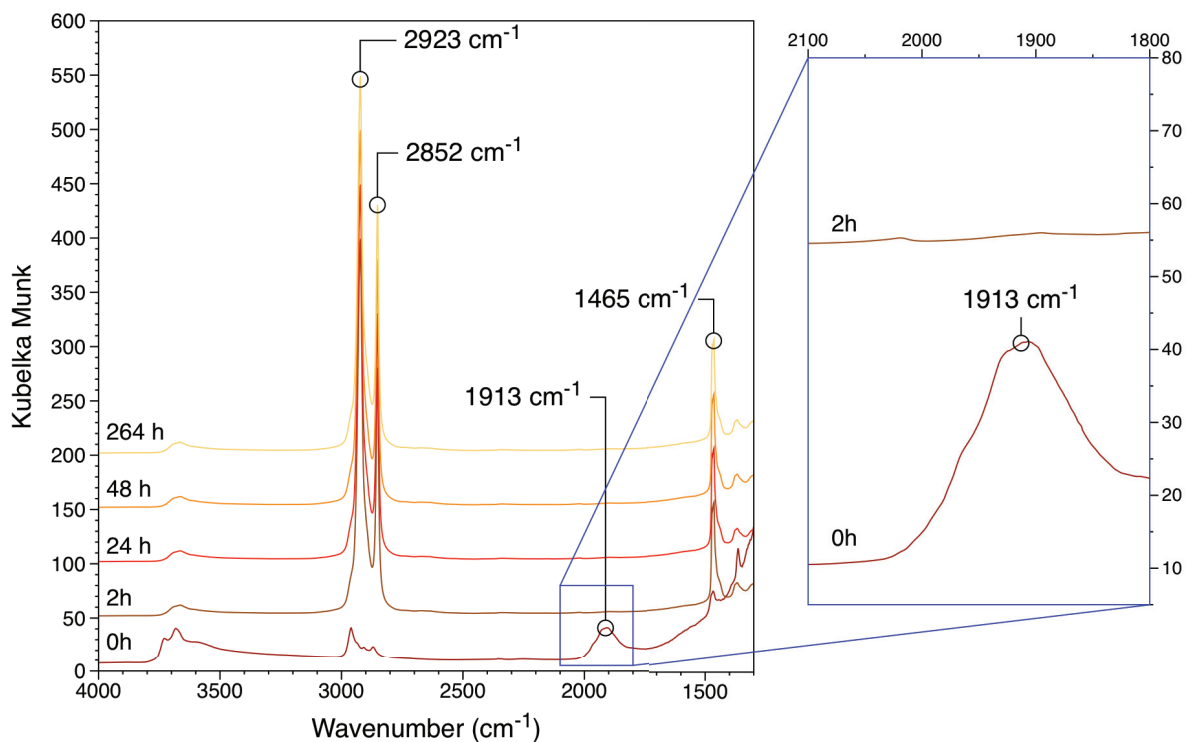


Figure 3.20 DRIFT spectra of the fresh catalyst and of the catalytic bed at different time on stream.

The DRIFT spectra of the used catalyst are similar whatever the time on stream. It is noteworthy that at 2 h on stream, all the W-H have already inserted ethylene as $\nu_{\text{(WH)}}$ has completely disappeared whereas bands between 2750 and 3000 cm^{-1} corresponding to $\nu_{\text{(CH)}}$ and bands 1360 and 1465 cm^{-1} corresponding with $\delta_{\text{(CH)}}$ are observed from 2 h on stream. These bands can be assigned to long chain alkyls formed by multiple insertions in the metal hydride bond. This metal can be the tungsten and/or the aluminum as the $\nu_{\text{(AlH)}}$ band at 1932 cm^{-1} , usually hidden by the $\nu_{\text{(WH)}}$ but evidenced by selective exchange with D₂ is also consumed (see Chapter 2). Thus this aluminum hydride has also inserted ethylene.

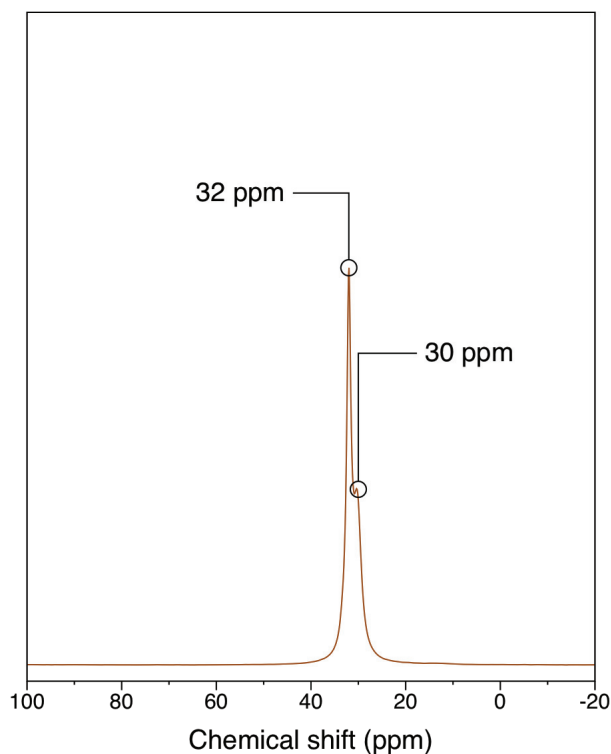


Figure 3.21 ^{13}C CPMAS NMR spectra of the catalyst after 48 h on stream

The formation of long chain alkyls is confirmed by the solid state NMR study. Only the spectrum after 48 h on stream is shown on Figure 3.21 as whatever the time on stream they are very similar. Peaks at 30 and 32 ppm are observed, corresponding to respectively crystallized and amorphous PE.²⁹ Even at short time on stream the chain ends (CH_3) are not visible on the NMR spectra, confirming chain growth of surface species since the early time of the catalysis

2.6.2. TGA and DSC study

In order to confirm the hypothesis of the formation of PE, the used catalyst were analyzed by TGA and DSC and compared to the fresh catalyst.

Figure 3.22 clearly shows that there is a fast formation of surface carbonaceous species on the surface of the catalyst, even at short time on stream. After 2 h, there is 17% of weight loss when the catalyst is completely calcinated.

On the DTG profiles (Figure 3.22, right) two weight loss peaks could be observed centered on 383°C and 525°C . It is interesting to note that at high time on stream, 264h, the first weight loss peak shifts to 433°C indicating that the species burns 50°C higher. The longer the time on stream, the more carbonaceous deposits are observed, the harder they are to burn.

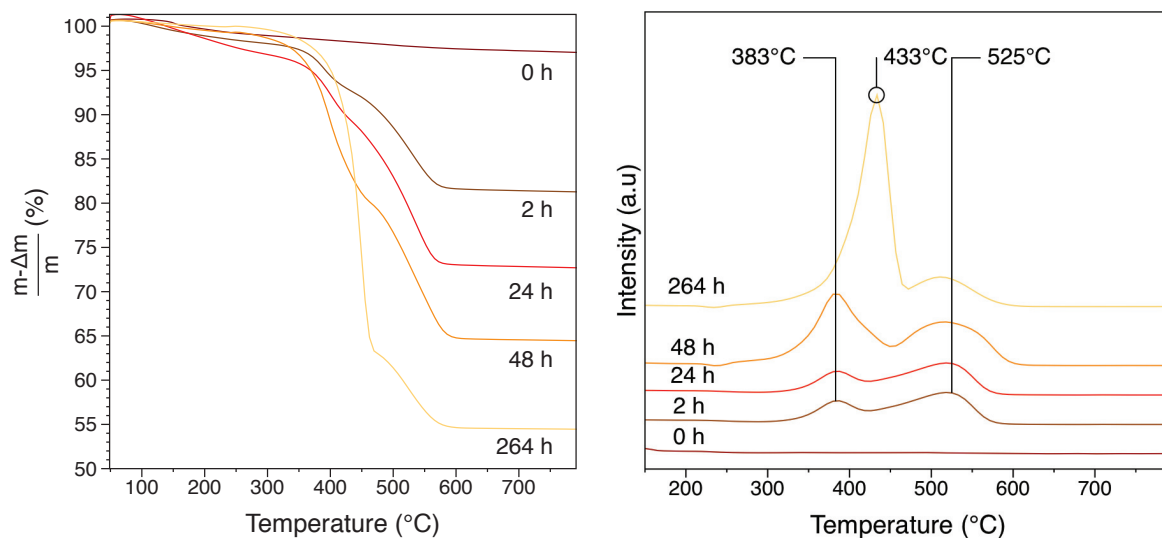


Figure 3.22 left: TGA profiles for of the catalyst for each time on stream; right: Differential thermo-gravimetric profiles of the catalyst for each time on stream

On Figure 3.23, the comparison between the amounts of carbonaceous deposits at the surface of the used catalyst (left) with the conversion of ethylene (right) let think that the formed carbonaceous products are involved in deactivation.

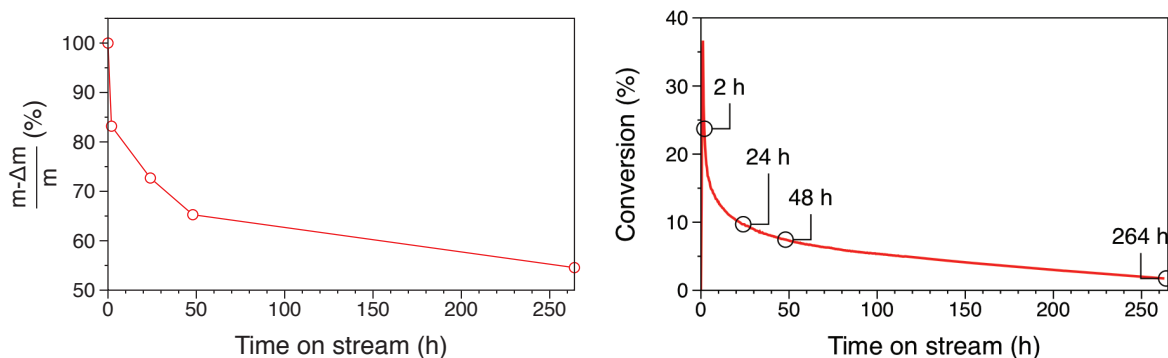


Figure 3.23 left: Weight loss of the fresh and used catalyst vs. time on stream; right: Conversion of ethylene vs. Time on stream for the ethylene to propylene reaction (idem Figure 3.19)

The fusion DSC profile presented on Figure 3.24 (left) shows that the melting point of the formed species increases with the time on stream: starting at 101°C after 2 h and reaching 136°C after 264 h. This is also clear that when the time on stream increases, more than one surface species is formed. This is confirmed by crystallization DSC profile on Figure 3.24 (right) with almost two crystallization peaks after 48h on stream.

The formation of different surface deposits may be explained by the different active sites of the catalyst as represented on scheme 6. It can be assumed that these different sites are sensitive to ethylene partial pressure. Hence, at short time on stream, the ethylene conversion is high, which reduces its partial pressure. Contrariwise, at long time on

stream, the conversion onto propylene has decreased leading to a higher ethylene partial pressure. It explains why the species with a high melting point ($>130^{\circ}\text{C}$) is observed in DSC only after 24 h on stream.

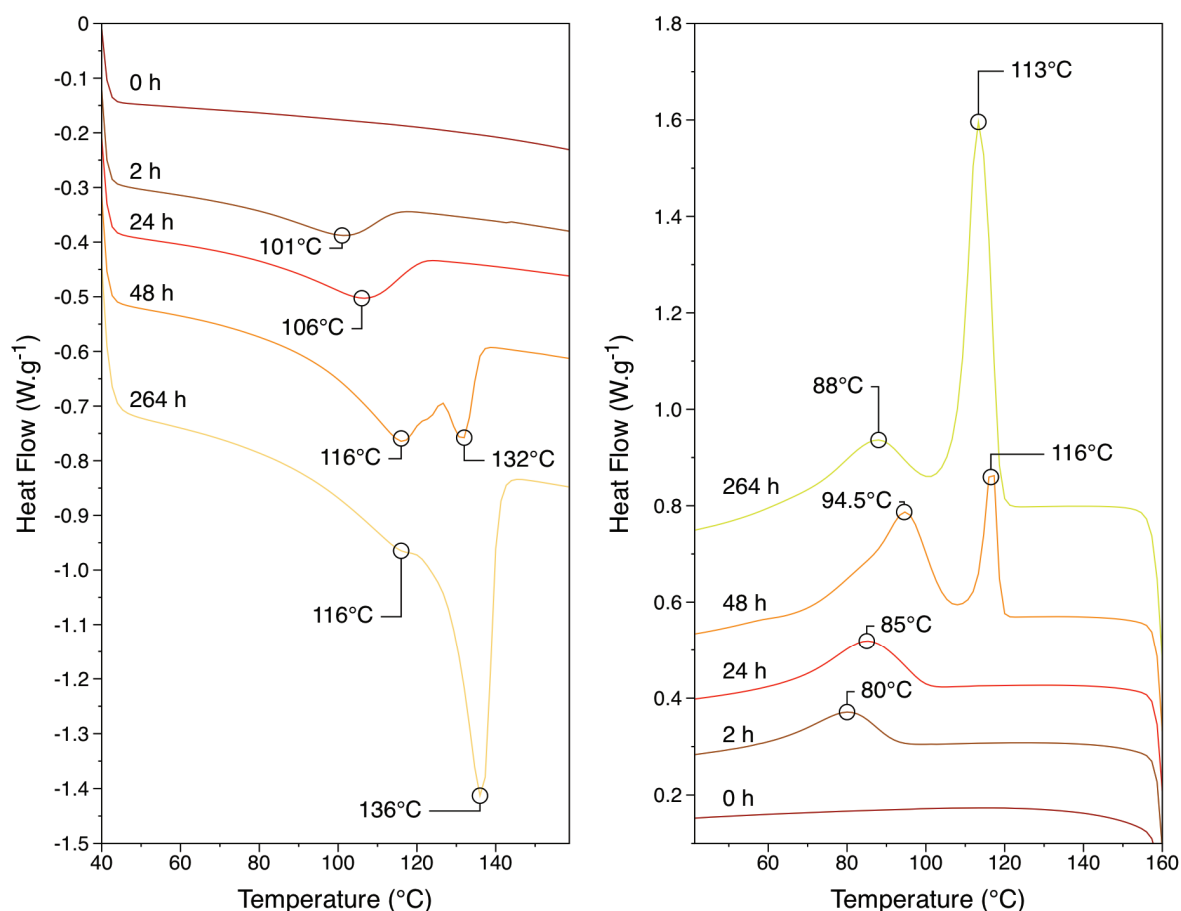


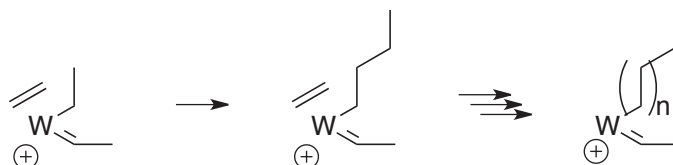
Figure 3.24 left: Fusion DSC profiles for each time on stream; right: Crystallization DSC profiles for each time on stream

It is also interesting to compare these results to with the results described in §2.5.2. Thus, in Figure 3.18 and Figure 3.24, it can be observed that at 24h on stream at 100°C the profile is similar the profile at 246h at 150°C . Indeed, the aging of the catalyst is fastened by a decrease of temperature.

2.6.3. Proposed deactivation mechanism

Regarding the last results, it seems that the deactivation of the catalyst is mainly due to the formation of two types of polymers. The drop of initial activity, *i.e.* before 48h on stream, is accompanied of formation of a low melting point polymer (116°C). This polyethylene species may be formed by multiple insertion of ethylene in the tungsten alkyl bond. In the literature, only one example of tungsten-based ethylene polymerization catalyst is described, which is a cationic species.³⁵ (Polymer international 44 1997 517) To the

best of our knowledge, no neutral tungsten species are described as polymerization catalysts. It can thus be proposed that the polyinsertion of ethylene occurs only on cationic tungsten site as presented in Scheme 3.8. Once this long chain is formed on the metal centre, the β -hydride elimination did not occur any more. The resulting species could not perform ethylene dimerization anymore and thus it cannot form 1-butene. The pseudo-plateau conversion may thus be attributed to neutral tungsten species, less reactive in dimerization as less electrophilic, but not affected by deactivation by polymerization.



Scheme 3.8 Mechanism of formation of the polyethylene surface species by poly insertion of ethylene in tungsten carbon bound

This neutral site has an important activity in olefin metathesis, as the introduction of small amount of 1-butene at the end of catalytic test is followed by a large increase in the ethylene conversion. It shows that dimerization is the rate-determining step but also the main step affected by deactivation.

The other surface species such as aluminum hydride or alkyl-aluminum may also play a role in this deactivation process by the formation of the polymer at 135°C (see Chapter 4).

The formation of carbonaceous deposits at the surface of the catalyst during metathesis reaction as been observed many time.³⁰⁻³² These deposits are assumed to be responsible of the deactivation of the catalyst, such as for WO₃/SiO₂, which is reactivated under air at 500°C to calcine these deposits and to retrieve the active species.³³ In the case of WH/Al₂O₃ the regeneration may be more difficult as the formation of the hydride species cannot occur under air.

2.7. Attempts of regeneration of the catalyst

After a certain time on stream the activity of the WH/Al₂O₃ catalyst for the conversion of ethylene to propylene decreases. The aging of the active site is due to the formation of polyethylene species. Hence, in order to retrieve the initial activity of the catalyst this species must be removed from the catalyst and the tungsten hydride regenerated.

Supported titanium hydrides have already shown a good activity in catalytic hydrogenolysis of parafin waxes at low temperature.³⁴ The tungsten system may be able to per-

form such a reaction. Indeed, the grafted tungsten is able to perform alkane hydrogenolysis, as during the treatment of $1/\text{Al}_2\text{O}_3$ under H_2 at 150°C the neopentane is cleaved in ethane and methane^{3,24} Treatment of the used catalyst by H_2 should thus regenerate the active species, using the ability of the surface species to break C-C bonds.

2.7.1. Regeneration after catalysis

The regeneration of the catalyst has been studied under a flow of hydrogen at different temperature. After 50 hours on ethylene stream, the following regeneration cycle has been experimented. First, the reactor is purged with argon ($4\text{mL}\cdot\text{min}^{-1}$). It is then heated to the regeneration temperature. Once the regeneration temperature reached, the gas flow is switched to hydrogen ($4\text{mL}\cdot\text{min}^{-1}$) until no hydrocarbon is detected on CPG. Finally the reactor is purged with argon ($4\text{mL}\cdot\text{min}^{-1}$), and cooled to 150°C .

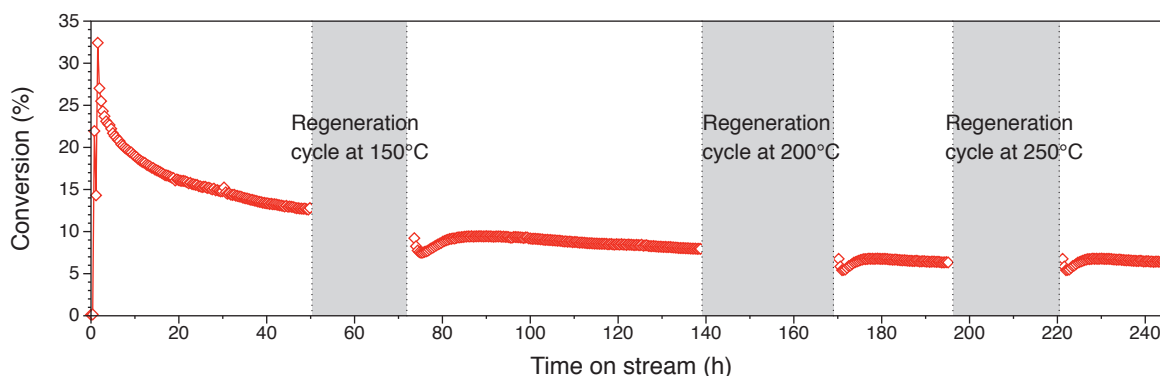


Figure 3.25 Conversion of ethylene vs. time on stream. Three regeneration temperatures have been experimented: 150°C , 200°C and 250°C .

Figure 3.25 shows that whatever the temperature used, the regeneration cycles have no influence on ethylene conversion. Indicating that the regeneration of the catalyst did not occur under hydrogen at these temperatures. Thus the regeneration was tested at 300°C .

At 300°C the active species seems to be irreversibly damaged. There is no more activity after the treatment. On the same sample the treatment commonly used to activate the WO_3/SiO_2 was tried. The powder was oxidized under dry air at 500°C the reduced under H_2 at 500°C . The resulting catalyst exhibits no activity, neither in direct conversion of ethylene to propylene nor in propylene metathesis.

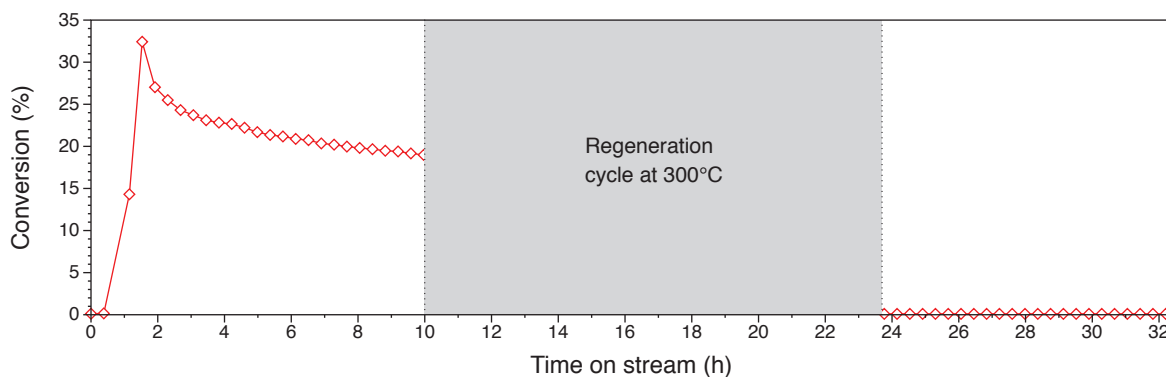


Figure 3.26 Conversion of ethylene vs. time on stream. Regeneration cycle at 300°C.

2.7.2. “On-stream” regeneration

As regeneration under hydrogen is not possible, an experiment to avoid the formation of the inactive species was envisaged. Thus, the reactivity of the catalyst for direct conversion of ethylene to propylene using hydrogen as a co-feed was tested. To avoid hydrogenation of ethylene, which is largely thermodynamically favored, small amount of hydrogen has to be used. The experiment was carried following the standard conditions with 8%vol hydrogen added to the ethylene flow rate. (The molar ratio is around 12%).

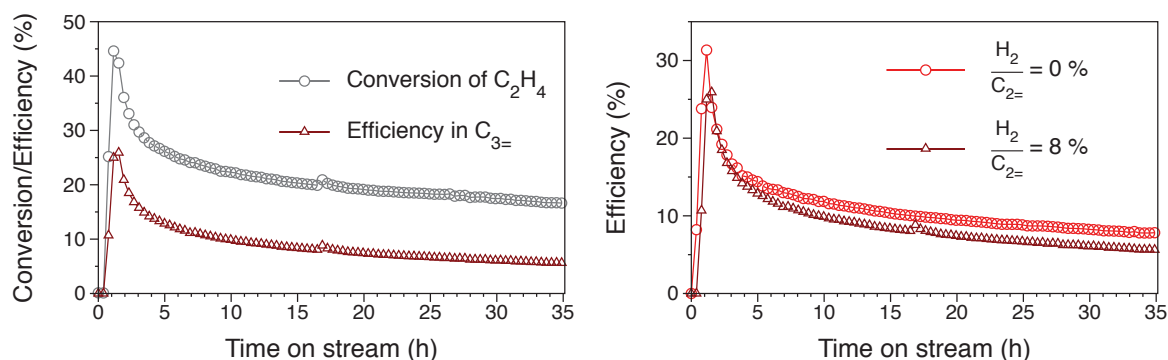


Figure 3.27 left: Conversion of ethylene and efficiency in propylene (conversion of ethylene \times selectivity in propylene) for the 8% H₂ co-feed ethylene to propylene experiment; right: Efficiency in propylene for the reference ethylene to propylene experiment and efficiency in propylene for the 8% H₂ co-feed ethylene to propylene experiment vs. time on stream.

A very high conversion of ethylene is reached when H₂ is added to the feed (Figure 3.27, left). Nevertheless the selectivity in propylene is much lower compared to the reference experiment. Efficiency in propylene (conversion of ethylene multiplied by selectivity in propylene) was thus plotted (Figure 3.27, left) and compared to the reference experiment (Figure 3.27, right). No significant changes in the deactivation profile are observed compared to the reference experiment.

Co-feeding the reactor with hydrogen decrease the selectivity in propylene (Figure 3.28, left). When the efficiency in ethane is plotted (Figure 3.28, right), the first hours on stream displays efficiency in ethane of 16%. Indeed, the formation of the active species converts ethylene to ethane. But after five hours of catalysis, the ethane production remains very high, and confirms that all the hydrogen (12%mol) reduce ethylene, which is largely thermodynamically favored.

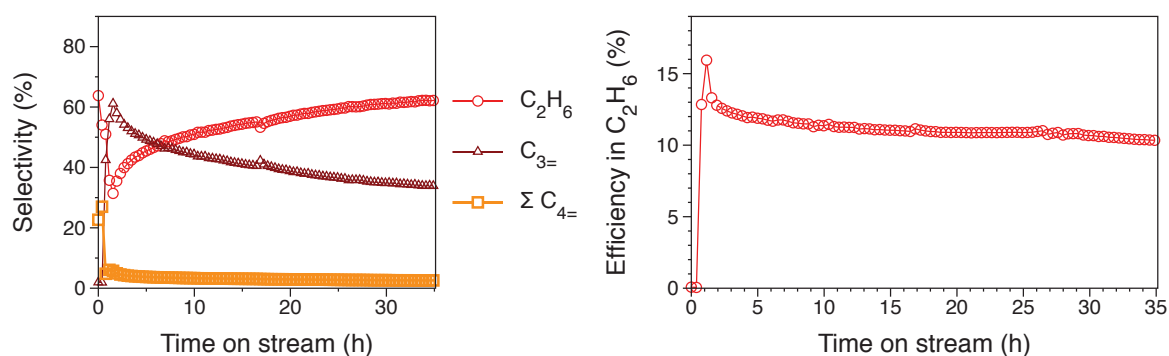


Figure 3.28 left: Selectivity for the 8% H_2 co-feed ethylene to propylene experiment; right: Efficiency (conversion of ethylene x selectivity in ethane) in ethane for the 8% H_2 co-feed ethylene to propylene experiment

Hence, an experiment with lower amount of H_2 was necessary to see if the same predominance of ethane was seen. Using 1% of H_2 as co-feed unfortunately gives the same results that the experiment with 8%. The efficiency is not affected and 1% of ethane is formed (Figure 3.29). Thus the hydrogenation of ethylene must be highly thermodynamically favored in comparison with regeneration reaction.

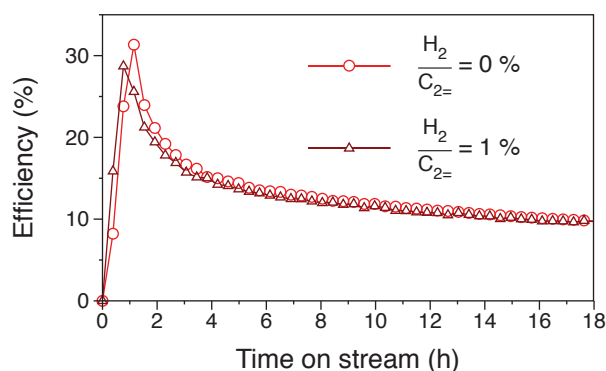
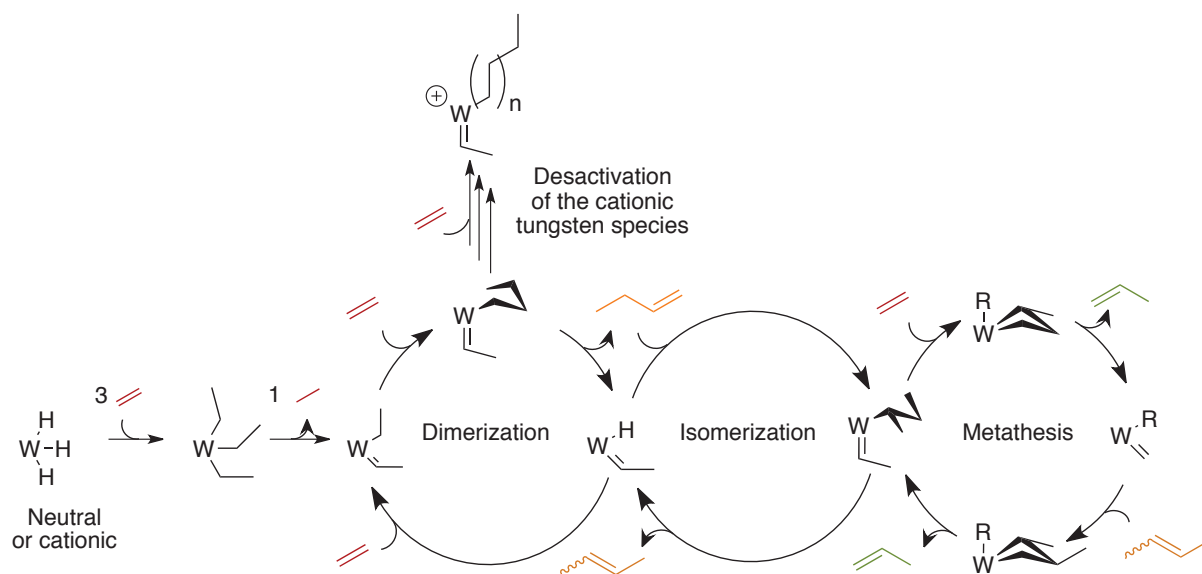


Figure 3.29 Comparison of efficiency (conversion of ethylene x selectivity in propylene) in propylene for the 1% H_2 co-feed and reference ethylene to propylene experiment

2.8. Conclusion

The WH/Al₂O₃₋₍₅₀₀₎ catalyst exhibits an outstanding activity in the direct conversion of ethylene to propylene. This reaction involves a threefold mechanism: dimerization, isomerization and cross-metathesis. The results of this chapter have shown that the dimerization is the rate-determining step of this catalytic mechanism. The ability of the WH/Al₂O₃₋₍₅₀₀₎ to perform the ethylene/2-butene cross-metathesis will be studied in more detail in Chapter 5. It has also been demonstrated that the two tungsten hydride surface species, *i.e.* neutral and cationic, may convert ethylene to propylene by the same trifunctional mechanism. Nevertheless, the most active cationic species is quickly deactivated by formation of a polymeric species with a melting point of 116°C. Unfortunately, after deactivation treatment under H₂ do not retrieves the active species.

As selective poisoning experiments of the different surface species of the WH/Al₂O₃₋₍₅₀₀₎ were not successful, it was decided to prepare isolated surface Al-H, Al-alkyls (see Chapter 4) and neutral tungsten oxo-alkyl-alkylidene (see Chapter 6) species, to study their role in this reaction.



Scheme 3.9 Global mechanism proposed for the direct conversion of ethylene to propylene on WH/Al₂O₃₋₍₅₀₀₎

3. Experimental section

The **WH/Al₂O₃-(500)** was prepared following the procedure described in Chapter 2. The preparation of **WH/SiAl₍₅₀₀₎**, **WH/Pural₍₅₀₀₎**, **WH/Al₂O₃-(300)**, **WH/Al₂O₃-(400)** and **WH/Al₂O₃-(800)** is described in Appendix 1.

The continuous flow reactor used for the catalytic test is presented in subsection 2.1 of Chapter 2 and Appendix 2.

Ethylene N35 Air Liquide, H₂ and Argon were purified over R3-11 BASF catalyst/MS4Å

Procedure for the catalytic tests: A stainless-steel half-inch cylindrical reactor that can be isolated from ambient atmosphere was charged with the desired amount of **WH/Al₂O₃-(500)** in a glovebox. After connection to the gas lines and purging of the tubing, the desired gas or mixture of gas was passed over the catalyst bed at 150°C, at atmospheric pressure, and at desired flow rate. Hydrocarbon products were analyzed online by GC (HP 8890 chromatograph fitted with an Al₂O₃/KCl 50 m x 0.32 mm capillary column, FID detector).

4. Reference and Notes

- (1) Propylene, *Chemical Profile, Chem. Market Reporter*, 2003.
- (2) Calamur, C. N. and Carrera, C. M. In *Kirk-Othmer Encyclopedia of Chemical Technology: Propylene*; John Wiley & Sons, Inc., 2005; p. 1-25.
- (3) Le Roux, E.; Taoufik, M.; Copèret, C.; de Mallmann, A.; Thivolle-Cazat, J.; Basset, J. -M.; Maunders, B. M.; and Sunley, G. J. *Angewandte Chemie International Edition*. 2005, *44*, 6755-6758.
- (4) Szeto, K. C.; Norsic, S.; Hardou, L.; Le Roux, E.; Chakka, S.; Thivolle-Cazat, J.; Baudouin, A.; Papaioannou, C.; Basset, J. M.; and Taoufik, M. *Chem Commun (Camb)*. 2010, *46*, 3985-7.
- (5) Stull, D. R. and Sinke, G. C. *The chemical thermodynamics of organic compounds*, Westrum, Ed.; Krieger: Malabar, Fla.; 1987.
- (6) O'Neill, P. P. and Rooney, J. J. *Journal of the American Chemical Society*. 1972, *94*, 4383-4384.
- (7) Hugues, F.; Besson, B.; and Basset, J. M. *Journal of the Chemical Society, Chemical Communications*. 1980, *1980*, 719-721.
- (8) Imamura, H. and Konishi, T. *Lanthanide and Actinide Research*. 1991, *3*, 387-9.
- (9) Yamaguchi, T.; Tanaka, Y.; and Tanabe, K. *Journal of Catalysis*. 1980, *65*, 442 - 447.
- (10) Suzuki, T.; Tanaka, K.; Toyoshima, I.; and Gotoh, H. *Applied Catalysis*. 1989, *50*, 15 - 25.
- (11) Suzuki, T. *Reaction Kinetics and Catalysis Letters*. 2004, *81*, 327-331.
- (12) Oikawa, H.; Shibata, Y.; Inazu, K.; Iwase, Y.; Murai, K.; Hyodo, S.; Kobayashi, G.; and Baba, T. *Applied Catalysis A: General*. 2006, *312*, 181 - 185.
- (13) Iwamoto, M. and Kosugi, Y. *J. Phys. Chem. C*. 2007, *111*, 13-15.

- (14) Iwamoto, M. *Catalysis Surveys from Asia*. 2008, 12, 28-37.
- (15) Taoufik, M.; LeRoux, E.; Thivolle-Cazat, J.; and Basset, J. -M. *Angewandte Chemie International Edition*. 2007, 46, 7202-7205.
- (16) Pillai, S. M.; Ravindranathan, M.; and Sivaram, S. *Chemical Reviews*. 1986, 86, 353-399.
- (17) Tolman, C. A. *Journal of the American Chemical Society*. 1972, 94, 2994-2999.
- (18) van Santen, R. A.; Moulijn, J. A.; van Leeuwen, P. W. N. M.; and Averill, B. A. In *Catalysis : an integrated approach*; Elsevier: Amsterdam ; New York, 1999; p. 375-431.
- (19) Basset, J. M.; Coperet, C.; Lefort, L.; Maunders, B. M.; Maury, O.; Le Roux, E.; Saggio, G.; Soignier, S.; Soulivong, D.; Sunley, G. J.; Taoufik, M.; and Thivolle-Cazat, J. *J. Am. Chem. Soc.* 2005, 127, 8604-8605.
- (20) Ivin, K. J. and Mol, J. C. *Olefin metathesis and metathesis polymerization*, Academic Press: San Diego ; 1997.
- (21) Hérisson, J. L. and Chauvin, Y. *Makromol. Chem.* 1971, 141, 161-176.
- (22) Arlman, E. J. and Cossee, P. *Journal of Catalysis*. 1964, 3, 99 - 104.
- (23) Cossee, P. *Journal of Catalysis*. 1964, 3, 80 - 88.
- (24) Le Roux, E.; Taoufik, M.; Copèret, C.; de Mallmann, A.; Thivolle-Cazat, J.; Basset, J. -M.; Maunders, B. M.; and Sunley, G. J. *Angewandte Chemie*. 2005, 117, 6913-6916.
- (25) Ballinger, T. H. and Yates, J. T. *Langmuir*. 1991, 7, 3041-3045.
- (26) Jezequel, M.; Dufaud, V.; Ruiz-Garcia, M. J.; Carrillo-Hermosilla, F.; Neugebauer, U.; Niccolai, G. P.; Lefebvre, F.; Bayard, F.; Corker, J.; Fiddy, S.; Evans, J.; Broyer, J. -P.; Malinge, J.; and Basset, J. -M. *Journal of the American Chemical Society*. 2001, 123, 3520-3540.
- (27) Ahn, H. and Marks, T. J. *Journal of the American Chemical Society*. 2002, 124, 7103-7110.
- (28) Robbins, J.; Bazan, G. C.; Murdzek, J. S.; O'Regan, M. B.; and Schrock, R. R. *Organometallics*. 1991, 10, 2902-2907.
- (29) Nowaczyk, G.; Glowinkowski, S.; and Jurga, S. *Solid State Nuclear Magnetic Resonance*. 2004, 25, 194-199.
- (30) Wills, G. B.; Fathikalajahi, J.; Gangwal, S. K.; and Tang, S. *Rec. Trav. Chim. Pays-Bas*. 1977, 96, M110-M114.
- (31) Spamer, A.; Dube, T. I.; Moodley, D. J.; van Schalkwyk, C.; and Botha, J. M. *Applied Catalysis a-General*. 2003, 255, 133-142.
- (32) Li, X.; Zhang, W.; Liu, S.; Huang, H.; Han, X.; Xu, L.; and Bao, X. *J. Phys. Chem.* 2009, 100, 8228-8233.
- (33) van Schalkwyk, C.; Spamer, A.; Moodley, D. J.; Dube, T.; Reynhardt, J.; and Botha, J. M. *Applied Catalysis a-General*. 2003, 255, 121-131.
- (34) Larabi, C.; Merle, N.; Norsic, S.; Taoufik, M.; Baudouin, A.; Lucas, C.; Thivolle-Cazat, J.; de Mallmann, A.; and Basset, J. -M. *Organometallics*. 2009, 28, 5647-5655.
- (35) Justino, J.; Marques, M. M.; Correia, S.; Dias, A. R.; Lemos, F.; and Ribeiro, F. R. *Polymer International*. 1997, 44, 517-522.

Chapter 4

Well-defined aluminum alkyl and hydride grafted on $\gamma\text{-Al}_2\text{O}_3$ – role in deactivation of WH/ Al_2O_3

1. Introduction	131
2. Results and discussions	132
2.1. Preparation and characterizations of Al^tBu/Al₂O₃₋₍₅₀₀₎	132
2.1.1. Choice of the support and precursor.....	132
2.1.2. Reactivity of Al(^t Bu) ₃ toward Al ₂ O ₃₋₍₅₀₀₎	132
2.1.3. NMR characterizations	133
2.1.4. Mass balance analysis.....	135
2.2. Preparation and characterizations of AlH/Al₂O₃₋₍₅₀₀₎	136
2.2.1. Treatment of 2/Al ₂ O ₃₋₍₅₀₀₎ under vacuum.....	136
2.2.2. Treatment of 2/Al ₂ O ₃₋₍₅₀₀₎ under H ₂	137
2.2.3. NMR characterizations	139
2.3. Catalytic activity of 2/Al₂O₃₋₍₅₀₀₎ and AlH/Al₂O₃₋₍₅₀₀₎	143
2.3.1. Catalytic activity of 2/Al ₂ O ₃₋₍₅₀₀₎ and AlH/Al ₂ O ₃₋₍₅₀₀₎ in ethylene to propylene conditions	144
• 2/Al ₂ O ₃₋₍₅₀₀₎	144
• AlH/Al ₂ O ₃₋₍₅₀₀₎	145
• Conclusion	146
2.3.2. Catalytic activity of AlH/Al ₂ O ₃₋₍₅₀₀₎ for ethylene polymerization	146
2.3.3. Catalytic activity of AlH/Al ₂ O ₃₋₍₅₀₀₎ for ethylene hydrogenation.....	148
2.4. Conclusion.....	149
3. Experimental section	150
3.1. General procedures.....	150
3.2. Preparation and characterizations of Al₂O₃₋₍₅₀₀₎ RP	151
3.3. Preparation of 2/Al₂O₃₋₍₅₀₀₎.....	151
3.4. Preparation of AlH/Al₂O₃₋₍₅₀₀₎	151
3.5. Catalytic application of 2/Al₂O₃₋₍₅₀₀₎ and AlH/Al₂O₃₋₍₅₀₀₎	152
3.5.1. Ethylene to propylene conditions	152
3.5.2. Ethylene polymerization.....	152
3.5.3. Ethylene hydrogenation.....	152
4. Reference and Notes	153

1. Introduction

Metal-hydrides are a class of species that holds a most peculiar position on the fringe of both inorganic and organometallic chemistry. Combining the lightest element of the periodic table to a wide range of transition- and main-group metals, they have found applications in hydrogen storage,¹ in organic synthesis² and catalysis.³ Comparatively, supported maingroup metal hydrides have been overlooked, as they are deemed as less catalytically attractive. However, considering recent advances in catalysis by main-group metals,⁴ it seems of interest to take a closer look at this class of compounds, as they may reveal unforeseen reactivity.

Moreover in the course of studies on (silica-)alumina-supported catalysts, the formation of surface aluminum hydrides was encountered on several occasions: Zr-H on alumina,⁵ W-H on silica-alumina,⁶ Ti-H on silica-alumina,⁷ Hf-H on silica-alumina⁸ and alumina⁹ and finally W-H on alumina (see chapter 2). It is notable that alkyl aluminum, counterpart of the cationic metal species, obtained by alkyl transfer on a Lewis acidic aluminum of the surface, are present at the surface of some metal-hydride catalyst. This species were observed for Zr-Np on alumina,¹⁰ Hf-H on alumina⁹ and **WH/Al₂O₃** (see chapter 2).

The chemical pathway leading to these species has only been the subject of assumptions, and their reactivity may be masked by that of the neighboring transitionmetal hydrides. Moreover, they may play a non-negligible role in the catalytic activity of this surface species and especially in the deactivation process. Therefore, it is highly desirable to efficiently and selectively synthesize surface aluminum alkyl and hydrides and to characterize them with the highest possible accuracy. Supported aluminum hydrides have been extensively studied by infrared spectroscopy,¹¹ but the low concentration of the species hampers their characterization by NMR spectroscopy, not only in ¹H but most crucially, in less responsive ²⁷Al NMR spectroscopy.

The high yield synthesis of supported aluminum alkyls and hydrides along with their deep characterization by IR spectroscopy, mass-balance analysis and particularly high-field, multinuclear NMR spectroscopy is presented in this chapter. Their reactivity toward ethylene has been tested to understand their potential role in the catalytic activity of **WH/Al₂O₃**.

2. Results and discussions

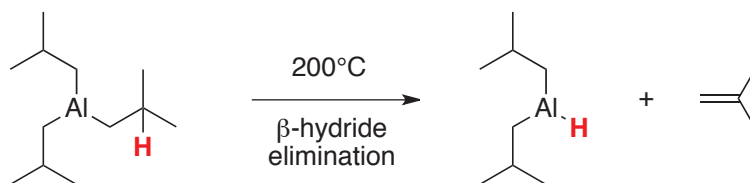
2.1. Preparation and characterizations of Al^{*i*}Bu/Al₂O₃₋₍₅₀₀₎

2.1.1. Choice of the support and precursor

Following on the work on tungsten catalyst supported on alumina, γ -alumina pretreated under *vacuum* at 500°C (Al₂O₃₋₍₅₀₀₎ RP), featuring a specific area of 200 m².g⁻¹ was chosen. Such material bears surface hydroxyl groups that may react with incoming organometallic species by protonolysis, with a density of about 2.0 OH.nm⁻² (650 μ mol.g⁻¹).

Furthermore, the thermal treatment creates Lewis acidic sites that are highly electrophilic and therefore, reactive towards organometallics either during the grafting step or in a consecutive pseudointramolecular step where grafted species react with neighbouring surface reactive centers by alkyl group transfer as observed in Chapter 2 for the tungsten species. This dual reactivity pattern stemming from alumina's complexity, coupled to the fact that the incoming reagent and the inorganic carrier are based on the same Al element, confers to the present study a most challenging character when attempting to understand molecular processes at hand and the structure of the formed surface species.

The organometallic precursor Al(^{*i*}Bu)₃ **2** (^{*i*}Bu = CH₂CH(CH₃)₂), was selected for the grafting. This choice was prompted by its commercial availability, the synthesis of Al(CH₂^{*i*}Bu)₃ will have demanded the use of very pyrophoric Al(Me)₃. Moreover Al(^{*i*}Bu)₃ is well known to form Al(^{*i*}Bu)₂H, around 200°C following an β -hydride elimination mechanism by releasing isobutene.¹² This property was another argument to choose **2** as precursor for the preparation of supported alkyls aluminum and aluminum hydrides.



Scheme 4.1 Formation of diisobutyl aluminum hydride from **2**¹²

2.1.2. Reactivity of Al(^{*i*}Bu)₃ toward Al₂O₃₋₍₅₀₀₎

Al₂O₃₋₅₀₀ reacts smoothly at room temperature with a pentane solution of Al(^{*i*}Bu)₃, **2**, to afford a surface-modified alumina bearing Al^{*i*}Bu moieties, **2**/Al₂O₃₋₍₅₀₀₎.

This is confirmed by infrared spectroscopy. The spectrum of **2**/ $\text{Al}_2\text{O}_3\text{-(500)}$ is almost devoid of bands in the $\nu_{(\text{AlO-H})}$ region (Figure 4.1). Thus, the grafting proceeds on all types of AlOH groups, without distinction, in contrast for instance to $[\text{W}(\equiv\text{C}^t\text{Bu})(\text{CH}_2^t\text{Bu})_3]$, **1**, which mostly reacts with hydroxyls on tetrahedral aluminum (see chapter 2 and reference ¹⁰). C-H related bands are observed at 3000-2800 and 1460-1320 cm^{-1} in agreement with the presence of alkyl groups on the surface.

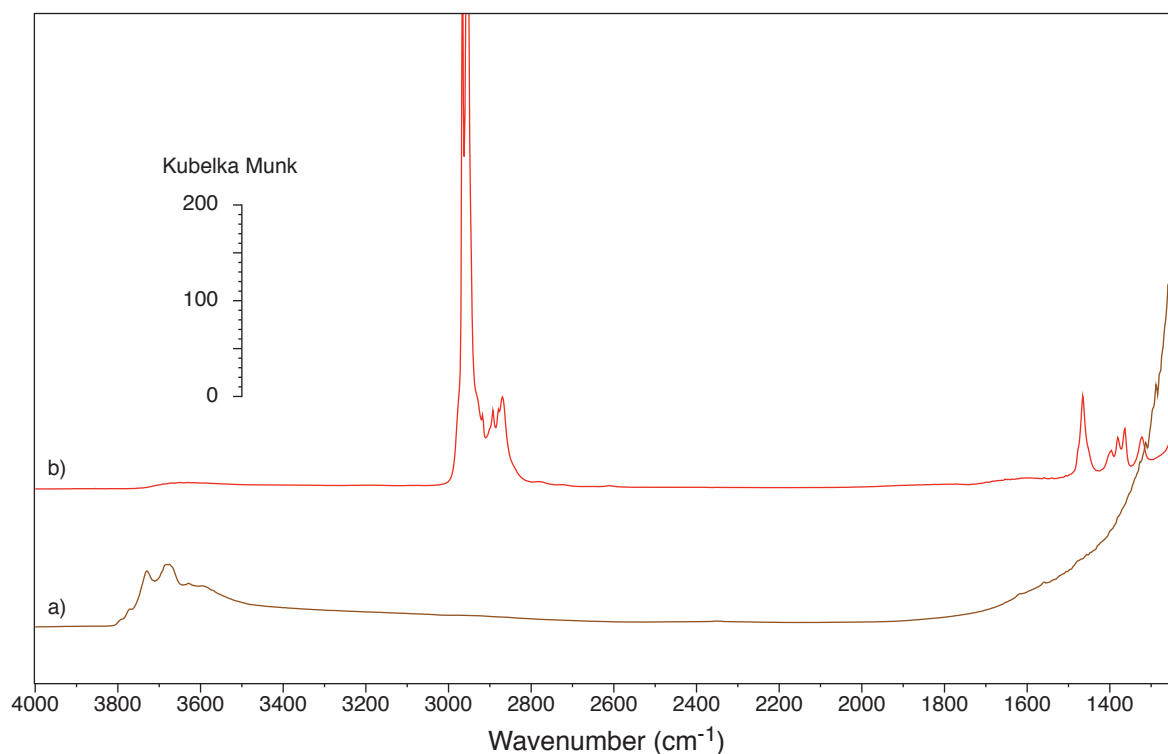


Figure 4.1 Diffuse reflectance infrared spectra of a) $\text{Al}_2\text{O}_3\text{-(500)}$, b) **2**/ $\text{Al}_2\text{O}_3\text{-(500)}$

2.1.3. NMR characterizations

The ^1H solid-state NMR spectrum of **2**/ $\text{Al}_2\text{O}_3\text{-(500)}$ comprises a peak at 1.2 ppm, with shoulders at 2.2 ppm and 0.0 ppm (Figure 4.2). Despite the high-field (18.8T, 800 MHz for ^1H resonance), only poor resolution was achieved, most probably as a consequence of strong dipolar interaction due the high density of surface alkyl groups (see the initial concentration of hydroxyl, of about 2 per nm^2).

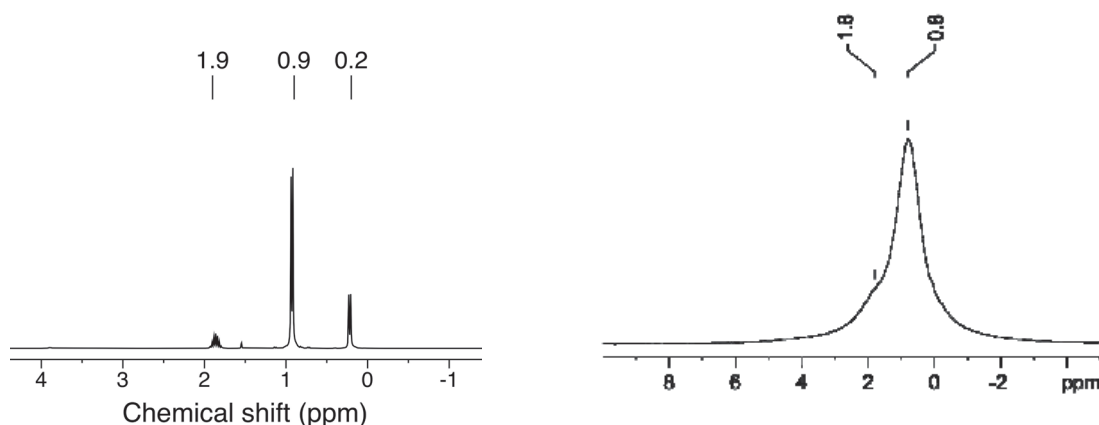


Figure 4.2 left: ^1H NMR spectrum of **2**; right: ^1H MAS NMR spectrum of **2**/ Al_2O_3 -(500)

The ^{13}C CP MAS NMR spectrum features a broad signal at 28 ppm, with broad shoulder at 26 ppm (Figure 4.3), which compares well with isobutyl groups signature in the molecular precursor where signals at 28 ppm and 26 ppm are observed at room temperature with no detectable AlCH_2 due to the quadrupolar aluminum ($\text{spin } 5/2$). This signal can however be observed at 23.4 ppm by thermal decoupling at -50°C .¹³

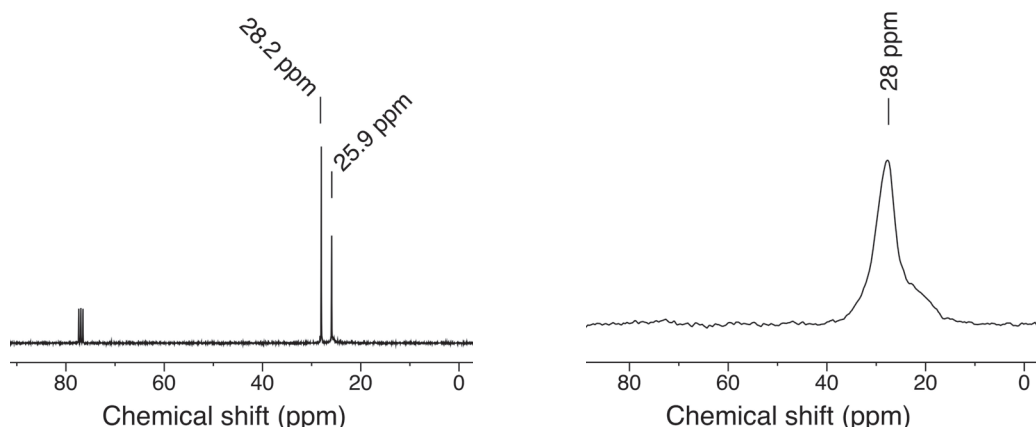


Figure 4.3 left: $^{13}\text{C}\{^1\text{H}\}$ NMR spectrum of **2**; right: ^{13}C MAS NMR spectrum of **2**/ Al_2O_3 -(500)

The ^{27}Al MAS NMR spectrum is uninformative, as the bulk atoms signal masks the resonances from the grafted aluminum nuclei (Figure 4.4 a). Taking advantage of the presence of alkyl protons, one can make use of a correlation pulse sequence such as HMQC in order to gather information on their neighboring aluminums. The ^{27}Al MAS NMR spectrum of **2**/ Al_2O_3 -(500) obtained with a dipolar filtering revealing only aluminum centers spatially close to protons is shown in Figure 4.4 b. The recoupling period set to a small value (500 μsec) keeps the bulk alumina at a low signal level. The spectrum features a broad signal spreading from 100 to 0 ppm, resulting from different aluminum coordinations. In the literature, tetra- penta- and hexa- coordinated aluminum sites are generally

found at chemical shift ranges of [100-40], [40-25] and [20-0] ppm, respectively.¹⁴ This means that all three coordination types are presumably present in close vicinity to alkyl fragments, mostly as AlⁱBu groups but also as surface Al₂O₃-aluminum centers. The major differences between the two spectra, which mostly result from alkyl-bearing aluminum centers, stand in i) an enhanced contribution in the penta-coordinated Al region, and ii) in the significant broadening of the tetra-coordinated aluminum signal.

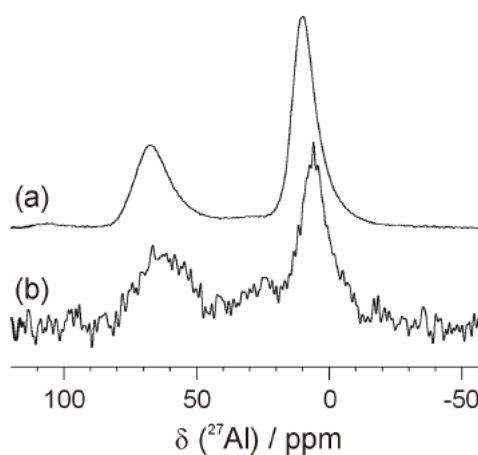
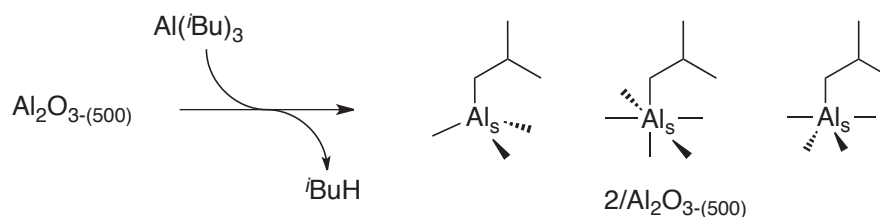


Figure 4.4 (a) ²⁷Al Hahn-echo MAS and (b) *D*-filtered HMQC ²⁷Al MAS NMR spectra of **2**/Al₂O₃₋₍₅₀₀₎ (208.50 MHz, spinning frequency of 20 kHz; spectrum b is the projection of the 2D correlation spectrum, acquired with 1536 transients and with SR4 recoupling scheme of 500 ms applied on 1H channel).

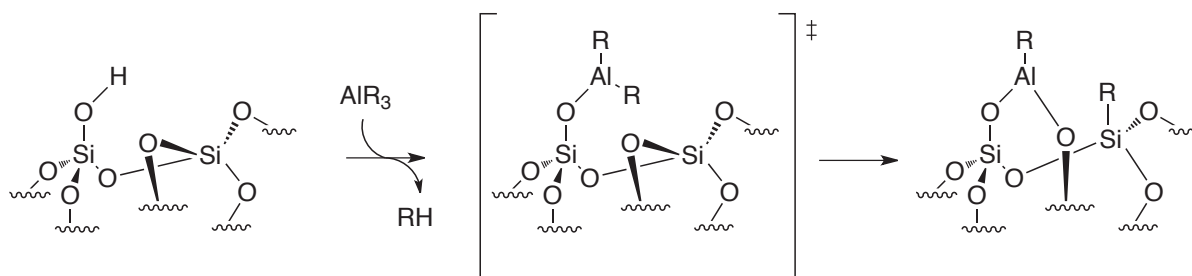
Even if spectral resolution in the Al_V region prevents their accurate measurement, it is likely that their electric field gradient, *ie.* the C_Q (quadrupolar coupling) value, is also in the upper range of reported pentacoordinated aluminum. The broadening of the Al_{IV} resonance observed in the HMQC-filtered spectrum accounts for higher C_Q values than that encountered in the pristine material.¹⁴ As a high C_Q value is diagnostic of high dissymmetry, this indicates severe anisotropy of the Al coordination sphere.

2.1.4. Mass balance analysis

Mass balance analysis indicates formation of 550 μmol.g⁻¹ of isobutane during the grafting step, while hydrolysis of surface alkyl groups leads to evolution of 1200 μmol.g⁻¹ of isobutane, which is consistent with the postulated reaction pattern as the major grafting reaction scheme (Scheme 4.2). These elements point out the introduction of ca. 600 μmol.g⁻¹ of additional Al centers onto the alumina surface, in line with quasi-quantitative consumption of surface hydroxyls.

Scheme 4.2 Reaction of **2** toward $\text{Al}_2\text{O}_3\text{-(500)}$ affording $2/\text{Al}_2\text{O}_3\text{-(500)}$

When considering the information extracted from the ^{27}Al HMQC NMR spectrum, the several types of alkyl aluminum coordination, *i.e.* tetra-, penta- and hexa- coordinate, can originate from protonolytic grafting, and from transfer of alkyl groups onto acidic Al-centers, accompanied with coordination of the support's oxygen atoms. These pathways are in line with the reactivity of aluminum alkyls with silica surfaces. Anwander *et al.* have reported the opening of siloxane bridges at the surface of silica after reaction with $\text{Al}(\text{Me})_3$ (Scheme 4.3).¹⁵ In that system, the resulting SiMe and AlMe group can easily be differentiated by ^{13}C solid state NMR with a chemical shift of respectively 0.1 and -9.5 ppm. These results have been confirmed by recent studies of reactivity of $\text{Al}(\text{iBu})_3$ toward silica performed in our laboratory.¹⁶

Scheme 4.3 Reactivity of alkyl aluminum with silica.^{15,16}

2.2. Preparation and characterizations of $\text{AlH}/\text{Al}_2\text{O}_3\text{-(500)}$

The preparation of aluminum hydrides by thermal treatment of $2/\text{Al}_2\text{O}_3\text{-(500)}$ is investigated in this subsection. Once obtained these hydride species have been characterized by IR spectroscopy, mass balance analysis and NMR spectroscopy.

2.2.1. Treatment of $2/\text{Al}_2\text{O}_3\text{-(500)}$ under vacuum

The formation of an aluminum hydride was expected by thermal treatment of $2/\text{Al}_2\text{O}_3\text{-(500)}$ under vacuum. Surprisingly, by treating $2/\text{Al}_2\text{O}_3\text{-(500)}$ gradually from 25°C to 350°C , only a small $\nu(\text{AlH})$ signals band at 1940 cm^{-1} is observed on the IR spectra from 200°C (Figure 4.5) and only $60\text{ }\mu\text{mol.g}^{-1}$ of isobutene are observed. At higher temperatures neither IR spectroscopy nor gas phase analysis show an evolution of the system. Most of the

alkyls remains on the surface as $\nu(\text{CH})$ and $\delta(\text{CH})$ signals are still present on the spectrum and only 5% of the surface isobutyl of $2/\text{Al}_2\text{O}_3-(500)$ has evolved as isobutene. The properties of this surface aluminum alkyl are thus different from its homogeneous precursor preventing the occurrence of $\beta\text{-H}$ transfer and concomitant generation of isobutene and AlH.

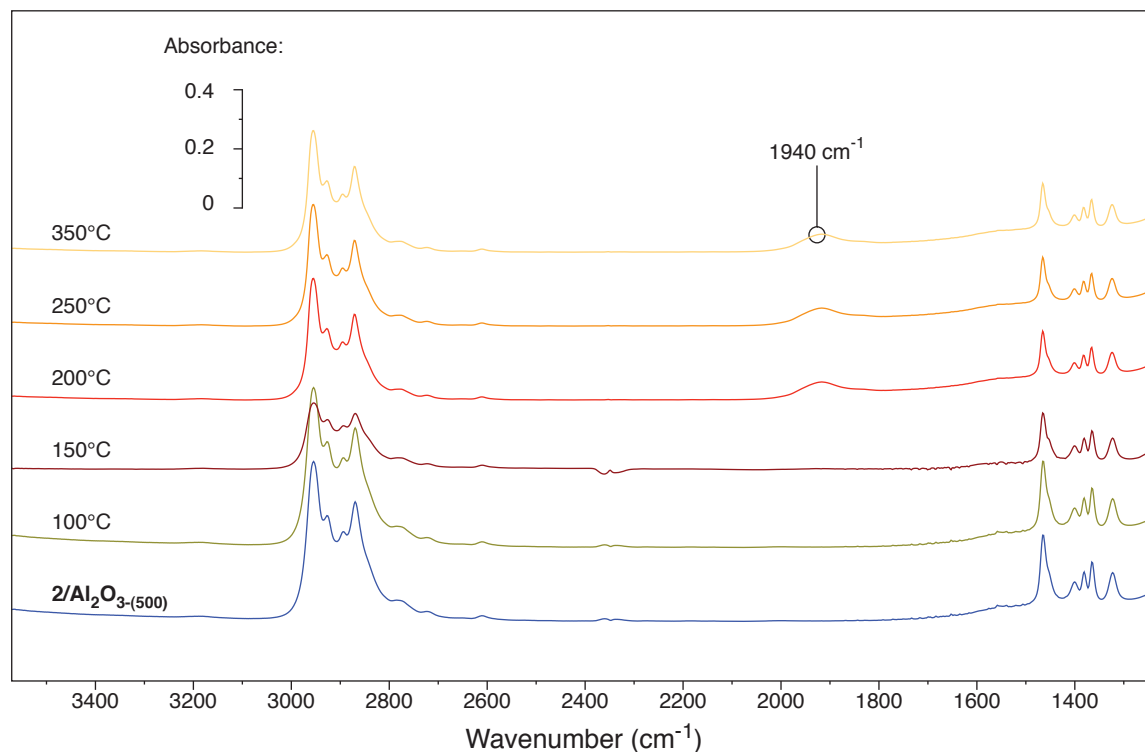
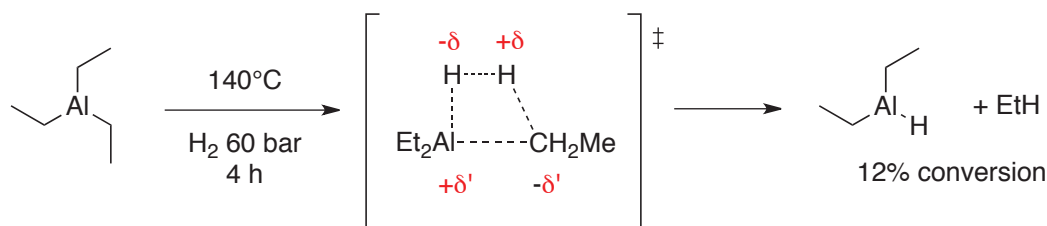


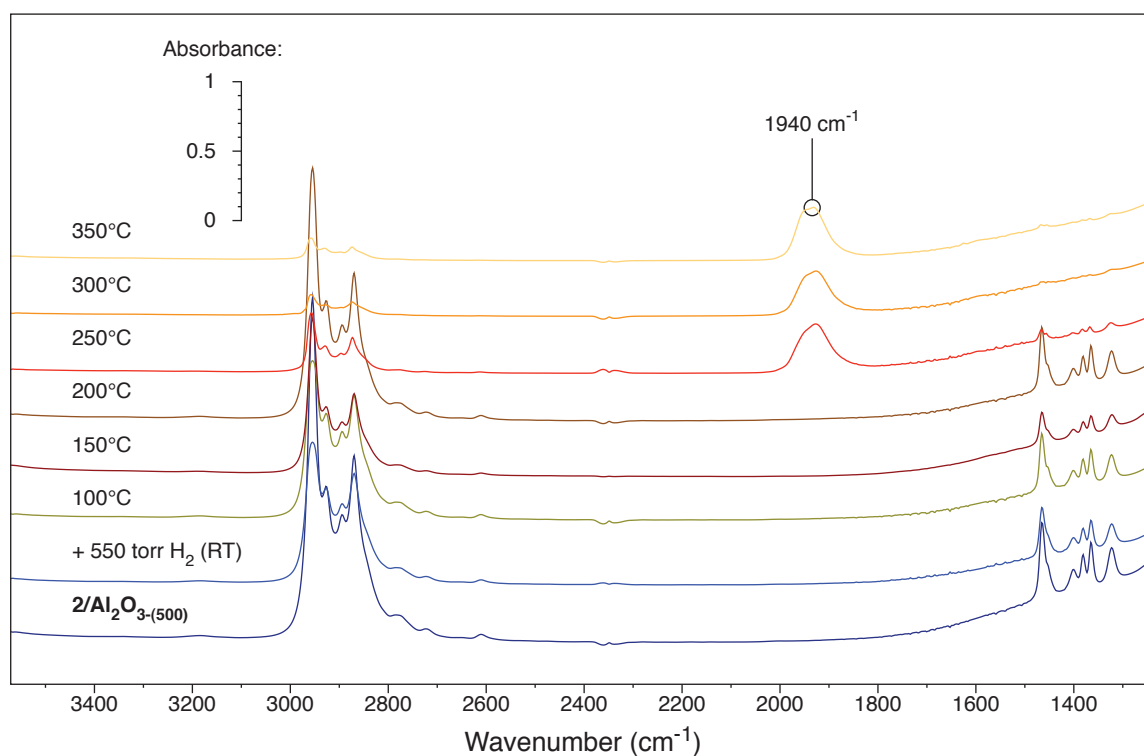
Figure 4.5 IR spectra of 75mg pellet of **2** grafted on $\text{Al}_2\text{O}_3-(500)$ by sublimation treated under *vacuum* from RT to 350°C (2 h at each temperature)

2.2.2. Treatment of $2/\text{Al}_2\text{O}_3-(500)$ under H_2

Having introduced alkyl groups onto the surface, it was set out to generate hydride groups from hydrogenolysis of metal–carbon bond. Hydrogenolysis of transition–metal bonds is well documented, and supported transition metal species generated in such a way have been extensively reported.¹⁷ However, main group metal alkyls reactivity toward hydrogen is less pronounced, and examples of such reactions usually imply forceful conditions (Scheme 4.4).¹⁸ It was reasonable to assume that the strong polarization of the Al–C bond by the electrodeficient support would ease the heterolytic splitting of H_2 .

Scheme 4.4 Hydrogenolysis of triethylaluminum and transition state proposed by Podall *et al.*¹⁸

A preliminary study of hydrogen treatment (550 Torr) was performed on an Al_2O_3 -(500) pellet where **2** has been grafted. The IR follow up reveals that a characteristic $\nu(\text{AlH})$ signals at 1940 cm^{-1} start to appear at 250°C .¹¹ This band rises while increasing the temperature to 350°C (Figure 4.6). Concomitant alkane formation is detected by GC analysis of the gas phase.

Figure 4.6 IR spectra of 65mg pellet of **2** grafted on Al_2O_3 -(500) by sublimation treated under hydrogen excess (550 Torr) from RT to 350°C (2 h at each temperature)

Regarding these preliminary results, $2/\text{Al}_2\text{O}_3$ -(500) was treated 4h at 400°C under a low H_2 pressure (550 Torr) and afforded $\text{AlH}/\text{Al}_2\text{O}_3$ -(500), along with formation of $4800 \mu\text{mol.g}^{-1}$ of C (alkane mixture) in the gas phase, which corresponds to 2.0 isobutyl per initially grafted Al.

The formation of the corresponding quantity of hydride is indicated by the stoichiometry of the hydrolysis, as $1200 \mu\text{mol}$ of H_2 are released upon exposure of

$\text{AlH}/\text{Al}_2\text{O}_3-(500)$ to excess water. On the infrared spectrum of $\text{AlH}/\text{Al}_2\text{O}_3-(500)$, the characteristic,¹¹ and noticeably intense, $\nu(\text{AlH})$ signals appeared at 1940 cm^{-1} , while those of the $i\text{Bu}$ groups almost completely vanished (Figure 4.7). Performing the reaction under D_2 leads to the formation of a $\nu(\text{AlD})$ band with the expected isotopic shift (1400 cm^{-1}) (see Appendix 3)

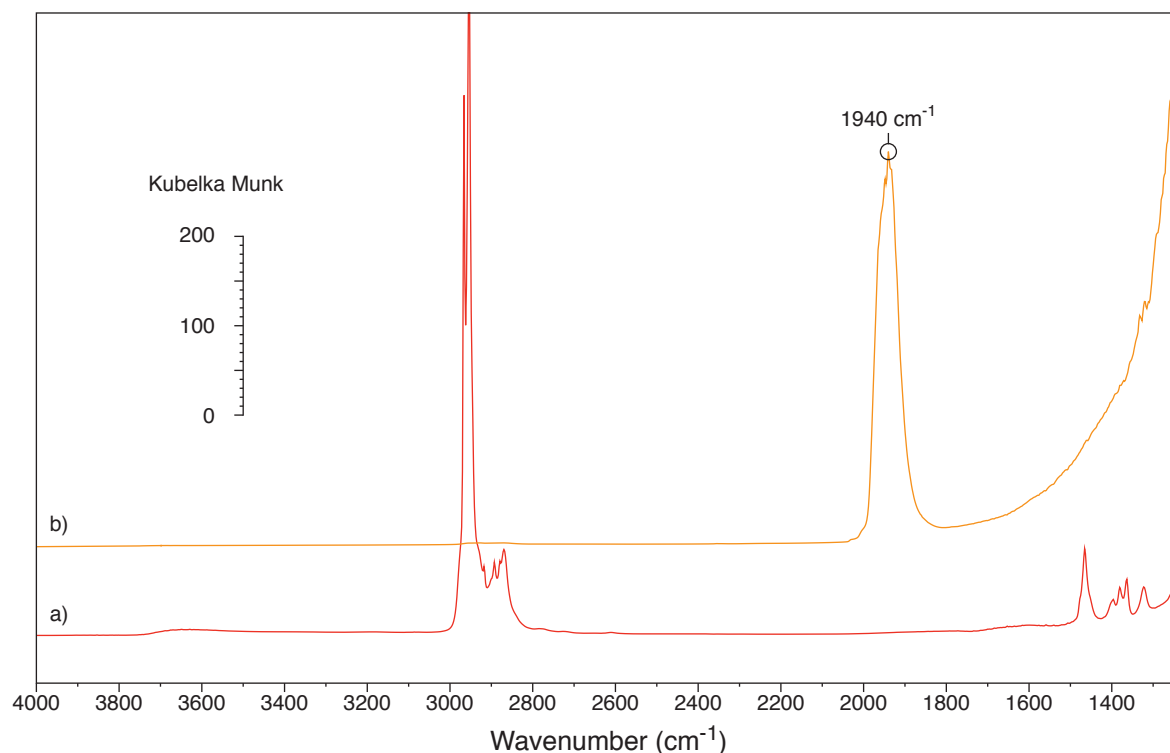


Figure 4.7 Diffuse reflectance infrared spectra of a) $2/\text{Al}_2\text{O}_3-(500)$ and b) $\text{AlH}/\text{Al}_2\text{O}_3-(500)$

2.2.3. NMR characterizations

^1H MAS NMR spectrum of $\text{AlH}/\text{Al}_2\text{O}_3-(500)$ has been acquired at two static magnetic fields, 9.4 T (a) and 18.8 T (b) (Figure 4.8). The main spectral feature is a multiplet centered at about 3.5 ppm, arising from the indirect spin-spin coupling with a spin 5/2 nucleus like ^{27}Al . Figure 4.8 (c) is a J-HMQC filtered ^1H MAS spectrum obtained with an ^{27}Al RA-MP decoupling,¹⁹ revealing the ^1H chemical shift region of hydride species. The spectrum reveals the presence of a ^1H site at a chemical shift of 3.3 ppm, in a major proportion. This chemical shift lies below the expected range for molecular aluminum hydrides,²⁰⁻²³ but is similar to what was observed in related materials.²⁴

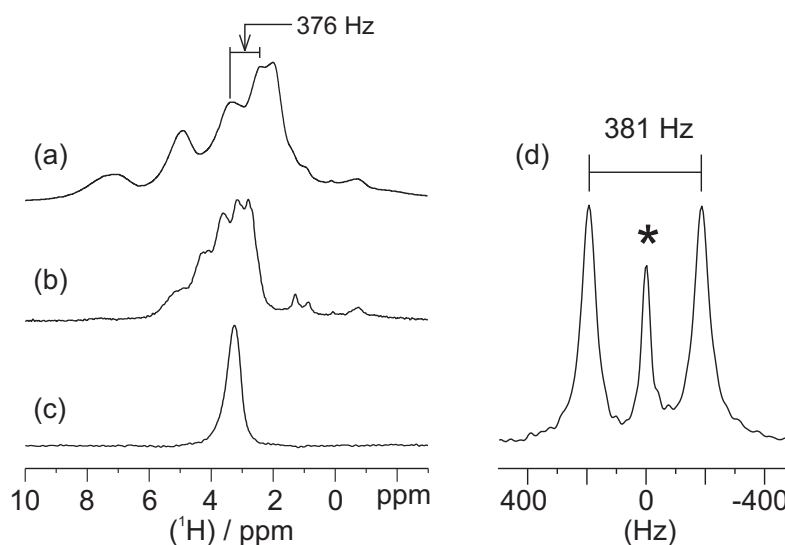


Figure 4.8 ^1H MAS NMR spectra of $\text{AlH}/\text{Al}_2\text{O}_3\text{-(500)}$ recorded at (a) $B_0=9.4$ T and (b) $B_0=18.8$ T at a spinning frequency of $nR=20$ kHz. (c) J -HMQC filtered ^1H MAS spectrum with ^{27}Al RA-MP decoupling ($B_0=18.8$ T, $\nu_R=20$ kHz). (d) J -resolved projection (see Appendix 3) ($B_0=18.8$ T, $\nu_R=20$ kHz). Central peak (*) results from the incomplete inversion produced by the ^{27}Al π pulse leading to refocusing of the heteronuclear scalar coupling.

The unusual asymmetric pattern observed in the non-decoupled ^1H MAS spectra at two magnetic fields is the result of a contribution from (a) the scalar coupling J_{iso} and (b) a second-order coupling arising from the strong dipolar coupling between ^1H and a neighboring quadrupolar nucleus, ^{27}Al .²⁵ The spacing of 376 Hz between the innermost lines (see spectrum at 9.4 T) is a direct measure of the ^1H - ^{27}Al scalar coupling. This J_{iso} value, higher than those reported so far in the literature,²⁶ denotes the specific characteristic of the present hydride species. The interval between the outermost lines of the multiplet is inversely proportional to the aluminum Larmor frequency ν_{Al} , which explains the larger spreading of the multiplet observed at 9.4 T with respect to that observed at 18.8 T. It is also directly proportional to the quadrupolar constant C_Q and the dipolar constant DIS . From crystallographic data, it is reasonable to consider the AlH distance superior to 1.50 Å¹³ that leads to a dipolar-coupling constant of about 9 kHz. A fair simulation points to high values of C_Q , about 15 MHz (Figure 4.9), much larger than those commonly reported in the literature,²⁶ but in line with those encountered in silica-supported aluminum alkyls.¹⁵ This large C_Q value directly reflects the large electric field gradient that is present around the considered Al-H . Therefore, the large splitting observed in Figure 4.8, which has not been reported previously, accounts for a large local dissymmetry around the aluminum. The first coordination sphere of aluminum is here highly distorted as a consequence of the surface heterogeneity. This is not surprising as heterolytic cleavage of the aluminum-carbon bond by H_2 is expected to yield hydride species on the formerly alkyl-substituted $\text{Al}_{\text{IV/V}}$ centers, for which we already observed large C_Q values. A J -Resolved

experiment²⁷ where an ^{27}Al π pulse is used to express the heteronuclear J coupling during a ^1H spin-echo, was performed on $\text{AlH}/\text{Al}_2\text{O}_3\text{-(500)}$. The signal presented in the frequency domain in Figure 4.8 (d), clearly evidences a doublet characteristic of a *terminal* aluminum hydride and separated by 381 Hz, in line with the scalar coupling J_{iso} measured on the ^1H MAS spectrum.

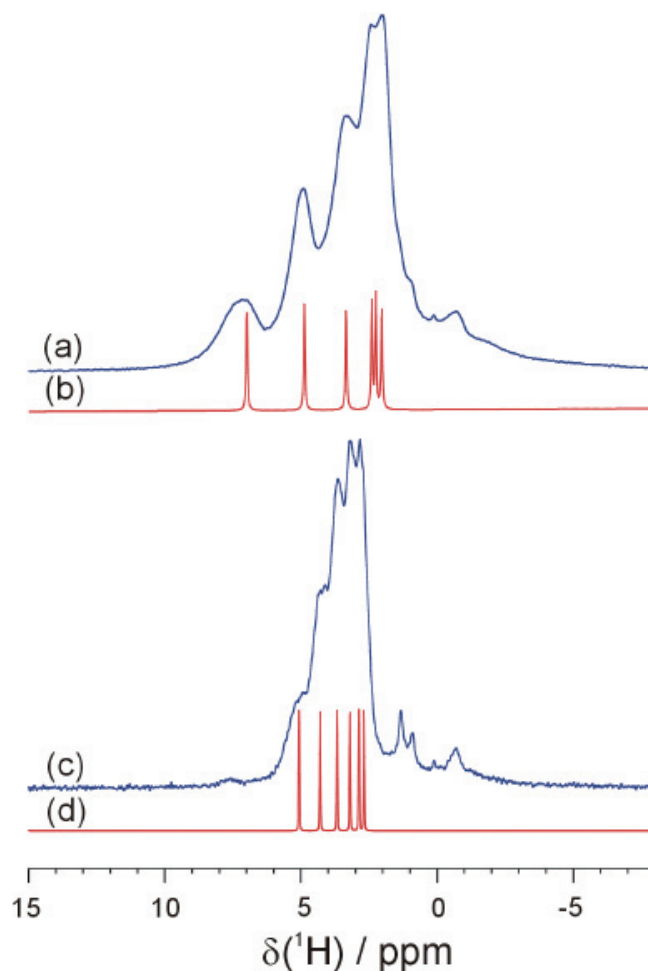


Figure 4.9 ^1H MAS spectra of **2** at 9.4 T (a) and 18.8 T (c). The positions of the lines in the multiplet were calculated with DMFIT4 using the expression of the complete shift given by eq. 23 in reference²⁷. The second-order shift itself, defined as $\Delta = -3/10 C_q D' / \nu_s$, was 390 Hz and 195 Hz at 9.4 T and 18.8 T, respectively. These values of D correspond to $C_Q=15\text{MHz}$ and $D'=9\text{kHz}$.

The ^{27}Al - ^1H correlation spectrum on Figure 4.10 was acquired using the J-HMQC pulse sequence which correlates nuclei *via* their scalar coupling, a well-suited method for hydride species presenting large $^1J_{\text{Al-H}}$ couplings.²⁶ The broad signal along the ^{27}Al dimension shows only those aluminum centers bearing hydride ligands. This spectrum confirms the major presence of highly distorted (*i.e.* with large C_Q values) $\text{Al}_{\text{IV/V-H}}$ in $\text{AlH}/\text{Al}_2\text{O}_3\text{-(500)}$. The narrow ^1H chemical shift range for the hydride signal prevents definitive conclusion regarding the absolute proportion of Al_{IV} in $\text{AlH}/\text{Al}_2\text{O}_3\text{-(500)}$. The pro-

portion of $\text{Al}_{\text{VI}}\text{-H}$ is small in $\text{AlH}/\text{Al}_2\text{O}_{3-(500)}$ (estimated to be less than 10%), as in $2/\text{Al}_2\text{O}_{3-(500)}$, where $\text{Al}_{\text{VI}}\text{-}i\text{Bu}$ species were assumed to be present in much weaker proportion than the tetra- and pentacoordinated aluminum alkyl centers. In the Al_{VI} case, the quadrupolar broadening is clearly reduced, indicating a comparatively more symmetrical environment. Interestingly, as the $\text{Al}_{\text{IV/V}}\text{-H}$ gives ^1H NMR signals in the [3.4-3.2] ppm range, the $\text{Al}_{\text{VI}}\text{-H}$ hydrides resonate at lower fields ([3.6-3.4] ppm). The NMR characteristics for the identified types of hydrides are gathered in Figure 4.10.

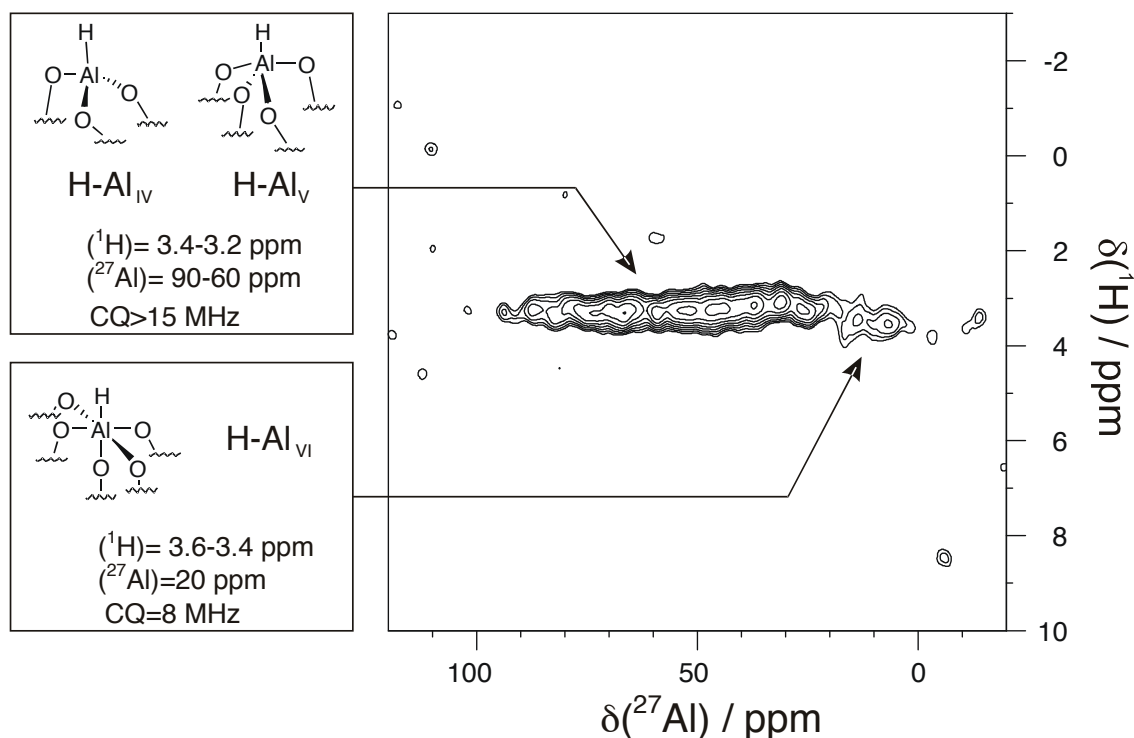
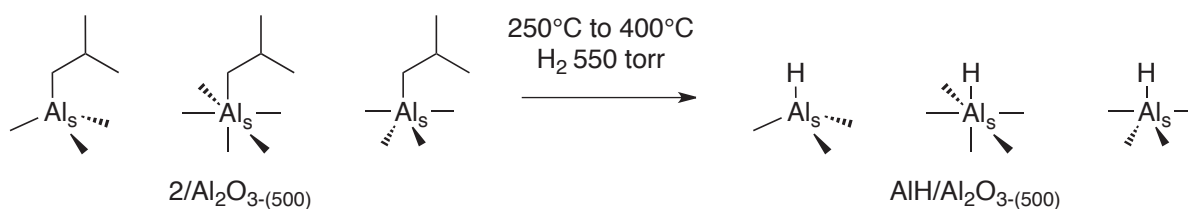


Figure 4.10 $^{27}\text{Al}\text{-}^1\text{H}$ J-HMQC MAS NMR spectrum of $\text{AlH}/\text{Al}_2\text{O}_{3-(500)}$ (18.8T, at a spinning frequency of 20 kHz, evolution delay of 2 ms, number of transients of 768, relaxation delay of 1s, number of t_1 increments of 100).

$\text{AlH}/\text{Al}_2\text{O}_{3-(500)}$ is the first example of material bearing isolated aluminum hydride supported on Alumina, which was prepared by heterolytic splitting of H_2 on Al-C of supported alkyl aluminum (Scheme 4.5).



Scheme 4.5 Treatment of $2/\text{Al}_2\text{O}_{3-(500)}$ under H_2 at 400°C afford $\text{AlH}/\text{Al}_2\text{O}_{3-(500)}$

2.3. Catalytic activity of $2/\text{Al}_2\text{O}_3-(500)$ and $\text{AlH}/\text{Al}_2\text{O}_3-(500)$

The exposure of $\text{AlH}/\text{Al}_2\text{O}_3-(500)$ to 550 Torr of ethylene at 100°C leads to formation of polyethylenic fragments and vanishing of Al-H bands, as shown by IR follow-up (Figure 4.11).

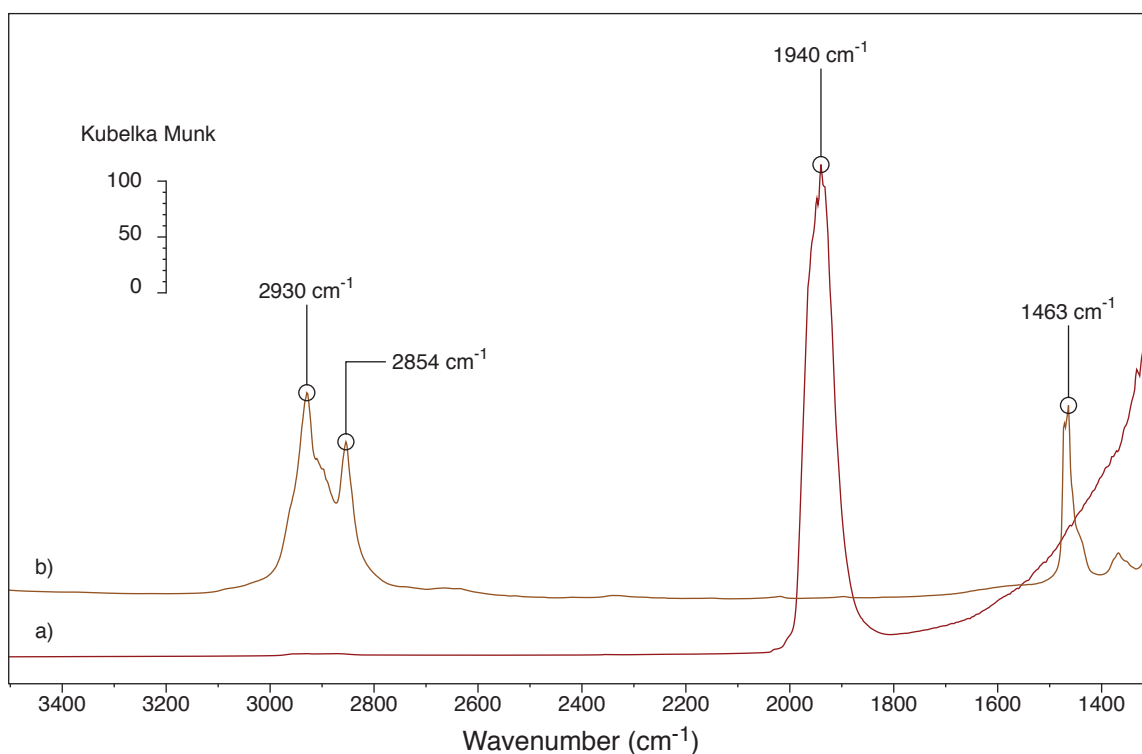


Figure 4.11 Diffuse reflectance infrared spectra of $\text{AlH}/\text{Al}_2\text{O}_3-(500)$ a) before and b) after exposition to excess of ethylene (550 Torr) at 100°C

In Chapter 2, the presence of aluminum alkyl and aluminum hydride at the surface of $\text{WH}/\text{Al}_2\text{O}_3-(500)$ have been spotted. As unsaturated $\text{C}=\text{C}$ bond can thus be inserted into Al-H they may have a role in the catalytic activity of $\text{WH}/\text{Al}_2\text{O}_3-(500)$.

In Chapter 3, it has been demonstrated that the mechanism of conversion of ethylene to propylene includes the transient formation 1-butene by ethylene dimerization. Hence, the preparation of surface aluminum alkyl and aluminum hydrides without their tungsten counterparts is a good opportunity to verify their potential role in dimerization. Moreover, it has also been shown that the deactivation mechanism of the active species occurs by formation of polyethylene at the surface of the catalyst. Thus, in order to understand the role of aluminum alkyls and hydrides in the catalytic activity of $\text{WH}/\text{Al}_2\text{O}_3-(500)$ for direct conversion of ethylene to propylene, the activity of $2/\text{Al}_2\text{O}_3-(500)$ and $\text{AlH}/\text{Al}_2\text{O}_3-(500)$ toward ethylene in continuous flow reactor will be first tested.

Considering the results obtained, $\text{AlH}/\text{Al}_2\text{O}_{3-(500)}$ was then tested for in autoclave for ethylene polymerization. Finally $\text{AlH}/\text{Al}_2\text{O}_{3-(500)}$ was tested for catalytic ethylene hydrogenation.

2.3.1. Catalytic activity of $2/\text{Al}_2\text{O}_{3-(500)}$ and $\text{AlH}/\text{Al}_2\text{O}_{3-(500)}$ in ethylene to propylene conditions

The two materials have been tested in similar conditions that the $\text{WH}/\text{Al}_2\text{O}_{3-(500)}$, *i.e.* in continuous flow reactor at 150°C and $4 \text{ mL}\cdot\text{min}^{-1}$ of ethylene.

- $2/\text{Al}_2\text{O}_{3-(500)}$

When $2/\text{Al}_2\text{O}_{3-(500)}$ was tested in continuous flow reactors, no trace of products were found by GC in the gas flow coming out from the reactor. Thus, aluminum alkyls do not perform the dimerization of ethylene. After 24 h, a 355 mg plug of polymeric material and catalyst was collected when the reactor was opened. During 24 h on stream 205 mg of polymer was formed. The resulting material (polymer + catalyst) was analyzed by TGA and DSC.

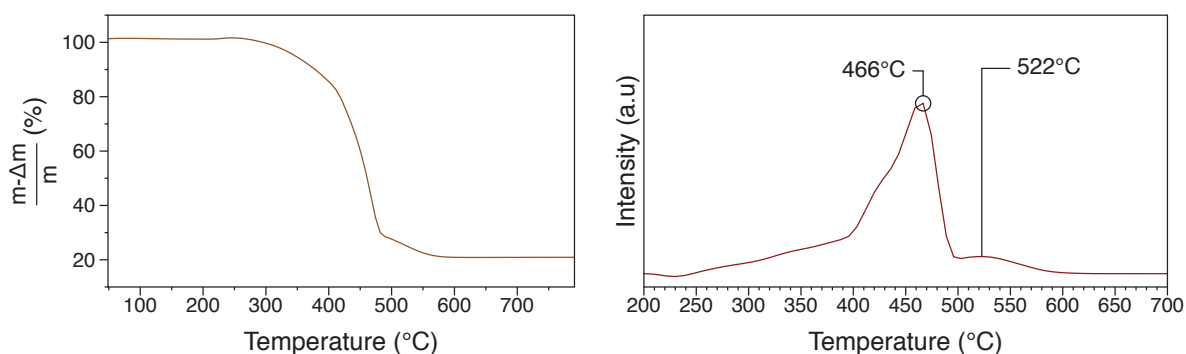


Figure 4.12 left: TGA profile of the material recovered after 24 h on stream over $2/\text{Al}_2\text{O}_{3-(500)}$; right: relative differential thermo-gravimetric profile.

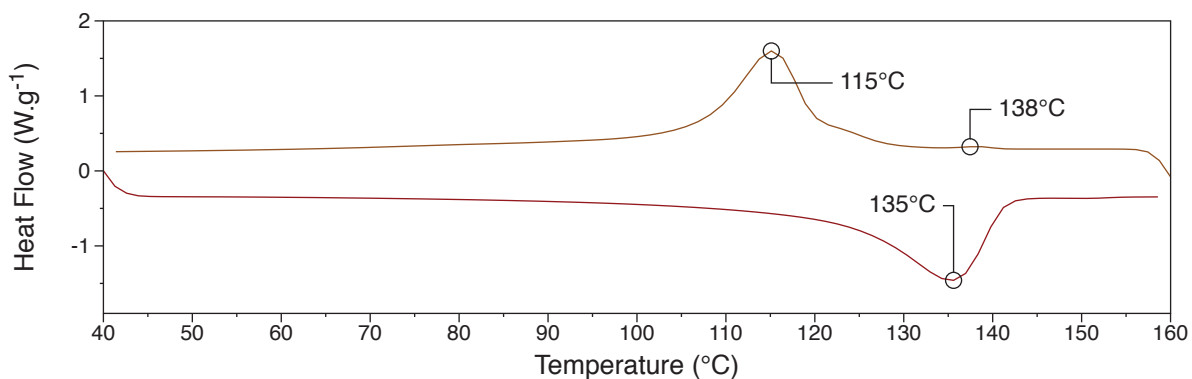


Figure 4.13 Fusion and crystallization DSC profile of the material recovered after 24 h on ethylene stream over $2/\text{Al}_2\text{O}_{3-(500)}$

The polymer formed burns mainly around 466°C as the DTG profile features a large peak at this temperature and minor one at 522°C (Figure 4.12). DSC reveals that the melting point of the polymer formed in 135°C (Figure 4.13). This melting point is similar to LHDPE.

- $\text{AlH}/\text{Al}_2\text{O}_3\text{-(500)}$

When $\text{AlH}/\text{Al}_2\text{O}_3\text{-(500)}$ was tested in continuous flow reactors, no trace of products were found by GC in the gas flow coming out from the reactor. Thus, aluminum hydrides do not perform the dimerization of ethylene either. Interestingly, after 24 h on stream the reactor clogged up. A 960 mg plug of polymeric material and catalyst was collected when the reactor was opened. Indeed, during 24 h on stream 850 mg of polymer was formed. The resulting material (polymer + catalyst) was analyzed by TGA and DSC.

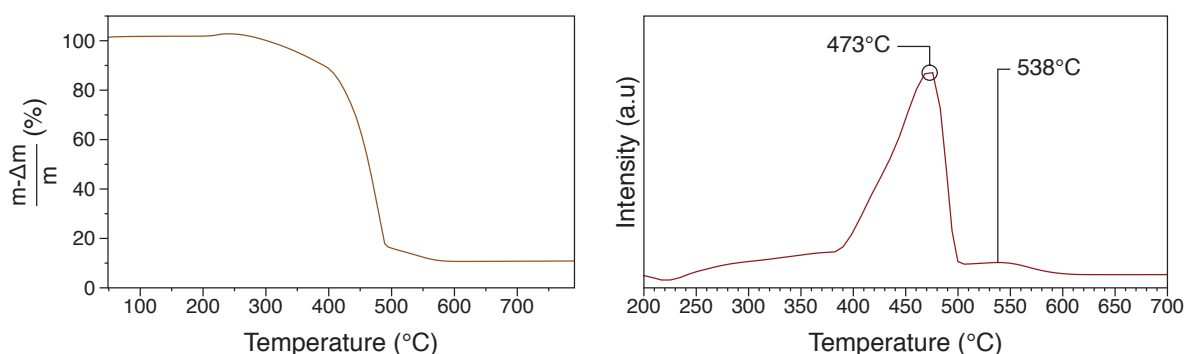


Figure 4.14 left: TGA profile of the material recovered after 24 h on stream over $\text{AlH}/\text{Al}_2\text{O}_3\text{-(500)}$; right: relative differential thermo-gravimetric profile.

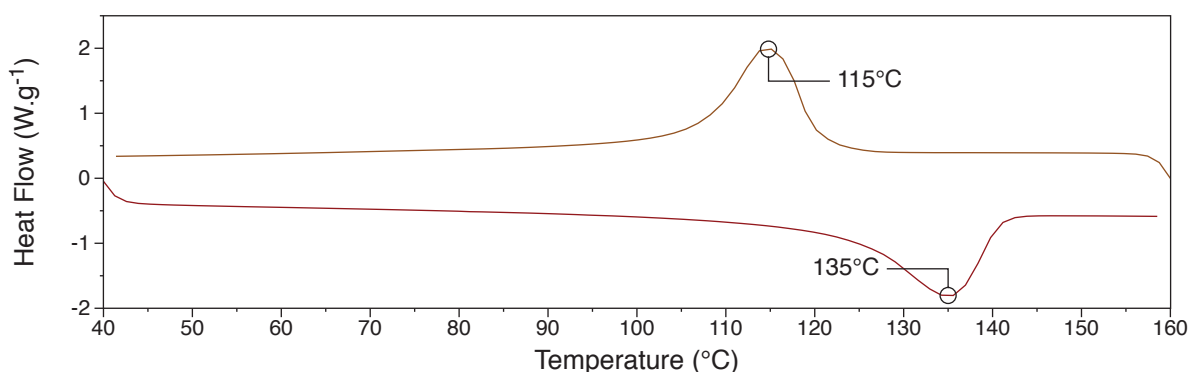


Figure 4.15 Fusion and crystallization DSC profile of the material recovered after 24 h on ethylene stream over $\text{AlH}/\text{Al}_2\text{O}_3\text{-(500)}$

TGA indicates that 90% of the material is burned during the analysis (Figure 4.14). The polymer formed burns mainly around 473°C as the DTG profile features a large peak at this temperature and minor one at 538°C. DSC reveals that the melting point of the polymer formed in 135°C (Figure 4.15). This melting point is similar to LHDPE.

- Conclusion

This values have to be compared to the results presented in Chapter 3, when $\text{WH}/\text{Al}_2\text{O}_3$ -(500) was analyzed after different time on ethylene stream. At low time on stream, polymers with low melting point are formed (*i.e.* 101-116°C). At higher time on stream two melting point are observed one at 116°C and one at 135°C. $2/\text{Al}_2\text{O}_3$ -(500) and $\text{AlH}/\text{Al}_2\text{O}_3$ -(500) provide after 24 h on stream a polymer with a single melting point of 135°C. It can be assumed that the formation of the polymeric species with a melting point of 116°C is promoted by tungsten surface species of $\text{WH}/\text{Al}_2\text{O}_3$ -(500).

2.3.2. Catalytic activity of $\text{AlH}/\text{Al}_2\text{O}_3$ -(500) for ethylene polymerization

As the previous results shows that $\text{AlH}/\text{Al}_2\text{O}_3$ -(500) is a catalyst for ethylene polymerization at atmospheric pressure, it was decided to performing the reaction at 35 bar of ethylene in autoclave. The polymerization time and the effect of temperature were studied.

Table 4.1 Ethylene polymerization results for $\text{AlH}/\text{Al}_2\text{O}_3$ -(500)

Run ^[a]	T (°C)	Polymerization time (h)	Yield (mg _{PE})	Activity ^[b]	M_n ^[c]	M_w/M_n	T_m (°C)	Cristalinity (%)
1	50	0.5	660	11.0	8.9	2.6	135	45
2	50	1	1155	9.6	8.3	2.6	134	53
3	50	4	3270	7.7	8.7	2.6	135	56
4	100	0.5	1314	21.9	8.7	2.7	136	53
5	150	0.5	953	15.8	7.4	3.0	137	53

[a] All polymerization experiments were conducted under 35 bar of ethylene, using 100 mg of $\text{AlH}/\text{Al}_2\text{O}_3$ -(500) ($1200 \mu\text{mol}_{(\text{AlH})}\cdot\text{g}^{-1}$) in 20 mL of toluene; [b] Average activity in $\text{kg}_{\text{PE}}\cdot\text{mol}_{(\text{AlH})}^{-1}\cdot\text{h}^{-1}$ calculated over the whole polymerization time. [c] Average molecular weight ($\times 10^5 \text{ g}\cdot\text{mol}^{-1}$) determined by HTSEC in 1,2,4-trichlorobenzene at 150 °C, measured with a relative calibration based on standard polystyrene. [d] Determined by DSC (second heating).

The results obtained for polymerization of ethylene over $\text{AlH}/\text{Al}_2\text{O}_3$ -(500) are summarized in Table 4.1. For each runs the polymeric material obtained have a similar melting temperature (T_m): from 134 to 137°C. This temperature is consistent with high density polyethylene HDPE. The average molar mass (M_n) of PE, measured with high temperature size exclusion and spanning from 8.3 to 8.9 $10^5 \text{ g}\cdot\text{mol}^{-1}$, is also in line with the formation of HDPE. The molar mass distribution (M_w/M_n) remains comparable for all runs, from 2.6 to 3.0, a mass distribution characteristic of single-site polymerization with a high $k_{\text{chain-growth}}/k_{\text{chain-transfer}}$ ratio. On all this polymers liquid ^{13}C NMR was performed at 100°C in 1,3,5-trichlobenzene (TCB). The presence of a single signal at 32.2 ppm is characteristic of a linear structure, as no branching carbon is detected (see Figure 4.16). However, the

yield and M_n values imply that, at most, only a small fraction (<1.25%) of Al centers produce polymer chains. Such a low fraction of active species has already been observed with homogeneous catalysts.^{28,29} Moreover, from the DFT calculation on the Insertion/Chain Transfer Balance Budzelaar *et al.* suggested that none of the reported aluminum catalysts so far were the active species and a transition metal contamination could not be excluded.³⁰

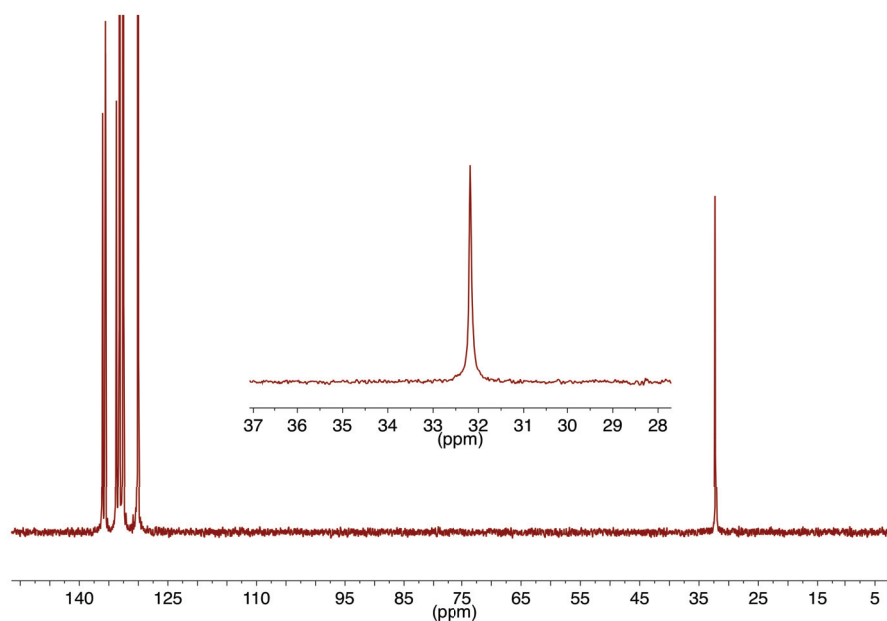
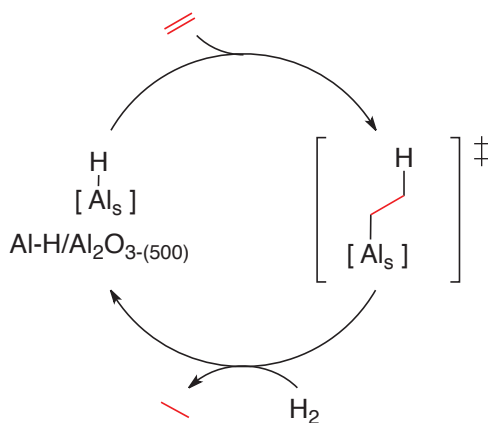


Figure 4.16 ^{13}C NMR in a TCB at 100°C of the material obtained after Ethylene polymerization over $\text{AlH}/\text{Al}_2\text{O}_3-(500)$

The study of polymerization time at 50°C (Run 1-3) shows that the activity of the catalyst slightly decreases with the polymerization time from 11.0 to $7.7 \text{ kg}_{\text{PE}} \cdot \text{mol}^{-1}_{(\text{AlH})} \cdot \text{h}^{-1}$. The study of the reaction temperature indicates that 100°C is the optimal temperature for the ethylene polymerization with an activity of $21.9 \text{ kg}_{\text{PE}} \cdot \text{mol}^{-1}_{(\text{AlH})} \cdot \text{h}^{-1}$ corresponding to a TOF of 782 h^{-1} . Yet again this result may be compared with the result of Chapter 3, when $\text{WH}/\text{Al}_2\text{O}_3-(500)$ was analyzed after exposure to ethylene stream at different temperatures. The formation of carbonaceous deposit reaches a maximum when the ethylene to propylene reaction was performed at 100°C . Moreover the polymeric residue on the used catalyst exhibits similar melting point (134°C) as the polymer obtained from $\text{AlH}/\text{Al}_2\text{O}_3-(500)$.

2.3.3. Catalytic activity of $\text{AlH}/\text{Al}_2\text{O}_3$ -(500) for ethylene hydrogenation

As the last results demonstrates that these surface aluminum hydrides are reactive toward double-bond insertion, and as the formation of aluminum hydride have shown that Al-C bonds can be cleaved through H_2 heterolytic cleavage, it is reasonable to expect that the combination of these two elementary steps, *i.e.* olefin insertion followed by Al-C hydrogenolysis, may be combined into olefin hydrogenation (Scheme 4.6).



Scheme 4.6 Postulated mechanism of ethylene hydrogenation over $\text{AlH}/\text{Al}_2\text{O}_3$ -(500)

Therefore, exposure of ethylene and H_2 to $\text{AlH}/\text{Al}_2\text{O}_3$ -(500) in a continuous flow reactor (H_2 and C_2H_4 : 4 mL.min⁻¹, 400°C) lead to sustained conversion into ethane, while Al_2O_3 -(500) proved inactive under identical conditions.

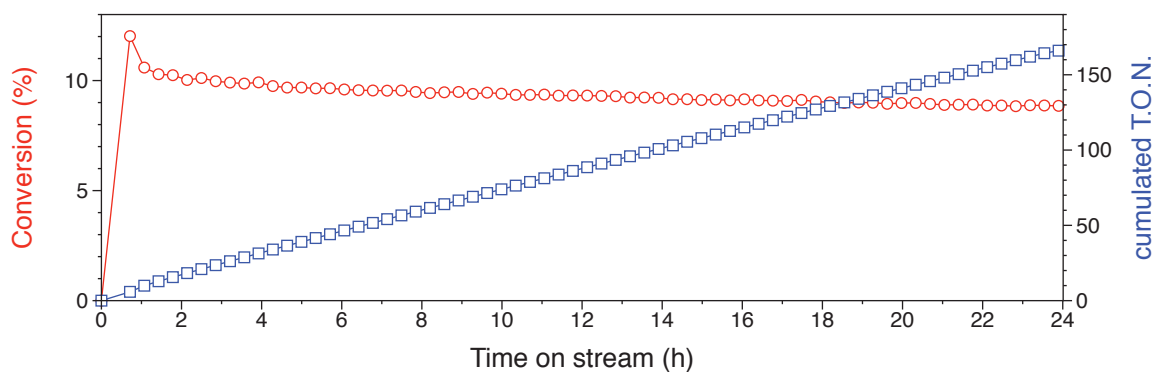


Figure 4.17 Conversion of ethylene (●), and TON (□)

This represents the first example of inactivated olefin hydrogenation by aluminum hydrides, which parallels recent findings in alkaline-earth metal catalysis³¹ and main group metal-based frustrated Lewis pairs (FLP).³² This most probably owes a lot to the peculiar structure of the supported hydrides, as enlighten by their NMR features. Hence, the uncommon highly strained molecular structure of the Al-H may well be the source of this unprecedented reactivity.

2.4. Conclusion

In order to observe the role of alkyl aluminum and aluminum hydride present at the surface of **WH/Al₂O₃**, isolated alkyl aluminum, **2/Al₂O₃₋₍₅₀₀₎**, and isolated aluminum hydride, **AlH/Al₂O₃₋₍₅₀₀₎**, supported on alumina have been prepared.

Supported aluminum alkyl, **2/Al₂O₃₋₍₅₀₀₎**, was prepared by reaction between Al(ⁱBu)₃ and the surface of Al₂O₃₋₍₅₀₀₎. The isobutyl fragment is located on all types of surface aluminum, *i.e.* tetra- penta- and hexa- coordinated. **2/Al₂O₃₋₍₅₀₀₎** has shown an activity in ethylene polymerization in continuous flow reactor at 150°C.

Treatment of **2/Al₂O₃₋₍₅₀₀₎** under hydrogen afford the corresponding aluminum hydrides, **AlH/Al₂O₃₋₍₅₀₀₎**. These species are formed by heterolytic splitting of H₂ on Al-C bond of alkyl aluminum. The use of High field NMR, and particularly ²⁷Al-¹H J-HMQC sequence, has proved the presence of aluminum hydride on all types of surface aluminum, with a large scalar coupling constant ¹J_{Al-H} of 380 Hz and a ¹H chemical shift of 3.3 ppm.

As **2/Al₂O₃₋₍₅₀₀₎**, **AlH/Al₂O₃₋₍₅₀₀₎** has shown an activity in ethylene polymerization in continuous flow reactor in the same conditions that direct conversion of ethylene to propylene. The resulting polymers have a melting point of 135°C, whereas two melting point, *i.e.* 116 and 135°C, are observed for the polymers formed on **WH/Al₂O₃₋₍₅₀₀₎** during the ethylene to propylene conversion. These results proves that alkyl aluminum and aluminum hydride are involved in the deactivation of **WH/Al₂O₃₋₍₅₀₀₎** during direct conversion of ethylene to propylene, and that tungsten species may promote the formation of the polymers with a melting point of 116°C.

AlH/Al₂O₃₋₍₅₀₀₎ have been tested for ethylene polymerization at 35 bar with a maximum activity of 21.9 kg_{PE}.mol⁻¹_(AlH).h⁻¹ at 100°C.

Finally, it has been found that **AlH/Al₂O₃₋₍₅₀₀₎** was able to perform catalytically ethylene hydrogenation by double bond insertion in Al-H followed of H₂ heterolytic splitting over Al-C at high temperature (400°C).

3. Experimental section

3.1. General procedures

All experiments were carried out under controlled atmosphere, using Schlenk and glove-box techniques for the organometallic synthesis. For the synthesis and treatments of the surface species, reactions were carried out using high-vacuum lines (10^{-5} Torr) and glove-box techniques. Gas-phase analyses were performed on a Hewlett-Packard 5890 series II gas chromatograph equipped with a flame ionisation detector and an Al₂O₃/KCl on fused silica column (50 m X 0.32 mm). IR spectra were recorded on a Nicolet 6700 FT-IR spectrometer by using a DRIFT cell equipped with CaF₂ windows. The samples were prepared under Ar within a glove-box. Typically, 64 scans were accumulated for each spectrum (resolution 4 cm⁻¹). Solution NMR spectra were recorded on an Avance-300 Bruker spectrometer. All chemical shifts were measured relative to residual ¹H or ¹³C resonance in the deuterated solvent: C₆D₆, δ 7.15 ppm for ¹H, 128 ppm for ¹³C. Solid-state NMR spectra were acquired on a Avance II 800 spectrometers (¹H: 800.13 MHz, ¹³C: 201.21 MHz). For ¹H experiments, the spinning frequency was 20 kHz, the recycle delay was 5 s and 16 scans were collected using a 90° pulse excitation of 3 μ s. The RA-MP ²⁷Al decoupling scheme was composed of pulses of 6 μ s at an RF field strength of 70 kHz interleaved a delay of 300 μ s. The HMQC experiments were set up with an ²⁷Al spin echo selective to the central transition, with pulses of 8.5 and 17 μ s. In the *J*-HMQC, the recoupling delay was set to 6 msec, with a p pulse on ¹H of 5.3 μ s, a recycling delay of 1 s and 768 added transients. For the *D*-HMQC, the recoupling scheme (SR4)³³ applied for 500 μ s. A total of 1536 transients were added with a recycling delay of 1 s. Chemical shifts were given in ppm with respect to TMS as external reference for ¹H and ¹³C NMR, and to Al(H₂O)₆³⁺ for ²⁷Al NMR. Differential scanning calorimetry (DSC) measurements for determination of polymer melting transition were performed on a Mettler DSC1 apparatus. Sample was heated from 40°C to 150 °C at 5°C.min⁻¹. Two successive heating and cooling of the samples were performed, and data obtained during the second run was considered. High temperature SEC analysis was performed using a Waters Alliance GPCV 2000 chromatograph equipped with three columns (PL gel Olexis 7x300 mm). Polymer was separate from catalyst by extraction with trichlorobenzene at 120°C. Sample (1 mg.mL⁻¹) was eluted with trichlorobenzene with a flow rate of 1 mL.min⁻¹ at 150°C. Online detection was performed by refractometry and viscosimetric measurements using Waters equipments. The system was calibrated with polystyrene standards in the range of 500 to 7106 g.mol⁻¹.

3.2. Preparation and characterizations of $\text{Al}_2\text{O}_{3-(500)}$ RP

$\gamma\text{-Al}_2\text{O}_{3-(500)}$ RP was used for details of preparation and characterization see section 3 in Chapter 2.

3.3. Preparation of $2/\text{Al}_2\text{O}_{3-(500)}$

A mixture of $\text{Al}(i\text{Bu})_3$, **1**, (360 mg, 1.614 mmol) and $\text{Al}_2\text{O}_{3-(500)}$ RP (1 g) in pentane (10 mL) was stirred at 25 °C for 4 h. After filtration, the solid was washed three times with pentane and all volatile compounds were condensed into another reactor (volume known > 6 L) in order to quantify isobutane evolved during the impregnation. The resulting white solid was dried under vacuum (10^{-5} Torr).

Hydrolysis procedure: $2/\text{Al}_2\text{O}_{3-(500)}$ was treated with an excess of H_2O in gas phase (17 Torr). The gaseous products were quantified by GC.

3.4. Preparation of $\text{AlH}/\text{Al}_2\text{O}_{3-(500)}$

Monitoring the treatment of $2/\text{Al}_2\text{O}_{3-(500)}$ under vacuum or H_2 at different temperature: Al_2O_3 RP (75mg, 65 mg) was pressed into an 17 mm self-supporting disk, adjusted in the sample holder, and introduced into a reactor equipped with CaF_2 windows. The supports were calcined under air and partly dehydroxylated under vacuum (10^{-5} Torr) at 500°C. **2** was then sublimed under *vacuum* onto the Alumina disk. The solid was reacted at RT for 2 h, and the excess of the molecular complex was removed by reverse sublimation at 60°C and condensed into a tube cooled by liquid N_2 , which was then sealed off using a blow torch. The resulting pellet was treated either under *vacuum* or under 550 Torr of H_2 and heated two hours at 100, 150, 200, 250, 300 and 350°C. An IR spectrum was recorded and gas phase was analyzed by GC at each step.

Preparation of $\text{AlH}/\text{Al}_2\text{O}_{3-(500)}$: $2/\text{Al}_2\text{O}_{3-(500)}$ was heated at 400 °C in the presence of a large excess of dry, deoxygenated H_2 (750 Torr). After 4 h, material **2** was obtained as a white solid, and the gaseous products were quantified by GC.

Hydrolysis procedure: $\text{AlH}/\text{Al}_2\text{O}_{3-(500)}$ was treated with an excess of H_2O in gas phase (17 Torr). The gaseous products were quantified by GC.

3.5. Catalytic application of $2/\text{Al}_2\text{O}_{3-(500)}$ and $\text{AlH}/\text{Al}_2\text{O}_{3-(500)}$

3.5.1. Ethylene to propylene conditions

A stainless-steel half-inch cylindrical reactor that can be isolated from the atmosphere was charged with $2/\text{Al}_2\text{O}_{3-(500)}$ or $\text{AlH}/\text{Al}_2\text{O}_{3-(500)}$ (110 mg; 0.19 mL) in a glovebox. After connection to the gas lines and purging of the tubes, a $4 \text{ ml}\cdot\text{min}^{-1}$ flow of ethylene ($\text{WHSV} (\text{C}_2\text{H}_2) = 2.5 \text{ h}^{-1}$, $\text{SV} (\text{C}_2\text{H}_2) = 1270 \text{ h}^{-1}$) was passed over the catalyst bed at 150°C . Hydrocarbon products and hydrogen were analyzed online by GC (HP 8890 chromatograph fitted with an $\text{Al}_2\text{O}_3/\text{KCl}$ 50 m x 0.32 mm capillary column, FID detector for hydrocarbons with a 3-m molecular sieve column and a catharometer for hydrogen). After 24 hour on stream the catalyst and the material formed was recovered for analysis.

3.5.2. Ethylene polymerization

A 80 mL autoclave was charged into a glovebox with 20 mL of toluene and 100 mg of $\text{AlH}/\text{Al}_2\text{O}_{3-(500)}$. The reactor was then heated to 100°C . Under magnetic stirring, the wanted ethylene pressure was established and kept constant over 30min. The reaction was quenched by removing ethylene and pouring the mixture into a EtOH (40 mL), H_2O (140 mL) and HCl (20 mL, 37%) solution. After 2h of stirring, the resulting solid polymer was filtered off and washed successively with water (80 mL) and EtOH (80 mL) and dried at 50°C under vacuum until constant mass. Average activity in $\text{g}_{\text{PE}}\cdot\text{mol}^{-1}_{(\text{AlH})}\cdot\text{h}^{-1}$ was calculated over the whole polymerization time (30 min).

3.5.3. Ethylene hydrogenation

A stainless-steel half-inch cylindrical reactor that can be isolated from the atmosphere was charged with $\text{AlH}/\text{Al}_2\text{O}_{3-(500)}$ (200 mg; 0.34mL) in a glovebox. After connection to the gas lines and purging of the tubes, a $4 \text{ ml}\cdot\text{min}^{-1}$ flow of H_2 and a $4 \text{ ml}\cdot\text{min}^{-1}$ flow of ethylene ($\text{WHSV} (\text{C}_2\text{H}_2) = 1.4 \text{ h}^{-1}$, $\text{SV} (\text{C}_2\text{H}_2) = 700 \text{ h}^{-1}$) was passed over the catalyst bed at 400°C . Hydrocarbon products and hydrogen were analyzed online by GC (HP 8890 chromatograph fitted with an $\text{Al}_2\text{O}_3/\text{KCl}$ 50 m x 0.32 mm capillary column, FID detector for hydrocarbons with a 3-m molecular sieve column and a catharometer for hydrogen).

4. Reference and Notes

- (1) Eberle, U.; Felderhoff, M.; and Schüth, F. *Angewandte Chemie International Edition*. 2009, *48*, 6608-6630.
- (2) Andersson, P. G. and Munslow, I. J. *Modern reduction methods*, Andersson, P. G. and Munslow, I. J., Ed.; Wiley-VCH : Weinheim ; 2008.
- (3) Cornils , B. and Herrmann, W. A. *Applied homogeneous catalysis with organometallic compounds : a comprehensive handbook in three volumes*, Cornils , B. and Herrmann, W. A., Ed.; 2nd.; Wiley-VCH; 2002.
- (4) Harder, S. *Chemical Reviews*. 2010, *110*, 3852-3876.
- (5) Joubert, J.; Delbecq, F.; Thieuleux, C.; Taoufik, M.; Blanc, F.; Copèreret, C.; Thivolle-Cazat, J.; Basset, J. -M.; and Sautet, P. *Organometallics*. 2007, *26*, 3329-3335.
- (6) Le Roux, E.; Taoufik, M.; Baudouin, A.; Copèreret, C.; Thivolle-Cazat, J.; Basset, J. -M.; Maunders, B. M.; and Sunley, G. J. *Advanced Synthesis & Catalysis*. 2007, *349*, 231-237.
- (7) Larabi, C.; Merle, N.; Norsic, S.; Taoufik, M.; Baudouin, A.; Lucas, C.; Thivolle-Cazat, J.; de Mallmann, A.; and Basset, J. -M. *Organometallics*. 2009, *28*, 5647-5655.
- (8) Tosin, G.; Delgado, M.; Baudouin, A.; Santini, C. C.; Bayard, F.; and Basset, J. -M. *Organometallics*. 2010, *29*, 1312-1322.
- (9) Delgado, M. *PhD Thesis*. 2010.
- (10) Joubert, J.; Delbecq, F.; Sautet, P.; Roux, E. L.; Taoufik, M.; Thieuleux, C.; Blanc, F.; Coperet, C.; Thivolle-Cazat, J.; and Basset, J. M. *J. Am. Chem. Soc.* 2006, *128*, 9157-9169.
- (11) Joubert, J.; Salameh, A.; Krakoviack, V.; Delbecq, F.; Sautet, P.; Copèreret, C.; and Basset, J. M. *The Journal of Physical Chemistry B*. 2006, *110*, 23944-23950.
- (12) Ziegler, K. *Angewandte Chemie*. 1956, *68*, 721-729.
- (13) Uchiyama, M.; Naka, H.; Matsumoto, Y.; and Ohwada, T. *Journal of the American Chemical Society*. 2004, *126*, 10526-10527.
- (14) MacKenzie, K. J. D. *Multinuclear solid-state NMR of inorganic materials*, Pergamon: Amsterdam ; London ; 2002.
- (15) Anwander, R.; Palm, C.; Groeger, O.; and Engelhardt, G. *Organometallics*. 1998, *17*, 2027-2036.
- (16) Espinas, J.; Pelletier, J.; and Taoufik, M. *Unpublished results*.
- (17) Basset, J. -M.; Psaro, R.; Roberto, D.; and Ugo, R. *Modern surface organometallic chemistry*, Basset, J. -M.; Psaro, R.; Roberto, D.; and Ugo, R., Ed.; Wiley-VCH ; 2009.
- (18) Podall, H. E.; Petree, H. E.; and Zietz, J. R. *The Journal of Organic Chemistry*. 1959, *24*, 1222-1226.
- (19) Delevoye, L.; Trébosc, J.; Gan, Z.; Montagne, L.; and Amoureux, J. -P. *Journal of Magnetic Resonance*. 2007, *186*, 94 - 99.
- (20) Healy, M. D.; Mason, M. R.; Gravelle, P. W.; Bott, S. G.; and Barron, A. R. *Journal of the Chemical Society, Dalton Transactions*. 1993, *1993*, 441-454.
- (21) Campbell, J. P. and Gladfelter, W. L. *Inorganic Chemistry*. 1997, *36*, 4094-4098.
- (22) Nöth, H.; Schlegel, A.; Knizek, J.; Krossing, I.; Ponikwar, W.; and Seifert, T. *Chemistry - A European Journal*. 1998, *4*, 2191-2203.
- (23) Veith, M.; Freres, J.; Huch, V.; and Zimmer, M. *Organometallics*. 2006, *25*, 1875-1880.
- (24) Liu, S.; Fookan, U.; Burba, C. M.; Eastman, M. A.; and Wehmschulte, R. J. *Chemistry of Materials*. 2003, *15*, 2803-2808.

- (25) Harris, R. K. and Olivieri, A. C. *Progress in Nuclear Magnetic Resonance Spectroscopy*. 1992, 24, 435 - 456.
- (26) Hervrmánek, S.; Krvrírřvz, O.; Fusek, J.; Cerny, Z.; and Cásensky, B. *Journal of the Chemical Society, Perkin Transactions 2*. 1989, 1989, 987-992.
- (27) Massiot, D.; Fayon, F.; Alonso, B.; Trebosc, J.; and Amoureux, J. -P. *Journal of Magnetic Resonance*. 2003, 164, 160 - 164.
- (28) Kim, J. S.; Wojcinski, L. M.; Liu, S.; Sworen, J. C.; and Sen, A. *Journal of the American Chemical Society*. 2000, 122, 5668-5669.
- (29) Korolev, A. V.; Ihara, E.; Guzei, I. A.; Young, ,. V. G.; and Jordan, R. F. *Journal of the American Chemical Society*. 2001, 123, 8291-8309.
- (30) Talarico, G.; Busico, V.; and Budzelaar, P. H. M. *Organometallics*. 2001, 20, 4721-4726.
- (31) Stephan, D. and Erker, G. *Angewandte Chemie International Edition*. 2010, 49, 46-76.
- (32) Spielmann, J.; Buch, F.; and Harder, S. *Angewandte Chemie International Edition*. 2008, 47, 9434-9438.
- (33) Brinkmann, A. and Kentgens, A. P. M. *Journal of the American Chemical Society*. 2006, 128, 14758-14759.

Chapter 5

Production of propylene from light olefins using the $\text{WH}/\text{Al}_2\text{O}_3$ catalyst

1. Introduction	157
• Propylene from 1-butene only	157
• Propylene from 1-butene/2-butene mixture	157
• Propylene from 2-butene/isobutene mixture	158
• Propylene from ethylene/2-butene mixture	158
• Propylene from 2-butene only	159
2. Results and discussions	160
2.1. Description of the reactor	160
2.2. Propylene metathesis	161
2.3. Production of propylene from 1-butene only	164
2.3.1. Catalytic test	164
2.3.2. Proposed mechanism	165
2.3.3. Influence of the pressure	168
2.4. Production of propylene from trans-2-butene only	170
2.4.1. Catalytic test	170
2.4.2. Proposed mechanism	171
2.4.3. Influence of the pressure	172
2.5. Production of propylene from 1-butene/trans-2-butene mixtures	174
2.6. Production of propylene from isobutene/trans-2-butene cross metathesis.....	176
2.7. Ethylene/trans-2-butene cross-metathesis over WH/Al₂O₃₋₍₅₀₀₎.....	179
2.8. Conclusion.....	184
3. Experimental section	185
4. Reference and Notes	186

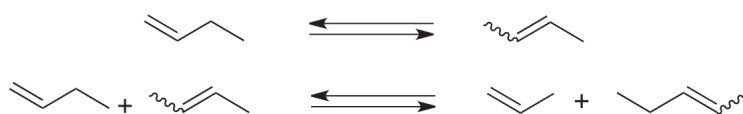
1. Introduction

The supported tungsten hydride catalyst has shown unprecedented results for the direct conversion of ethylene to propylene (see Chapter 3). Nevertheless, deactivation occurs during this reaction, and no methods were found for the regeneration of the catalyst. The study of the reaction mechanism reported in Chapter 3 shows that: i) $\text{WH}/\text{Al}_2\text{O}_3$ may be able to perform olefin metathesis; ii) butenes are the primary products and iii) ethylene is involved in the deactivation process by polymerization which is assumed to occur on cationic tungsten, Al-R and Al-H sites. Taking into account these results, it was decided to use $\text{WH}/\text{Al}_2\text{O}_3$ for metathesis reactions involving butenes and with a lower amount of ethylene to produce propylene. The reduction of ethylene partial pressure in the gas feed may generate less deactivation in metathesis.

The production of propylene using olefin metathesis is usually performed by ethylene/but-2-ene cross-metathesis using the reverse reaction of the Philips tri-olefin process.¹ Several examples report the valorizations of butenes cut for the production of propylene:

- Propylene from 1-butene only

Liu *et al.* have reported the preparation of a tungsten oxide catalyst supported on a mixture of $\gamma\text{-Al}_2\text{O}_3$ and 10%_{wt} of HY zeolite. This catalyst has shown interesting activity for propylene production from 1-butene only, with, after 1 hour on stream, a conversion of $5.7 \text{ mmol}_{\text{C}_3\text{=}}\cdot\text{h}^{-1}\cdot\text{g}^{-1}$ (selectivity 53%) at 180°C and 1 bar.² The selectivity in ethylene is explained by the isomerization of 1-butene to 2-butene performed on the acidic sites. The newly formed 2-butene reacts further with 1-butene by cross metathesis reaction on tungsten sites (Scheme 5.1).



Scheme 5.1 Production of propylene from 1-butene²

- Propylene from 1-butene/2-butene mixture

An example of homogenous system based on Grubbs 1st generation catalyst has been reported by Meyer *et al.*³ This system allows the production of propylene, in a high pressure closed reactor, from a mixture of 1-butene and 2-butene (Scheme 5.2). At 20 bar and 60°C , with a molar ratio, R ($\text{mol}_{\text{butenes}}/\text{mol}_{\text{catalyst}}$), of 14,000 and a 1-butene:2-butene ratio of 1:1, the thermodynamic equilibrium is reached in 60 min with a propylene yield of 25.9%. This system does not provide propylene from 1-butene alone.

Scheme 5.2 Production of propylene from 1-butene/2-butene mixture³

- Propylene from 2-butene/isobutene mixture

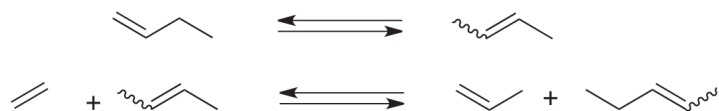
The use of isobutene in olefin metathesis reaction has been described by Banks *et al.* for the synthesis of isoamylene.⁴ In this reaction isobutene is reacted with 2-butene over a WO₃/SiO₂ catalyst to produce 2-methyl-2-butene (isoamylene) and propylene (Scheme 5.3). When the reactor is fed with a 1:1 ratio, ethylene, propylene, pentenes (n and iso) and hexenes (n plus iso) are produced with the following molar distribution: 10:40:35:15.

Scheme 5.3 Production of propylene and 2-methyl-2-butene from 2-butene/isobutene mixture⁴

The use of isobutene mixed with butenes is also presented in a BASF patent.⁵ In that multistage process the first stage is the reaction of 1-butene, 2-butene and isobutene to give propylene, 2-pentene and 2-methyl-2-butene. The second stage is the separation of propylene and 2-pentene/2-methyl-2-butene. The third stage is reaction of 2-pentene and 2-methyl-2-butene with ethylene to give propylene, 1-butene and isobutene. The latter are separated from propylene in the fourth stage of the process and are recycled in the first stage.

- Propylene from ethylene/2-butene mixture

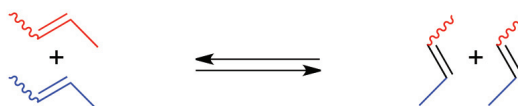
The Olefin Conversion Technology provided by ABB Lummus enhances the amount of propylene produced by naphta steam cracker units. This process converts the raw C₂ and C₄ feedstock coming from the steam cracker into propylene. The reaction occurs over a mixture of WO₃/SiO₂ and MgO at a temperature higher than 260°C and a pressure of 30-35 bars. The 1-butene feed is isomerized to 2-butene, over an MgO isomerzation catalyst, and then consumed along with the original 2-butene by the ethylene/2-butene cross metathesis (Scheme 5.4).⁶



Scheme 5.4 Production of propylene from ethylene/2-butene metathesis after enrichment of the feed in 2-butene by 1-butene isomerization.

- Propylene from 2-butene only

As for all symmetrical olefins, the reaction of butene-2 with typical olefin metathesis catalyst ($\text{MoO}_3/\text{Al}_2\text{O}_3$, $\text{WO}_3/\text{SiO}_2\dots$) always leads, to the best of our knowledge, to degenerated products, and thus no conversion of butene-2 to higher or smaller olefins is observed (Scheme 5.5). Only cis-trans isomerization occurs by metathesis pathway. No example of systems, are reported to produce propylene from 2-butene only.



Scheme 5.5 Degenerated 2-butene metathesis

Most of the catalysts allowing the production of propylene from butenes need acid or basic materials to achieve isomerization before the metathesis reaction. It has been seen in Chapter 3, that the tungsten carbene-hydride $\text{W}(\text{H})(=\text{CHR})$ present on the surface of $\text{WH}/\text{Al}_2\text{O}_3$ during the ethylene to propylene reaction, is able to perform olefin metathesis, *via* the carbene ligand, and dimerization-isomerization, *via* the hydride ligand. It can be presumed that $\text{WH}/\text{Al}_2\text{O}_3$ may perform the different catalytic reactions described previously. Experiments in Chapter 3 have also demonstrated that ethylene is the reagent that induces deactivation of the cationic tungsten sites by polymerization. One can wonder if this phenomenon also occurs with other olefins, such as propylene? The conversion of propylene on $\text{WH}/\text{Al}_2\text{O}_3$ will thus be studied first, to assess whether the fast deactivation observed in the early stage of ethylene to propylene reaction also occurs when starting with higher olefin.

2. Results and discussions

2.1. Description of the reactor

The continuous flow reactor described in subsection 2.1 of Chapter 3 and Appendix B was used for the following study.

In this chapter, different reactions involving olefins are presented. As some of these reactions involve two different reagents their conversion can be plotted separately. Nevertheless, for the sake of comparison, the reference in this chapter is the total olefin volumetric, and therefore the molar, flow rate. It is thus appropriate to compare the total carbon conversion, calculated as follow:

$$\text{Total carbon conv.} = \frac{\sum_i \text{mol of reagent}_i \text{ converted}}{\sum_j \text{mol of reagent}_j \text{ introduced}}$$

$$\text{Selectivity}_k = \frac{\text{mol of product}_k \text{ formed}}{\sum_i \text{mol of reagent}_i \text{ converted}}$$

The definition of the total carbon conversion is the sum of number of moles of each reagent converted divided by the sum of number of moles of each reagent introduced. The selectivity of a product k is equal to the number of mol of product k formed divided by sum of number of moles of each reagent converted.

2.2. Propylene metathesis

The main drawback of the production of propylene by direct conversion of ethylene over **WH/Al₂O₃** is the deactivation of the catalyst by ethylene polymerization presumably due to the cationic species (see Chapter 3). Before studying new routes of production of propylene, the reactivity of propylene over **WH/Al₂O₃** will first be tested in order to determine its catalytic performances for olefin metathesis. A particular attention will be pointed on the deactivation profile, which will be compared to those of direct conversion of ethylene to propylene.

The catalytic performances of **WH/Al₂O₃-(500)**, have been tested for propylene metathesis in continuous flow reactor following the conditions given in Table 5.1.

Table 5.1 Experimental conditions

Propylene flow rate (NmL.min ⁻¹)	20
Mass of catalyst (mg)	135
Tungsten loading (%wt)	5.5
Temperature (°C)	150
R (mol _{C₃=} .mol _w ⁻¹ .min ⁻¹)	20
P _{C₃=}	atm. pres.
VHSV (h ⁻¹)	5200

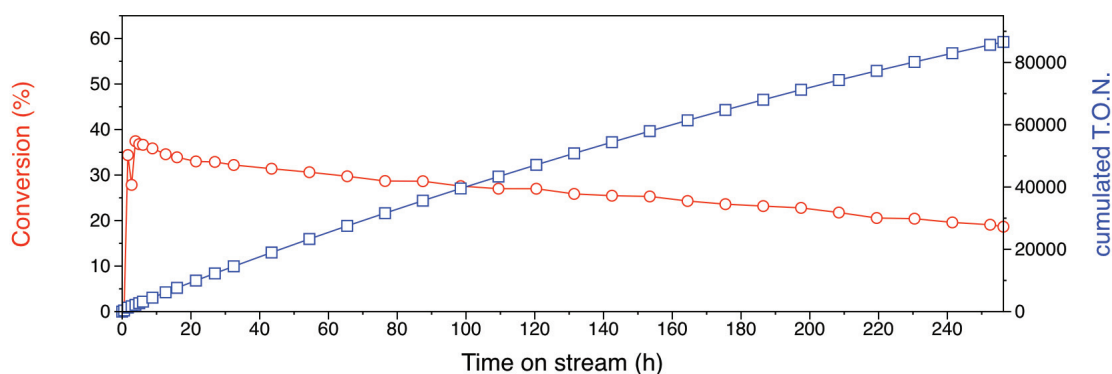


Figure 5.1 Conversion of propylene (●) and cumulated TON (□) vs. time on stream for propylene metathesis on **WH/Al₂O₃-(500)** at 150°C

The reaction presents an initial steep maximal conversion rate of 7.8 mol_{C₃=}.mol_w⁻¹.min⁻¹ (148 mol_{C₃=}.g⁻¹.h⁻¹), reaching 4 mol_{C₃=}.mol_w⁻¹.min⁻¹ (74 mol_{C₃=}.g⁻¹.h⁻¹) with an overall TON of 88,000 after 260h (Figure 5.1). The conversion profile of the reaction is linear with a low deactivation rate of 0.4%.h⁻¹, whereas deactivation was very fast in the ten first hours of catalysis for the direct conversion of ethylene to propylene (2.40%.h⁻¹). This difference spots the influence of ethylene in the deactivation of the catalyst. No deac-

tivation by polymerization is observed, probably due to the fact that polymerization of propylene on cationic sites did not occur as observed for cationic tungsten catalysts.⁷ It can also be emphasized that the linear deactivation profile observed is characteristic of poisoning by impurities of the feed.⁸

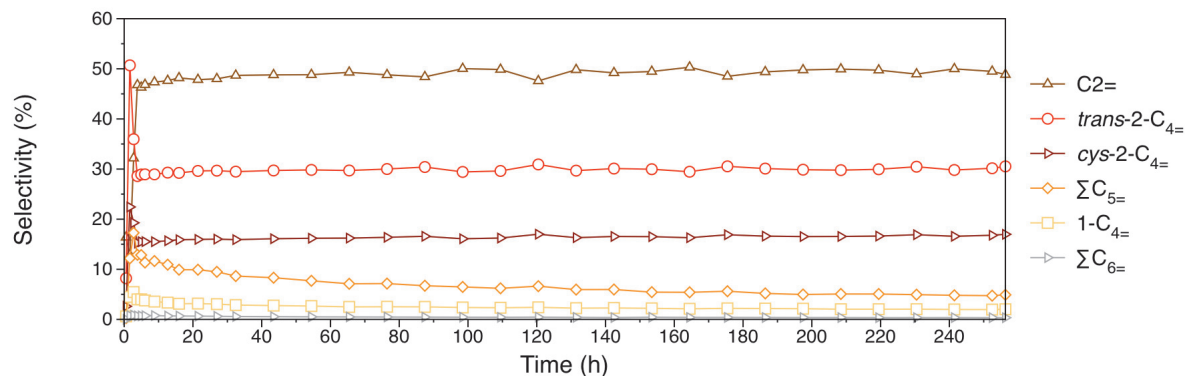
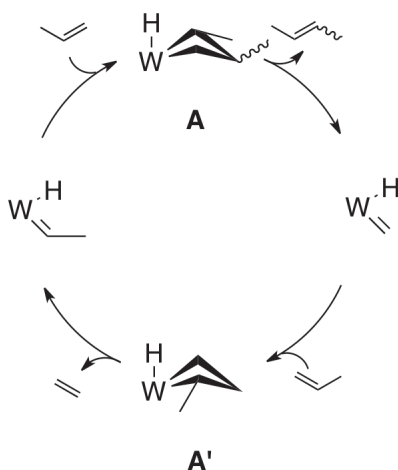


Figure 5.2 Selectivity vs. time on stream for propylene metathesis on WH/Al₂O₃-(500) at 150°C

The maximum conversion rate of the propylene metathesis is far higher than the maximum rate of direct conversion of ethylene to propylene ($7.8 \text{ mol}_{\text{C}_3=} \cdot \text{mol}_{\text{W}}^{-1} \cdot \text{min}^{-1}$ vs. $0.6 \text{ mol}_{\text{C}_2\text{H}_4} \cdot \text{mol}_{\text{W}}^{-1} \cdot \text{min}^{-1}$). This high activity has dictated the molar ratio used in this catalytic test ($R = 20 \text{ mol}_{\text{C}_3=} \cdot \text{mol}_{\text{W}}^{-1} \cdot \text{h}^{-1}$), in order to work under thermodynamic equilibrium (38% conversion of propylene).⁹

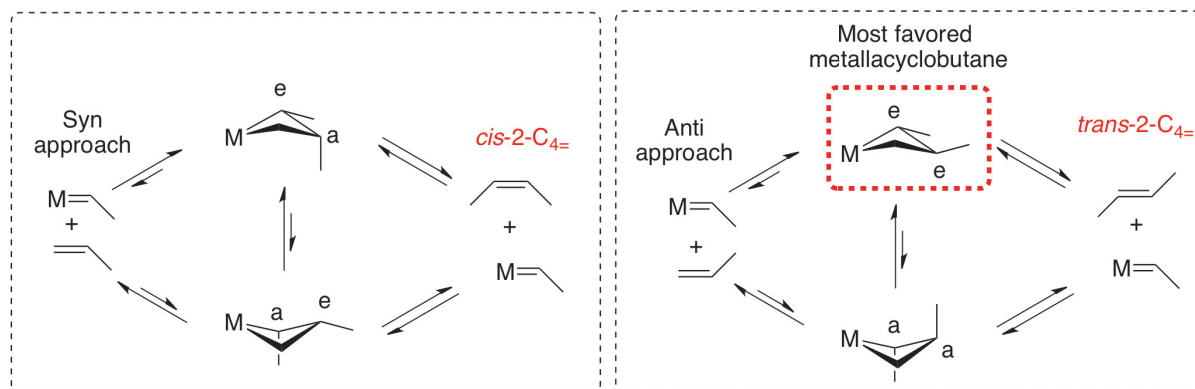
The reaction produces ethylene (49%), trans-2-butene (29%), cis-2-butene (16%), pentenes (5%) and less than 0.2% of hexenes and isobutene (Figure 5.2). The formation of ethylene and butenes, occurs according to the Chauvin mechanism (Scheme 5.6).¹⁰



Scheme 5.6 Intermediates for the production of ethylene and 2-butenes from propylene

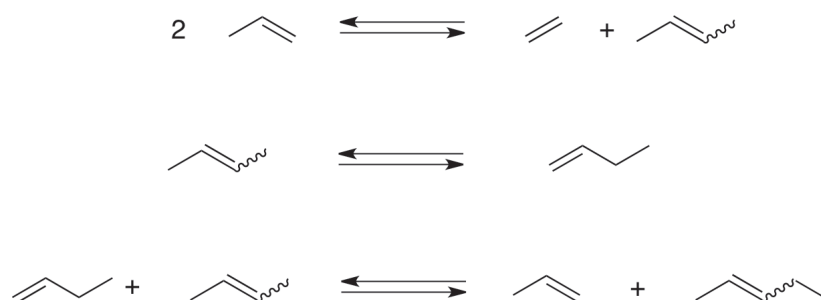
The trans/cis 2-butene ratio stays at a constant value of 1.8 (therm. eq. = 2.1),¹¹ in agreement with that observed in the literature for other d⁰ systems, where terminal alkenes

typically give the *trans*-alkene as the major kinetic product, due to the easier formation of the least sterically hindered metallacyclobutane (**A**) by an *anti* approach (Scheme 5.7).¹² Nevertheless, Leconte *et al.* have pointed out that this model is limited in the case of propylene where (1,3) or (1,2) interactions in the metallacyclobutane **A** are not very significant.¹³ Therefore, as shown in Chapter 3, the active site of the **WH/Al₂O₃**, which is able to perform olefin isomerization, might also account for the observed ratio by converting *cis*-2-butene to *trans*-2-butene.



Scheme 5.7 The stability of the intermediary metallacyclobutane dictates the selectivity of butenes^{12,13}

These results clearly demonstrate the ability of the **WH/Al₂O₃** to perform olefin metathesis. The formation of 1-butene and pentenes also shows that the 2-butenes produced during the metathesis reaction can be isomerized to 1-butene, which will react with 2-butenes to form pentenes and propylene (Scheme 5.8). This finding may be exploited to produce propylene from butenes feeds.



Scheme 5.8 Successive reactions leading to the formation of pentenes from propylene

2.3. Production of propylene from 1-butene only

2.3.1. Catalytic test

The catalytic performances of **WH/Al₂O₃-(500)**, have been tested for 1-butene conversion in continuous flow reactor following the conditions given in Table 5.2. As **WH/Al₂O₃** is a reliable metathesis catalyst, it may be assumed that the main products of the reaction will be the result from 1-butene self-metathesis, *i.e.* ethylene and 3-hexenes (Scheme 5.9).



Scheme 5.9 1-butene self-metathesis

Table 5.2 Experimental conditions

1-butene flow rate (NmL.min ⁻¹)	20
Mass of catalyst (mg)	135
Tungsten loading (% _{wt})	5.5
Temperature (°C)	150
R (mol _{C4=} .mol _W ⁻¹ .min ⁻¹)	20
P _{C4=}	atm. pres.
VHSV (h ⁻¹)	5200

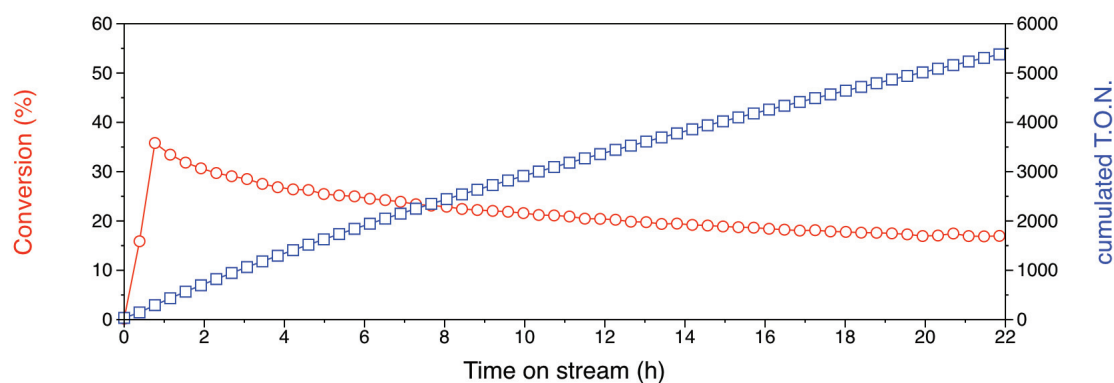


Figure 5.3 Conversion of 1-butene (●) and cumulated TON (□) vs. time on stream on **WH/Al₂O₃-(500)** at 150°C

The 1-butene conversion reaches a maximum of 7.2 mol_{C4=}.mol_W⁻¹.min⁻¹ at 1 h on stream and, after 22 h on stream, 3.4 mol_{C4=}.mol_W⁻¹.min⁻¹ with a cumulated TON of 5450 after 22 h. Yet again the conversion profile is quite linear with a deactivation rate of 0.8%.h⁻¹ (Figure 5.3). This deactivation is faster than that observed for propylene metathesis, and may be related, for a part, to the purity of the feed. In contrast to the propylene feed, 1-butene has not been purified on molecular sieve to avoid isomerization to 2-butene. Nevertheless, the maximum initial conversion rate is similar for the two gases and yet again no polymerization is observed 1-butene is even more difficult to polymerize.

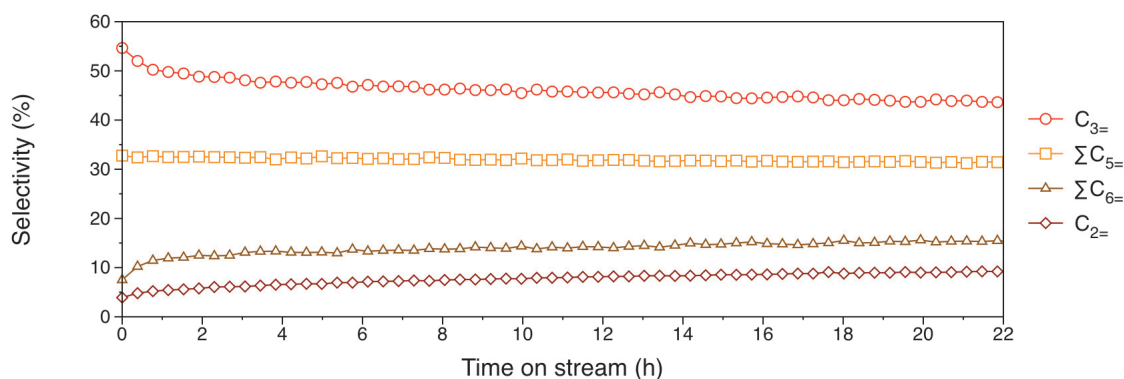
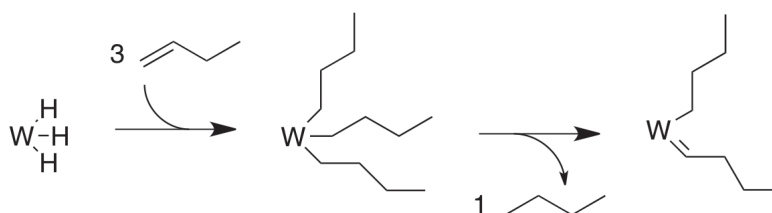


Figure 5.4 Selectivity vs. time on stream for 1-butene conversion on **WH/Al₂O₃-(500)** at 150°C

Surprisingly the selectivity of the reaction is not in favor of the expected hexenes and ethylene. An outstanding selectivity of 50% in propylene is observed giving a maximum productivity of $64.8 \text{ mmol}_{\text{C}_3=}\cdot\text{g}_{\text{cata}}^{-1}\cdot\text{h}^{-1}$ after 1 h on stream, which is 13 times faster than observed with the system described by Liu *et al.* (*vide supra*).² Even after 22 h on stream propylene is still the major product with 44% selectivity (productivity of $27.7 \text{ mmol}_{\text{C}_3=}\cdot\text{g}_{\text{cata}}^{-1}\cdot\text{h}^{-1}$). The other products of the reaction are n-pentenes, n-hexenes and ethylene, with respectively 32%, 15% and 9% selectivity at 22 h on stream (Figure 5.4).

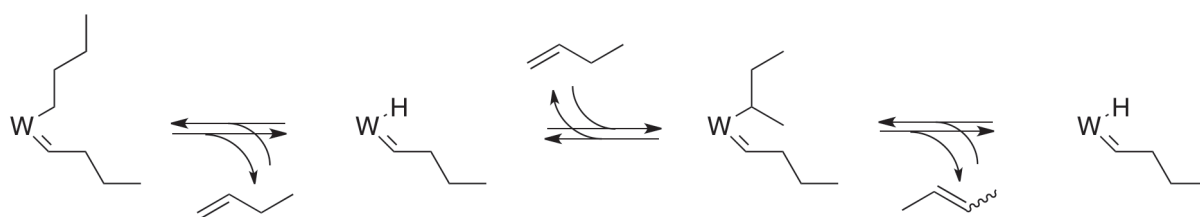
2.3.2. Proposed mechanism

It is reasonable to postulate that initiation of the **WH/Al₂O₃** catalyst occurs with a similar mechanism than that described for the direct conversion of ethylene to propylene: in the early stage of catalysis, butane is observed in the feed, while with ethylene ethane was observed. When an excess of 1-butene is contacted to **WH/Al₂O₃** at 150°C in a batch reactor, after 3 h, 1 equivalent of butane per grafted tungsten is observed in the gas phase. It can be assumed that three 1-butene molecules insert in the trishydride affording a tungsten trisalkyl species, $[\text{W}((\text{CH}_2)_3\text{CH}_3)_3]$, one of this alkyl ligand is then released following an α -H abstraction mechanism giving an butyl-butylidene species, $[\text{W}(=\text{CH}(\text{CH}_2)_2\text{CH}_3)((\text{CH}_2)_3\text{CH}_3)]$ (Scheme 5.10).



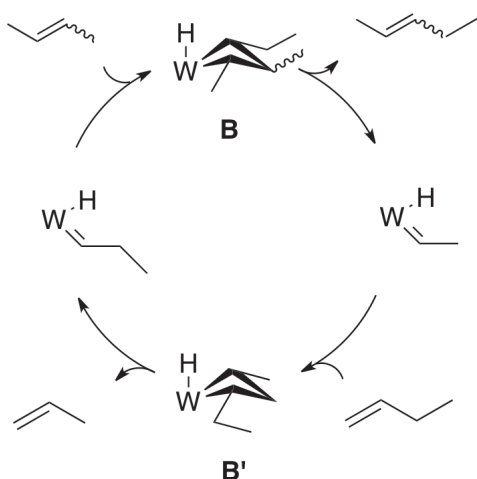
Scheme 5.10 Hypothetical formation of the active species as deduced from butane evolution

The first reaction expected when contacting 1-butene to an olefin metathesis catalyst is the self-metathesis. Nevertheless, the resulting product distribution reveals the occurrence of other reactions. As presented in Chapter 3, $\text{WH}/\text{Al}_2\text{O}_3$ is not only an olefin metathesis catalyst, the alkyl alkylidene species is in equilibrium with an hydride alkylidene species allowing olefin isomerization. 1-butene can insert in the W-H bond, following the Cosse-Arlman mechanism,^{14,15} either by 1,2-insertion or by 2,1-insertion, the later, may be followed by a β -hydride elimination of the hydrogen allowing the formation of 2-butene (Scheme 5.11). This reaction is equilibrated and thermodynamics is in favor of the formation of 2-butenes with a 1-butene:2-butenes ratio of 1:33.¹¹ It can be assumed that these elementary steps occurs on both cationic and neutral sites.



Scheme 5.11 Isomerization of butenes on $\text{WH}/\text{Al}_2\text{O}_3$

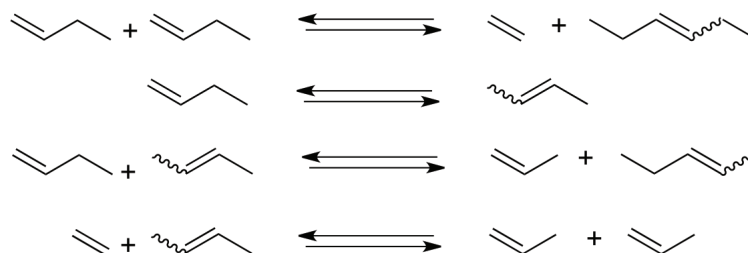
During the initiation of the metathesis reaction, the butylidene-hydride tungsten species can react either with 1-butene or 2-butene to form respectively 1-pentene or 2-hexenes and propylidene-hydride or ethylidene-hydride species. These two newly formed carbenes will react in cross metathesis to afford propylene and pentenes from 1-butene and 2-butene, following the classical Chauvin mechanism (Scheme 5.12).¹⁰



Scheme 5.12 Intermediates for the production of propylene and 2-pentenes from 1-butene and 2-butene

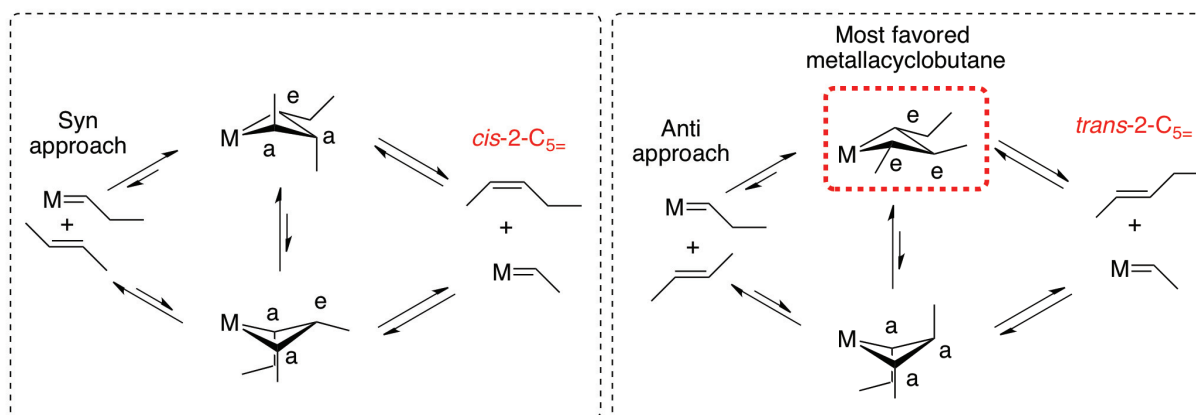
If only the self-metathesis of 1-butene and 1-butene/2-butenes cross-metathesis take place, the relative proportion of hexenes to ethylene and propylene to pentenes should be

1:1. The excess of propylene *vs.* pentenes and the deficit of ethylene *vs.* hexenes can be explained by the cross metathesis between 2-butenes resulting from isomerization and ethylene resulting from 1-butene self-metathesis (Scheme 5.13). Therefore, as this reaction gives 2 mol of propylene per mol of ethylene, it explains the difference in selectivities with the difference between propylene and pentenes (12%) being twice the difference between hexenes and ethylene (6%).



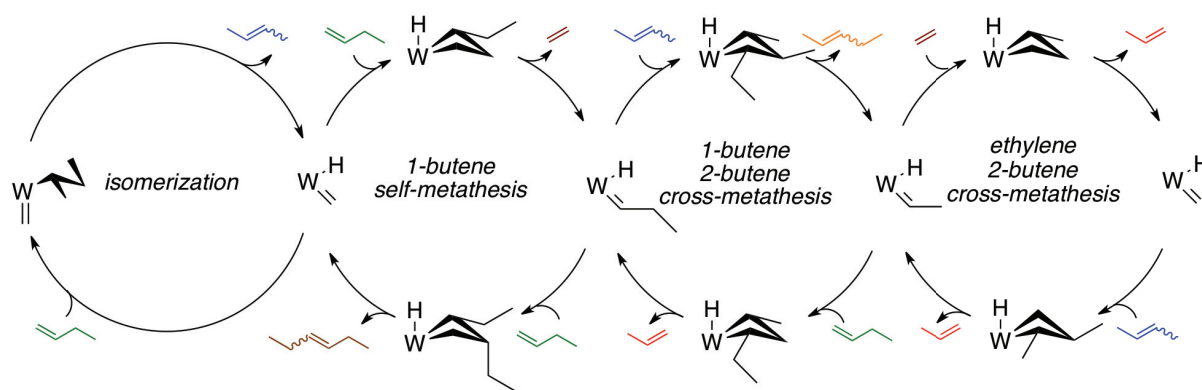
Scheme 5.13 Reactions occurring during the conversion of 1-butene on $\text{WH}/\text{Al}_2\text{O}_3$

As observed for propylene metathesis, the *trans* to *cis* ratio of 2-pentenenes is in favor of the *trans* isomer, *i.e.* 2.9:1 (constant with time on stream), and superior to thermodynamic ratio (1.5:1).¹¹ In this case the pentenes produced by metathesis are mostly *trans*, regarding the stability of the intermediate metallacyclobutane **B** (Scheme 5.14).



Scheme 5.14 The stability of the intermediary metallacyclobutane dictates the selectivity of pentenes^{12,13}

A catalytic cycle that involves all these reactions, *i.e.* i) isomerization of 1-butene to 2-butenes, ii) 1-butene self metathesis, iii) 1-butene/2-butenes cross metathesis and iv) ethylene/2-butenes cross metathesis, can be proposed (Scheme 5.15). This mechanism highlights the importance of the dual functionality of the active site, since tungsten carbene-hydride is required. From the data obtained it appears that 1-butene isomerization is the fastest of all other reactions occurring in this system.

Scheme 5.15 Catalytic cycle for the conversion of 1-butene on WH/Al₂O₃

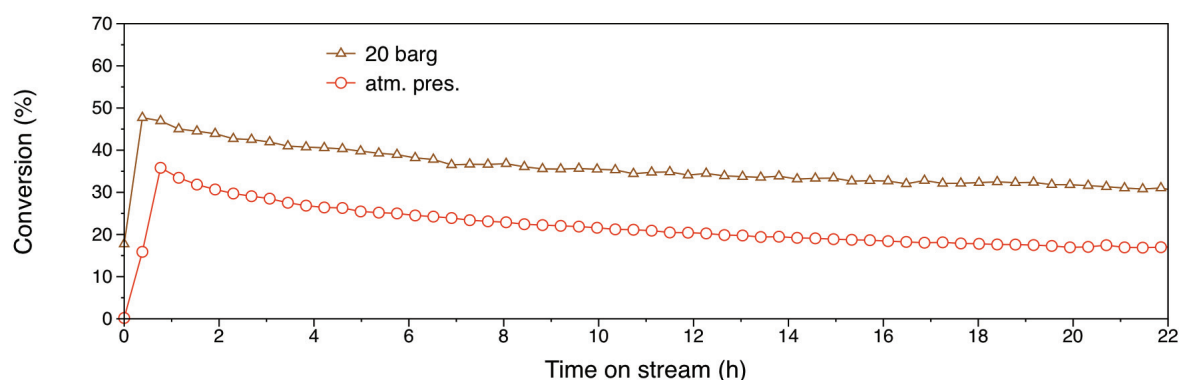
2.3.3. Influence of the pressure

In last subsection, the conversion of 1-butene on WH/Al₂O₃₋₍₅₀₀₎ has been presented. Herein, a study of the influence of the pressure in activity and selectivity in propylene for this reaction is reported.

The catalytic tests have been performed at 20 barg following the conditions given in Table 5.3. The results are compared to the same experiment performed at atmospheric pressure.

Table 5.3 Experimental conditions

1-butene flow rate (NmL.min ⁻¹)	20
Mass of catalyst (mg)	135
Tungsten loading (% _{wt})	5.5
Temperature (°C)	150
R (mol _{C4=} .mol _W ⁻¹ .min ⁻¹)	20
P _{C4=} (barg)	20
VHSV (h ⁻¹)	5200

Figure 5.5 Conversion of 1-butene on WH/Al₂O₃₋₍₅₀₀₎ at 150°C at atmospheric pressure (●) and 20 barg (Δ) vs. time on stream

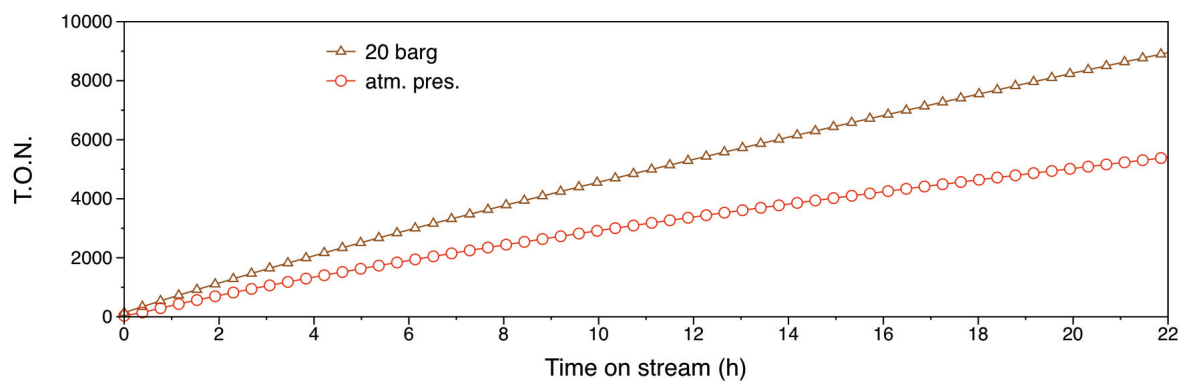


Figure 5.6 Cumulated TON vs. time on stream for conversion of 1-butene on **WH/Al₂O₃-(500)** at 150°C at atmospheric pressure (●) and 20 barg (△)

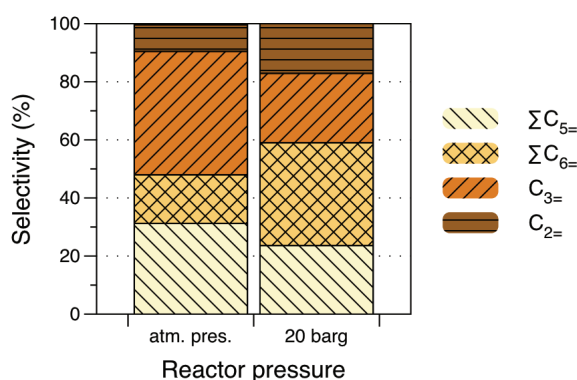


Figure 5.7 Selectivity at 10 h on stream for conversion of 1-butene on **WH/Al₂O₃-(500)** at 150°C at atmospheric pressure and 20 barg

The increase of the pressure shows a beneficial impact on the conversion rate, which rises from 45% to 58% at the beginning of the catalysis (Figure 5.5). At 22 h on stream the cumulate TON reaches 9000 at 20 barg while it was 5450 at atmospheric pressure (Figure 5.6). Nevertheless, the selectivity in propylene severely drops in favor of hexenes: from 42% to 24% for propylene and 17% to 35% for hexenes (Figure 5.7).

This change in selectivity is not in favor of the production of propylene as the maximum productivity rate is only $51.5 \text{ mmol}_{\text{C}_3=} \cdot \text{g}_{\text{cata}}^{-1} \cdot \text{h}^{-1}$. For this reaction, increasing reactor pressure has not a valuable effect on propylene productivity.

2.4. Production of propylene from trans-2-butene only

In last subsection, the activity of WH/Al₂O₃₋₍₅₀₀₎ for conversion of 1-butene has been studied. The awaited 1-butene self-metathesis was not the only reaction observed, isomerization of 1-butene to 2-butenes afford after metathesis reactions a high selectivity in propylene. This finding suggests that WH/Al₂O₃₋₍₅₀₀₎ may also convert a symmetrical olefin such as trans-2-butene whereas conventional olefin metathesis catalyst only perform degenerated metathesis (Scheme 5.5).³

2.4.1. Catalytic test

The catalytic performances of WH/Al₂O₃₋₍₅₀₀₎, have been tested for conversion of 2-butene in continuous flow reactor following the conditions given in Table 5.4.

Table 5.4 Experimental conditions

Trans-2-butene flow rate (NmL.min ⁻¹)	20
Mass of catalyst (mg)	135
Tungsten loading (% _{wt})	5.5
Temperature (°C)	150
R (mol _{C4=} .mol _W ⁻¹ .min ⁻¹)	20
P _{C4=}	atm. pres.
VHSV (h ⁻¹)	5200

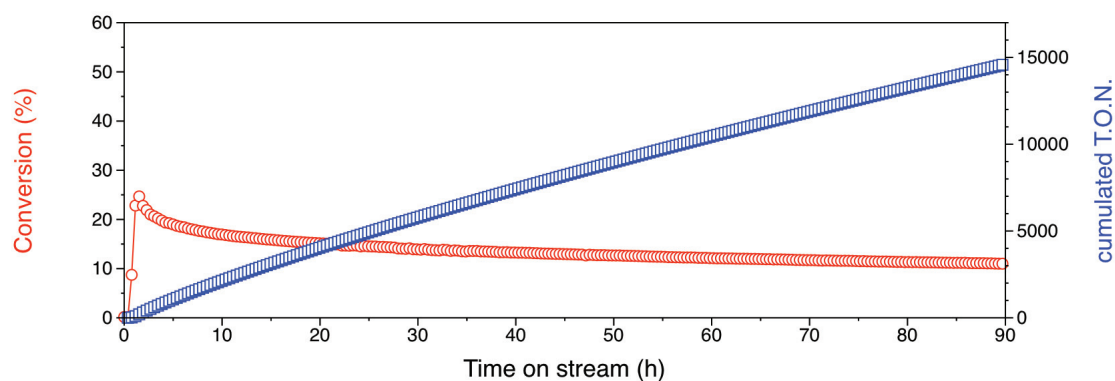


Figure 5.8 Conversion of 2-butene (●) and cumulated TON (□) vs. time on stream on WH/Al₂O₃₋₍₅₀₀₎ at 150°C

The trans-2-butene conversion reaches a maximum of 4.9 mol_{C4=}.mol_W⁻¹.min⁻¹ at 2 h on steam and, after 90 h, 2.2 mol_{C4=}.mol_W⁻¹.min⁻¹ with a cumulated TON of 14500. Yet again the conversion profile is quite linear with a deactivation rate of 0.12%.h⁻¹ (Figure 5.8).

For this reaction the selectivity in propylene is very high 52.5% and remains constant for the entire test. This correspond to a maximum propylene production of $50.5 \text{ mmol}_{\text{C}_3=} \cdot \text{g}_{\text{cata}}^{-1} \cdot \text{h}^{-1}$ at 2 h on stream and $21.3 \text{ mmol}_{\text{C}_3=} \cdot \text{g}_{\text{cata}}^{-1} \cdot \text{h}^{-1}$ after 90 h on stream. The reaction also produces pentenes (36.5%), hexenes (9.0%) and ethylene (2.0%). The trans to cis 2-pentenes ratio is 2.9:1 and constant with time on stream (thermodynamic equilibrium 1.5:1). This ratio is the same than in the case of 1-butene conversion, it can, yet again, be explain by the interactions of the substituents of the metallacyclobutane intermediate (see Scheme 5.14).

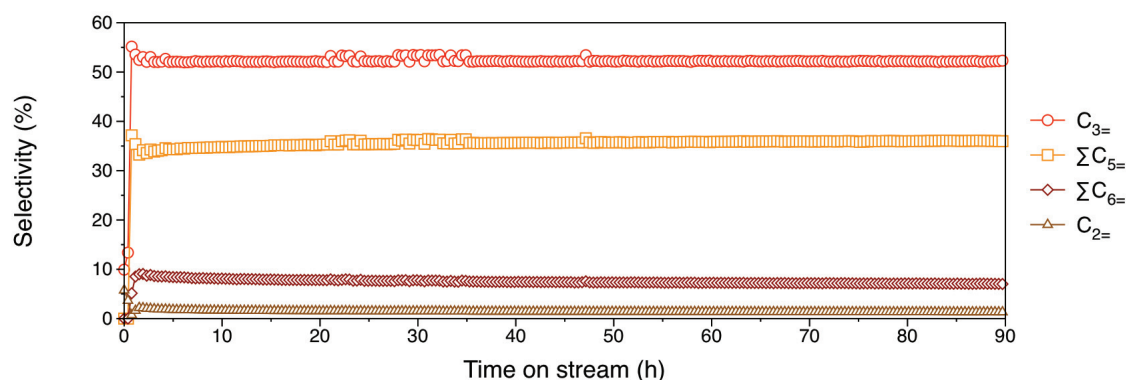


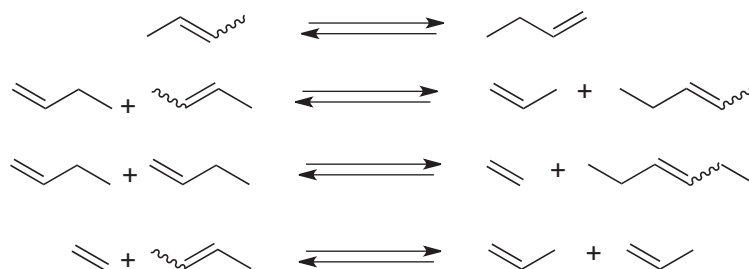
Figure 5.9 Selectivity vs. time on stream for 2-butene conversion on **WH/Al₂O₃₋₍₅₀₀₎** at 150°C

2.4.2. Proposed mechanism

The mechanism of this reaction is very similar to the mechanism described for 1-butene conversion in last subsection. As in the case of 1-butene, butane is observed in the early stage of catalysis and performing the reaction in batch reactor confirms the evolution a stoichiometric butane equivalent per tungsten centre.

Then, as metathesis catalyst should only promote degenerated metathesis, the conversion of trans-2-butene to other olefins must be explained by an isomerization step generating 1-butene from trans-2-butene. At thermodynamic equilibrium the 1-butene:2-butenes ratio of 1:33 is reached. This value explains both the lower activity and the higher selectivity in propylene than for the same reaction carried out with 1-butene. As the formation of 1-butene is less favored by thermodynamics, its cross-metathesis with 2-butenes does not occur easily. Moreover, the 1-butene self-metathesis, producing hexenes and ethylene, is statistically less possible. Here also the excess of propylene produced regarding pentene can be interpreted by ethylene/trans-2-butene cross metathesis, as the difference between propylene and pentene (14%) is twice the difference between hexenes and ethylene (7%). This difference is a bit higher than for 1-butene conversion, *i.e.* 14% vs. 12%,

and may be induced by the high partial pressure of trans-2-butene in the feed. It also explains the higher selectivity of this reaction.



Scheme 5.16 Reactions occurring during the conversion of trans-2-butene on **WH/Al₂O₃**

To the best of our knowledge, **WH/Al₂O₃** is the first system reported allowing the direct conversion of 2-butene in propylene.

2.4.3. Influence of the pressure

Herein, a study of the influence of the pressure on the conversion of trans-2-butene on **WH/Al₂O₃-(500)** has been presented. The catalytic tests have been performed at 20 barg following the conditions given in Table 5.5. The results are compared to the same experiment performed at atmospheric pressure.

Yet again the increase of the pressure shows a benefic impact on the conversion, which rises from 25% to 35% at the beginning of the catalysis (Figure 5.10). At 35 h on stream the cumulate TON reaches 10000 at 20 barg while it was 6000 at atmospheric pressure (Figure 5.11). In contrast to what was observed with 1-butene, the drop of selectivity in propylene is small, it remains the major product, decreasing from 52.5% to 50%. This change of selectivity is in favor of pentenes, which selectivity slightly increases from 36.5% to 44% (Figure 5.12). Increasing the pressure afford an higher propylene productivity, as after 2 h on stream under 20 bar the productivity rate is 64.8 mmol_{C₃}·g_{cata}⁻¹·h⁻¹.

Table 5.5 Experimental conditions

2-butene flow rate (NmL.min ⁻¹)	20
Mass of catalyst (mg)	135
Tungsten loading (% _{wt})	5.5
Temperature (°C)	150
R (mol _{C₄} ·mol _w ⁻¹ ·min ⁻¹)	20
P _{C₄} (barg)	20
VHSV (h ⁻¹)	5200

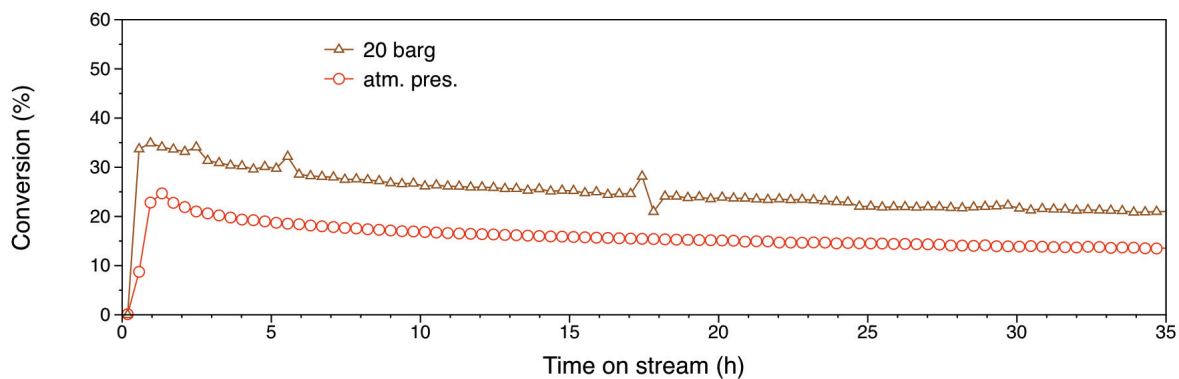


Figure 5.10 Conversion of 2-butene on **WH/Al₂O₃₋₍₅₀₀₎** at 150°C at atmospheric pressure (○) and 20 barg (Δ) vs. time on stream

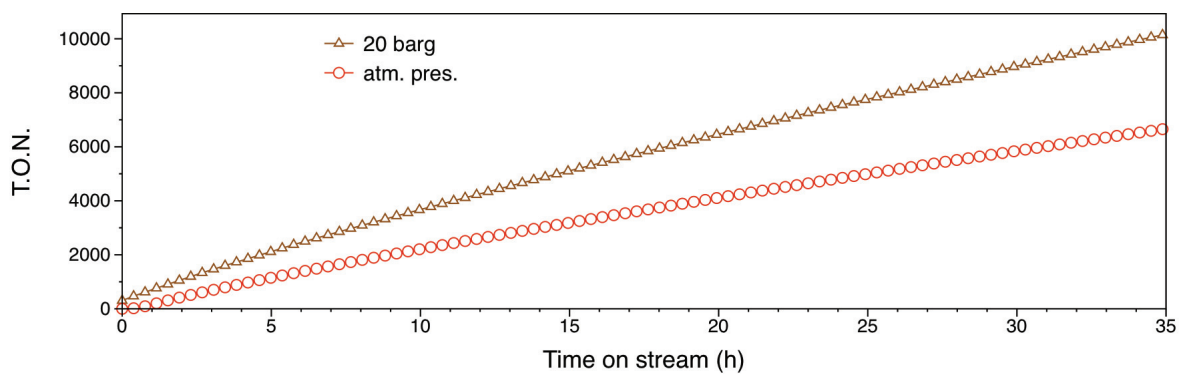


Figure 5.11 Cumulated TON vs. time on stream for conversion of 2-butene on **WH/Al₂O₃₋₍₅₀₀₎** at 150°C at atmospheric pressure (○) and 20 barg (Δ)

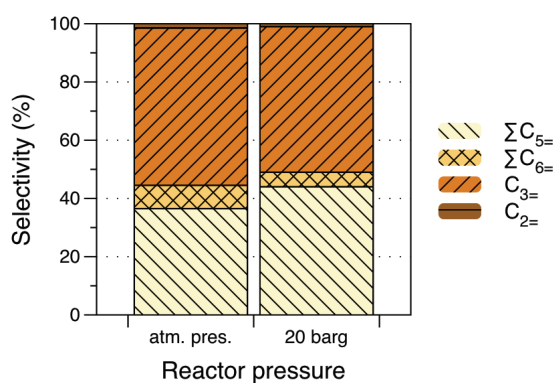


Figure 5.12 Selectivity at 10 h on stream for conversion of 2-butene on **WH/Al₂O₃₋₍₅₀₀₎** at 150°C at atmospheric pressure and 20 barg

2.5. Production of propylene from 1-butene/trans-2-butene mixtures

The reactions of butene-1 and trans-2-butene separately with WH/Al₂O₃₋₍₅₀₀₎ have been presented in previous subsections. Herein is described the reactivity of a mixture of these two gases with the WH/Al₂O₃₋₍₅₀₀₎ and the influence of the 1-butene/trans-2-butene ratio. The study has been conducted according to the conditions presented in Table 5.6 and varying the proportion of butene-1 from 0%, 33%, 50%, 66% to 100% in butene-2 feed.



Scheme 5.17 1-butene/trans-2-butene conversion on WH/Al₂O₃₋₍₅₀₀₎

Table 5.6 Experimental conditions

Total flow rate (NmL.min ⁻¹)	20
Mass of catalyst (mg)	135
Tungsten loading (% _{wt})	5.5
Temperature (°C)	150
R (mol _{C4=} .mol _W ⁻¹ .min ⁻¹)	20
P _{C4=}	atm. pres.
VHSV (h ⁻¹)	5200

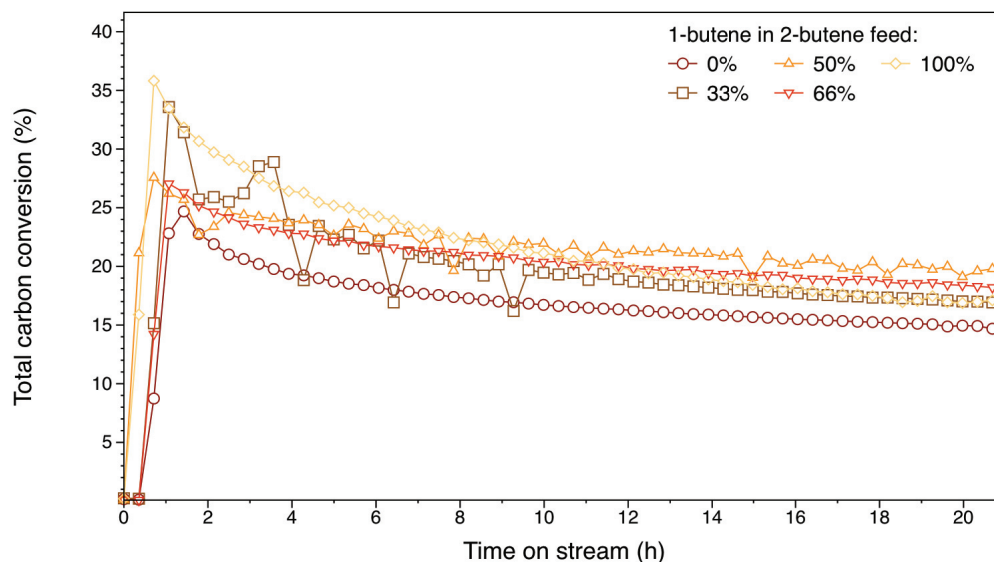


Figure 5.13 Total carbon conversion vs. time on stream for 1-butene/trans-2-butene metathesis on WH/Al₂O₃₋₍₅₀₀₎ at 150°C for different feed compositions 0%, 33%, 50%, 66% and 100% mol. of 1-butene in the 2-butene feed

For each experiment, the conversion profile is very similar, with a maximum conversion for the experiment where the feed is only composed of 1-butene. It is also notable

that this experiment shows the fastest deactivation rate. After 20 h on stream the 50% mixture gives conversion rate with $3.8 \text{ mol}_{C_4=}\cdot\text{mol}_W^{-1}\cdot\text{min}^{-1}$ (Figure 5.13).

As expected, the selectivity in propylene is slightly better when 1-butene is a minor component of the feed. This selectivity decreases when the molar percentage of 1-butene increases, raising the selectivity in hexenes and ethylene, produced by self-metathesis of 1-butene. Operating with 33% of 1-butene in the feed gives the best selectivity in propylene with 55% (Figure 5.14).

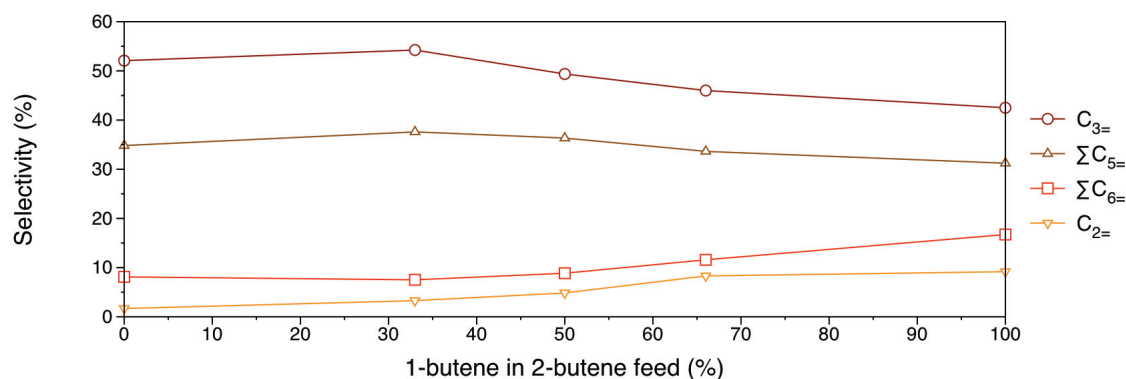


Figure 5.14 Selectivity at 20 h on stream for 1-butene/2-butene metathesis on **WH/Al₂O₃₋₍₅₀₀₎** at 150°C vs. 1-butene molar percentage in the 2-butene feed

At 20h on stream the productivity rate span from 26.9 to 36.0 $\text{mmol}_{C_3=}\cdot\text{g}_{\text{cata}}^{-1}\cdot\text{h}^{-1}$. The maximum productivity is reached with a one to one ratio 1-butene to trans-2-butene (Figure 5.15).

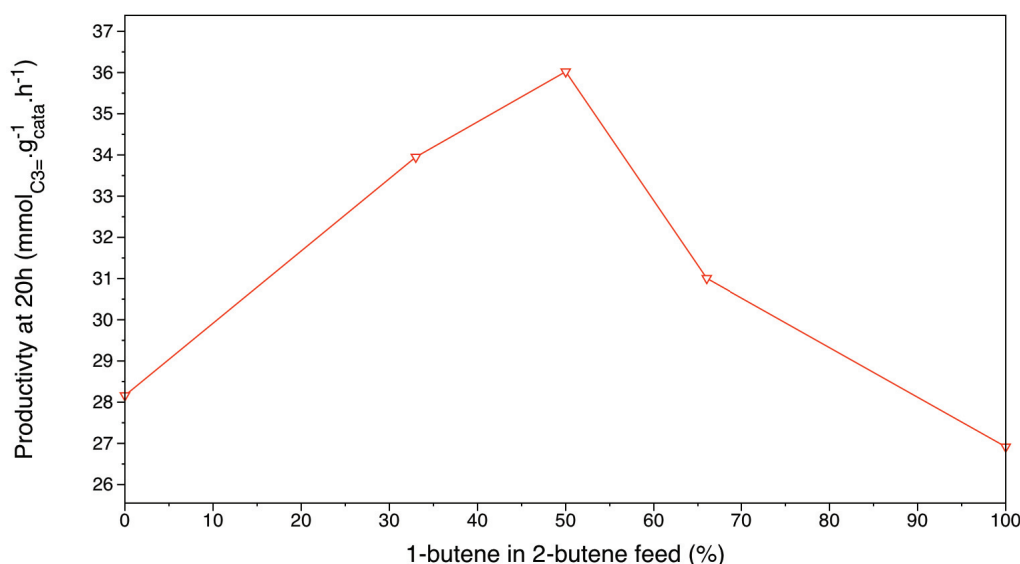
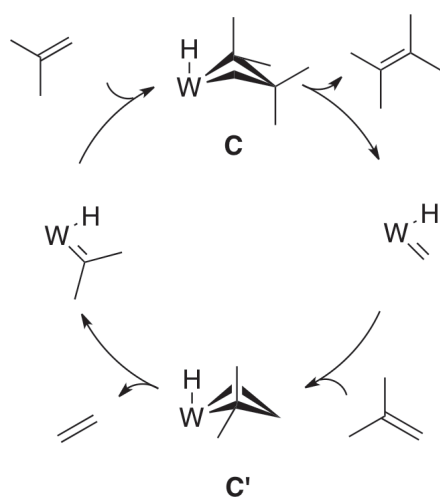


Figure 5.15 Productivity in propylene at 20 h on stream for 1-butene/trans-2-butene metathesis on **WH/Al₂O₃₋₍₅₀₀₎** at 150°C vs. 1-butene molar percentage in the trans-2-butene feed

These results demonstrate that WH/Al₂O₃₋₍₅₀₀₎ is able to produce propylene with good yield from linear C₄ olefins. The activity of WH/Al₂O₃₋₍₅₀₀₎ toward branched C₄ olefin, *i.e.* should be investigated.

2.6. Production of propylene from isobutene/trans-2-butene cross metathesis

As described in last subsection, the conversion of 1-butene/trans-2-butene mixtures on WH/Al₂O₃₋₍₅₀₀₎ lead to the formation of propylene by cross-metathesis. Moreover, this reaction produces hexenes by self-metathesis of 1-butene. The next step of our study of the valorization of C₄ olefin cut into propylene, is the study of the conversion of isobutene/trans-2-butene. This reaction may also give isobutene self-metathesis. The conversion of isobutene only on this catalyst has been recently studied,¹⁶ and unprecedented results have been found. Therefore this reaction is not thermodynamically favored (13.8% conversion at 150°C).¹¹ The reaction presented an initial maximal conversion rate of 0.61 mol_{i-C₄}·mol_W⁻¹·min⁻¹ before reaching a pseudo-plateau of 0.22 mol_{i-C₄}·mol_W⁻¹·min⁻¹, with an overall turnover number (TON) of 235 after 16 h. At the pseudo-steady state, the product selectivities were 2,3-dimethylbutenes 50%. The metathesis of isobutene is usually known as a degenerate process with the classical olefin metathesis catalysts,^{17,18} WH/Al₂O₃₋₍₅₀₀₎ proves to be the first compound capable of catalyzing the productive self-metathesis of isobutene into 2,3-dimethylbutene.

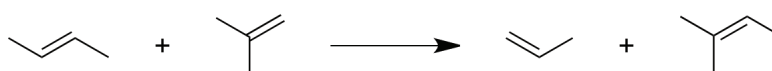


Scheme 5.18 Intermediates for the production of 2,3-dimethylbutene from isobutene by self-metathesis

As known in the classical olefin metathesis mechanism¹⁰ isobutene can react with the hydrido-tungsta-carbene giving the corresponding metallacyclobutanes intermediates C and C' (Scheme 5.18). The metallacyclobutane C is *a priori* the less thermodynamically favored intermediate, since it has gem-methyl substituents in the 1,2-positions gen-

erating a sterically encumbered intermediate. Productive metathesis of isobutene involving **C** is thus disfavored for steric reasons which accounts for the fact that a moderate activity is observed with **WH/Al₂O₃-(500)** by comparison with metathesis of linear olefins, such as propylene or butenes (*vide supra*).

In light of this results, **WH/Al₂O₃-(500)** may be active for the isobutene/trans-2-butene cross metathesis (Scheme 5.19), with a good selectivity as 2,3-dimethylbutene is not favored. The catalytic test has been performed following the conditions reported in Table 5.7.



Scheme 5.19 isobutene/trans-2-butene cross-metathesis

Table 5.7 Experimental conditions

Trans-2-butene flow rate (NmL.min ⁻¹)	5
Isobutene flow rate (NmL.min ⁻¹)	5
Mass of catalyst (mg)	400
Tungsten loading (% _{wt})	5.5
Temperature (°C)	150
R (mol _{C4=} .mol _W ⁻¹ .min ⁻¹)	3.5
P _{C4=}	atm. pres.
VHSV (h ⁻¹)	875

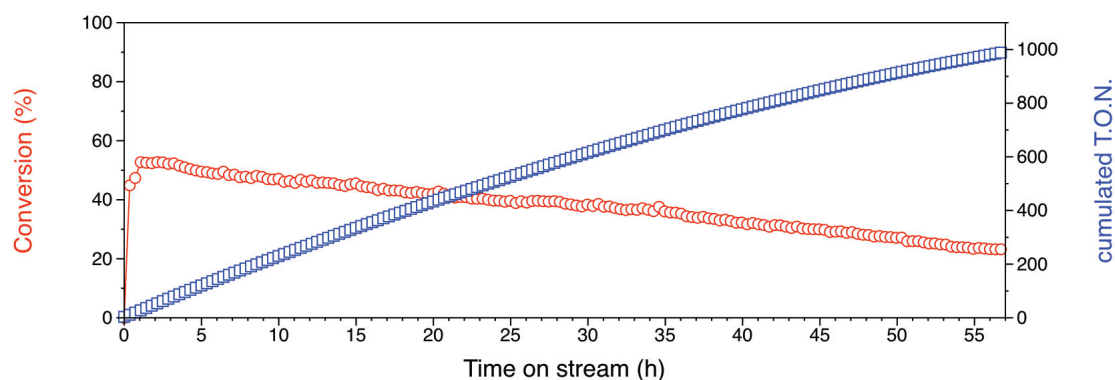


Figure 5.16 Total carbon conversion (●) and cumulated TON (□) vs. time on stream for isobutene/trans-2-butene cross metathesis on **WH/Al₂O₃-(500)** at 150°C

The maximum conversion rate is reached after 2 h on stream with 1.8 mol_{C4=}.mol_W⁻¹.min⁻¹. This conversion decreases linearly at 0.5%.h⁻¹ to reach 0.8 mol_{C4=}.mol_W⁻¹.min⁻¹ after 57 h with an overall TON of 1000 (Figure 5.16).

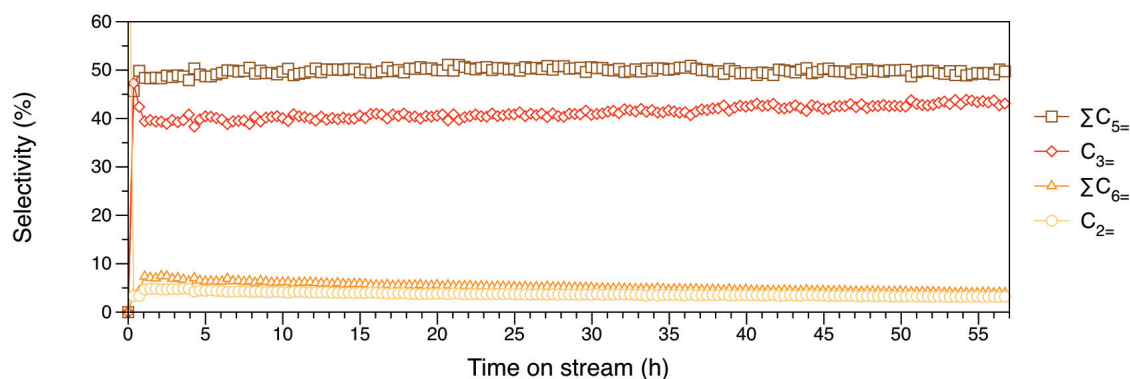
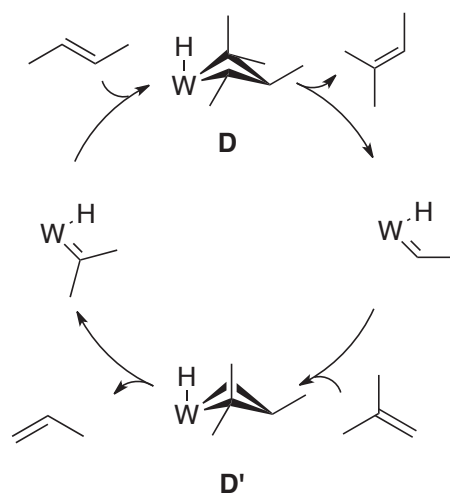


Figure 5.17 Selectivity vs. time on stream for isobutene/trans-2-butene cross metathesis on WH/Al₂O₃₋₍₅₀₀₎ at 150°C

The selectivity of the reaction is in favor of pentenes, 50%, followed by propylene, 40%, linear hexenes, 6%, and ethylene 4% (Figure 5.17). It is noticeable that mostly isopentenes, and only linear hexenes are produced. The propylene production rate for this reaction is thus $17.2 \text{ mmol}_{\text{C}_3=} \cdot \text{g}_{\text{cata}}^{-1} \cdot \text{h}^{-1}$ at maximum conversion and $5.8 \text{ mmol}_{\text{C}_3=} \cdot \text{g}_{\text{cata}}^{-1} \cdot \text{h}^{-1}$ after 57 h on stream.

During the initiation of the reaction, isobutene probably inserts more easily than 2-butenes (α -olefin vs. 2,3-substituted olefin), leading to isobutylidene-hydride after α -H elimination of isobutane as proposed in the case of 1-butene. This tungsten species can react either with isobutene or trans-2-butene to form respectively isopentene or 3-methyl-2-pentenes and tungsten isopropylidene-hydride or tungsten ethylidene-hydride species. These two newly formed carbenes will react in cross metathesis to afford propylene and isopentenes from isobutene and 2-butene, following the classical Chauvin mechanism (Scheme 5.20).¹⁰ As, in mechanism presented in Scheme 5.18, the intermediate metallacyclobutane **D** is *a priori* the less thermodynamically favored intermediate, since it has gem-methyl substituents in the 1-position and two methyl substituents in the 2- and 3-position. The steric crowding of this intermediate is nevertheless less pronounced than for intermediate **C** obtained during isobutene self-metathesis. This explains both the lower of this reaction compared to linear olefins and the higher activity compared to isobutene self-metathesis.



Scheme 5.20 Intermediates for the production of isopentenes and propylene from isobutene/trans-2-butene cross-metathesis

As 2,3-dimethylbutene is not observed, the linear hexenes are produced by butene-1 self-metathesis, isobutene self-metathesis did not occur.

Whatever the route employed to produce propylene from butenes, the selectivity in propylene is limited to 55%. The activities of **WH/Al₂O₃-(500)** for butenes conversion is related to the nature of the reagent, and therefore related to the sterical hindrance of the intermediate metallacyclobutane.

2.7. Ethylene/trans-2-butene cross-metathesis over **WH/Al₂O₃-(500)**

The most commonly used process to produce propylene by metathesis is ethylene/trans-2-butene cross metathesis, as this reaction should achieve 100% selectivity in propylene (Scheme 5.21). Nevertheless, we have seen that ethylene is responsible of the deactivation of the catalyst by polymerization. This reaction will be studied in order to determine the optimal ethylene to trans-2-butene ratio, affording i) the best conversion rate, ii) the highest selectivity in propylene and iii) the lowest deactivation rate, *i.e.* by limiting ethylene polymerization. The performances of the **WH/Al₂O₃-(500)** for ethylene/trans-2-butene cross-metathesis have been evaluated in continuous flow reactor following the conditions given in Table 5.8.



Scheme 5.21 Ethylene/trans-2-butene cross-metathesis

Table 5.8 Experimental conditions

Trans-2-butene flow rate (NmL.min ⁻¹)	10
Ethylene flow rate (NmL.min ⁻¹)	10
Mass of catalyst (mg)	135
Tungsten loading (%wt)	5.5
Temperature (°C)	150
R (mol _{C4+=C2=} .mol _W ⁻¹ .min ⁻¹)	20
P _{C4+=C2=}	atm. pres.
VHSV (h ⁻¹)	5200

The maximum conversion rate is reached after 1 h on stream with 7.4 mol_{C4+=C2=}.mol_W⁻¹.min⁻¹. This conversion decreases linearly at 0.03%.h⁻¹ to reach 5.4 mol_{C4+=C2=}.mol_W⁻¹.min⁻¹ after 45 h with an overall TON of 16000 (Figure 5.18). A very high selectivity in propylene of 97.9% is observed. The other products of the reaction are pentenes (1.6%) and hexenes (0.5%) (Figure 5.19). The propylene production rate for this reaction is thus 133.4 mmol_{C3=}.g_{cata}⁻¹.h⁻¹ at maximum and 97.9 mmol_{C3=}.g_{cata}⁻¹.h⁻¹ after 45 h on stream.

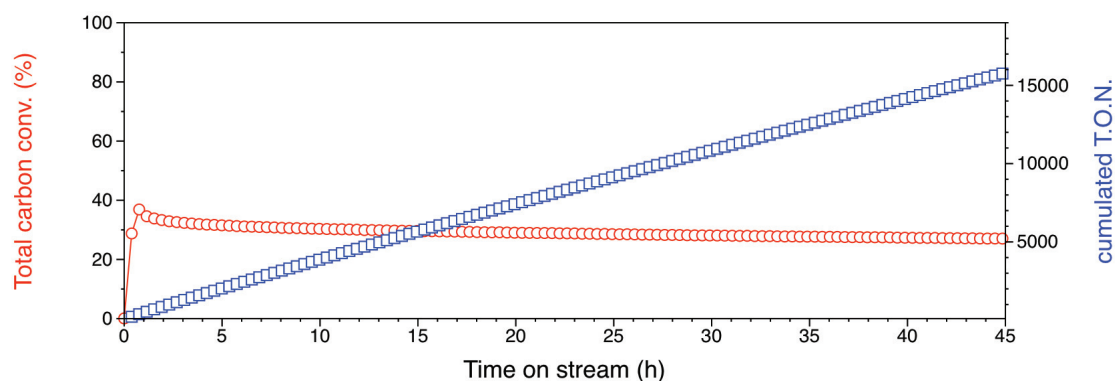


Figure 5.18 Total carbon conversion (●) and cumulated TON (□) vs. time on stream for ethylene/trans-2-butene cross metathesis on WH/Al₂O₃₋₍₅₀₀₎ at 150°C

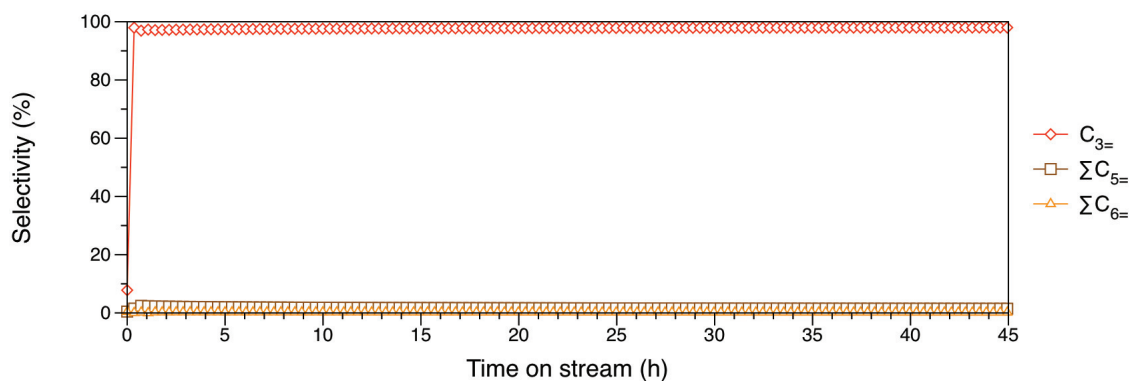


Figure 5.19 Selectivity vs. time on stream for ethylene/trans-2-butene cross metathesis on WH/Al₂O₃₋₍₅₀₀₎ at 150°C

It is interesting to compare the conversion rates observed for this reaction with those of the direct conversion of ethylene to propylene described in Chapter 3. The **WH/Al₂O₃ (500)** catalyst is clearly more active for ethylene/trans-2-butene cross-metathesis than for the conversion of ethylene to propylene (7.4 to 5.4 mol_{C₄+C₂=}.mol_W⁻¹.min⁻¹ vs. 0.6 to 0.1 mol_{C₂H₄}.mol_W⁻¹.min⁻¹). It suggests that the metathesis is not the rate-determining step of the ethylene to propylene mechanism, confirming that dimerization of ethylene is the slowest step. Furthermore, the deactivation profile is linear, with 0.03%.h⁻¹, a value close to the pseudo-plateau of the ethylene to propylene reaction (*i.e.* 0.05%.h⁻¹), while no fast deactivation occurs in the early stage of catalysis. Among all the reactions producing propylene from butenes cross-metathesis, described in this chapter, the ethylene/trans-2-butene cross-metathesis exhibits the highest selectivity in propylene (97.8%) and activity (7.4 mol_{C₄+C₂=}.mol_W⁻¹.min⁻¹). This later can be explained by a less sterically hindered metallacyclobutane intermediate, the reaction intermediates are the same than for propylene metathesis (**A** and **A'** in Scheme 5.6), where the methyl substituents are in 1,2-positions where the interactions are minimal in equatorial-equatorial position. The activity is quite similar to the activity of propylene production.

The influence of the nature of aluminas supports provided by UOP on this reaction has been studied. The different tungsten hydride catalysts presented in Appendix A have been tested. No major trend can be determined from these results.

The influence of ethylene proportion in this reaction was then studied to optimize the reaction conditions, but also to see its influence on deactivation rate. The study has been conduct in conditions presented in Table 5.6 and varying the proportion of ethylene from 0%, 10%, 18%, 35%, 45 to 70%mol. in trans-2-butene feed.

Table 5.9 Experimental conditions

Total flow rate (NmL.min ⁻¹)	20
Mass of catalyst (mg)	135
Tungsten loading (% _{wt})	5.5
Temperature (°C)	150
R (mol _{C₄+C₂=} .mol _W ⁻¹ .min ⁻¹)	20
P _{C₄ C₄+C₂=}	atm. pres.
VHSV (h ⁻¹)	5200

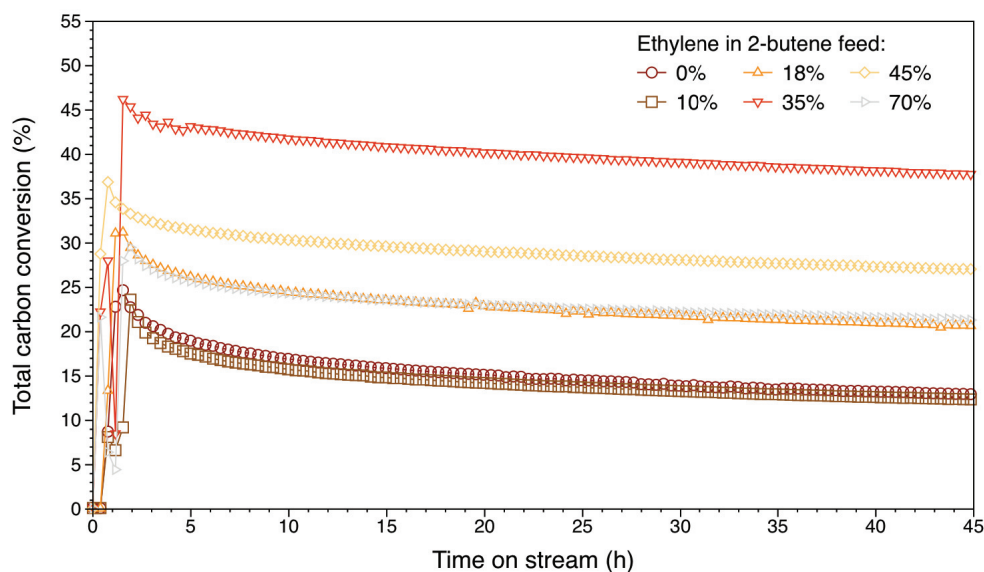


Figure 5.20 Total carbon conversion vs. time on stream for ethylene/trans-2-butene metathesis on $\text{WH}/\text{Al}_2\text{O}_3(500)$ at 150°C for different feed compositions 0%, 10%, 18%, 35%, 45% and 70% mol. of ethylene in the 2-butene feed

The maximum conversion rates span from 5.0 to $9.2 \text{ mol}_{\text{C}_4+\text{C}_2} \cdot \text{mol}_W^{-1} \cdot \text{min}^{-1}$, whereas the deactivation rate is quite constant for all ratio: ca. $0.11\% \cdot \text{h}^{-1}$ (Figure 5.20). The selectivity in propylene increases with proportion of ethylene in the feed, starting from 52.5% when no ethylene was in the feed to 98.7% when 70% of ethylene was added in the trans-2-butene feed (Figure 5.21). The maximum propylene production rate is obtained when the reactor is fed with 35% of ethylene in the 2-butene feed, with $142.8 \text{ mmol}_{\text{C}_3} \cdot \text{g}_{\text{cata}} \cdot \text{h}^{-1}$ at 20 h on stream. This optimum, observed at substoichiometric proportion of ethylene, can be explained by the occurrence of trans-2-butene conversion to propylene as seen in subsection 2.4, concomitantly to the ethylene/trans-2-butene cross-metathesis.

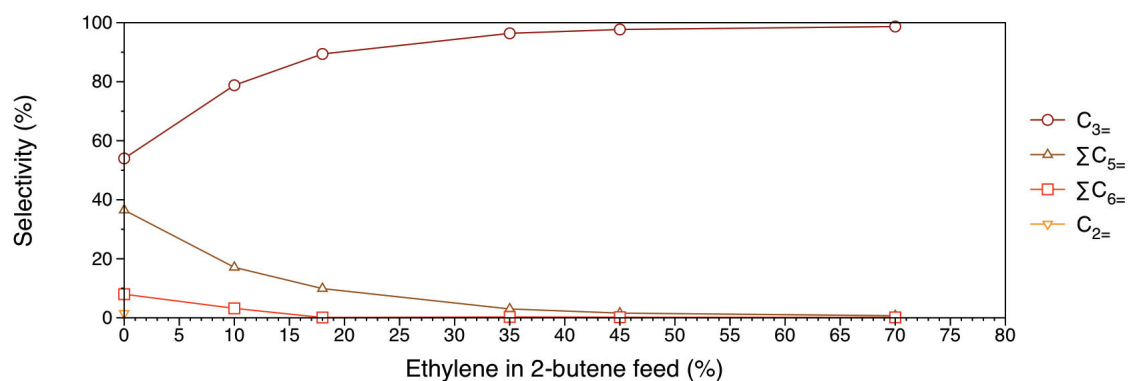


Figure 5.21 Selectivity at 20 h on stream for ethylene/trans-2-butene metathesis on $\text{WH}/\text{Al}_2\text{O}_3(500)$ at 150°C vs. ethylene molar percentage in the trans-2-butene feed

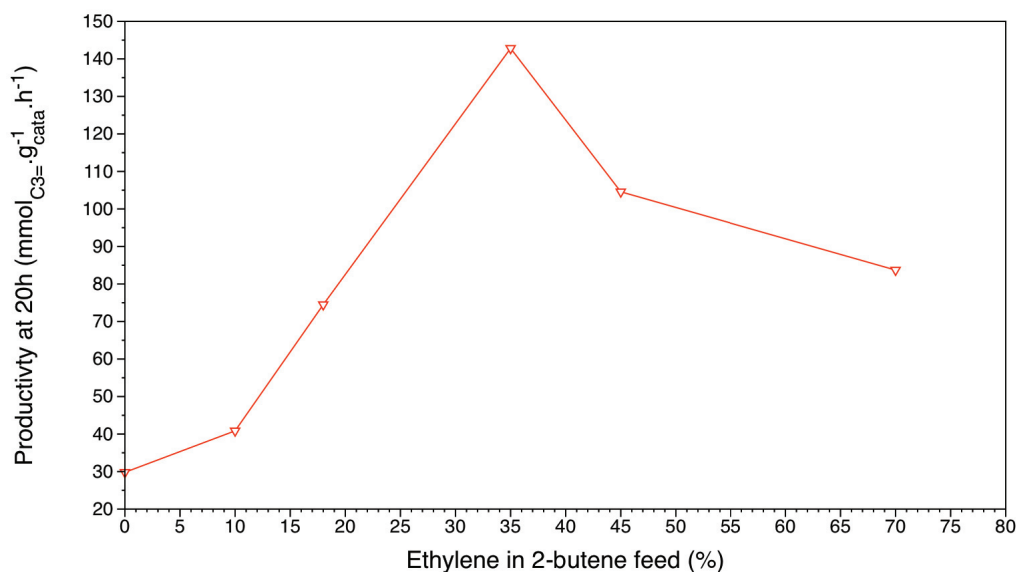


Figure 5.22 Productivity in propylene at 20 h on stream for ethylene/trans-2-butene metathesis on **WH/Al₂O₃** (500) at 150°C vs. 1-butene molar percentage in the trans-2-butene feed

As no trend could be established between ethylene ratio and deactivation rate, it can be assumed that ethylene is not a major element for the deactivation of the catalyst for metathesis reaction and therefore the rate of metathesis reaction is much higher than the rate of insertion of ethylene responsible of deactivation. It confirms the results obtained in Chapter 3, where it has been seen that ethylene was deactivating the cationic tungsten sites, which are the most active dimerization sites, whereas the neutral sites were still performing the reaction but at a slower rate.

2.8. Conclusion

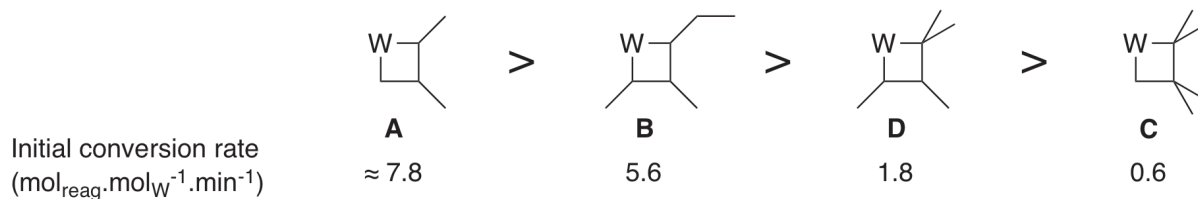
In this chapter, a study of the propylene metathesis has confirmed the ability of the tungsten hydride to perform olefin metathesis with high activities. Different routes allowing the production of propylene were then investigated. The results are summarized in Table 5.10.

Table 5.10 Productivity of the different routes to propylene

Reaction	Propylene selectivity (%)	Productivity at 20h on stream (mmol _{C₃=} .g _{cata} ⁻¹ .h ⁻¹)
1-butene conversion	42.5	28.1
Trans-2-butene conversion	52.1	26.9
1-butene/trans-2-butene cross-metathesis	49.9	36.0
Isobutene/trans-2-butene cross-metathesis	40.0	10.5
Ethylene/trans-2-butene cross-metathesis (45% ethylene)	97.7	115.9
Ethylene/trans-2-butene cross-metathesis (35% ethylene)	96.4	142.8

Using **WH/Al₂O₃(500)**, the best route, in term of selectivity and productivity in propylene, is high ethylene/2-butene cross-metathesis, with a low deactivation rate (ca. 0.11%.h⁻¹).

During this study, it has been observed, for metathesis reaction involving a stoichiometric ratio of reagent, that the number of substituent of the less thermodynamically favored metallacyclobutane governs the conversion rate of metathesis reaction (Scheme 5.22). The different reaction can thus be classified from higher to lower activity: i) Propylene self-metathesis or ethylene/trans-2-butene cross-metathesis where **A** is the less thermodynamically favored intermediate, ii) 1-butene/trans-2-butene cross-metathesis (metallacyclobutane **B**), iii) isobutene/trans-2-butene cross-metathesis (metallacyclobutane **D**) and iv) isobutene self-metathesis (metallacyclobutane **C**).



Scheme 5.22 Influence of the substituent of the metallacyclobutane on the conversion rate of metathesis reactions.

3. Experimental section

The $\text{WH}/\text{Al}_2\text{O}_3\text{-(500)}$ was prepared following the procedure described in Chapter 2. The continuous flow reactor used for the catalytic test is presented in subsection 2.1 of Chapter 2 and Appendix B.

Propylene (N35 Air Liquide) and Argon were purified over R3-11 BASF catalyst/MS4Å, 1-butene (Scott), trans-2-butene (Scott), Isobutene (Linde) were used as received to avoid isomerization or dimerization.

Procedure for the catalytic tests: A stainless-steel half-inch cylindrical reactor that can be isolated from ambient atmosphere was charged with the desired amount of $\text{WH}/\text{Al}_2\text{O}_3\text{-(500)}$ in a glovebox. After connection to the gas lines and purging of the tubing, the desired gas or mixture of gas was passed over the catalyst bed at 150°C at desired pressure and flow rate. For experience under pressure, the reactor was filled with argon at the desired pressure before feeding it with piston pump. Hydrocarbon products were analyzed online by GC (HP 8890 chromatograph fitted with an $\text{Al}_2\text{O}_3/\text{KCl}$ 50 m x 0.32 mm capillary column, FID detector).

4. Reference and Notes

- (1) Bailey, G. C. *Catalysis Reviews*. 1970, 3, 37-60.
- (2) Liu, H.; Zhang, L.; Li, X.; Huang, S.; Liu, S.; Xin, W.; Xie, S.; and Xu, L. *Journal of Natural Gas Chemistry*. 2009, 18, 331-336.
- (3) Meyer, W. H.; Radebe, M. M. D.; Serfontein, D. W.; Ramdhani, U.; du Toit, M.; and Nicolaidis, C. P. *Applied Catalysis A: General*. 2008, 340, 236-241.
- (4) Banks, R. L. and Regier, R. B. *Product R&D*. 1971, 10, 46-51.
- (5) Schwab, P. and Schulz, M. *DE19746040*. 1999.
- (6) Mol, J. C. *Journal of Molecular Catalysis A: Chemical*. 2004, 213, 39-45.
- (7) Justino, J.; Marques, M. M.; Correia, S.; Dias, A. R.; Lemos, F.; and Ribeiro, F. R. *Polymer International*. 1997, 44, 517-522.
- (8) Behr, A.; Schuller, U.; Bauer, K.; Maschmeyer, D.; Wiese, K. D.; and Nierlich, F. *Applied Catalysis A General*. 2009, 357, 34-41.
- (9) Kapteijn, F.; Homburg, E.; and Mol, J. C. *The Journal of Chemical Thermodynamics*. 1983, 15, 147-152.
- (10) Hérisson, J. L. and Chauvin, Y. *Makromol. Chem*. 1971, 141, 161-176.
- (11) Stull, D. R. and Sinke, G. C. *The chemical thermodynamics of organic compounds*, Westrum, Ed.; Krieger: Malabar, Fla.; 1987.
- (12) Bilhou, J. L.; Basset, J. M.; Mutin, R.; and Graydon, W. F. *Journal of the American Chemical Society*. 1977, 99, 4083-4090.
- (13) Leconte, M. and Basset, J. M. *Journal of the American Chemical Society*. 1979, 101, 7296-7302.
- (14) Arlman, E. J. and Cossee, P. *Journal of Catalysis*. 1964, 3, 99 - 104.
- (15) Cossee, P. *Journal of Catalysis*. 1964, 3, 80 - 88.
- (16) Merle, N.; Stoffelbach, F.; Taoufik, M.; Le Roux, E.; Thivolle-Cazat, J.; and Basset, J. M. *Chem Commun (Camb)*. 2009, 2523-5.
- (17) Ivin, K. J. and Mol, J. C. *Olefin metathesis and metathesis polymerization*, Academic Press: San Diego; 1997.
- (18) Kawai, T.; Kudo, H.; Suzuki, T.; and Iyoda, T. *Journal of Molecular Catalysis A: Chemical*. 2000, 158, 533 - 540.

Chapter 6

Well-defined surface models of the active sites of WO_3/SiO_2 and $\text{WH}/\text{Al}_2\text{O}_3$ catalysts

1. Introduction	190
2. Results and discussions	193
2.1. Preparation of the molecular precursors	193
2.1.1. Alkyls complexes: [W=O(CH ₂ ¹ Bu) ₄] (3), [W=N(2,6- ¹ PrC ₆ H ₃)(CH ₂ ¹ Bu) ₂ (=CH ¹ Bu)] (4) ...	193
• [W=O(CH ₂ ¹ Bu) ₄] (3)	193
• [W=N(2,6- ¹ PrC ₆ H ₃)(CH ₂ ¹ Bu) ₂ (=CH ¹ Bu)] (4)	195
2.1.2. Fluorinated complexes: [W=N(C ₆ H ₅)(CH ₂ ¹ Bu) ₃ F] (5) and [W=O(CH ₂ ¹ Bu) ₃ F] (6)	195
• [W=N(C ₆ H ₅)(CH ₂ ¹ Bu) ₃ F] (5)	195
• [W=O(CH ₂ ¹ Bu) ₃ F] (6)	199
2.2. Grafting of the molecular precursors and characterizations	201
2.2.1. Reactivity of [W=O(CH ₂ ¹ Bu) ₄] (3) with Al ₂ O ₃₋₍₅₀₀₎	201
• IR study	201
• Mass balance analysis	202
• Conclusion	203
2.2.2. Reactivity of [W=O(CH ₂ ¹ Bu) ₄] (3) with SiO ₂₋₍₇₀₀₎	203
• DRIFT	204
• RAMAN	204
• Mass balance analysis	205
• Solid-state NMR study	205
• EXAFS	206
• DFT Calculations	207
• Thermal stability and carbene formation	208
• Conclusion	209
2.2.3. Reactivity of [W=N(2,6- ¹ PrC ₆ H ₃)(CH ₂ ¹ Bu) ₂ (=CH ¹ Bu)] (4) with SiO ₂₋₍₇₀₀₎	209
2.2.4. Reactivity of [W=N(C ₆ H ₅)(CH ₂ ¹ Bu) ₃ F] (5) with SiO ₂₋₍₇₀₀₎	211
• IR Study	211
• Mass balance analysis	213
• Conclusion	213
2.2.5. Reactivity of [W=O(CH ₂ ¹ Bu) ₃ F] (6) with SiO ₂₋₍₇₀₀₎	213
• IR study	213
• RAMAN	214
• Mass balance analysis	215
• Solid-state NMR study	215
• DFT calculations	216
• Using POSS as models of SiO ₂	218
• EXAFS	219
• Thermal stability and carbene formation	220
• Conclusion	220
2.3. Catalytic activity of the different species prepared	221
2.3.1. Compared catalytic performances toward direct conversion of ethylene to propylene	221
2.3.2. Compared catalytic performances toward propylene metathesis	221
2.4. Conclusion	226
3. Experimental section	228
3.1. General procedures	228
3.2. Preparation of the organometallic precursors	229
3.2.1. Preparation of ¹ BuCH ₂ Na	229
3.2.2. Preparation of 3	229
3.2.3. Preparation and of 5	230
3.2.4. Preparation and characterization of 6	231
• Method 1	231
• Method 2	231

3.3. Reactivity of the organometallic precursors with oxides and characterizations.....	231
3.3.1. Preparation and characterization of 3/Al₂O₃₋₍₅₀₀₎	231
3.3.2. Preparation and characterization of 3/SiO₂₋₍₇₀₀₎	232
3.3.3. Preparation and characterization of 5/SiO₂₋₍₇₀₀₎	232
3.3.4. Monitoring the synthesis of 5/SiO_{2-(700)D} by IR spectroscopy.....	232
3.3.5. Preparation and characterization of 6/SiO₂₋₍₇₀₀₎	233
3.3.1. Preparation and characterization of 6/POSS	233
3.3.2. DFT calculations	234
3.4. Catalytic tests.....	234
3.4.1. Reactivity toward ethylene in batch reactor	234
3.4.2. Propylene metathesis	234
4. Reference and Notes	235

1. Introduction

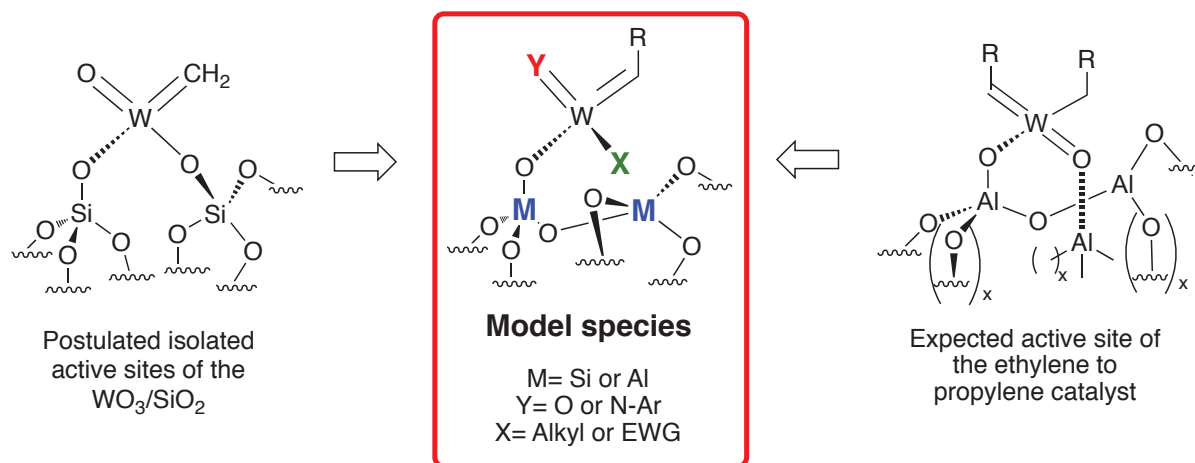
WO₃/SiO₂ is an efficient catalyst for olefin metathesis used in industrial processes since the discovery of Banks and Bailey in the 1960s.¹⁻⁴ However, as already explained in chapter 1, the structure of the actual active species is still a matter of debate, which prevents efficient and rational development.⁵⁻⁹ Several observations suggest the existence of isolated metal centers as the active site, and based on the validity of Chauvin mechanism both in homogeneous and heterogeneous systems,¹⁰ it is reasonable to expect that carbene species are involved, possibly bearing an oxo ligand in the metal's coordination sphere^{11,12} (Scheme 6.1 left). Owing to the strategic importance of olefins as building blocks for the world chemical industry, development of efficient processes is of utmost relevance. More specifically, tailored heterogeneous catalysts with known structure-activity relationships may improve lifetimes and activity by increasing the numbers of active sites.¹³

Moreover, interesting similarities between the active site of WO₃/SiO₂ and the neutral active site of WH/Al₂O₃ catalyst described in Chapter 2 must be noted. Hence the active tungsten seems to bear an oxo ligand in its coordination sphere. Moreover, mechanistic considerations, reported in Chapter 3, indicate that the active site of the catalyst for the direct conversion of ethylene to propylene must be an alkyl-alkylidene tungsten species (Scheme 6.1 right). Consequently, the preparation of new surface species with similar coordination sphere will confirm the characterizations of the neutral active site of WH/Al₂O₃ and deepen the understanding of its catalytic activity.

This chapter details the preparation of new, well-defined single site supported catalysts, as models of the active site of tungsten oxide supported on silica and tungsten hydride supported on alumina. These new surface species were prepared according to SOMC methodology using the strategy described in Scheme 6.1 (centre).

In order to establish a reliable structure-reactivity relationship of the grafted tungsten complexes, it was decided to explore the influence of the coordination sphere of the tungsten atom by changing: i) the nature of **M**, *i.e.* the oxide support (**M** = Si or Al) ii) the nature of the double bonded ancillary ligand **Y** (**Y** = O or N-Ar); iii) the nature of the single bonded ancillary ligand **X** (**X** = alkyl or an electron-withdrawing group (EWG)). Regarding this last parameter, one should mention that only the alkyl **X** ligand can afford the alkyl-alkylidene tungsten species needed for the direct conversion of ethylene to propylene (see Chapter 3). When this ligand will be replaced by an EWG, it is *a priori* expected that the dimerization site will not be available any more, but nevertheless the electrophil-

icity of the metal center may be strengthened and this may provide better metathesis catalysts. This structure-reactivity relationship strategy study will thus afford new catalysts and is expected to confirm the necessity of a carbene-hydride or carbene-alkyl sites for performing direct conversion of ethylene to propylene.



Scheme 6.1 left: Expected isolated active sites of the WO_3/SiO_2 metathesis catalyst; centre: template used for the preparation of model species; right: Expected active site of the $\text{WH}/\text{Al}_2\text{O}_3$ ethylene to propylene catalyst.

When considering the design of single-site heterogeneous catalysts with a controlled coordination sphere, SOMC has emerged as a powerful approach. The reaction of molecular species with an oxide surface may be understood by comparison to their known reactivity in solution, and therefore targeted species may be obtained through judicious selection of the molecular precursors. The support and the homogeneous organometallic precursors were chosen carefully to match the described model (Scheme 6.1 centre).

As a result, the support used for the grafting of these organometallic species were SiO_2 and Al_2O_3 in order to obtain species having respectively $\mathbf{M} = \text{Si}$ and Al regarding the notation of Scheme 6.1. The variation of support will thus provide models of the active site of the WO_3/SiO_2 when $\mathbf{M} = \text{Si}$ and the active site of $\text{WH}/\text{Al}_2\text{O}_3$ when $\mathbf{M} = \text{Al}$.

Bearing in mind the active sites of WO_3/SiO_2 or $\text{WH}/\text{Al}_2\text{O}_3$ catalyst, and in the view of developing realistic model surface species, it was targeted, as tungsten molecular precursors, oxo carbenes or their alkyl precursors that are amenable to carbene generation upon α -H abstraction. Then, tungsten oxo-alkylidene derivatives and their alkyl precursors were considered ($\mathbf{Y}=\text{O}$).

The first example of such complexes was provided by Schrock *et al.*, who reported the synthesis of $[\text{W}=\text{OCl}_2(=\text{CHR})(\text{PR}'_3)_n]$ derivatives which catalyze olefin metathesis in presence of a Lewis acid.^{14,15} Later they developed a bisaryloxy complex $[\text{W}=\text{O}(\text{OAr})(=\text{CHR})(\text{PR}'_3)]$ which catalyses ROMP of norbornadiene derivatives without co-

catalyst.¹⁶ These complexes were not selected as candidates for grafting, as the formation of metal-support bond by protonolysis will lead to the evolution of HCl or ArOH respectively for chlorine or aryloxy complexes. These acidic products may be consecutively added to the carbene to form a σ -alkyl species¹⁷ inactive in olefin metathesis.

Chen *et al.* have also reported the formation of an oxo carbene tungsten complex [W=O(=C^tBu)(Si^tBuPh₂)(CH₂^tBu)₂] by addition of 1 equivalent of oxygen on [W(=C^tBu)(CH₂^tBu)₂(Si^tBuPh₂)].¹⁸ The mechanism of formation of this oxo has been investigated through theoretical calculations. The authors describe a silyl migration, leading to a tungsten IV species, induced by the highly exothermic addition of oxygen on that species.¹⁹ Nevertheless, the poor yield of the reaction (1.7%), which has only been reported on NMR tube, discards this complex as a precursor for grafting.

Osborn and Kress described tungsten oxotrisalkyl complexes [W=O(CH₂^tBu)₃X] (X = Cl, Br, ONp) that are efficient metathesis catalysts with high, sustained activity upon activation by Lewis acids and photoinitiation.²⁰⁻²² These oxo alkyls appear as promising candidates for this purpose.

The key step in grafting, namely formation of the metal-support bond by protonolysis of a metal-alkyl, must occur irreversibly with high selectivity. This rules out using of halide (*i.e.* Cl, Br, I) or alkoxides as the X species in [W=O(CH₂^tBu)₃X], as competition between W-C and W-R bond protonolysis may occur upon grafting. A typical example is the formation of binuclear [W₂O₃(CH₂^tBu)₆] upon hydrolysis of [W=O(CH₂^tBu)₃Cl].^{23,24} Fluorine may be envisaged as an X, since tungsten fluorine bond is stronger than the other tungsten halide bond (W-F = 131±15 kcal.mol⁻¹; W-Cl = 101±10 kcal.mol⁻¹).²⁵ The following new tungsten oxo complexes, *i.e.* [W=O(CH₂^tBu)₄] (**3**) and [W=O(CH₂^tBu)₃F] (**5**), seem to meet all these constraints, and have thus been prepared.

In contrast to these oxo-alkylidene tungsten derivatives, numerous examples of compounds bearing the isoelectronic imido ligand have been described (Y=N-R). Indeed, due to their easier synthesis, enhanced stability and high activity in olefin metathesis in absence of cocatalysts, this approach proved to be rewarding both for homogeneous and heterogenized systems.²⁶ It was also decided to use the tungsten imido alkylidene complex [W=N(2,6-ⁱPrC₆H₃)(CH₂^tBu)₂(=CH^tBu)] (**4**), as its grafting on silica was already studied in the laboratory.^{27,28} This supported complex will be compared with isoelectronic oxo (Y=O) complexes.

The first part of this chapter will be focused on the preparation and characterizations of the homogeneous precursors, *i.e.* tetraalkyl derivative [W=O(CH₂^tBu)₄] (**3**), carbene

bisalkyl derivative $[W=N(2,6\text{-}^i\text{PrC}_6\text{H}_3)(\text{CH}_2^t\text{Bu})_2(=\text{CH}^t\text{Bu})]$ (**4**) and fluorinated derivatives $[W=N(\text{C}_6\text{H}_5)(\text{CH}_2^t\text{Bu})_3\text{F}]$ (**5**) and $[W=O(\text{CH}_2^t\text{Bu})_3\text{F}]$ (**6**).

The second part of the chapter describes the grafting and characterizations of these complexes. The most obvious pathway for the immobilization of these organometallic species is the protonolysis of a W-C bond with the remaining silanols or aluminols of the pre-treated support. The grafting of **3** and **4** will afford species bearing **X** as an alkyl ligand and **Y** as an oxide or imido ligand, whereas the grafting of **5** and **6** is expected to give surface species bearing **X** as a fluoride and **Y** as an oxide or imido ligand according to the defined strategy (Scheme 6.1 centre). However, the fate of the W-F was particularly studied, and the resulting species do not have the expected structure.

The third part of this chapter discloses the catalytic activity of the different catalysts obtained for ethylene to propylene and propylene metathesis. The structure-reactivity relationship will be studied and particularly the deactivation pathway of the active species.

2. Results and discussions

2.1. Preparation of the molecular precursors

Four different organometallic precursors of the model species have been prepared, in this subsection their synthesis and characterizations are presented.

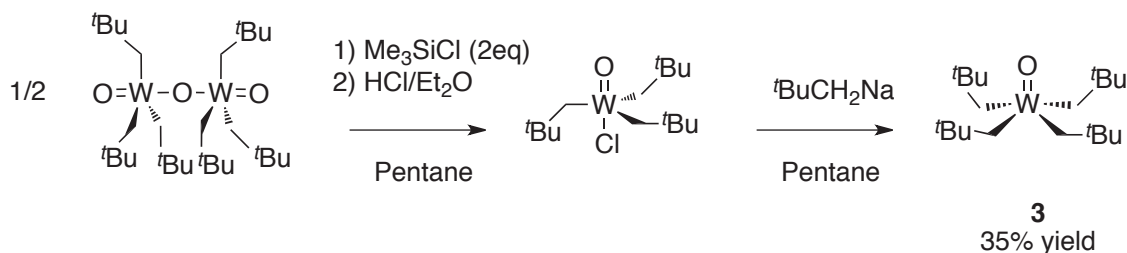
2.1.1. Alkyls complexes: $[W=O(\text{CH}_2^t\text{Bu})_4]$ (**3**),
 $[W=N(2,6\text{-}^i\text{PrC}_6\text{H}_3)(\text{CH}_2^t\text{Bu})_2(=\text{CH}^t\text{Bu})]$ (**4**)

The Alkyls complexes, *i.e.* complexes that may afford model species with **X** = alky are presented herein.

- $[W=O(\text{CH}_2^t\text{Bu})_4]$ (**3**)

The tungsten oxo-tetraalkyl complex $[W=O(\text{CH}_2^t\text{Bu})_4]$, **3**, has not been reported yet even though Kress *et al.* reported the synthesis of $[W=O(\text{CH}_2^t\text{Bu})_3(\text{OCH}_2^t\text{Bu})]$ mistakenly attributed to **3** starting from $[W=OCl_4]$.^{20,21} Thus a new route to the desired complex **3** was investigated. The reaction of $[W=O(\text{CH}_2^t\text{Bu})_3\text{Cl}]$, prepared from $[W_2O_3(\text{CH}_2^t\text{Bu})_6]$,²⁴ with several alkylating agents was studied. Among $(^t\text{BuCH}_2)_2\text{Mg}\cdot\text{dioxane}$, $^t\text{BuCH}_2\text{MgCl}$ or $^t\text{BuCH}_2\text{Li}$, only unconventional $^t\text{BuCH}_2\text{Na}$ afforded a tractable product, $[W=O(\text{CH}_2^t\text{Bu})_4]$, **3**, as a colourless, light- and highly moisture-sensitive oil in a 35% yield.

The alkylating agent, $^t\text{BuCH}_2\text{Na}$, was prepared, by analogy with $(\text{C}_6\text{H}_5)\text{CH}_2\text{K}$,^{29,30} by transmetallation of $^t\text{BuCH}_2\text{Li}$ ³¹ with $^t\text{BuONa}$.

Scheme 6.2 Synthesis of **3**

NMR features indicate the presence of equivalent neopentyl moieties, with the methylenic group giving rise to a singlet at 1.83 ppm and 85.60 ppm ($^1J_{\text{W-C}} = 48.1$ Hz) on the ^1H and ^{13}C NMR spectra, respectively. Alkylation results in significant shielding as the CH₂ signals in ^1H and ^{13}C NMR are 2.46 and 100.9 ppm in $[\text{W}=\text{O}(\text{CH}_2^t\text{Bu})_3\text{Cl}]$, respectively (Figure 6.1).

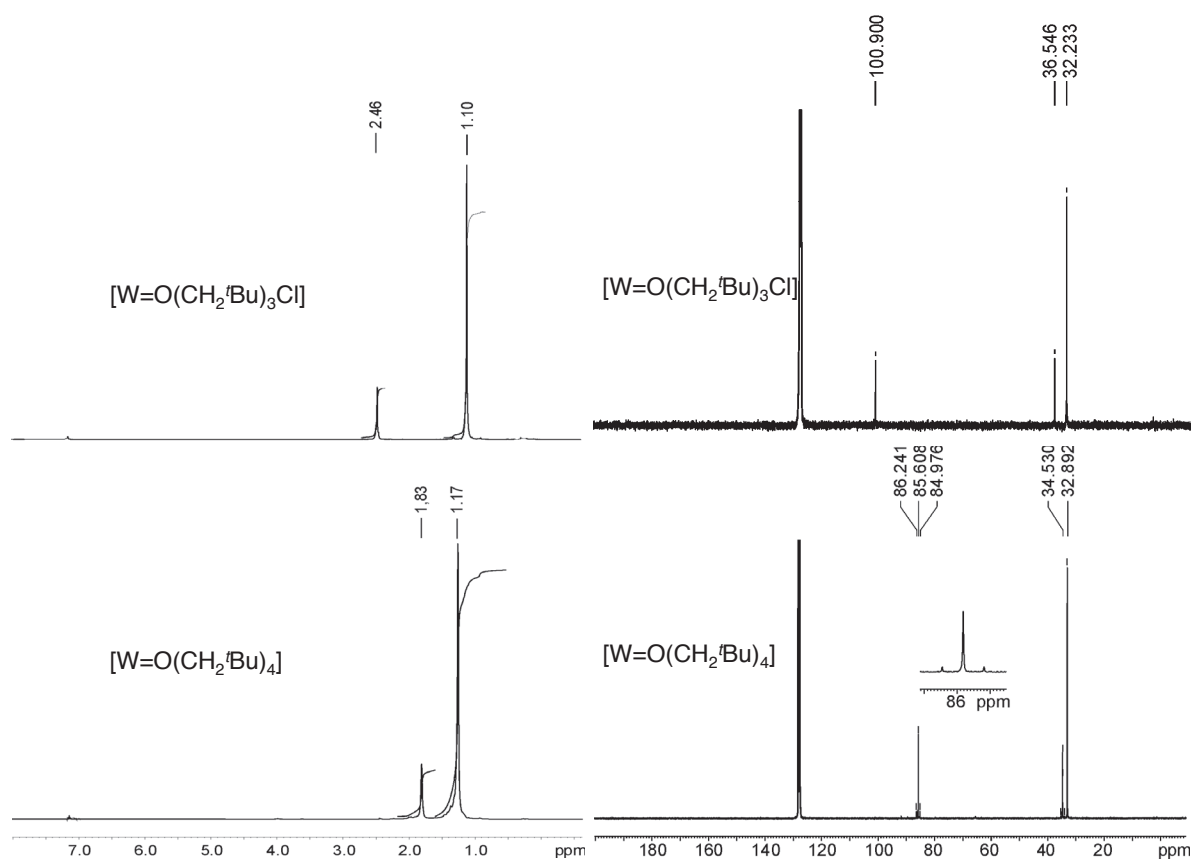


Figure 6.1 Compared ^1H (left) and ^{13}C (right) NMR spectra of $[\text{W}=\text{O}(\text{CH}_2^t\text{Bu})_3\text{Cl}]$ (top) and **3** (bottom) (C_6D_6 , 295K, ^1H : 300 MHz, ^{13}C : 75 MHz)

As this product was obtained as an extremely air and light sensitive oil, which slowly decomposes at room temperature, neither XRD nor elemental analysis could have been performed. However, DFT calculations (B3PW91/SDDall) indicate that **3** adopts a distorted trigonal bipyramidal geometry, with the oxo and two neopentyl ligands in the

equatorial positions, while the axial sites are occupied by alkyl moieties (Figure 6.2), which is consistent with equivalent neopentyl ligands on the NMR time scale at room temperature.

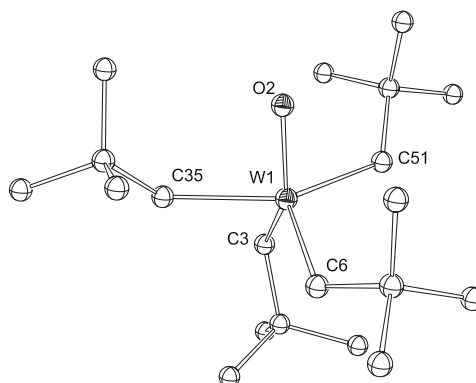
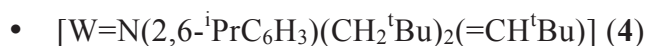
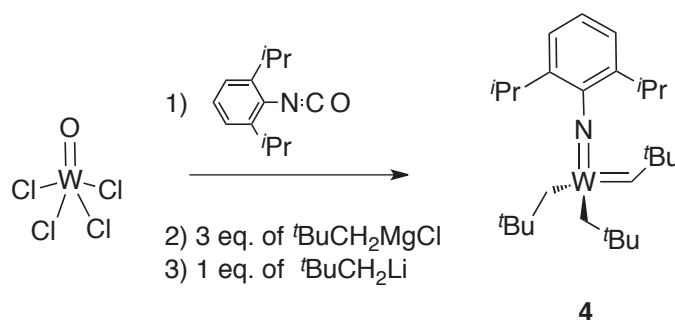


Figure 6.2 DFT calculated structure of **3**



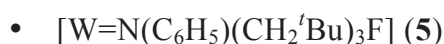
The compound $[W=N(2,6\text{-}^i\text{PrC}_6\text{H}_3)(\text{CH}_2^t\text{Bu})_2(=\text{CH}^t\text{Bu})]$, **4**, is known and several preparation methods, are described in the literature.^{32,33} It was found that the most convenient method, in term of number of steps, yield and purification, was the following. The synthesis begins with the reaction of WOC1_4 with $(2,6\text{-}^i\text{PrC}_6\text{H}_3)\text{NCO}$, followed by a first alkylation with three equivalent of neopentylmagnesiumchloride affording $[W=N(2,6\text{-}^i\text{PrC}_6\text{H}_3)(\text{CH}_2^t\text{Bu})_3\text{Cl}]$ which is alkylated a second time using the more nucleophilic neopentyllithium to afford **4**.



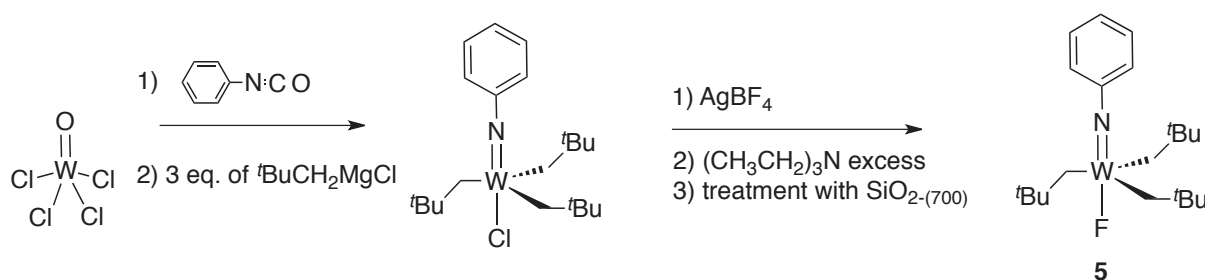
Scheme 6.3 Synthesis of **4**

2.1.2. Fluorinated complexes: $[W=N(\text{C}_6\text{H}_5)(\text{CH}_2^t\text{Bu})_3\text{F}]$ (**5**) and $[W=O(\text{CH}_2^t\text{Bu})_3\text{F}]$ (**6**)

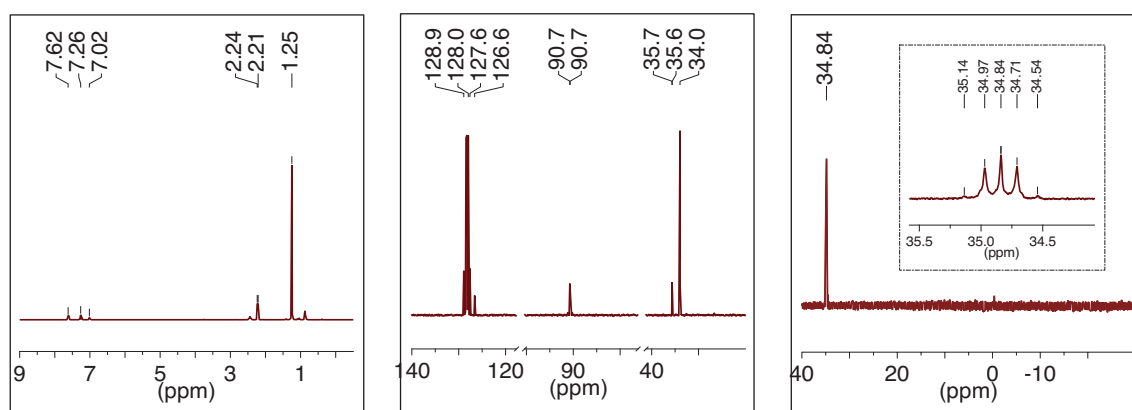
The preparation of organometallic complexes containing a fluorine ligand acting as an electron-withdrawing group, $\text{X} = \text{F}$, are presented in this subsection.



The phenyl substituent of the imido ligand was chosen, without bulky substituents in ortho and ortho' position, to be as close as possible to the oxo ligand in term of steric hinderance. The synthesis of **5** was adapted from the synthesis of [W=N(2,6-ⁱPrC₆H₃)(CH₂^tBu)₃F] described by Le Ny *et al.*³⁴ Thus, **5** has been synthesized by reaction of WOC1₄ with C₅H₅NCO, followed by alkylation with neopentylmagnesiumchloride. The chlorine atom has been substituted by a fluorine using AgBF₄ (Scheme 6.4). Et₃N was not efficient to fully remove BF₃, it has only been fully removed by reaction with SiO₂₋₍₇₀₀₎, as ¹¹B NMR gives no signal and elemental analysis did not spot the presence of boron. This method, in spite of its drastic impact of the reaction yield (31%), afford pure [W=N(2,6-ⁱPrC₆H₃)(CH₂^tBu)₃F], **5**, as a pale yellow solid.

Scheme 6.4 Synthesis of **5**

The NMR study of **5** confirms its structure (Figure 6.3). As the obtained species, **5**, contains five NMR active nuclei (*i.e.* ¹H (Nat. Ab. = 99.98%, ¹³C (Nat. ab. = 1.11%), ¹⁴N (Nat. ab. = 9.63%), ¹⁸F (Nat. ab. = 100%) and ¹⁸³W (Nat. ab. = 14.31%)), a particular attention has been turned to the study of the scalar coupling of the nuclei bounded to the tungsten.

Figure 6.3 liquid NMR spectra of **5**: left ¹H NMR; centre ¹³C{¹H} NMR and right ¹⁹F{¹H} NMR

On the ¹H NMR spectrum, the only protons affected by scalar couplings are the methylenic ones in β of the tungsten atom (Figure 6.4): i) coupling with ¹⁸F, spin 1/2, sepa-

rated by three bonds, with a coupling constant ${}^3J_{\text{F-H}} = 10.6$ Hz ii) 14.31% of these protons have a coupling with ${}^{183}\text{W}$, spin $\frac{1}{2}$, separated by two bond with a coupling constant ${}^2J_{\text{W-H}} = 10.1$ Hz iii) ${}^3J_{\text{N-H}}$ and ${}^3J_{\text{H-H}}$ are too small to be observed. Thus the resulting multiplet has the intensity 3.5:43:7:43:3.5, which is in line with the observed signal.

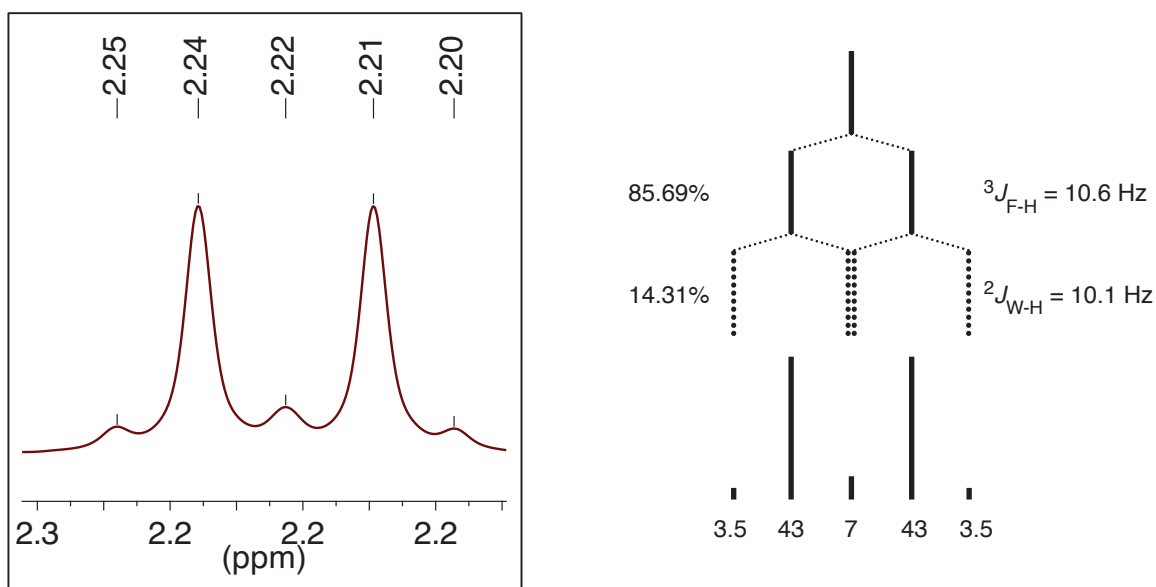


Figure 6.4 left: zoom on the ${}^1\text{H}$ NMR spectra of **5**; right: interpretation of the multiplet pattern

Then, on the ${}^{13}\text{C}\{{}^1\text{H}\}$ NMR spectrum, the only carbons affected by scalar couplings, as the spectrum is proton decoupled, are the methylenic ones in α of the tungsten atom (Figure 6.5): i) coupling with ${}^{18}\text{F}$, spin $\frac{1}{2}$, separated by two bonds, with a coupling constant ${}^2J_{\text{F-C}} = 6.8$ Hz ii) 14.31% of these carbons have a coupling with ${}^{183}\text{W}$, spin $\frac{1}{2}$, separated by one bond with a coupling constant ${}^1J_{\text{W-C}} \approx 46$ Hz iii) ${}^2J_{\text{N-C}}$ is too small to be observed. Thus the resulting multiplet has the intensity 3.5:3.5:43:43:3.5:3.5, which is in line with the observed signal.

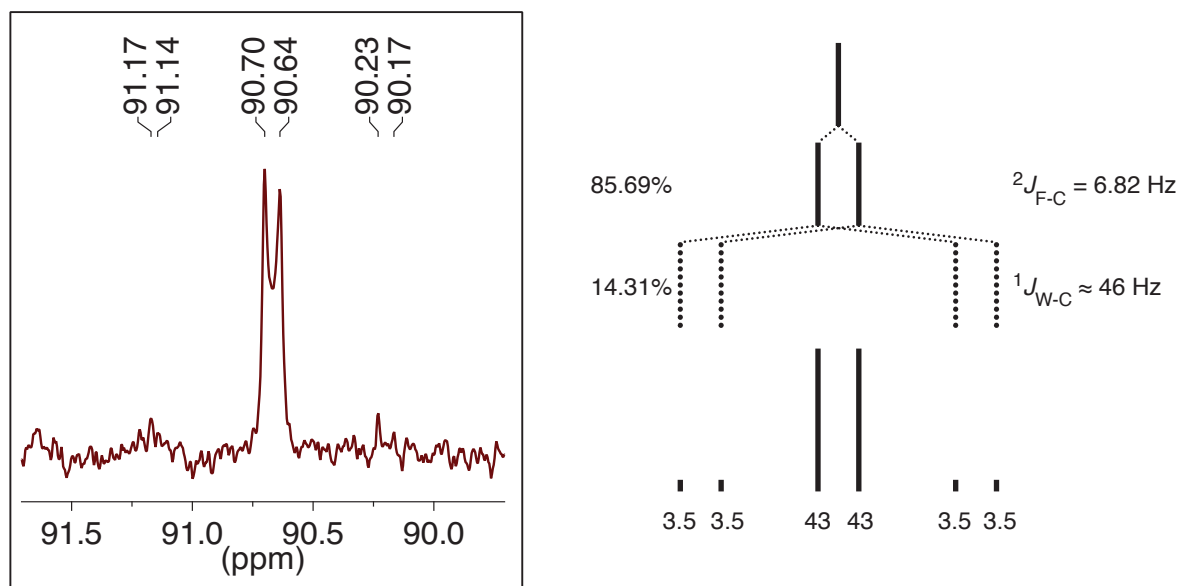


Figure 6.5 left: zoom on the ¹³C{¹H} NMR spectra of 5; right: interpretation of the multiplet pattern

Finally, the ¹⁸F{¹H} NMR spectrum presents, as expected, only one fluorine signal with a chemical shift at 34.8 ppm (Figure 6.6). It is affected by scalar couplings: i) coupling with ¹⁴N, spin 1, separated by two bonds, with a coupling constant $^2J_{N-F} = 49$ Hz, forming a spin 1 triplet ii) 14.31% of these fluorines have a coupling with ¹⁸³W, spin 1/2, separated by one bond with a coupling constant $^1J_{W-F} \approx 50$ Hz. Thus the resulting multiplet has the intensity 2:31:34:31:25, which is in line with the observed signal.

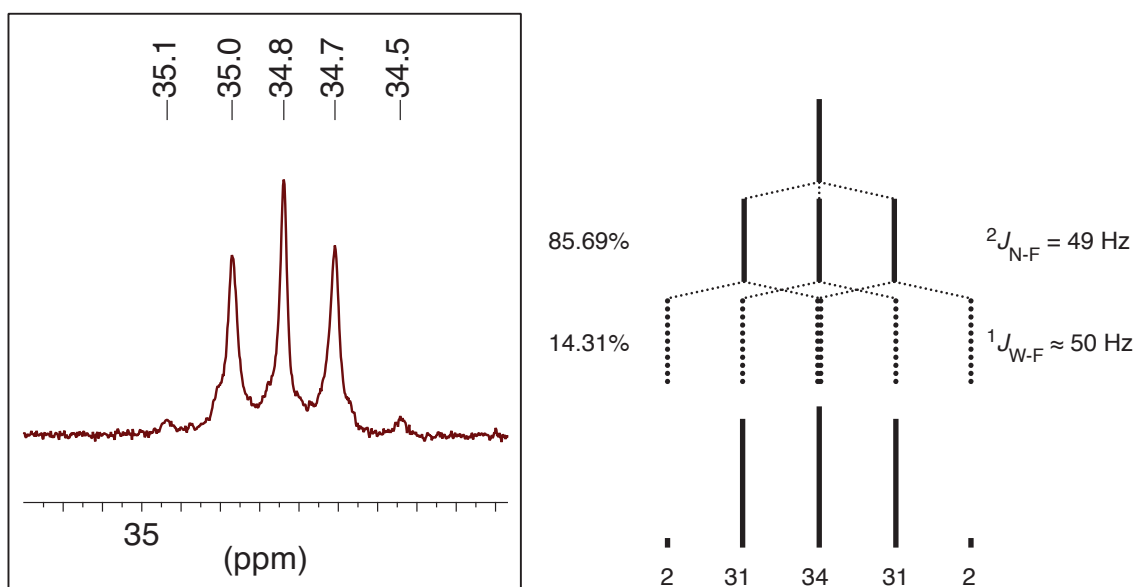
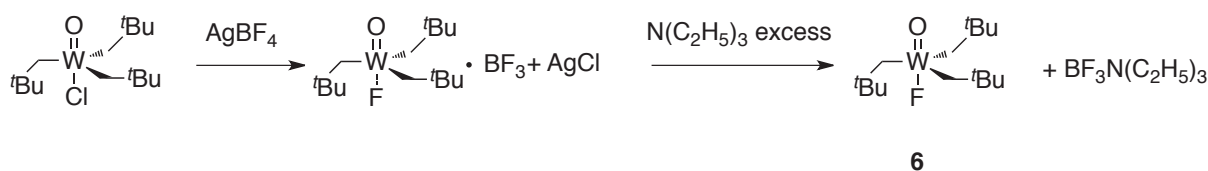


Figure 6.6 left: zoom on the ¹⁹F{¹H} NMR spectra of 5; right: interpretation of the multiplet pattern

Thus, the study of the scalar coupling of the nuclei bounded to the tungsten confirms the presence of three equivalent neopentyl moieties, one imido ligand and a single fluorine atom bounded to the tungsten.

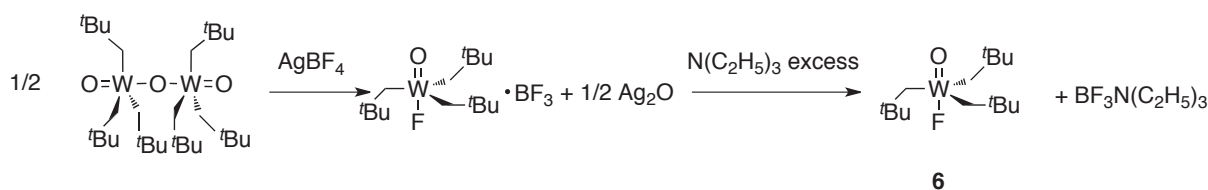


For the synthesis of $[W=O(CH_2^tBu)_3F]$, **6**, which has not been reported yet, $AgBF_4$ was also used as a fluorinating agent. A first method employed was the reaction of a stoichiometric equivalent of $AgBF_4$ with $[W=O(CH_2^tBu)_3Cl]$ with formation of an $AgCl$ precipitate (Scheme 6.5). The BF_3 moiety still in interaction with the complex was then eliminated by precipitation of $BF_3 \cdot N(C_2H_5)_3$ formed by addition of an excess of triethylamine. The removing of BF_3 was easier for this complex than for its imido equivalent **5**. This may be due to a weaker interaction between BF_3 and the oxo ligand.³⁵



Scheme 6.5 Synthesis of **6** from $[W=O(CH_2^tBu)_3Cl]$

An original method, was then applied, starting from the $[W_2O_3(CH_2^tBu)_6]$, which is the $[W=O(CH_2^tBu)_3Cl]$ precursor, reducing the synthesis of **3** of one step (Scheme 6.6). Hence, during the reaction of two equivalent of $AgBF_4$ with $[W_2O_3(CH_2^tBu)_6]$, an Ag_2O precipitate is observed. After removing the BF_3 moiety with an excess of triethylamine, $[W=O(CH_2^tBu)_3F]$ (**6**) was obtained as a white solid in a 80% yield from the dimeric complex.



Scheme 6.6 Synthesis of **6** from $[W_2O_3(CH_2^tBu)_6]$

NMR features of **6** (Figure 6.7) indicate the presence of equivalent neopentyl moieties, with the methylenic group giving rise to a doublet with satellites at 2.24 ppm ($^2J_{W-H} = 10.1$ Hz, $^3J_{F-H} = 8.6$ Hz) and a doublet with satellites at 94.8 ppm ($^1J_{W-C} = 46.0$ Hz; $^3J_{F-C} = 6.3$ Hz) on the 1H and ^{13}C NMR spectra, respectively. As expected for this complex bearing the more electronegative fluorine ligand both signals are shifted upfield in comparison with the chlorine ligand (*vide supra*). The quaternary carbon of the neopentyl moieties gives a singlet at 35.5 ppm whereas the terminal methyl groups give a singlet at 1.26 ppm and 32.6

ppm on the ¹H and ¹³C NMR spectra, respectively. On ¹⁹F{¹H} NMR spectrum, only a singlet with satellites is observed at -0.36 ppm. These satellites results from the strong coupling between tungsten and fluorine, ¹J_{W-F} = 82.2 Hz. The BF₃ has been fully removed as ¹¹B NMR gives no signal and elemental analysis did not spot the presence of boron. The latter has confirmed the formula of **6**.

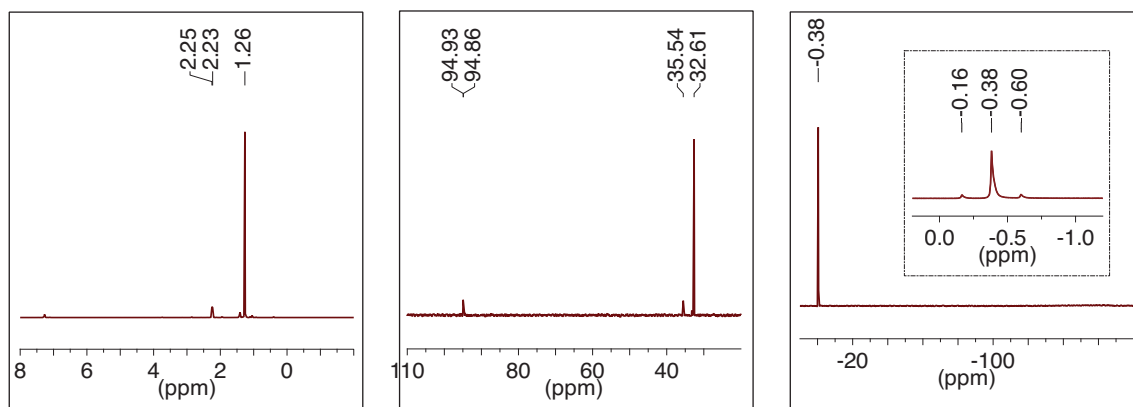
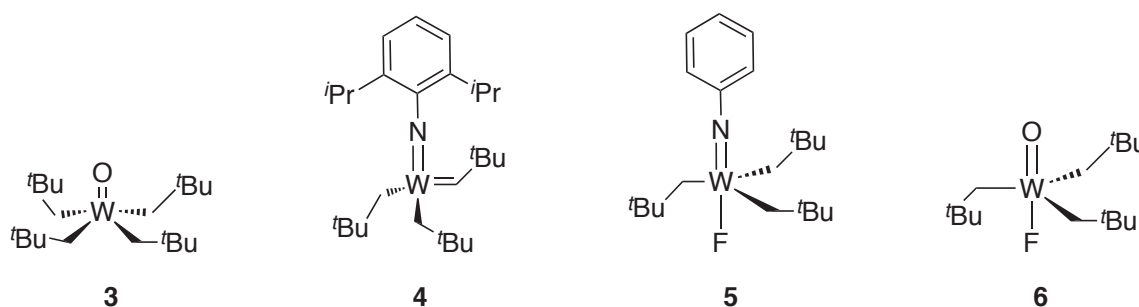


Figure 6.7 liquid NMR of **6**: left ¹H NMR; centre ¹³C{¹H} NMR and right ¹⁹F{¹H} NMR

Three novel tungsten complexes, *i.e.* [W=O(CH₂^tBu)₄] (**3**), [W=N(C₆H₅)(CH₂^tBu)₃F] (**5**) and [W=O(CH₂^tBu)₃F] (**6**), have thus been successfully synthesized. They will be used along with [W=N(2,6-ⁱPrC₆H₃)(CH₂^tBu)₂(=CH^tBu)] (**4**), as precursors for grafted catalyst (Scheme 6.7).



Scheme 6.7 Different precursors synthesized

It is interesting to compare all these organometallic complexes, as only **4** exhibits a carbenic ligand. The formation of this carbenic ligand only occurs when the alkylation of the complex is complete. Hence, the action of one equivalent of ^tBuCH₂Li on [W=N(2,6-ⁱPrC₆H₃)(CH₂^tBu)₃Cl], which bears three neopentyl ligand, lead to **4**, which bears two neopentyl and one neopentylidene ligand in a tetrahedral geometry. Schrock postulates the formation of a sterically crowded [W=N(2,6-ⁱPrC₆H₃)(CH₂^tBu)₄] intermedi-

ate³³ that undergoes α -hydrogen abstraction leading to the evolution of ${}^t\text{BuCH}_3$ and the formation of the carbenic ligand.^{35,36}

The oxo ligand is thus less bulky than the arylimido $\text{N}(2,6\text{-}{}^i\text{PrC}_6\text{H}_3)$ leaving, **3**, stable toward α -hydrogen abstraction as no carbenic ligand is formed during its synthesis.

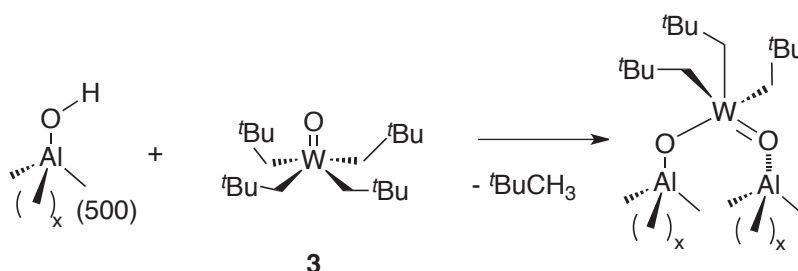
Le Ny and Osborn have made a complete study of $[\text{W}=\text{N}(\text{R})(\text{CH}_2{}^t\text{Bu})_3\text{X}]$ systems (X = halide, R = Me, ${}^i\text{Pr}$, ${}^t\text{Bu}$, $2,6\text{-}{}^i\text{PrC}_6\text{H}_3$) have also revealed they are stable toward α -hydrogen abstraction.³⁴ They have performed an NMR study to understand their structure. For all these complexes the neopentyl ligands were demonstrated equivalent and that the complex adopt a trigonal bipyramid geometry. Moreover ${}^{14}\text{N}$ NMR indicates that $\text{W}=\text{N}-\text{R}$ bonds are linear on the $[\text{W}=\text{N}(\text{R})(\text{CH}_2{}^t\text{Bu})_3\text{X}]$. It can be reasonably assumed that **5** and **6** have the same geometry.

2.2. Grafting of the molecular precursors and characterizations

The reactivity of the molecular precursors **3**, **4**, **5** and **6** toward partially dehydroxylated oxides is presented in this section.

2.2.1. Reactivity of $[\text{W}=\text{O}(\text{CH}_2{}^t\text{Bu})_4]$ (**3**) with $\text{Al}_2\text{O}_{3-(500)}$

Once the molecular precursor prepared and characterized, the grafting onto the oxide surface was performed. The first oxide chosen for the grafting is $\gamma\text{-Al}_2\text{O}_3$. Using this support may explain its influence in the active site of the $\text{WH}/\text{Al}_2\text{O}_3$ system. In order to achieve the selective synthesis of species singly bound to the support, $\text{Al}_2\text{O}_{3-(500)}$ was used. This synthesis may afford a surface site with the expected desired structure (Scheme 6.8), close to that of the active site of the $\text{WH}/\text{Al}_2\text{O}_{3-(500)}$ (Scheme 6.1 right).



Scheme 6.8 Expected reactivity of **3** toward $\text{Al}_2\text{O}_{3-(500)}$

- IR study

An excess of $[\text{W}=\text{O}(\text{CH}_2{}^t\text{Bu})_4]$, **3**, was sublimed at 60°C under dynamic vacuum on an alumina disk (40 mg) partially dehydroxylated at 500°C ($\text{Al}_2\text{O}_{3-(500)}$). These operations

were monitored by FTIR (Figure 6.8). The resulting spectra shows that the $\nu_{(\text{OH})}$ vibrations at 3793, 3775, and 3731 cm⁻¹ disappeared (Figure 3), while some OHs appear as a large band centered at 3645 cm⁻¹. This is very close from what was observed during the grafting of [W(≡C^tBu)(CH₂^tBu)₃] (**1**) where mostly HO- μ_1 -Al_{IV} reacts with the tungsten complex (Chapter 2). Moreover, the characteristic bands in the 3000-2700 cm⁻¹ and 1470-1110 cm⁻¹ regions associated with the $\nu_{(\text{CH})}$ and $\delta_{(\text{CH})}$ of the perhydrocarbyl ligands around W also have appeared.

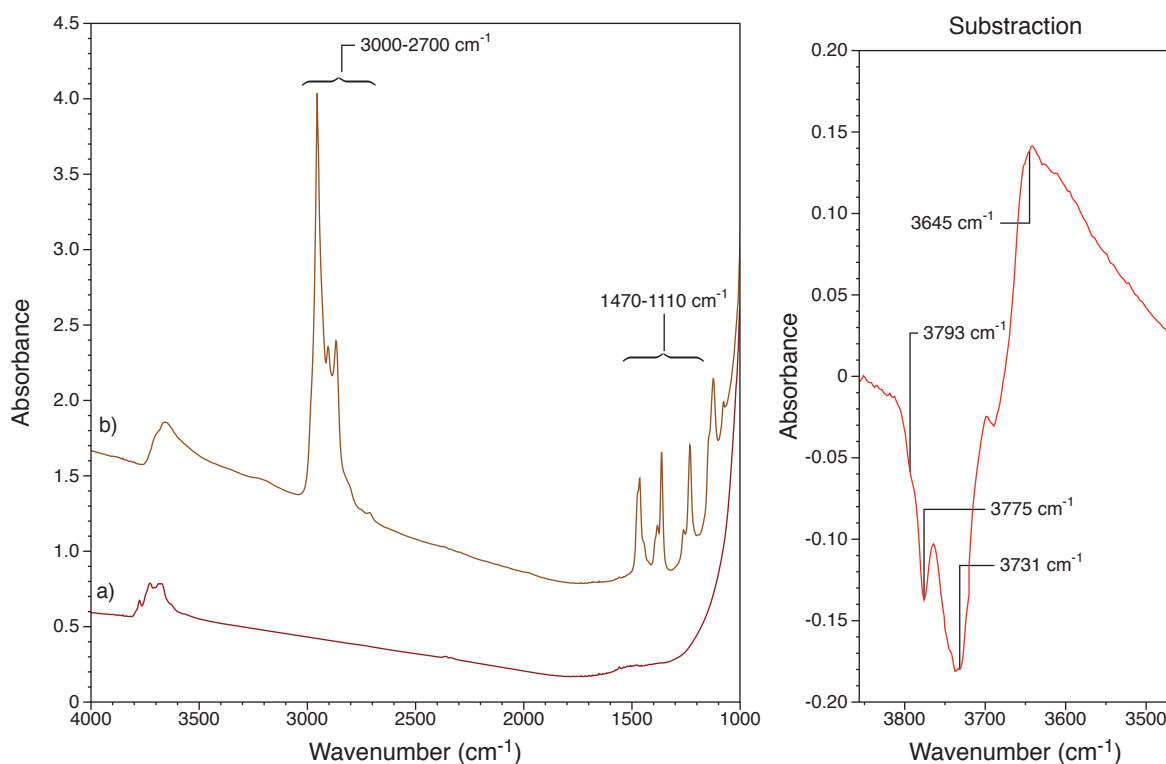
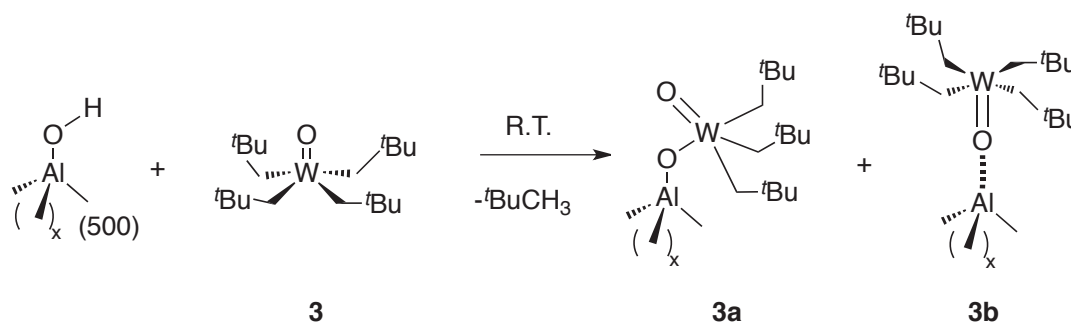


Figure 6.8 left: IR spectra of a) Al₂O₃₋₍₅₀₀₎ and b) **3**/Al₂O₃₋₍₅₀₀₎; right: subtraction of the two spectra in the $\nu_{(\text{OH})}$ region.

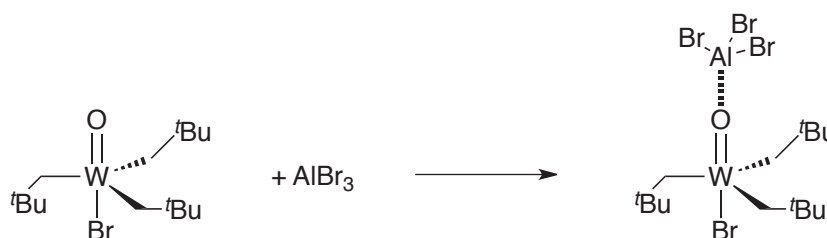
- Mass balance analysis

The reaction of **3** and γ -Al₂O₃₋₍₅₀₀₎ at RT in pentane in absence of light for 15 h generates 0.05 mmol of ^tBuCH₃.g⁻¹ of alumina, and the corresponding solid is washed 3 times with pentane before drying under vacuum. Elemental analysis shows the presence of W to the extent of 4.0 wt %, which corresponds to 0.22 mmol of W.g⁻¹. As only 0.25 equiv of ^tBuCH₃ evolved per grafted W, 0.05 mmol of OH/g of alumina has been consumed. Moreover, an average of 18.7 C per grafted W is found on the resulting solid by elemental analysis. Overall, the data are consistent with the formation of a mixture of two surface complexes (Scheme 6.9), which contains 25% of **3a** (15 C/W) and 75% of **3b** (20 C/W) giving an average of 18.75 C/W and for which 0.25 ^tBuCH₃/grafted W is expected during grafting (Scheme 6.9).

Thus **3a** is formed by the expected protonolysis of W-C bond whereas **3b** is formed by coordination of the oxide ligand with Lewis acid sites of the alumina.³⁶ This coordination has been evidenced for homogeneous tungsten oxo complexes using AlBr_3 as a Lewis acid (Scheme 6.10).^{21,35}



Scheme 6.9 Grafting of **3** on $\text{Al}_2\text{O}_{3-(500)}$



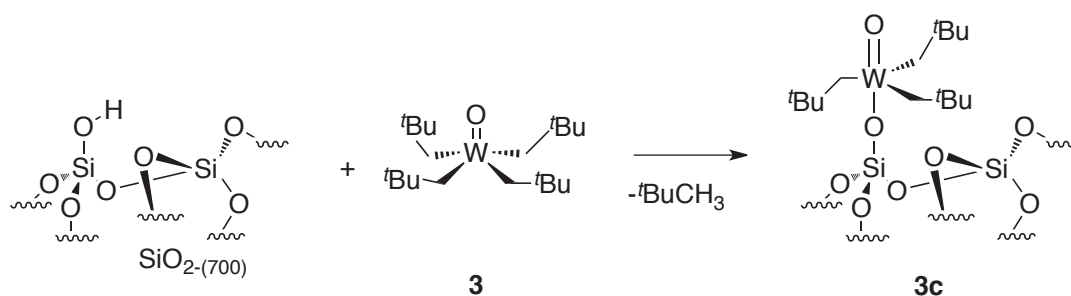
Scheme 6.10 Coordination of $[\text{W}=\text{O}(\text{CH}_2^t\text{Bu})_3\text{Br}]$ with AlBr_3 ³⁵

- Conclusion

The grafting of **3** on $\text{Al}_2\text{O}_{3-(500)}$ provide a mixture of two surface species (**3a**, **3b**). As the target of the study was the formation of well-defined single-sites models, it was decided to exclude Alumina and switch to Silica, a support that does not present Lewis acid character. Only silanols are expected to react through the protonolysis of W-C bounds.

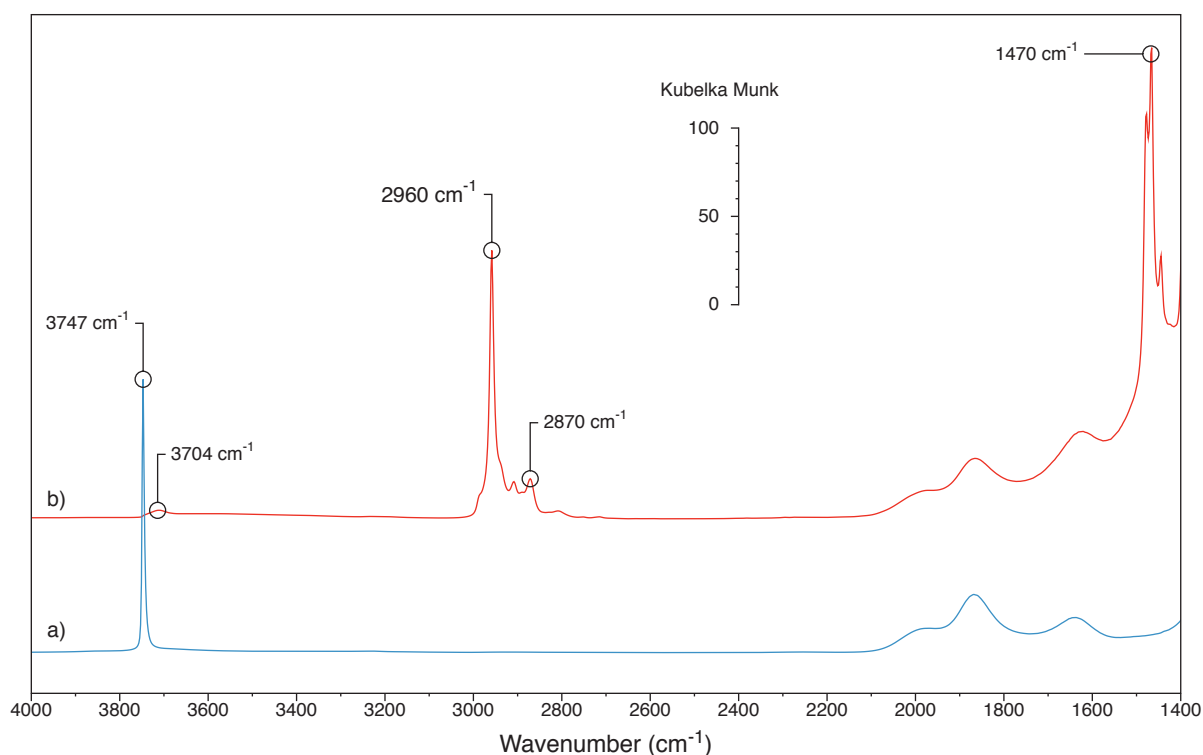
2.2.2. Reactivity of $[\text{W}=\text{O}(\text{CH}_2^t\text{Bu})_4]$ (**3**) with $\text{SiO}_{2-(700)}$

In order to achieve the selective synthesis of species singly bound to the support, we selected a silica that solely bears isolated silanols surface groups, namely silica heated under vacuum at 700°C (SiO_2-700). Grafting of **3** was carried out in absence of light at room temperature in pentane (Scheme 6.11).

Scheme 6.11 Grafting of **3** on $\text{SiO}_2-(700)$

- DRIFT

Infrared studies revealed the disappearance of the isolated silanol peak, and minor quantities of interacting SiOH (3704 cm^{-1}), indeed the small amount of untouched OH exhibits Van der Waals interaction with the alkyls ligands of the grafted complex.³⁷ Other main spectral features are $\nu_{(\text{C-H})}$ and $\delta_{(\text{C-H})}$ ($2990\text{--}2800$ and $1460\text{--}1480\text{ cm}^{-1}$, respectively; Figure 6.9) corresponding to the alkyl fragments of the grafted complex.

Figure 6.9 Diffuse reflectance infrared spectra of a) $\text{SiO}_2-(700)$ and b) $3/\text{SiO}_2-(700)$

- RAMAN

In order to gain information on the $\text{W}=\text{O}$ bond, the vibration band of which is hidden by the silica network's absorption in the infrared spectrum, Raman spectroscopy was applied (Figure 6.10). A characteristic broad line of medium intensity is observed in $3/\text{SiO}_2-(700)$ at

around 958 cm^{-1} . This is close to the values observed for WO_3/SiO_2 systems. Tomas *et al.* have observed, on WO_3/SiO_2 catalysts, a broad band at 970 cm^{-1} . They demonstrate that this band is not related to WO_3 crystallites.⁷ Kim *et al.* also observed a band at 975 cm^{-1} on low tungsten loaded WO_3/SiO_2 catalyst (1%_wt W). They attributed this band to surface tungsten oxides.³⁸ The lines at about 910 , 935 and 990 cm^{-1} result from neopentyl-related modes.

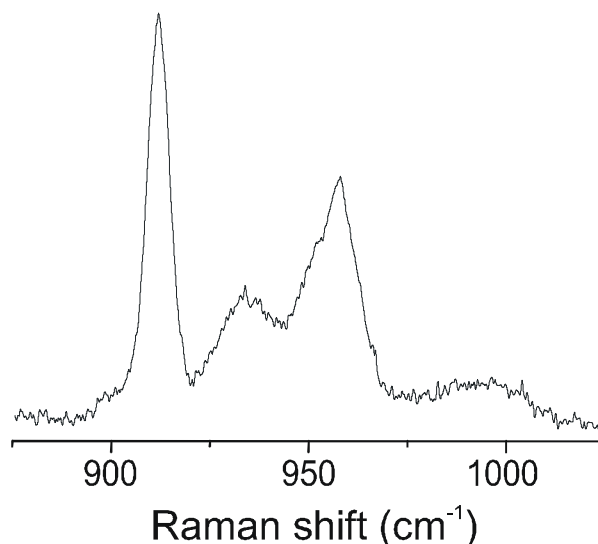


Figure 6.10 Selected region of Raman spectrum of $3/\text{SiO}_{2-(700)}$.

- Mass balance analysis

The resulting material ($3/\text{SiO}_{2-(700)}$) was stable to light exposure, and contained 4.1 wt% of tungsten and 4.2 wt% of carbon ($\text{C}/\text{W} = 14.9 \pm 0.1$, theory=15). Gas phase analysis indicates evolution of 0.9 equivalent of NpH per metal center. Thus mass balance analysis is fully in agreement with the $[(\equiv\text{SiO})(\text{W}=\text{O})(\text{CH}_2^t\text{Bu})_3]$ (**3c**) formulation.

- Solid-state NMR study

Solid-state NMR data are in line with the **3c** proposed structure (Figure 2). The ^1H NMR spectrum shows a set of signals at 1.93 (CH_2) and 1.01 ($\text{C}(\text{CH}_3)_3$) ppm. On the ^{13}C NMR spectrum of $3/\text{SiO}_{2-(700)}$, neopentyl groups resonate at 91 (CH_2), 34 ($\text{C}(\text{CH}_3)_3$) and 31 ppm ($\text{C}(\text{CH}_3)_3$). This compares favorably with NMR features of the model alkoxide species $[\text{W}=\text{O}(\text{CH}_2^t\text{Bu})_3(\text{OCH}_2^t\text{Bu})]$ (1.93 and 87.3 ppm for WCH_2 groups in ^1H and ^{13}C NMR, respectively).^{20,21} No resonances originating from carbenic species were detected. Assignments have been confirmed by ^1H - ^{13}C HETCOR 2D NMR, indicating the expected correlation between the 1.93 (^1H) and 91 (^{13}C) ppm methylenic fragments' signals (Figure 2).

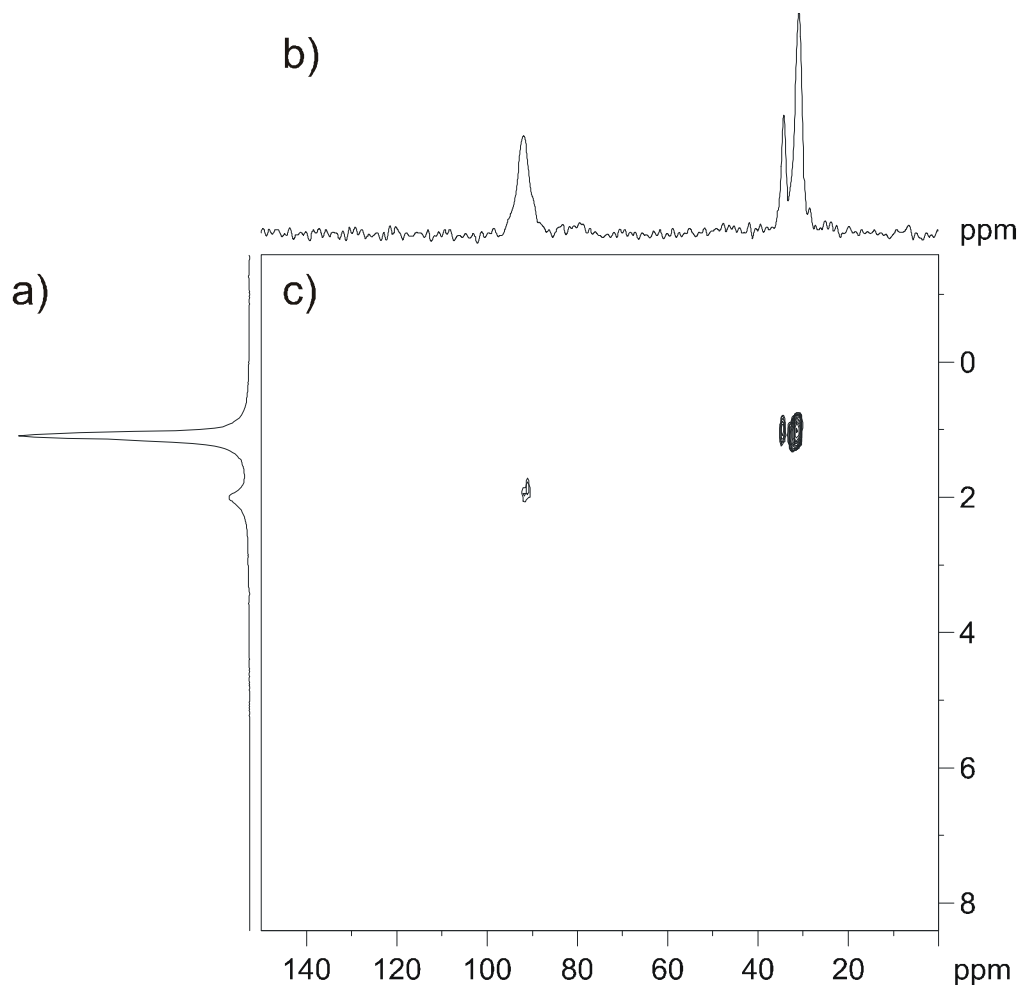


Figure 6.11 Solid state NMR data (18.8T) of **3**/SiO₂₋₍₇₀₀₎: a) ¹H MAS, b) ¹³C CP MAS and c) ¹H-¹³C HETCOR CP MAS.

- EXAFS

The structure **3c** of the supported tungsten complex **3**/SiO₂₋₍₇₀₀₎ was further confirmed by analysis of the W L_{III}-edge extended X-ray absorption fine structure (EXAFS) data (Figure 6.12 and Table 6.1). The results are consistent with a W coordination sphere comprising one oxygen atom at 1.71(1) Å, one oxygen at 1.97(3) Å and three carbons at 2.12(3) Å, assigned to an oxo ligand, a siloxide's σ-bonded oxygen, and methylenic carbons from neopentyl ligands, respectively. This is consistent with the bond distances found in [W₂O₃(CH₂^tBu)₆]²⁴ where the W=O_{terminal} (1.676–1.736 Å), W-O_{bridging} (1.913–1.987 Å) and W-C (2.113–2.150 Å) bond lengths are in the same range. W-O distances for σ-bonded siloxide ligands are usually shorter, *e. g.* (1.876–1.882 Å) in the case of [W=O(^tBu₃SiO)₂(C₂H₅)₂].³⁹ The rather long ≡SiO-W bond distance found here pleads for a *trans* mutual arrangement of the oxo and siloxy ligands, following from the strong *trans* influence of terminal M=O.⁴⁰⁻⁴² Moreover, the fit was improved when considering further layers of backscatterers: (i) three C atoms at 3.24(4)Å, assigned to the neopentyl ligands'

quaternary carbons, corresponding to a $126 \pm 8^\circ$ W-C-C angle, in agreement with the $123.7\text{--}127.4^\circ$ range found for $[\text{W}_2\text{O}_3(\text{CH}_2^t\text{Bu})_6]$;²⁴ (ii) *ca.* one silicon at $3.60(4)$ Å, corresponding to a $171 \pm 9^\circ$ W-O-Si angle: combined with the *trans* arrangement of the oxo and siloxy ligands, this indicates a quasi-linear O=W-O-Si framework; and (iii) *ca.* one oxygen atom at $2.98(8)$ Å, assigned to siloxane bridges of the silica surface.²⁸

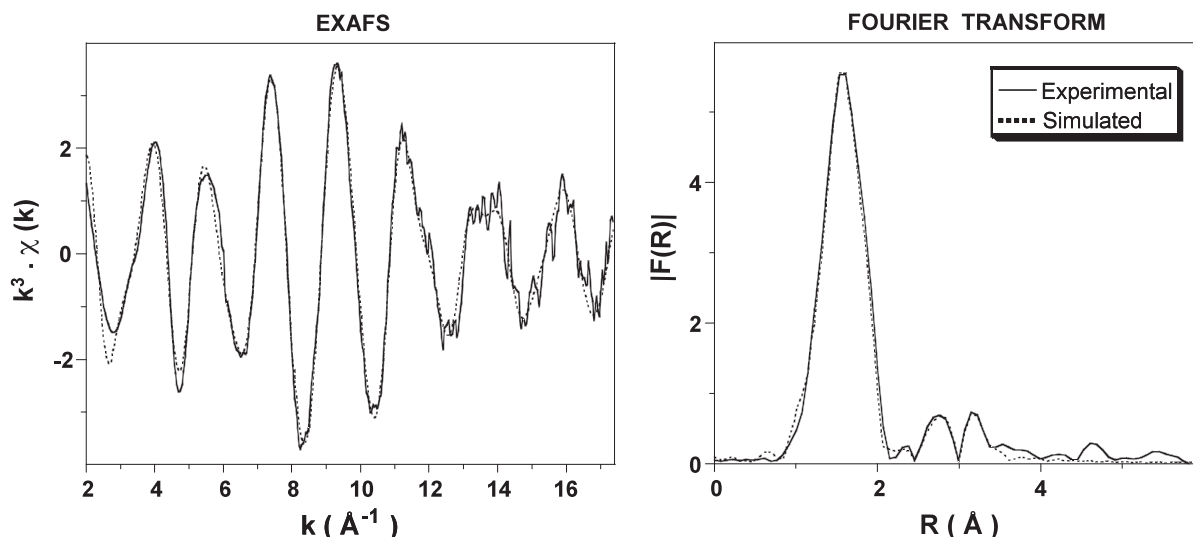


Figure 6.12 Tungsten L_{III} -edge k^3 -weighted EXAFS (left) and corresponding Fourier transform (right) with comparison to simulated curves for the W-containing surface species in $3/\text{SiO}_{2-(700)}$. Solid lines: experimental; dashed lines: spherical wave theory.

Table 6.1 EXAFS parameters for $3/\text{SiO}_{2-(700)}$ and DFT calculated distances for $3/\text{POSS}$

Type of neighbour	Number of neighbours	Distance (Å)	DFT calculated distance (Å)	σ^2 (Å ²)
W=O	1.1(3)	1.71(1)	1.755	0.0018(9)
W-O Si≡	1.2(6)	1.97(3)	1.990	0.002(2)
W-CH₂ CMe ₃	3.1(15)	2.12(3)	2.150–2.153	0.003(2)
W-CH₃ CMe ₃	3.1	3.24(4)	3.321–3.324	0.004(3)
W-O Si≡	0.8(4)	3.60(4)	3.637	0.004(4)
W-O (Si≡) ₂	0.8(7)	2.98(7)	-	0.007(8)

Errors between parentheses; fit residue: $\rho = 3.4\%$

- DFT Calculations

These structural propositions have been corroborated by DFT calculations (G03 program, B3PW91 level with the Sddall basis set) using polyhedral oligomeric silsesquioxane (POSS) as a model of $\text{SiO}_{2-(700)}$. Of the two possible structures (A and B on Figure 6.13), the most stable one (A with $\Delta E=65$ kJ) consists of a distorted trigonal bipyramid with mutually *trans* oxo and siloxide as axial ligands, and with equatorial positions occupied by alkyl moieties as observed in EXAFS. Moreover, the calculated bond lengths and angles

are in very good agreement with the EXAFS data, giving a clear picture of the surface organometallic fragment (Table 6.1).

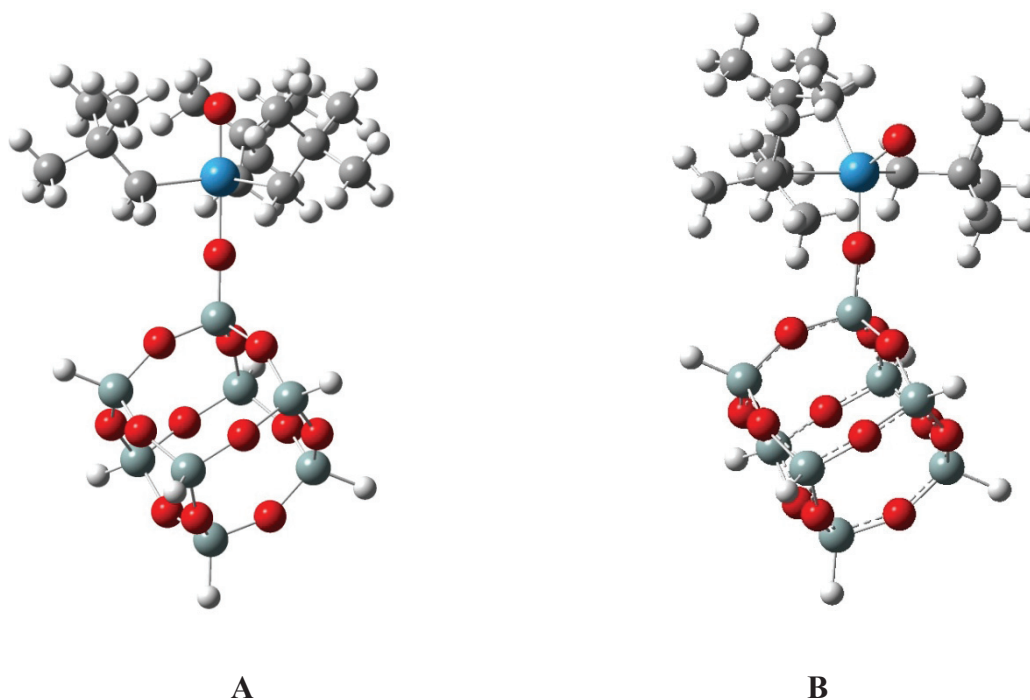
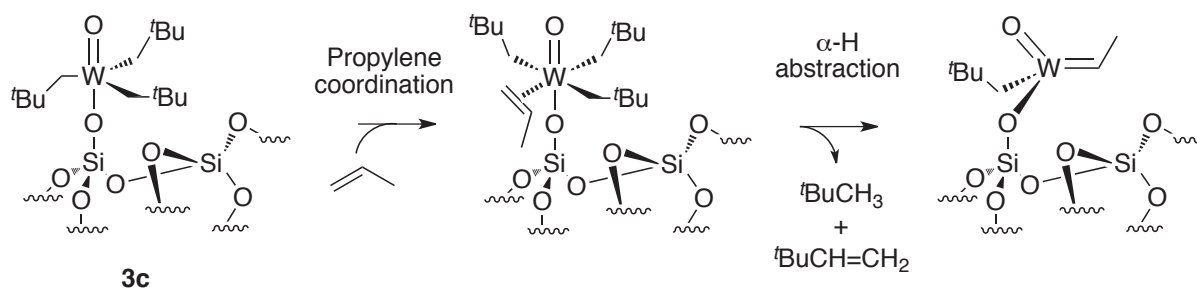


Figure 6.13 DFT calculated isomers of **3/POSS**

- Thermal stability and carbene formation

Hybrid material **3/SiO₂-(700)** proved to be thermally stable. Neither spectral (IR, RMN) modification nor gas evolution was detected upon heating under vacuum at 80°C. Thus, generation of carbene species from **3c** through thermally induced α -H abstraction does not seem to be operative. However, exposure to 40 equivalent of propylene at the same temperature (80°C) in a batch reactor led to the formation of equilibrated mixture of metathesis products: propylene, ethylene and 2-butene (trans/cis ratio of 2.3), along with 0.9 equivalent of neopentane per tungsten and trace amounts of nohexene, in agreement with the formation of the expected carbenic catalytic active species $[(\equiv\text{SiO})(\text{W}=\text{O})(\text{CH}_2^t\text{Bu})(=\text{CHCH}_2)]$ (Scheme 6.12). The coordination of the olefin to the highly electro-deficient tungsten centre increase the sterical crowding of the complex coordination sphere, going from a trigonal bipyramid to an octahedral geometry, and therefore favors the α -H abstraction.^{43,44} DFT calculations indicated that generation of this species from alkyl compound **3c** is thermodynamically favored ($\Delta E = -29 \text{ kJ}\cdot\text{mol}^{-1}$ for the corresponding species with H-substituted POSS as surface surrogate).



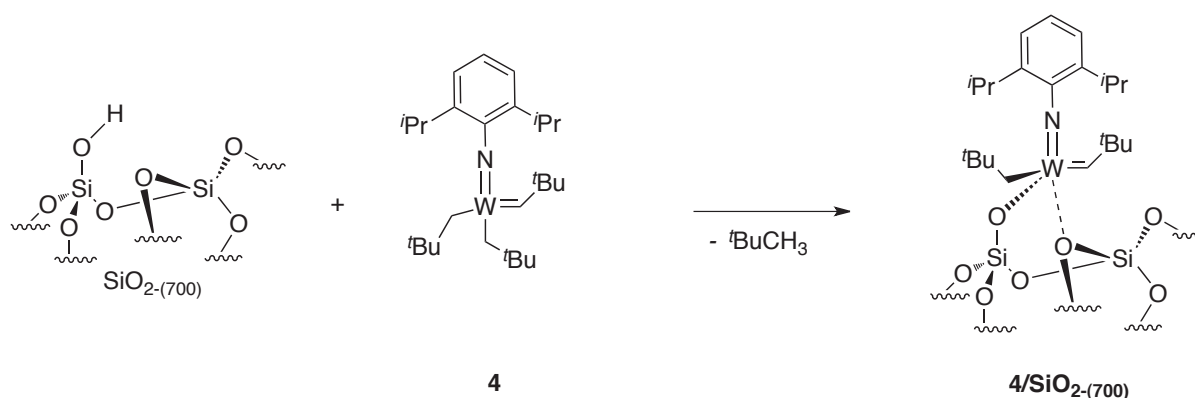
Scheme 6.12 Expected pathway of formation of a carbenic species from **3c** by propylene coordination followed by α-H abstraction

- Conclusion

The reaction of $[W=O(CH_2^tBu)_4]$ (**3**) with $SiO_{2-(700)}$ lead to the formation of a predominant single site species $[(\equiv SiO)(W=O)(CH_2^tBu)_3]$ **3c** which structure have been confirmed by IR, NMR, RAMAN and EXAFS spectroscopies, mass balance analysis and DFT calculations. This species is the first example of a well-defined tungsten surface species that solely combines oxo and alkyl ligands.

2.2.3. Reactivity of $[W=N(2,6\text{-}^iPrC_6H_3)(CH_2^tBu)_2(=CH^tBu)]$ (**4**) with $SiO_{2-(700)}$

In order to compare the impact of isoelectronic oxo and imido ligands on catalytic performances, the behavior of parent species $[(\equiv SiO)W=N(2,6\text{-}^iPrC_6H_3)(=CH^tBu)(CH_2^tBu)]$ (**4/SiO₂₋₍₇₀₀₎**) have been studied. This supported complex was prepared according the literature procedure (Scheme 6.13).²⁸ This procedure is briefly reported in this subsection, the characterizations obtained, which are fully in line with the described ones are also presented.



Scheme 6.13 Grafting of **4** on $SiO_{2-(700)}$

The grafting of **2** over $\text{SiO}_{2-(700)}$ was carried out at room temperature. The nature of **2**/ $\text{SiO}_{2-(700)}$ was confirmed by mass balance analysis, DRIFT and Solid state NMR which were fully in line with the literature characterizations.²⁸

The comparison between the DRIFT spectra of $\text{SiO}_{2-(700)}$ and **4**/ $\text{SiO}_{2-(700)}$ shows a complete consumption of the silanol band at 3740 cm^{-1} . Two groups of bands appear between $3100\text{-}2700\text{ cm}^{-1}$ and $1500\text{-}1300\text{ cm}^{-1}$ corresponding to the ν_{CH} and δ_{CH} of the neopentyl and disisopropylaryl ligands. Moreover, two broad bands also appear at 3700 and 3600 cm^{-1} . While the former is typical of residual surface hydroxyls in interaction with perhydrocarbyl groups, the latter is attributed to the interaction of other hydroxyls with the arylimido ligand.²⁸

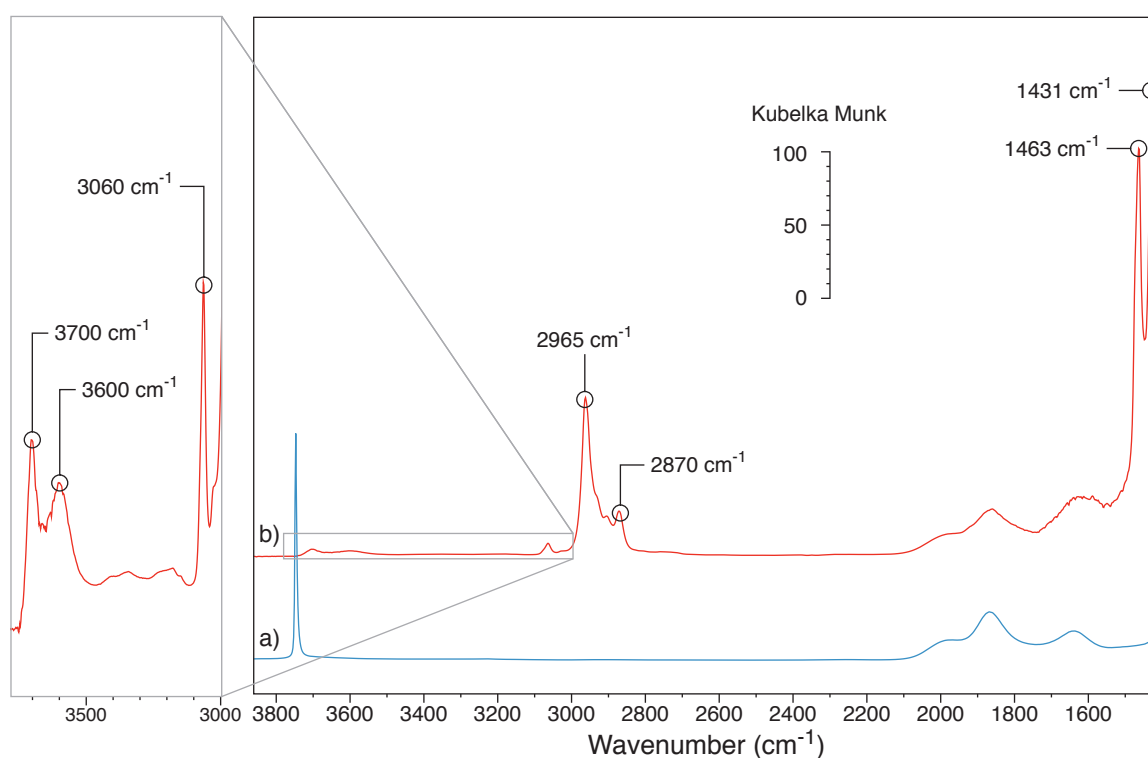
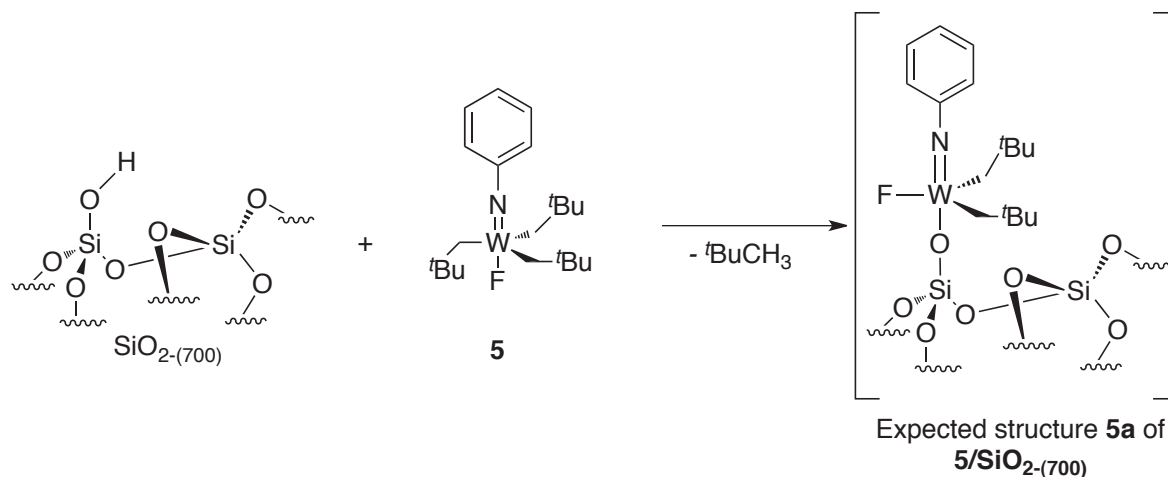


Figure 6.14 Diffuse reflectance infrared spectra of a) $\text{SiO}_{2-(700)}$ and b) **4**/ $\text{SiO}_{2-(700)}$

2.2.4. Reactivity of $[W=N(C_6H_5)(CH_2^tBu)_3F]$ (**5**) with $SiO_{2-(700)}$

The reactivity of $[W=N(C_6H_5)(CH_2^tBu)_3F]$ (**5**) toward $SiO_{2-(700)}$ have been then studied in pentane at room temperature.



Scheme 6.14 Expected reactivity of **5** toward $SiO_{2-(700)}$

- IR Study

Infrared studies revealed the disappearance of $\nu_{(OH)}$ bands associated to isolated silanols, and small intensity peaks corresponding to interacting SiOH with other functional groups (3695 cm^{-1}), as observed in related materials (Figure 6.15). As for **4/SiO₂₋₍₇₀₀₎** a group of bands appear between $3100\text{--}2700\text{ cm}^{-1}$, corresponding to the $\nu_{(CH)}$ of aromatic ($>3000\text{ cm}^{-1}$) and aliphatic parts of the ligands, and a band at 1489 cm^{-1} corresponding to $\delta_{(CH)}$ vibrations of the ligands. Contrary to the spectrum of **4/SiO₂₋₍₇₀₀₎**, the spectrum of **5/SiO₂₋₍₇₀₀₎** does not exhibit the signal at 3600 cm^{-1} . Moreover other features are notable on this spectrum. A weak broad band at 3330 cm^{-1} and a sharp signal at 1587 cm^{-1} that can be assigned to respectively $\nu_{(NH)}$ and $\delta_{(NH)}$ vibration modes.⁴⁵

With deuterated silica ($SiO_{2-(700)D}$), 80% of SiOD according to IR), a broad band at 2485 cm^{-1} appears whereas the adsorptions at 3330 cm^{-1} and 1587 cm^{-1} decrease (remaining signal due to the 20% of undeuterated SiOH). This confirms the assignment of an amino moiety (NH vs. ND).

This amine group can result from the 1,2 addition of surface silanols across the imido tungsten fragment of **5**. This singular reactivity has never been observed for **4** despite the fact **4** also bears an imido ligand. The bulkiness of isopropyl substituent of the aromatic ring might protect the nitrogen of the imido ligand.

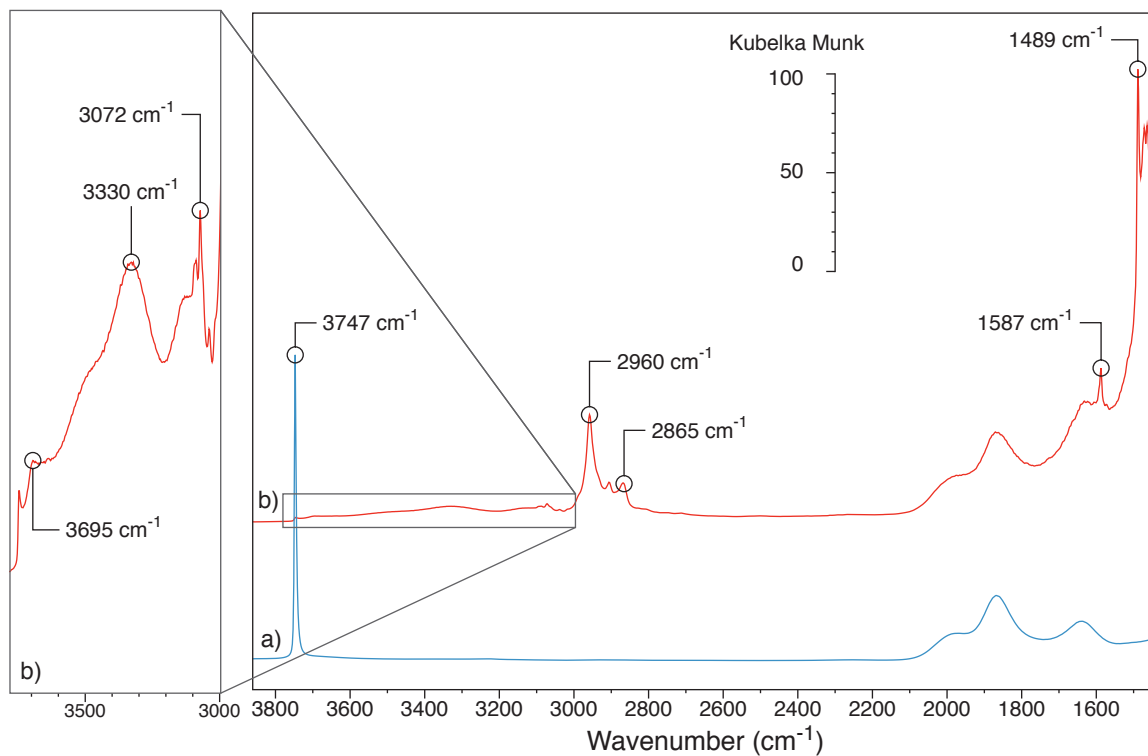


Figure 6.15 Diffuse reflectance infrared spectra of a) $\text{SiO}_2-(700)$ and b) $5/\text{SiO}_2-(700)$

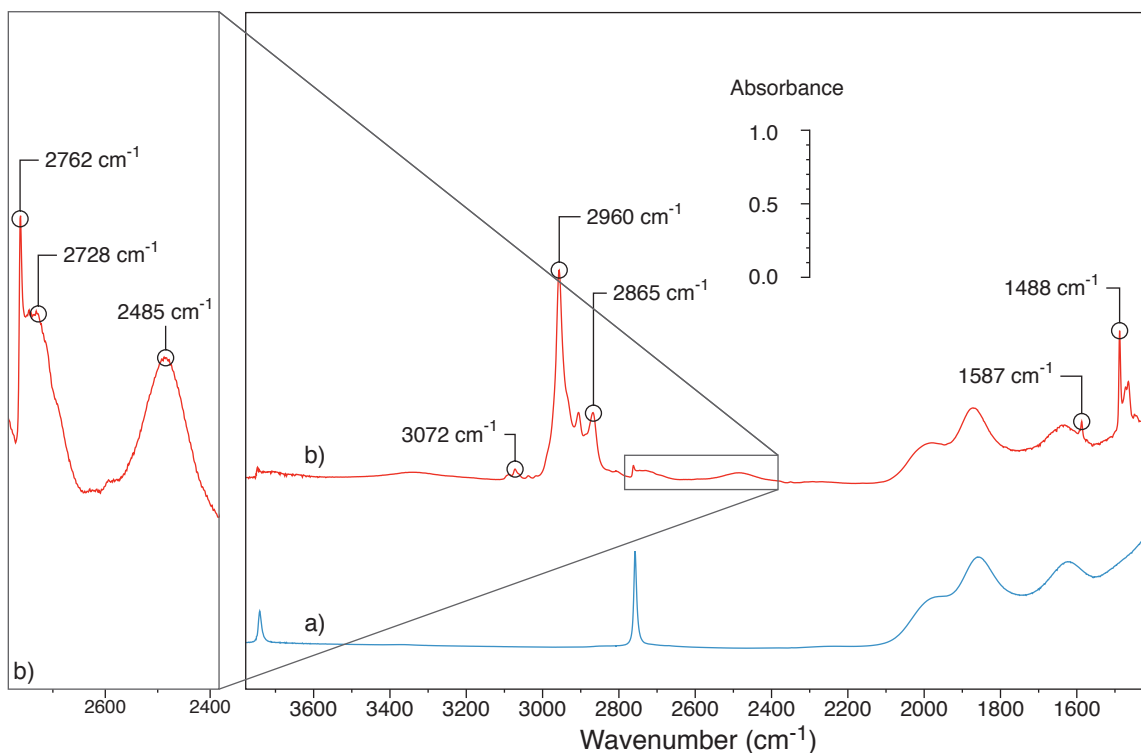


Figure 6.16 Infrared spectra of a) $\text{SiO}_2-(700)\text{D}$ and b) $5/\text{SiO}_2-(700)\text{D}$

- Mass balance analysis

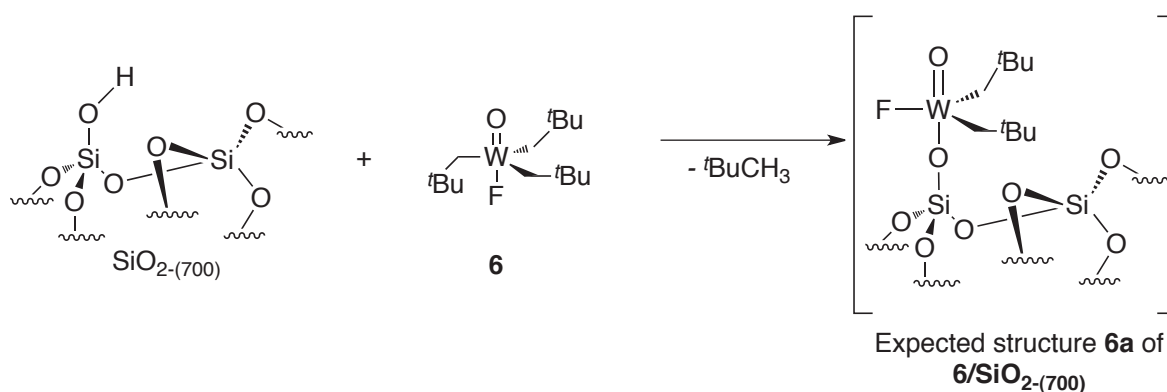
The formation of amino species is confirmed by the analysis of gas evolved during grafting, as less than 0.05 equivalent of neopentane per grafted tungsten is detected. The grafting occurs thus only by addition of a proton of a silanol on the imido ligand to form an amido. Comparable reactivity has been observed for $[\text{Mo}=\text{N}(\text{CH}^t\text{Bu})(\text{CH}_2^t\text{Bu})]$ that reacts with $\text{SiO}_2-(700)$ to form $[\equiv\text{SiO}-\text{Mo}=\text{NH}(\text{CH}^t\text{Bu})(\text{CH}_2^t\text{Bu})]^{46}$ but to our knowledge it is the first example of the addition of a silanol to an imido. Moreover elemental analysis of $5/\text{SiO}_2-(700)$ gives a tungsten loading of 4.8%_{wt}, 0.5%_{wt} of nitrogen and 6.5%_{wt} of carbon corresponding to 1.3 N/W and 20.6 C/W, *i.e.* three neopentyl and a phenylimido ligands per tungsten.

- Conclusion

These results confirm the transformation of the imido ligand to an amino ligand and it is clear that **5a** is not present at the surface of the catalyst. As the target of this chapter was to obtain species bearing a carbene and a double-bonded ligand (**Y**), characterizations of this material were not deepened further.

2.2.5. Reactivity of $[\text{W}=\text{O}(\text{CH}_2^t\text{Bu})_3\text{F}]$ (**6**) with $\text{SiO}_2-(700)$

In order to achieve the selective synthesis of species singly bound to the support, as presented in Scheme 6.15, silica that solely bears isolated silanol surface groups was selected, namely silica heated under vacuum at 700°C ($\text{SiO}_2-(700)$). Grafting of **6** was carried out in pentane at room temperature.



Scheme 6.15 Expected reactivity of **6** toward $\text{SiO}_2-(700)$

- IR study

As for $3/\text{SiO}_2-(700)$, infrared studies revealed the disappearance of $\nu_{(\text{OH})}$ bands associated to isolated silanols, and minor quantities of $\nu_{(\text{OH})}$ bands associated to interacting silanols

(3700 cm^{-1}), as already observed in related materials. Other main spectral features are $\nu_{(\text{C-H})}$ and $\delta_{(\text{C-H})}$ ($2990\text{-}2800$ and $1460\text{-}1480\text{ cm}^{-1}$, respectively; Figure 6.17)

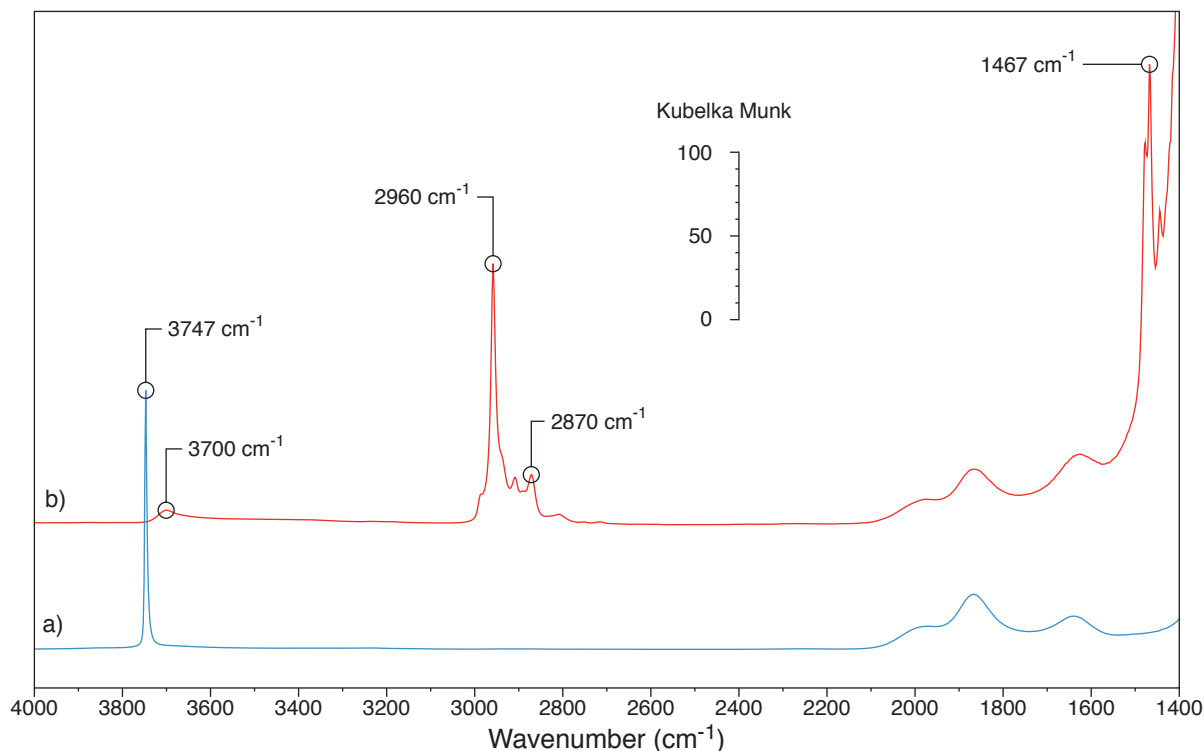


Figure 6.17 Diffuse reflectance infrared spectra of a) $\text{SiO}_2\text{-(700)}$ and b) $6/\text{SiO}_2\text{-(700)}$

- RAMAN

In order to gain information on the $\text{W}=\text{O}$ bond, Raman spectroscopy was performed on **6** and $6/\text{SiO}_2\text{-700}$ (Figure 6.18). The molecular complex spectrum features band at 905, 935, 975 and a weak broad band at 990 cm^{-1} . Only the intensity of the bands at 905, 935 and 990, attributed to neopentyl-related modes varies, during the grafting of **6** on silica. After grafting on silica the band at 975 cm^{-1} , attributed to $\text{W}=\text{O}$,³⁸ shift to 960 cm^{-1} indicating a modification of the tungsten coordination sphere. The same bands, but with different intensities are observed the spectrum obtained for $3/\text{SiO}_2\text{-(700)}$ (Figure 6.10).

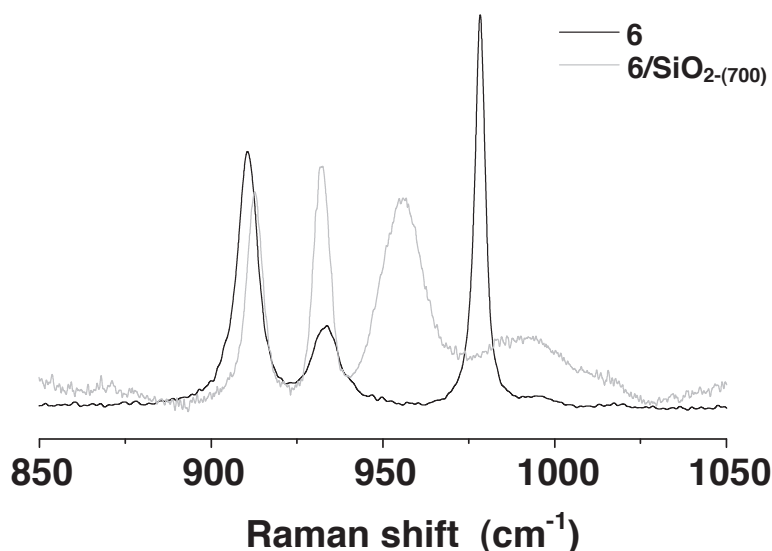


Figure 6.18 Selected region of Raman spectrum of **6** and **6/SiO₂-(700)**.

- Mass balance analysis

The resulting material (**6/SiO₂-(700)**) contained 4.43 wt% of tungsten and 3.27 wt% of carbon ($C/W = 11.3 \pm 0.1$, theory=10). Gas phase analysis indicates evolution of 1.0 equivalent of NpH per metal center. The mass balance analysis is similar to the one obtained for **3/SiO₂-700**, which is in favor of a monografted species such as: $[(\equiv\text{SiO})(\text{W}=\text{O})(\text{CH}_2^t\text{Bu})_2\text{F}]$ (**6a**).

- Solid-state NMR study

Solid-state NMR data were crucial to elucidate the structure of the **6/SiO₂-(700)** surface species (Figure 6.19). The ^1H NMR spectrum presents signals at 2.0 (CH_2) and 1.0 ($\text{C}(\text{CH}_3)_3$) ppm. On the ^{13}C NMR spectrum, neopentyl groups resonate at 91.6 (CH_2), 34.1 ($\text{C}(\text{CH}_3)_3$) and 30.5 ppm ($\text{C}(\text{CH}_3)_3$). These results confirm the presence of equivalent neopentyl moieties on the surface species. The ^{19}F NMR spectrum presents only one signal at -121 ppm surrounded by spinning bands. This single signal is in favor of the presence of a single site surface species. Nevertheless, a large shift of the ^{19}F signal between the molecular (-0.36 ppm) and the grafted species (-121 ppm) raise the question of the fate of the W-F bond during the grafting.

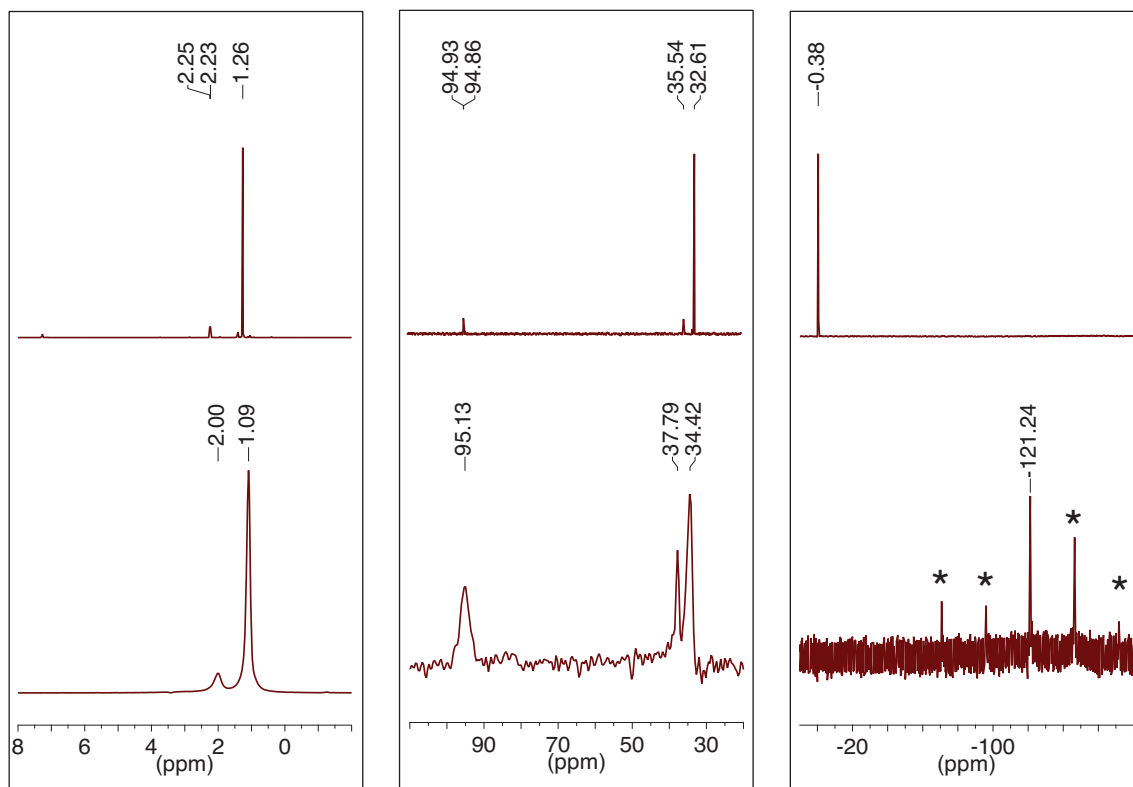


Figure 6.19 compared NMR of **6** (top) and **6/SiO₂-(700)** (bottom); left ¹H NMR; centre ¹³C NMR and right ¹⁹F NMR. (* = spinning bands, evidenced by changing the spinning frequency)

- DFT calculations

In order to understand the large shift of the ¹⁹F NMR signal from the homogeneous to the supported species, DFT calculations have been performed (G03 program B3LYP level with the Sddall basis set). These calculations have been performed, yet again, using polyhedral oligomeric silsesquioxane (POSS) as a model of SiO₂-(700). These calculations estimate the energy of the complex and the ¹⁹F chemical shift. First the calculation has been performed for the expected structure of **6a_{poss}** (Figure 6.20). In this structure, Si-O-W=O are aligned as in **1c**. The energy was set at 0 kcal.mol⁻¹ and the ¹⁹F chemical shift was calculated at -18 ppm. Then, when Si-O-W-F are aligned, **6b_{poss}** in Figure 6.21, the calculations gives a more stable structure with -3 kcal.mol⁻¹ but a ¹⁹F chemical shift of +75 ppm. Finally, the opening of a siloxane bridge followed by the formation of a Si-F bond and a bipodal tungsten species was envisaged (structure **6c_{poss}** in Figure 6.22). This was the most stable structure calculated with an energy estimated at -7 kcal.mol⁻¹ and a ¹⁹F chemical shift of -180 ppm.

The driving force of opening of the siloxane bridge reaction is the stability of the formation of the highly stable Si-F bond: W-F = 131±15 kcal.mol⁻¹ vs. Si-F = 166.1

kcal.mol^{-1} .^{25,47} Moreover, the calculated ^{19}F chemical shift of -180 ppm is in agreement with Si-F compound already described such as a soluble fluorinated POSS giving ^{19}F signal at -137.7 and -138.5 ppm⁴⁸ or a fluorinated silica with a ^{19}F signal assigned to isolated $[\equiv\text{Si-F}]$ at -156 ppm.⁴⁹

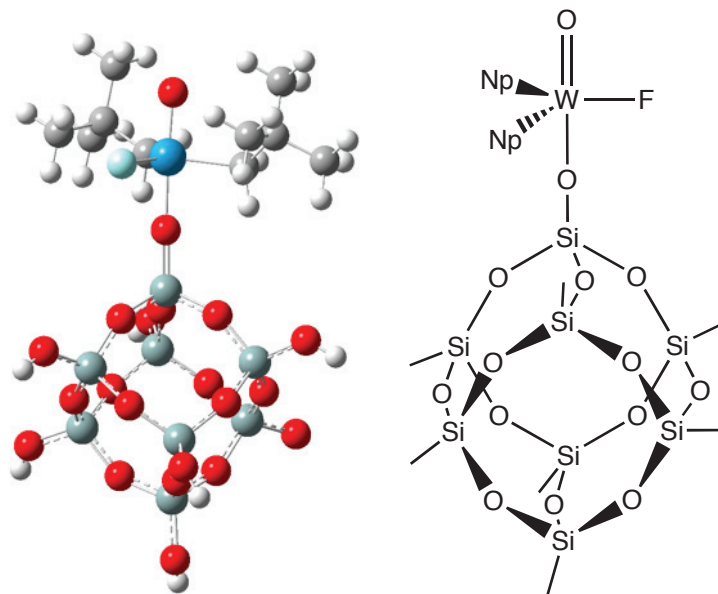


Figure 6.20 Calculated structure of **6a_{POSS}**: Energy = 0.0 kcal.mol^{-1} ; ^{19}F chemical shift = -18 ppm

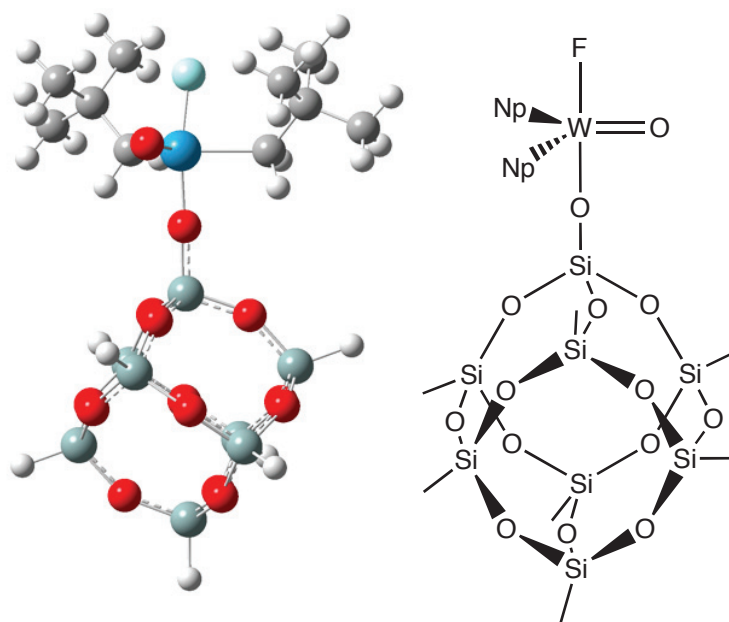


Figure 6.21 Calculated structure of **6b_{POSS}**: Energy = -3.0 kcal.mol^{-1} ; ^{19}F chemical shift = +75 ppm

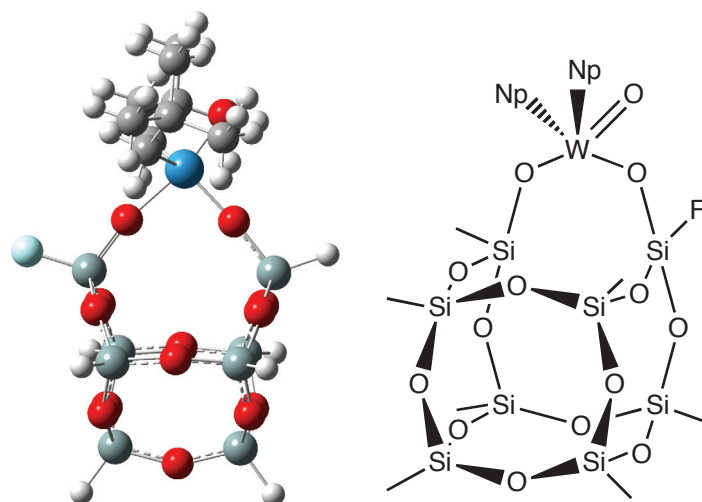


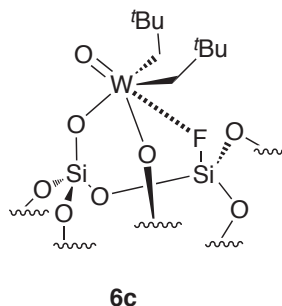
Figure 6.22 Calculated structure of **6c_{poss}**: Energy = -7.0 kcal.mol⁻¹; ¹⁹F chemical shift = -180 ppm

These DFT calculations contradict the hypothesis of the formation of a monografted tungsten surface species bearing a fluorine and an oxide ligand as presented for structure **6a** on Scheme 6.15. Further characterizations have to be performed in order to fully understand the structure of the surface species.

- Using POSS as models of SiO₂

The utilization of POSS as soluble model of silica was taken in consideration to solve the structure of the silica-grafted species. Hence, liquid NMR spectroscopy, which affords a better resolution than solid state NMR spectroscopy may bring information about the fluorine location, in particular with coupling constants. Thus, **6** was reacted with one equivalent of **POSS_{OH}** (R₇Si₈O₁₂(OH), R = C₅H₉), which is a good model for isolated silanols.^{50,51} The resulting product, **6/POSS** was analyzed by NMR spectroscopy in C₆D₆. The comparison with **6/SiO₂-(700)** shows that all corresponding ¹H, ¹³C and ¹⁹F signals were found in the molecular analogue. In particular, methylenes of the neopentyl moieties appear at 2.20 ppm as a singlet with satellites (²J_{W-H} = 11.7 Hz) and with the same pattern at 91.7 ppm (²J_{W-C} = 46.7 Hz), in the ¹H and ¹³C{¹H} NMR spectrum respectively. The notable absence of scalar coupling with ¹⁹F supports the disappearance of the fluorine from the tungsten coordination sphere. Moreover, in the ¹⁹F{¹H} spectrum, a singlet at -149.6 ppm, consistent with the signal at -121 ppm for **6/SiO₂-(700)** is observed. Yet again, no coupling with ¹⁸³W can be noticed, which confirms the cleavage of the W-F bond, which confirms the cleavage of the W-F bond, in agreement with DFT calculation. Similar reactivity has been observed during reaction of WF₆ with Me₃SiOMe, which leads to the formation of WF₅OMe and Me₃SiF.⁵² Nevertheless, there is a difference of ¹⁹F chemical shift in solid-state NMR between fluorinated silica ([≡Si-F] at -156 ppm)⁴⁹ and **6/SiO₂-(700)**

(-121 ppm). This difference can be induced by a π -donating coordination between fluorine and tungsten (**6c**, Figure 6.16). EXAFS experiment may confirm this hypothesis.



Scheme 6.16 Proposed structure for the surface species of **6**/ SiO_2 -₍₇₀₀₎

- EXAFS

The structure of the supported tungsten complex **6**/ SiO_2 -₍₇₀₀₎ was further studied by analysis of the W L_{III} -edge extended X-ray absorption fine structure (EXAFS) data.

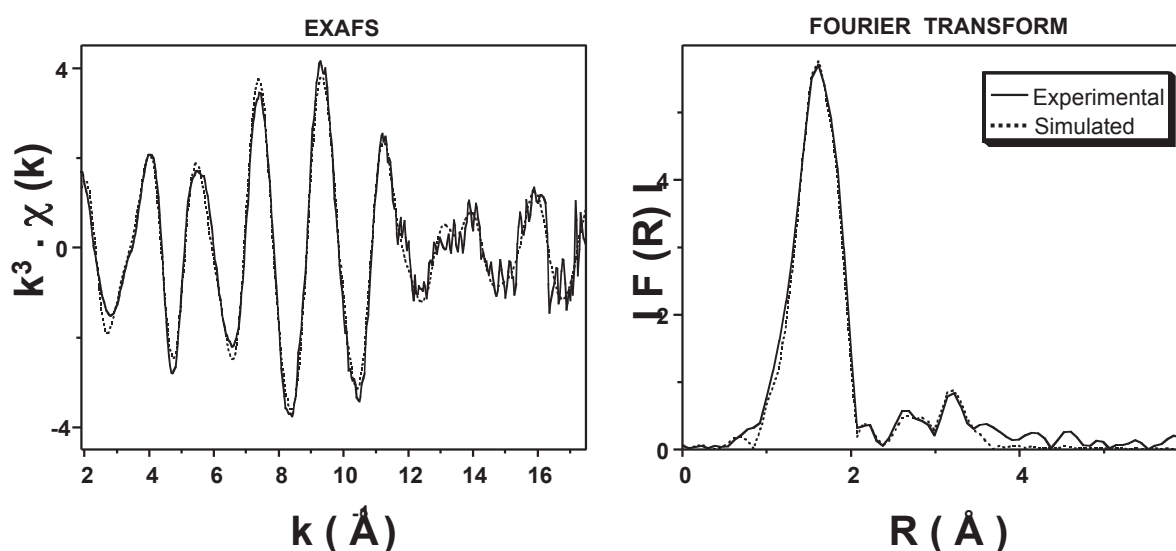


Figure 6.23 Tungsten L_{III} -edge k^3 -weighted EXAFS (left) and corresponding Fourier transform (right) with comparison to simulated curves for the W-containing surface species in **6**/ SiO_2 -₍₇₀₀₎. Solid lines: experimental; dashed lines: spherical wave theory.

The results are consistent with a W coordination sphere comprising one oxygen atom at 1.71(1) Å, two oxygen at 1.9(7) Å and two carbons at 2.12(2) Å, assigned to an oxo ligand, two siloxide's σ -bonded oxygen, and methylenic carbons from neopentyl ligands, respectively. This is consistent with the bond distances found in $[\text{W}_2\text{O}_3(\text{CH}_2^t\text{Bu})_6]^{24}$ where the $\text{W}=\text{O}_{\text{terminal}}$ (1.676–1.736 Å), $\text{W}-\text{O}_{\text{bridging}}$ (1.913–1.987 Å) and $\text{W}-\text{C}$ (2.113–2.150 Å) bond lengths are in the same range. $\text{W}-\text{O}$ distances for σ -bonded siloxide ligands are usually shorter, *e. g.* (1.876–1.882 Å) in the case of $[\text{W}=\text{O}(^t\text{Bu}_3\text{SiO})_2(\text{C}_2\text{H}_5)_2]^{39}$. Moreover, the fit was improved when considering further lay-

ers of backscatterers: (i) two C atoms at 3.28(4)Å, assigned to the neopentyl ligands' quaternary carbons, corresponding to a $126 \pm 8^\circ$ W-C-C angle, in agreement with the 123.7–127.4° range found for [W₂O₃(CH₂^tBu)₆];²⁴ (ii) less than two silicon at 3.61(3) Å, (iii) *ca.* one fluorine atom at 2.53(7) Å which can be in interaction with the tungsten as the W-F distance is quite long for a covalent bond.

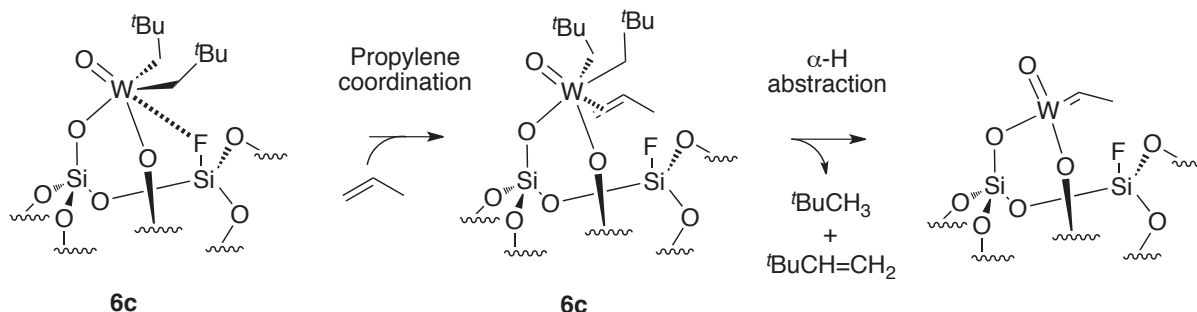
Table 6.2 EXAFS parameters for **6**/SiO₂₋₍₇₀₀₎

Type of neighbour	Number of neighbours	Distance (Å)	σ^2 (Å ²)
W=O	1.1(2)	1.71(1)	0.0023(9)
W-OSi=	1.9(7)	1.99(3)	0.003(2)
W-CH₂CMe₃	2.1(6)	2.12(2)	0.002(1)
W-CH₂CMe₃	2.1	3.28(4)	0.005(3)
W-OSi=	1.5(7)	3.61(3)	0.005(3)
W--F	1.1(8)	2.53(7)	0.019(14)

Errors between parentheses; Δk : [2.0 - 17.5 Å⁻¹] - ΔR : [0.6-3.6 Å]; $S_0^2 = 0.98$; $\Delta E_0 = 7.9 \pm 1.0$ eV (the same for all shells); Fit residue: $\rho = 3.4$ %; Quality factor: $(D\chi)^2/n = 1.65$ ($n = 9 / 31$). Two multiple-scattering pathway has been considered for this fit.

- Thermal stability and carbene formation

Thermal treatment of **6**/SiO₂₋₍₇₀₀₎ at 80°C under vacuum cause neither spectral (IR, RMN) modification nor gas evolution. As for **3**/SiO₂₋₍₇₀₀₎, the generation of carbene species from **6c** through thermally induced α -H abstraction is not operative. Its exposition, at 80°C, to 40 equivalent of propylene in a batch reactor led to the evolution of 1 equivalent of neopentane and traces of neohexene and the formation of the same equilibrated mixture of metathesis products than observed for **3**/SiO₂₋₍₇₀₀₎ (see section 2.2.2), *i.e.* propylene, ethylene and 2-butene (trans/cis ratio of 2.3). It can be assumed that the catalytic active carbenic species [(≡SiO)₂(W=O)(=CHR)(≡SiF)] can be generated from **6c** by addition of propylene (Scheme 6.17).

Scheme 6.17 Expected pathway of formation of a carbenic species from **6c** by propylene coordination followed by α -H abstraction

- Conclusion

The grafting of $[W=O(CH_2^tBu)_3F]$ (**6**) on $SiO_{2-(700)}$ has been performed. The singular reactivity of the W-F bond, by opening siloxane bridges, leading to **6c**, $[(\equiv SiO)_2(W=O)(CH_2^tBu)_2(\equiv SiF)]$, has been evidenced by IR, NMR, and EXAFS spectroscopies, mass balance analysis and DFT calculations. The use of POSS as a model of silica has been particularly useful to attest the disappearance of W-F bond during grafting.

2.3. Catalytic activity of the different species prepared

The catalytic activity of **3/SiO₂₋₍₇₀₀₎**, **4/SiO₂₋₍₇₀₀₎** and **6/SiO₂₋₍₇₀₀₎** have been tested for direct conversion of ethylene to propylene and propylene metathesis.

2.3.1. Compared catalytic performances toward direct conversion of ethylene to propylene

The reactivity of the three catalysts toward 700 eq. ethylene have been tested in batch reactor at 80°C.

Noteworthy, after 24h, neopentane is observed for **3/SiO₂₋₍₇₀₀₎** and **6/SiO₂₋₍₇₀₀₎**, which may be characteristic of to the formation of a carbenic species (see section 2.2.5 and Scheme 6.17). After 24h, **3/SiO₂₋₍₇₀₀₎** and **4/SiO₂₋₍₇₀₀₎** have converted ca. 0.5% of ethylene to propylene (cumulated T.O.N. \approx 20) while no propylene is produced over **6/SiO₂₋₍₇₀₀₎**. It confirms the necessity of a dimerization site to produce butenes, which can later react by cross metathesis with ethylene. Hence, **3c** and **4a** have an alkyl ligand (**X** regarding Scheme 6.1 centre), while **6c** have siloxy ligand that did not afford olefin insertion. Nevertheless, the activity of **3/SiO₂₋₍₇₀₀₎** and **4/SiO₂₋₍₇₀₀₎** is very low regarding the **WH/Al₂O₃** catalyst (see Chapter 3). It can be assumed that the silica do not provide the same electronic character to the tungsten centre.

2.3.2. Compared catalytic performances toward propylene metathesis

In a further step, catalytic performances of **3/SiO₂₋₍₇₀₀₎**, **4/SiO₂₋₍₇₀₀₎** and **6/SiO₂₋₍₇₀₀₎** were probed in continuous flow reactor (reactor as described in subsection 2.1 of Chapter 3 and Appendix 2, $20 \text{ NmL}_{C_3H_6} \cdot \text{min}^{-1}$; $R = 30 \text{ mol}_{C_3H_6} \cdot \text{mol}_W^{-1} \cdot \text{min}^{-1}$) at 80°C.

The oxo derivatives exhibit very similar activities. For **3/SiO₂₋₍₇₀₀₎** an initial conversion rate of $4.9 \text{ mol}_{C_3H_6} \cdot \text{mol}_W^{-1} \cdot \text{min}^{-1}$ (ca. 16% conversion) was reached (Figure 6.24), and 22000 cumulated turnover numbers (TON) were achieved after 95 hours (Figure 6.25). For **6/SiO₂₋₍₇₀₀₎**, the maximum conversion rate is a bit higher, with $5.5 \text{ mol}_{C_3H_6} \cdot \text{mol}_W^{-1} \cdot \text{min}^{-1}$ (ca. 18% conversion, Figure 6.24). It is though reached after a longer time (20 h

vs. 5 h). 25200 cumulated TON were achieved after 95 hours (Figure 6.25). For both complexes, the selectivity remained constant with time on stream, with equimolar quantities of ethene and 2-butenes, no other alkene were detected (Figure 6.26 and Figure 6.27). After the onset of the catalysis, the trans/cis 2-butene selectivity kept to a constant value of 1.8 (therm. eq. = 2.3),⁵³ in agreement with that observed in the literature for other d^0 systems; that is, terminal alkenes typically give the trans-alkene as the major kinetic product, due to the easier formation of the least sterically hindered metallacyclobutane by an *anti* approach (see subsection 2.2 in chapter 5).^{54,55}

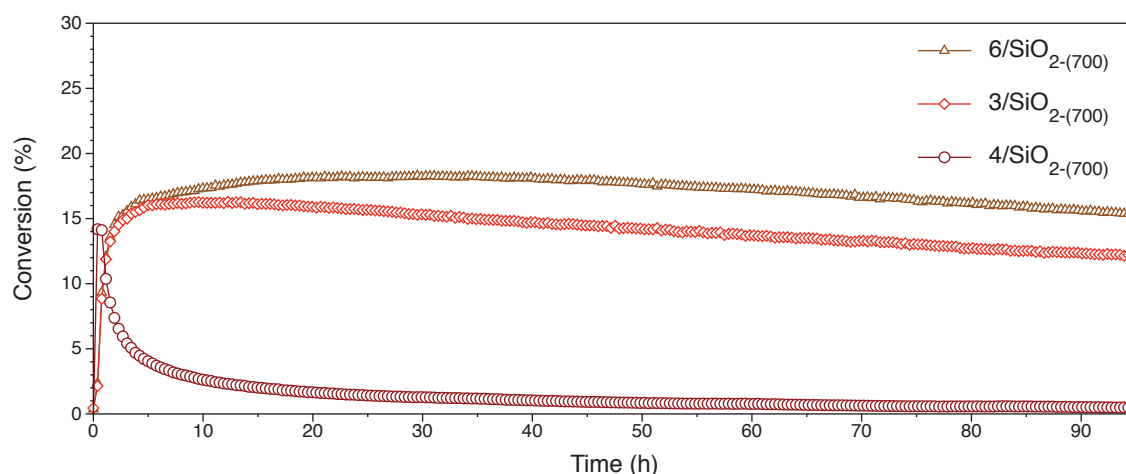


Figure 6.24 Conversion vs. time of $3/\text{SiO}_2-(700)$, $4/\text{SiO}_2-(700)$ and $6/\text{SiO}_2-(700)$ in propene metathesis (80°C , $20 \text{ mL}\cdot\text{min}^{-1}$)

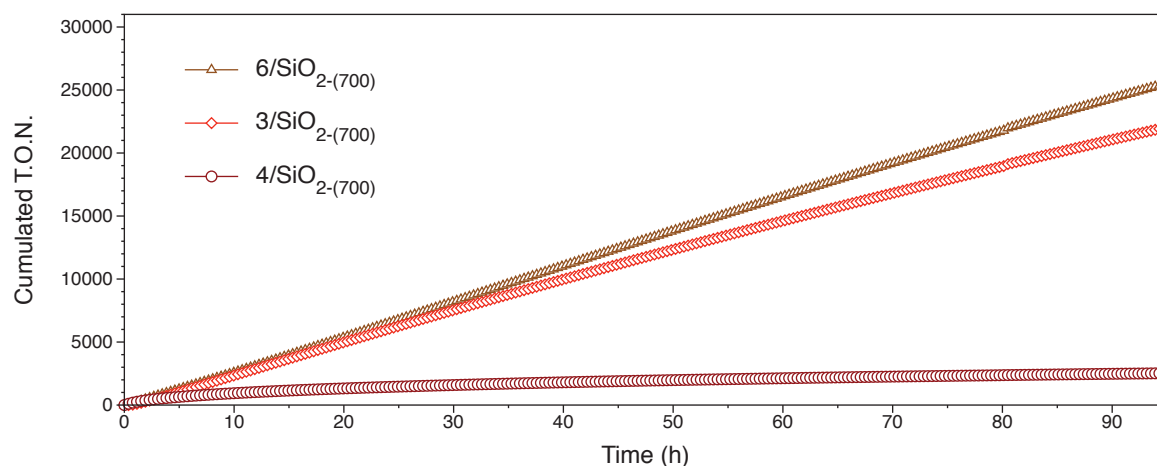


Figure 6.25 Cumulated TON vs. time of $3/\text{SiO}_2-(700)$, $4/\text{SiO}_2-(700)$ and $6/\text{SiO}_2-(700)$ in propene metathesis (80°C , $20 \text{ mL}\cdot\text{min}^{-1}$)

Regarding the catalytic performances, of the imido species $4/\text{SiO}_2-(700)$, three sharp differences are to be emphasized in comparison with $3/\text{SiO}_2-(700)$ and $6/\text{SiO}_2-(700)$. First the conversion profile is completely different. Although a comparable initial rate is observed for $4/\text{SiO}_2-(700)$ ($4.5 \text{ mol}_{\text{C}_3\text{H}_6}\cdot\text{mol}_\text{W}^{-1}\cdot\text{min}^{-1}$, *ca.* 15% conversion), fast deactivation quickly

followed (Figure 6.24): conversion dropped to about 4% after 5 hours, and slower but steady deactivation led to 2500 cumulated TONs after 95 hours (Figure 6.25).

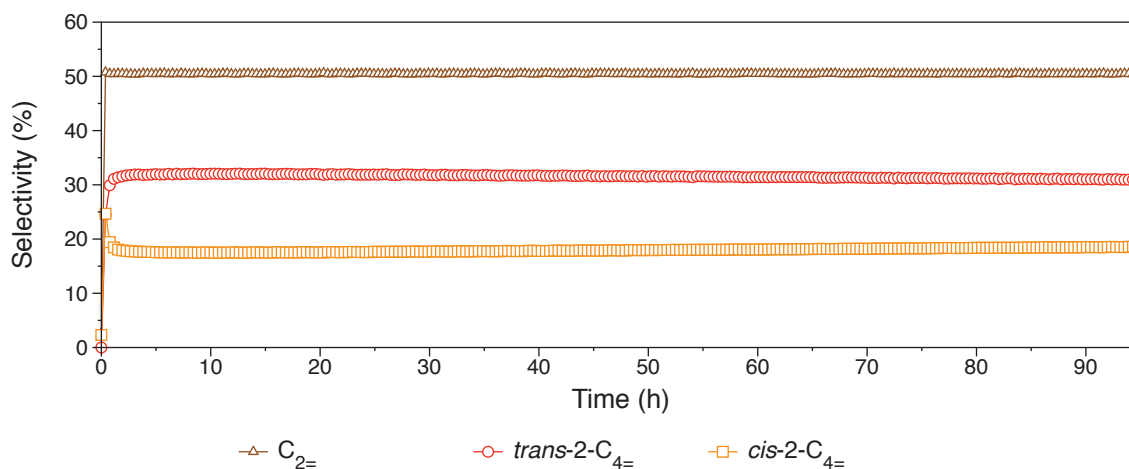


Figure 6.26 Selectivity of propylene metathesis vs. time for **3**/SiO₂-(700)

Then, regarding selectivity, along with the expected formation of ethylene (49.3%) and 2-butenes (48.5%), other products were formed, namely isobutene (0.05%), C₅ olefins (0.6%) and C₆ olefins (1.3%) (Figure 6.28); the trans/cis 2-butene ratio is 0.9, twice lower than for **3**/SiO₂-(700) and **6**/SiO₂-(700): This can be explained by the difference of steric hindrance between oxo and imido ligand that impacts on the relative stabilities of the tung-stacyclobutanes.

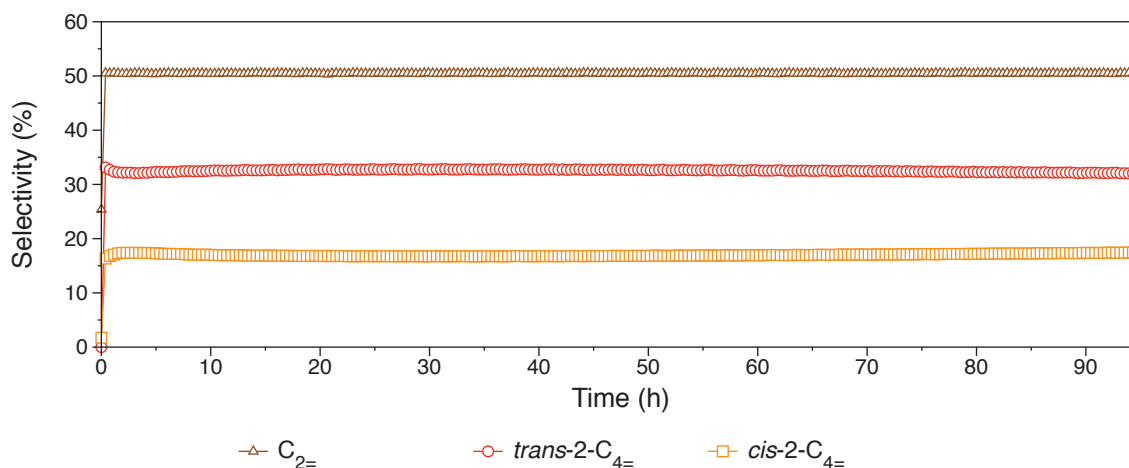


Figure 6.27 Selectivity of propylene metathesis vs. time for **6**/SiO₂-(700)

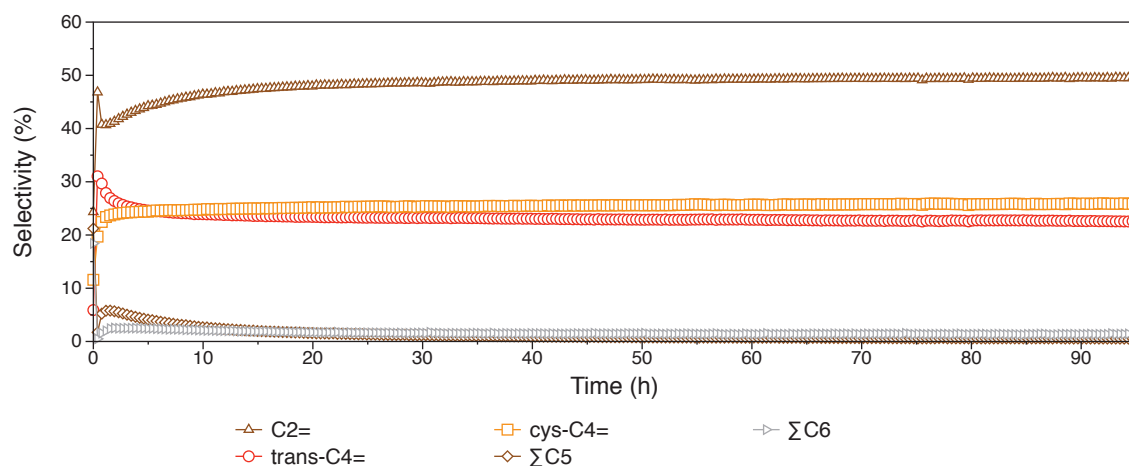


Figure 6.28 Selectivity of propylene metathesis vs. time for $4/\text{SiO}_2-(700)$

Finally, whereas the above mentioned higher alkenes (C_5 and C_6) are secondary cross-metathesis products, formation of isobutene can only be tracked back to a well-established olefin metathesis catalyst decomposition pathway, namely rearrangement of metallacyclobutanes by β -H transfer.⁵⁶⁻⁵⁸ Indeed, a 2-methyltungstacyclobutane thus affords a 2-methyltungsten hydride that further reductively eliminates isobutene and generates reduced, inactive tungsten species (Scheme 6.18). As the profile of isobutene formation (Figure 6.29) closely follows that of deactivation of $4/\text{SiO}_2-(700)$, one can assume that this mechanism plays a significant role in the imido species deactivation. Importantly, such a pathway does not seem to operate in the case of $3/\text{SiO}_2-(700)$ and $6/\text{SiO}_2-(700)$. This emphasizes the importance of the oxo ligand in enforcing catalyst stability.

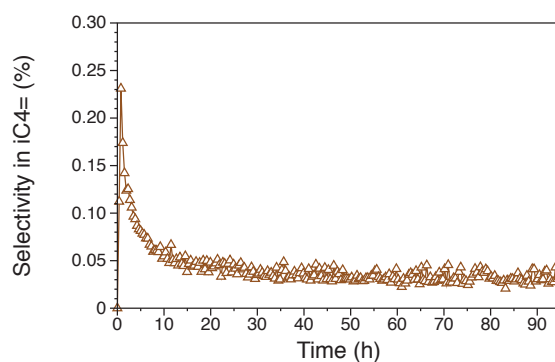
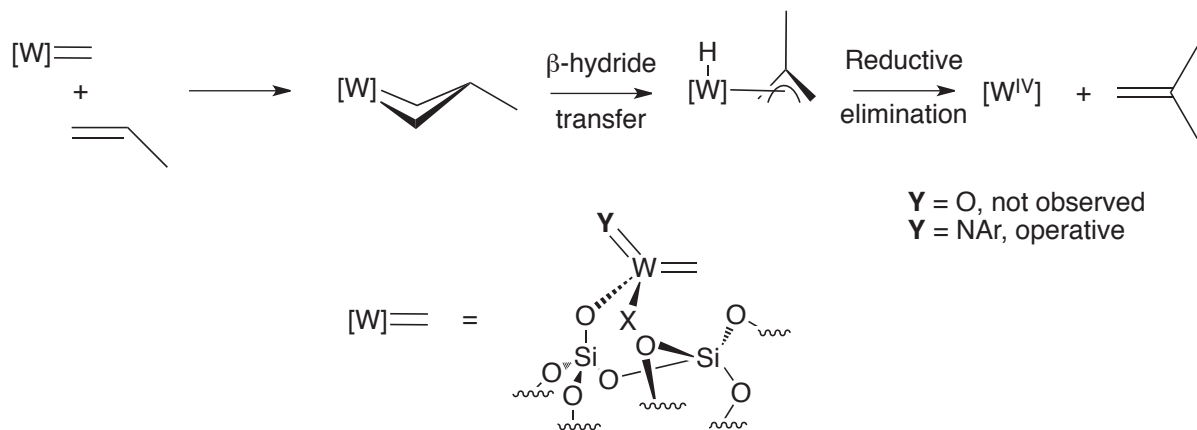


Figure 6.29 Selectivity in isobutene during propylene metathesis vs. time for $4/\text{SiO}_2-(700)$

Scheme 6.18 Catalyst deactivation by β -H transfer in the metallacyclobutane

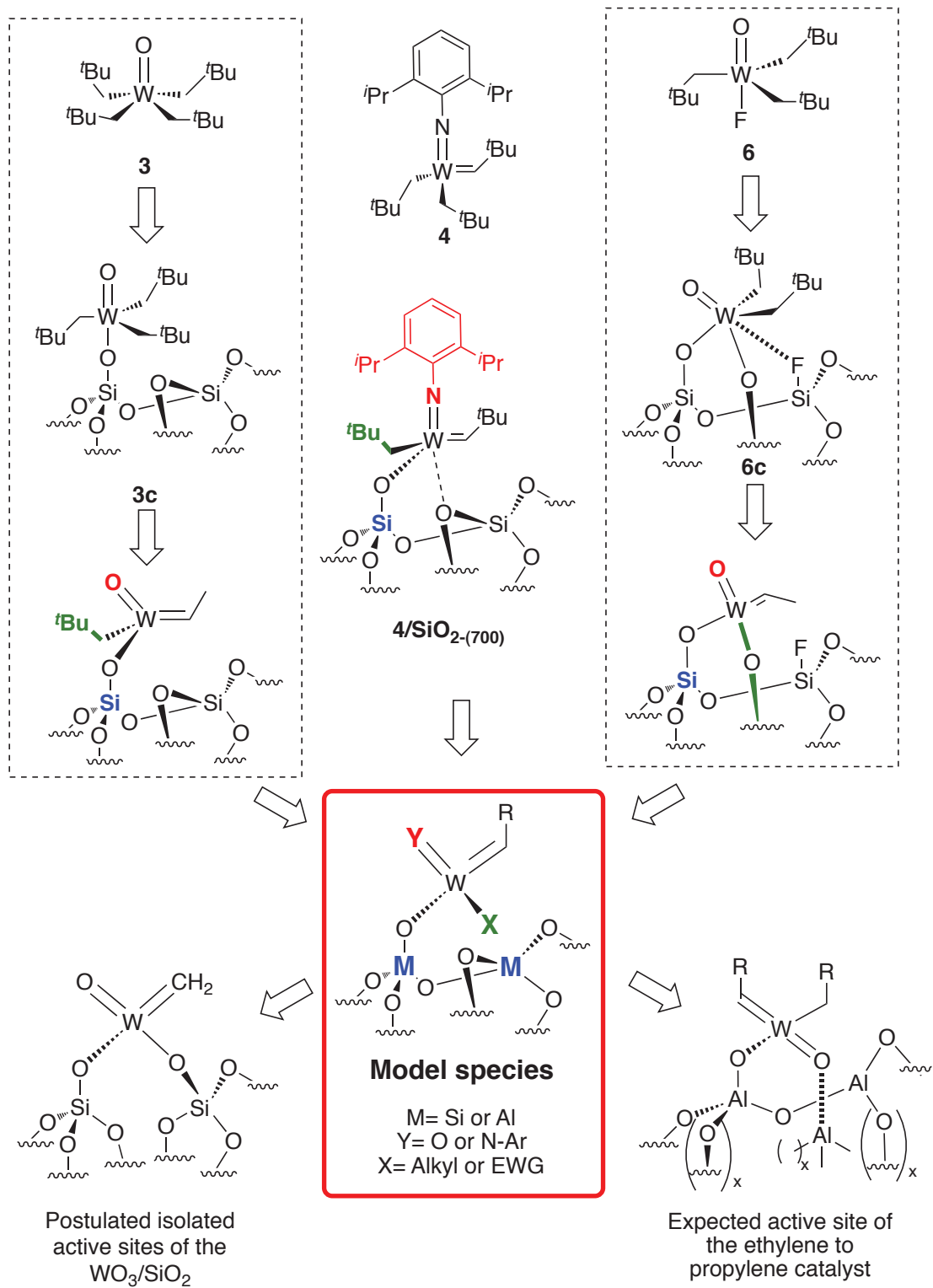
2.4. Conclusion

Three novel tungsten complexes, *i.e.* [W=O(CH₂^tBu)₄] (**3**), [W=N(C₆H₅)(CH₂^tBu)₃F] (**5**) and [W=O(CH₂^tBu)₃F] (**6**), have been successfully synthesized. Their reactivity toward partially dehydroxylated oxides have been investigated and compared to the reactivity of [W=N(2,6-ⁱPrC₆H₃)(CH₂^tBu)₂(=CH^tBu)] (**4**).

The grafting of these species have afforded new, well-defined, oxo alkyl tungsten surface species **3c** and **6c**. These species are assumed to form a carbene at 80°C when they are contacted to an olefin. The obtained species although not fully characterized yet are thus very close to the expected active site of the WO₃/SiO₂.

The new supported complexes, **3/SiO₂-(700)** and **6/SiO₂-(700)**, present a very high activity in propylene metathesis, under mild conditions and without need of a co-catalyst. These systems shows a sustained conversion, in contrast to the parent imido-derived material, **4/SiO₂-(700)**. This imido species deactivate by reduction of the tungsten centre by decomposition of the metallacyclobutane and formation of isobutene, whereas this mechanism does not occur for the oxo species.

This represents a significant step toward the understanding of the WO₃/SiO₂ system, as that isolated single site organometallic metal oxo fragments give rise to high performance catalyst for propylene metathesis.



Scheme 6.19 General overview of the species presented in this chapter

3. Experimental section

3.1. General procedures

All experiments were carried out by using standard Schlenk and glove-box techniques. Solvents were purified and dried according to standard procedures.⁵⁹ C₆D₆ (SDS) was distilled over Na/benzophenone and stored over 3 Å molecular sieves. [W=O(CH₂^tBu)₃Cl] and supported [(≡SiO)W=N(2,6-ⁱPrC₆H₃)(=CH^tBu)(CH₂^tBu)] (2/SiO₂₋₍₇₀₀₎) were synthesized following the literature procedure.^{24,28} Ethylene (N35, air liquide) and propylene (N35, air liquide) were purified by passing through a mixture of freshly regenerated molecular sieves (3 Å) and R-3-15 catalysts (BASF). Al₂O₃₋₍₅₀₀₎ was prepared as described in chapter 2. SiO₂₋₍₇₀₀₎ was prepared from Aerosil silica from Degussa (specific area of 200 m² g⁻¹), which was partly dehydroxylated at 700 °C under high vacuum (10⁻⁵ Torr) for 15 h to give a white solid having a specific surface area of 190 m² g⁻¹ and containing 0.7 OH nm⁻². Gas-phase analyses were performed on a Hewlett-Packard 5890 series II gas chromatograph equipped with a flame ionisation detector and an Al₂O₃/KCl on fused silica column (50 m X 0.32 mm). Elemental analyses were performed at the CNRS Central Analysis Department of Solaize (metal analysis), in the LSEO (Dijon, for C, H analysis) or at Pascher Mikrolabor. IR spectra were recorded on a Nicolet 6700 FT-IR spectrometer by using a DRIFT cell equipped with CaF₂ windows. The samples were prepared under Ar within a glove-box. Typically, 64 scans were accumulated for each spectrum (resolution 4 cm⁻¹). Confocal Raman spectra were acquired using the 488nm line of a Ar-ion laser (Melles Griot). The excitation beam was focused on the sample by a 50X long working distance microscope and the scattered light was analyzed by an air-cooled CCD (Labram HR, Horiba Jobin Yvon). The fluorescence was subtracted from the spectra for clarity. Solution NMR spectra were recorded on an Avance-300 Bruker spectrometer. All chemical shifts were measured relative to residual ¹H or ¹³C resonance in the deuterated solvent: C₆D₆, δ 7.15 ppm for ¹H, 128 ppm for ¹³C and relative to CF₃COOH for ¹⁸F. Solid-state NMR spectra were acquired on a Avance II 800 spectrometers (¹H: 800.13 MHz, ¹³C: 201.21 MHz, ¹⁹F: 752.96 MHz). For ¹H and ¹⁹F experiments, the spinning frequency was 20 kHz, the recycle delay was 5 s and 16 scans were collected using a 90° pulse excitation of 3 μs. The ¹³C CP MAS experiment was obtained at a spinning frequency of 20 kHz, with a recycle delay of 5 s and 10312 scans were collected. Optimal resolution was achieved using the PISARRO decoupling scheme⁶⁰ at a RF field strength of 70 kHz and with a decoupling pulse unit of 45 μs, corresponding to 0.9*τ_R (where τ_R is the rotor period). The Hartmann-Hahn conditions were optimized with a ramped radio

frequency (RF) field centered at 50 kHz applied on protons, while the carbon RF field was matched to obtain optimal signal. The contact time was set to 10 ms. The same CP and decoupling conditions were used for the acquisition of the two-dimensional HETCOR spectrum. The number of collected scans was limited to 688, with a recycling delay of 5s and 50 t_1 increments in the ^1H dimension, leading to a total experimental time of 48 hours. Chemical shifts were given in ppm with respect to TMS as external reference for ^1H and ^{13}C NMR. Procedures related to Extended X-ray Absorption Fine Structure Spectroscopy (EXAFS) are described in Chapter 2.

3.2. Preparation of the organometallic precursors

3.2.1. Preparation of $^t\text{BuCH}_2\text{Na}$

$^t\text{BuCH}_2\text{Na}$ was prepared from $^t\text{BuCH}_2\text{Li}^{31}$ following a procedure analogous to that used for $\text{C}_6\text{H}_5\text{CH}_2\text{K}$.^{29,30} A mixture of neopentyl chloride (20 g) and *ca.* 6 g (excess) of finely chopped Li wire (1% Na) in *ca.* 200ml of heptane was stirred and refluxed under argon for 10 days. The LiCl and excess Li was filtered off and the neopentyl lithium isolated from the filtrate by reducing the volume under vacuum, yield 12 g (60%) of white crystalline $^t\text{BuCH}_2\text{Li}$. ^1H NMR (δ , 295 K, C_6D_6 , 300 MHz): 8.88 (2H, s) 10.68 (9H, s). A mixture of 5.0 g of $^t\text{BuCH}_2\text{Li}$ in 100 mL of THF was added dropwise to a stirred and -78°C cooled solution of 6.1 $^t\text{BuONa}$ in 100 mL of THF. The solution was stirred at this temperature for 1-2 hours and turned yellow. Subsequently, the solution was slowly warmed to RT, the solution was filtered to remove the $^t\text{BuOLi}$ precipitate and the solvent was removed under *vacuum*. 5g (80%) of $^t\text{BuCH}_2\text{Na}$ as a yellow fine powder was obtained.

3.2.2. Preparation of **3**

$[\text{W}=\text{O}(\text{CH}_2^t\text{Bu})_3\text{Cl}]$ (1.500 g, 3.34 mmol) was dissolved in 10 cm^3 of Et_2O and a solution of NpNa (0.314 g, 3.34 mmol) in 10 cm^3 of Et_2O was added dropwise in absence of light while stirring at -78°C . After one hour, the volatiles were removed under *vacuum*. Pentane was added and the reaction mixture was filtered to remove insoluble NaCl. Pentane was evaporated to afford a colourless oil. The crude material was distilled twice at 60°C under reduced pressure (3.10^{-5} Torr) to yield 0.570 g of pure product (35 % yield). ^1H NMR (δ , 295 K, C_6D_6 , 300 MHz): 1.83 (8 H, s, $\text{CH}_2\text{C}(\text{CH}_3)_3$), 1.17 (36 H, s, $\text{CH}_2\text{C}(\text{CH}_3)_3$). $^{13}\text{C}\{^1\text{H}\}$ NMR (δ , 295 K, C_6D_6 , 75 MHz): 85.6 (s, $\text{CH}_2\text{C}(\text{CH}_3)_3$, ^{183}W satellites: $^1J_{\text{W-C}} = 48.1$ Hz), 34.5 (s, $\text{CH}_2\text{C}(\text{CH}_3)_3$), 32.9 (s, $\text{CH}_2\text{C}(\text{CH}_3)_3$). As the product was a heat, light and air sensitive oil, elemental analyses were not successful.

3.2.3. Preparation and of 5

Freshly distilled phenylisocyanate (3,214 g, 27 mmol) was added to a suspension of crude [W=OC₄] (9.000 g, 26 mmol) 200 mL of heptane. This mixture was heated to reflux for 4 days and a dark brown precipitate is formed. The volatiles are removed under *vacuum* and Et₂O (20mL) is added to afford a green solution. This solution is filtered to remove the insoluble impurities and Et₂O is then removed under *vacuum* affording 8.4g (65%) of dark green crystalline [W=N(C₆H₅)Cl₄]•(Et₂O). To the rapidly stirred dark green solution of [W=N(C₆H₅)Cl₄]•(Et₂O) (10.6 g, 21.6 mmol) in toluene at -78 °C was added dropwise 30 mL of 2.17 M ether solution of neopentylmagnesium chloride. The mixture was allowed to warm slowly to room temperature with continuous stirring. The volatiles were removed under *vacuum*. The product was extracted with pentane, and the extract was treated with activated carbon and stirred for 30 minutes. The mixture was filtered through a bed of celite, and the solvent was removed from the filtrate under *vacuum*. The yellow brown residue was collected on a frit, washed with chilled pentane and dried to give 3.8 g of [W=N(C₆H₅)(CH₂^tBu)₃Cl] as a brown powder (33 % yield). [W=N(C₆H₅)(CH₂^tBu)₃Cl] (2.000 g, 3.8 mmol) and AgBF₄ (0.740 g, 3.8 mmol) were stirred in 20 mL of toluene for one hour at room temperature. The reaction mixture was filtered to remove the insoluble AgCl, and NEt₃ (1.1 mL, 7.70 mmol) was added. The resulting solution was stirred for 16 h at room temperature and the reaction mixture was filtered over celite. The solvent was then removed under *vacuum* to leave a yellow pale solid. After this treatment boron was still spotted in ¹¹B NMR. A solution of the product in pentane was thus added to SiO₂-(700) (500mg) and let react for 4 hours. The silica was extracted 3 times with pentane. The solvent was then removed under *vacuum* to leave a yellow pale solid. This crude material was sublimed at 60°C under reduced pressure (3.10⁻⁵ Torr) to yield 580 mg of pure product (31 % yield). ¹H NMR (δ, 295 K, C₆D₆, 300 MHz): 7.72 (2 H, d, ³J_{HH}=8.2 Hz), 7.26 (2 H, t, ³J_{HH}=7.7 Hz), 7.02 (1 H, d, ³J_{HH}=7.1 Hz), 2.22 (6 H, m, CH₂C(CH₃)₃, ²J_{WH}=10.1 Hz, ³J_{FH}=10.6 Hz), 1.25 (27 H, s, CH₂C(CH₃)₃); ¹³C{¹H} NMR (δ, 295 K, C₆D₆, 75 MHz): 128.9, 128.0, 127.6, 126.6, 90.7 (m, CH₂C(CH₃)₃, ¹J_{WC}= 46 Hz, ²J_{FC}=6.82 Hz), 35.7 (s, CH₂C(CH₃)₃), 34.0 (s, CH₂C(CH₃)₃); ¹⁹F{¹H} NMR (δ, 295 K, C₆D₆, 280 MHz): 34.84 (m, ¹J_{WF}=50 Hz, ²J_{NF}=49 Hz). Anal. Calcd for C₂₁H₃₈FNW: C, 49.71; H, 7.55; F, 3.74; N, 2.76; W, 36.23% Found: C, 48.86; H, 7.38; F, 4.54; N, 2.74; W, 34.90%

3.2.4. Preparation and characterization of **6**

- Method 1

[W=O(CH₂^tBu)₃Cl] (1.500 g, 3.34 mmol) and AgBF₄ (0.65 g, 3.34 mmol) were stirred in 20 mL of toluene for one hour at room temperature. The reaction mixture was filtered to remove the insoluble AgCl, and NEt₃ (1.1 mL, 7.70 mmol) was added. The resulting solution was stirred for 16 h at room temperature and the reaction mixture was filtered over celite. The solvent was then removed under *vacuum* to leave a white solid. The crude material was sublimed at 60°C under reduced pressure (3.10⁻⁵ Torr) to yield 1.13 g of pure product (78 % yield).

- Method 2

[W₂O₃(CH₂^tBu)₆] (2.000 g, 2.37 mmol) and AgBF₄ (0.9 g, 4.74 mmol) were stirred in 20 mL of toluene for one hour at room temperature. The reaction mixture was filtered to remove the insoluble Ag₂O, and NEt₃ (1.1 mL, 7.70 mmol) was added. The resulting solution was stirred for 16 h at room temperature and the reaction mixture was filtered over celite. The solvent was then removed under *vacuum* to leave a white solid. The crude material was sublimed at 60°C under reduced pressure (3.10⁻⁵ Torr) to yield 1.68 g of pure product (82 % yield).

¹H NMR (δ, 295 K, C₆D₆, 300 MHz): 2.24 (6 H, m, CH₂C(CH₃)₃, ²J_{WH}=10.1 Hz, ³J_{FH}=8.6 Hz), 1.26 (27 H, s, CH₂C(CH₃)₃). ¹³C{¹H} NMR (δ, 295 K, C₆D₆, 75 MHz) 94.9 (m, CH₂C(CH₃)₃, ¹J_{WC}= 46 Hz, ²J_{FC}=6.3 Hz), 35.5 (s, CH₂C(CH₃)₃), 32.6 (s, CH₂C(CH₃)₃). ¹⁹F{¹H} NMR (δ, 295 K, C₆D₆, 280 MHz): -0.38 (m, ¹J_{WF}=82.2 Hz). Anal. Calcd for C₁₅H₃₃O₃FW: C, 41.69; H, 7.69; F, 4.42 %. Found: C, 41.47; H, 7.89; F, 4.72%.

3.3. Reactivity of the organometallic precursors with oxides and characterizations

3.3.1. Preparation and characterization of **3**/Al₂O₃₋₍₅₀₀₎

A mixture of **3** (500 mg, 1.03 mmol) and Al₂O₃₋₍₅₀₀₎ (2 g) in pentane (10 mL) was stirred at 25°C 15 hours in absence of light. After filtration, the solid was washed 5 times with pentane and all volatile compounds were condensed into another reactor (of known volume) in order to quantify neopentane evolved during grafting. The resulting white powder was dried under vacuum (10⁻⁵ Torr). Analysis by gas chromatography indicated the formation of 55 μmol of neopentane during the grafting (0.25 ±0.1 NpH/ W). Elemental analysis: W 4.0%_{wt} C 4.9%_{wt}.

3.3.2. Preparation and characterization of 3/SiO₂₋₍₇₀₀₎

A mixture of **3** (500 mg, 1.03 mmol) and SiO₂₋₍₇₀₀₎ (2 g) in pentane (10 mL) was stirred at 25°C overnight. After filtration, the solid was washed 5 times with pentane and all volatile compounds were condensed into another reactor (of known volume) in order to quantify neopentane evolved during grafting. The resulting white powder was dried under vacuum (10⁻⁵ Torr). Analysis by gas chromatography indicated the formation of 403 μmol of neopentane during the grafting (0.9±0.1 NpH/ W). Elemental analysis: W 4.2%_{wt} C 4.1%_{wt}. ¹H MAS NMR (800 MHz) δ 1.93, 1.01 ppm. ¹³C CP MAS NMR (200 MHz) δ 91, 34, 31 ppm.

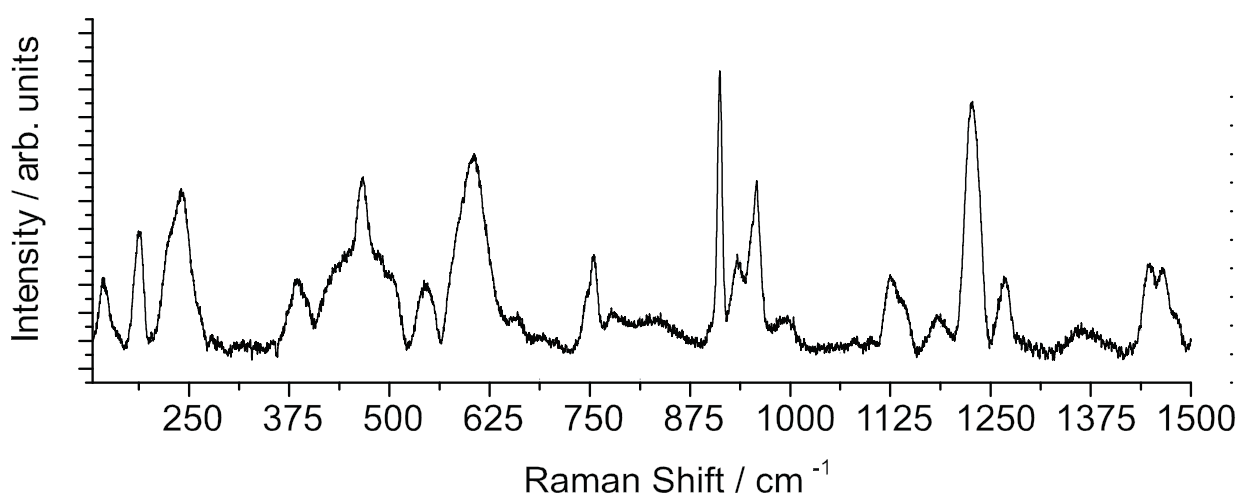


Figure 6.30 Raman spectrum of 3/SiO₂₋₍₇₀₀₎

3.3.3. Preparation and characterization of 5/SiO₂₋₍₇₀₀₎

A mixture of **5** (500 mg, 0.98 mmol) and SiO₂₋₍₇₀₀₎ (2 g) in pentane (10 mL) was stirred at 25°C overnight. After filtration, the solid was washed 5 times with pentane and all volatile compounds were condensed into another reactor (of known volume) in order to quantify neopentane evolved during grafting. The resulting white powder was dried under vacuum (10⁻⁵ Torr). Analysis by gas chromatography indicated the formation of 10 μmol of neopentane during the grafting (> 0.05 NpH/ W). Elemental analysis: W 4.8%_{wt} C 6.5%_{wt} N 0.5%_{wt}.

3.3.4. Monitoring the synthesis of 5/SiO_{2-(700)D} by IR spectroscopy.

The SiO₂ (25 mg) was pressed into a 17 mm self-supporting disk, adjusted in the sample holder, and introduced into a quartz reactor equipped with CaF₂ windows. Deuterated silica (SiO_{2-(700)D}) was prepared by heating this pellet under D₂O (>90% D, 22mmHg) at

500°C for 3-4 h followed by evacuation at 700°C temperature for 3-4 h. This procedure was repeated three times before a final dehydroxylation at 700°C for 15 h. The disk was then immersed in a solution of **5** (30mg, 0.059 mmol) in pentane (12 mL) for 3 h, washed 3 times in pentane, dried under vacuum for 30 min, and then an IR spectrum was recorded.

3.3.5. Preparation and characterization of **6/SiO₂₋₍₇₀₀₎**

A mixture of **6** [WO(CH₂CMe₃)₃F] (500 mg, 1.2 mmol) in pentane (10 mL) and SiO₂₋₍₇₀₀₎ (2 g) was stirred at 25°C overnight. After filtration, the solid was washed 5 times with pentane and all volatile compounds were condensed into another reactor (of known volume) in order to quantify neopentane evolved during grafting. The resulting white powder was dried under vacuum (10⁻⁵ Torr). Analysis by gas chromatography indicated the formation of 290 μmol of neopentane during the grafting (1,0±0.1 NpH/ W). Elemental analysis of: W 4.43 %_{wt} C 3.27 %_{wt}. ¹H MAS solid state NMR (800 MHz) δ 2.0, 1.1 ppm. ¹³C CP/MAS solid state NMR (200 MHz) δ 95, 38 and 34 ppm. ¹⁸F MAS solid state NMR (750 MHz) δ -121.2 ppm

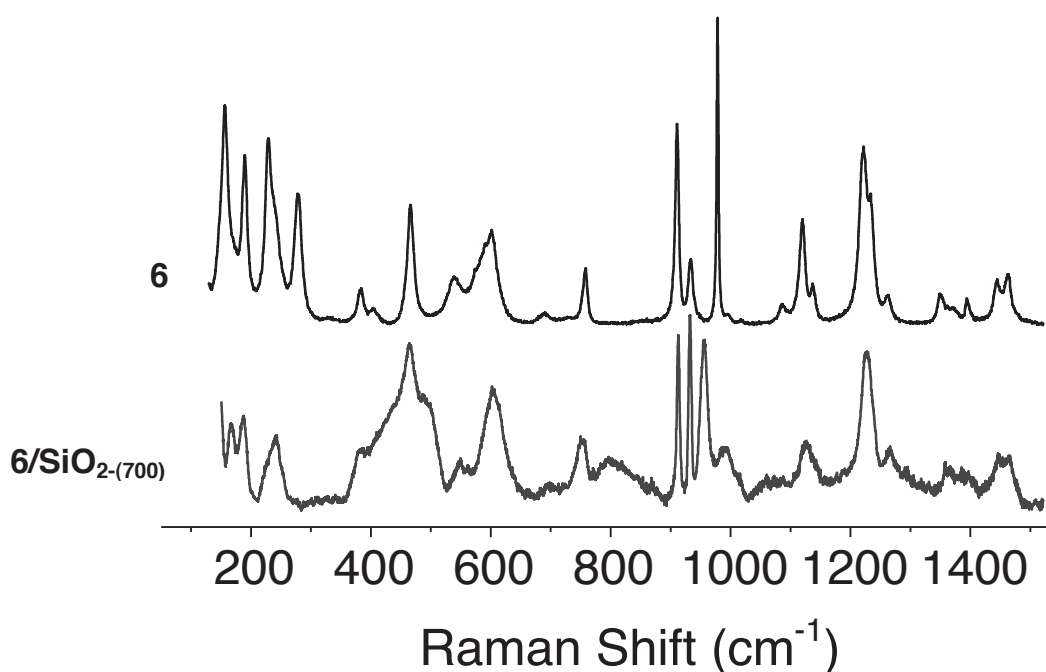


Figure 6.31 Raman spectrum of **6** and **6/SiO₂₋₍₇₀₀₎**

3.3.1. Preparation and characterization of **6/POSS**

A pentane solution of [(c-C₅H₉)₇Si₇O₁₂SiOH] (75 mg, 82 μmol, 1 mL pentane) was added at -78°C to a stirred pentane solution of **6** (36 mg, 82 μmol, 1 mL pentane). The mixture was allowed to warm slowly to room temperature with continuous stirring. And the volatile were removed under *vacuum* to afford **6/POSS**. ¹H NMR (δ, 295 K, C₆D₆, 300 MHz): 2.20 (m, CH₂C(CH₃)₃, ²J_{WH}=11.7 Hz), 1.26 (s, CH₂C(CH₃)₃), 1.87-1.22 (m, c-CH(CH₂)₄), 1.11 (m, c-CH(CH₂)₄). ¹³C{¹H} NMR (δ, 295 K, C₆D₆, 75 MHz) 91.7 (m, CH₂C(CH₃)₃, ¹J_{WC}= 46.7 Hz), 35.5 (s, CH₂C(CH₃)₃), 32.0 (s, CH₂C(CH₃)₃), 27.7, 27.5, 27.1, 27.0 (m, c-CH(CH₂)₄), 22.7, 22.1(m, c-CH(CH₂)₄). ¹⁹F{¹H} NMR (δ, 295 K, C₆D₆, 280 MHz): -149.6 (s).

3.3.2. DFT calculations

All the calculations have been performed using the G03 program.⁶¹ The geometries have been fully optimized without any symmetry constraints at the B3PW91 level with the Sddall basis set.

3.4. Catalytic tests

3.4.1. Reactivity toward ethylene in batch reactor

A mixture of solid **3/SiO₂-(700)** (100 mg), **4/SiO₂-(700)** (107 mg) or **6/SiO₂-(700)** (95 mg) and ethylene (550 Torr, 700 equiv) were heated at 80°C in a batch reactor of known volume (500 mL). Aliquot were drawn and analyzed by gas chromatography every 2 hours.

3.4.2. Propylene metathesis

Procedure in a batch reactor: A mixture of **3/SiO₂-(700)** (100 mg) or **6/SiO₂-(700)** (95 mg) and propene (500 Torr, 40 equiv) were heated at 80°C in a batch reactor of known volume (28 mL). An aliquot was drawn and analyzed by gas chromatography after 24 hours.

Procedure in a flow reactor: A stainless-steel half-inch cylindrical reactor that can be isolated from ambient atmosphere was charged with catalyst **3/SiO₂-(700)** (135 mg, % W = 4.2 %, 30 mol_{C₃H₆}.mol_W⁻¹.min⁻¹), **4/SiO₂-(700)** (145 mg, % W = 3.5 %, 30 mol_{C₃H₆}.mol_W⁻¹.min⁻¹) or **6/SiO₂-(700)** (128 mg, % W = 4.4 %, 30 mol_{C₃H₆}.mol_W⁻¹.min⁻¹) in a glovebox. After connection to the gas lines and purging of the tubing, a 20 ml.min⁻¹ flow of propylene was passed over the catalyst bed at 80°C. Hydrocarbon products were analyzed online by GC (HP 8890 chromatograph fitted with an Al₂O₃/KCl 50 m x 0.32 mm capillary column, FID detector).

4. Reference and Notes

- (1) Mol, J. C. *Journal of Molecular Catalysis A: Chemical*. 2004, 213, 39-45.
- (2) Heckelsberg, L. F.; Banks, R. L.; and Bailey, G. C. *Ind. Eng. Chem. Prod. Res. Dev.* 1968, 7, 29-31.
- (3) van Schalkwyk, C.; Spamer, A.; Moodley, D. J.; Dube, T.; Reynhardt, J.; Botha, J. M.; and Vosloo, H. C. M. *Applied Catalysis a-General*. 2003, 255, 143-152.
- (4) Spamer, A.; Dube, T. I.; Moodley, D. J.; van Schalkwyk, C.; and Botha, J. M. *Applied Catalysis a-General*. 2003, 255, 133-142.
- (5) Westhoff, R. and Moulijn, J. A. *Journal of Catalysis*. 1977, 46, 414-416.
- (6) Thomas, R.; Moulijn, J. A.; and Kerhkov, F. P. J. M. *Recl. Trav. Chim. Pay. B.* 1977, 96, M121-M126.
- (7) Kerhkov, F. P. J. M.; Thomas, R.; and Moulijn, J. A. *Recl. Trav. Chim. Pay. B.* 1977, 96, M134-M135.
- (8) Thomas, R. and Moulijn, V. H. J. *Journal of Molecular Catalysis*. 1980, 8, 161-174.
- (9) Spamer, A.; Dube, T. I.; Moodley, D. J.; van Schalkwyk, C.; and Botha, J. M. *Applied Catalysis a-General*. 2003, 255, 153-167.
- (10) Hérisson, J. L. and Chauvin, Y. *Makromol. Chem.* 1971, 141, 161-176.
- (11) Shelimov, B. N.; Elev, I. V.; and Kazansky, V. B. *Journal of Molecular Catalysis*. 1988, 46, 187 - 200.
- (12) Grünert, W.; Feldhaus, R.; Anders, K.; Shpiro, E. S.; and Minachev, K. M. *Journal of Catalysis*. 1989, 120, 444-456.
- (13) Thomas, J. M.; Raja, R.; and Lewis, D. W. *Angewandte Chemie International Edition*. 2005, 44, 6456-6482.
- (14) Schrock, R.; Rocklage, S.; Wengrovius, J.; Rupprecht, G.; and Fellmann, J. *Journal of Molecular Catalysis*. 1980, 8, 73 - 83.
- (15) Wengrovius, J. H.; Schrock, R. R.; Churchill, M. R.; Missert, J. R.; and Youngs, W. J. *Journal of the American Chemical Society*. 1980, 102, 4515-4516.
- (16) O'Donoghue, M. B.; Schrock, R. R.; LaPointe, A. M.; and Davis, W. M. *Organometallics*. 1996, 15, 1334-1336.
- (17) Xue, Z.; Li, L.; Hoyt, L. K.; Diminnie, J. B.; and Pollitte, J. L. *Journal of the American Chemical Society*. 1994, 116, 2169-2170.
- (18) Chen, T.; Wu, Z.; Li, L.; Sorasaene, K. R.; Diminnie, J. B.; Pan, H.; Guzei, I. A.; Rheingold, A. L.; and Xue, Z. *Journal of the American Chemical Society*. 1998, 120, 13519-13520.
- (19) Chen, T.; Zhang, X. H.; Wang, C. S.; Chen, S. J.; Wu, Z. Z.; Li, L. T.; Sorasaene, K. R.; Diminnie, J. B.; Pan, H. J.; Guzei, I. A.; Rheingold, A. L.; Wu, Y. D.; and Xue, Z. L. *Organometallics*. 2005, 24, 1214-1224.
- (20) Kress, J. R. M.; Russell, M. J. M.; Wesolek, M. G.; and Osborn, J. A. *Journal of the Chemical Society-Chemical Communications*. 1980, 431-432.

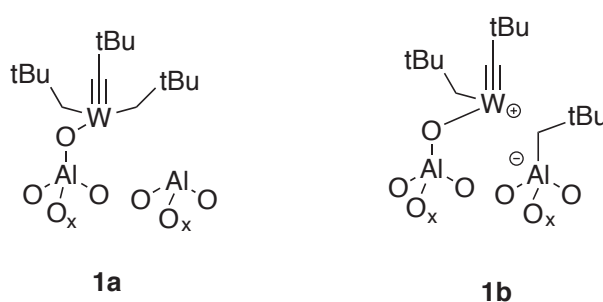
- (21) Kress, J.; Wesolek, M.; Leny, J. P.; and Osborn, J. A. *Journal of the Chemical Society-Chemical Communications*. 1981, 1039-1040.
- (22) *In the last reference WONp₃(ONp) was mistakenly assigned as WONp₄.*
- (23) Feinstein-Jaffe, I.; Pedersen, S. F.; and Schrock, R. R. *Journal of the American Chemical Society*. 1983, *105*, 7176-7177.
- (24) Feinsteinjaffe, I.; Gibson, D.; Lippard, S. J.; Schrock, R. R.; and Spool, A. *J. Am. Chem. Soc.* 1984, *106*, 6305-6310.
- (25) Gurvich, L. V.; Karachevtsev, G. V.; Kondratiev, V. N.; Lebedev, Y. A.; Medvedev, V. A.; and Potapov, N. K. *Energies of Dissociation of Chemical Bonds, Ionization Potentials and Electron Affinitie (in Russian)*, Nauka: Moscow; 1974.
- (26) Schrock, R. R. *Chem Rev.* 2009, *109*, 3211-26.
- (27) Rhers, B.; Quadrelli, E. A.; Baudouin, A.; Taoufik, M.; Copéret, C.; Lefebvre, F.; Basset, J. M.; Fenet, B.; Sinha, A.; and Schrock, R. R. *Journal of Organometallic Chemistry*. 2006, *691*, 5448-5455.
- (28) Rhers, B.; Salameh, A.; Baudouin, A.; Quadrelli, E. A.; Taoufik, M.; Coperet, C.; Lefebvre, F.; Basset, J. -M.; Solans-Monfort, X.; Eisenstein, O.; Lukens, W. W.; Lopez, L. P. H.; Sinha, A.; and Schrock, R. R. *Organometallics*. 2006, *25*, 3554-3557.
- (29) Schlosser, M. and Hartmann, J. *Angewandte Chemie*. 1973, *85*, 544-545.
- (30) Schlosser, M. and Hartmann, J. *Angewandte Chemie International Edition in English*. 1973, *12*, 508-509.
- (31) Schrock, R. R. and Fellmann, J. D. *Journal of the American Chemical Society*. 1978, *100*, 3359-3370.
- (32) Schrock, R. R.; DePue, R. T.; Feldman, J.; Yap, K. B.; Yang, D. C.; Davis, W. M.; Park, L.; DiMare, M.; and Schofield, M. *Organometallics*. 1990, *9*, 2262-2275.
- (33) Lopez, L. P. H. and Schrock, R. R. *Journal of the American Chemical Society*. 2004, *126*, 9526-9527.
- (34) Le Ny, J. P. and Osborn, J. A. *Organometallics*. 1991, *10*, 1546-1550.
- (35) Fischer, J.; Kress, J.; Osborn, J. A.; Ricard, L.; and Wesolek, M. *Polyhedron*. 1987, *6*, 1839-1842.
- (36) Ballinger, T. H. and Yates, J. T. *Langmuir*. 1991, *7*, 3041-3045.
- (37) Nedez, C.; Theolier, A.; Lefebvre, F.; Choplin, A.; Basset, J. M.; and Joly, J. F. *Journal of the American Chemical Society*. 1993, *115*, 722-729.
- (38) Kim, D. S.; Ostromecki, M.; and Wachs, I. E. *Journal of Molecular Catalysis a-Chemical*. 1996, *106*, 93-102.
- (39) Rosenfeld, D. C.; Kuiper, D. S.; Lobkovsky, E. B.; and Wolczanski, P. T. *Polyhedron*. 2006, *25*, 251 - 258.
- (40) Cotton, F. A. and Lippard, S. J. *Inorganic Chemistry*. 1966, *5*, 9-16.
- (41) Cotton, F. A. and Lippard, S. J. *Inorganic Chemistry*. 1966, *5*, 416-423.
- (42) Jeannin, Y.; Launay, J. P.; Livage, J.; and Nel, A. *Inorganic Chemistry*. 1978, *17*, 374-378.

- (43) Schrock, R. R. *Reactions of coordinated ligands vol. 2*, Paul, S. S., Ed.; Plenum Press: New York; 1989.
- (44) Feldman, J. and Schrock, R. R. In *Progress in inorganic chemistry vol. 39*; Wiley: New York ; Chichester , 1991; p. 1-73.
- (45) Silverstein, R. M. *Spectrometric identification of organic compounds*, 5th ed. / R. M. Silverstein, G. Clayton Bassler, Terence C. Morrill.; Wiley: New York, N.Y. ; 1991.
- (46) Herrmann, W. A.; Stumpf, A. W.; Priermeier, T.; Bogdanovi&ccacute;, S.; Dufaud, V.; and Basset, J. -M. *Angewandte Chemie International Edition in English*. 1996, *35*, 2803-2805.
- (47) Braun, M.; Nestler, K.; and Marx, G. *Thermochimica Acta*. 2003, *405*, 73 - 84.
- (48) Feher, F. J.; Phillips, S. H.; and Ziller, J. W. *J. Am. Chem. Soc.* 1997, *119*, 3397-3398.
- (49) Lataste, E.; Legein, C.; Body, M.; , J. -Y. B.; Tressaud, A.; and Demourgues, A. *The Journal of Physical Chemistry C*. 2009, *113*, 18652-18660.
- (50) Duchateau, R.; Abbenhuis, H. C. L.; van Santen, R. A.; Thiele, S. K. -H.; and van Tol, M. F. H. *Organometallics*. 1998, *17*, 5222-5224.
- (51) Quadrelli, E. A. and Basset, J. -M. *Coordination Chemistry Reviews*. 2010, *254*, 707 - 728.
- (52) Handy, L. B.; Sharp, K. G.; and Brinckman, F. E. *Inorganic Chemistry*. 1972, *11*, 523-531.
- (53) Stull, D. R. and Sinke, G. C. *The chemical thermodynamics of organic compounds*, Westrum, Ed.; Krieger: Malabar, Fla.; 1987.
- (54) Bilhou, J. L.; Basset, J. M.; Mutin, R.; and Graydon, W. F. *Journal of the American Chemical Society*. 1977, *99*, 4083-4090.
- (55) Leconte, M. and Basset, J. M. *Journal of the American Chemical Society*. 1979, *101*, 7296-7302.
- (56) Robbins, J.; Bazan, G. C.; Murdzek, J. S.; O'Regan, M. B.; and Schrock, R. R. *Organometallics*. 1991, *10*, 2902-2907.
- (57) Tobisch, S. *Organometallics*. 2007, *26*, 6529-6532.
- (58) Leduc, A. M.; Salameh, A.; Soulivong, D.; Chabanas, M.; Basset, J. M.; Copéret, C.; Solans-Monfort, X.; Clot, E.; Eisenstein, O.; Böhm, V. P.; and Röper, M. *J Am Chem Soc*. 2008, *130*, 6288-97.
- (59) Armarego, W. L. F. and Chai, C. L. L. *Purification of laboratory chemicals*, Butterworth Heinemann; 2009.
- (60) Weingarth, M.; Tekely, P.; and Bodenhausen, G. *Chemical Physics Letters*. 2008, *466*, 247 - 251.
- (61) M. J. Frisch, G. W. Trucks, H. B. Schlegel, G. E. Scuseria, M. A. Robb, J. R. Cheeseman, J. A. Montgomery, Jr., T. Vreven, K. N. Kudin, J. C. Burant, J. M. Millam, S. S. Iyengar, J. Tomasi, V. Barone, B. Mennucci, M. Cossi, G. Scalmani, N. Rega, G. A. Petersson, H. Nakatsuji, M. Hada, M. Ehara, K. Toyota, R. Fukuda, J. Hasegawa, M. Ishida, T. Nakajima, Y. Honda, O. Kitao, H. Nakai, M. Klene, X. Li, J. E. Knox, H. P. Hratchian, J. B. Cross, V. Bakken, C. Adamo, J. Jaramillo, R. Gomperts, R. E. Stratmann, O. Yazyev, A. J. Austin, R. Cammi, C. Pomelli, J. W. Ochterski, P. Y. Ayala, K. Morokuma, G. A. Voth, P. Salvador, J. J. Dannenberg, V. G. Zakrzewski, S. Dapprich, A. D. Daniels, M. C. Strain, O. Farkas, D. K. Malick, A. D. Rabuck, K. Raghavachari, J. B. Foresman, J. V. Ortiz, Q. Cui, A. G. Baboul, S. Clifford, J.

Cioslowski, B. B. Stefanov, G. Liu, A. Liashenko, P. Piskorz, I. Komaromi, R. L. Martin, D. J. Fox, T. Keith, M. A. Al-Laham, C. Y. Peng, A. Nanayakkara, M. Challacombe, P. M. W. Gill, B. Johnson, W. Chen, M. W. Wong, C. Gonzalez, and J. A. Pople, *Gaussian G03, Revision D.0.1*. 2004.

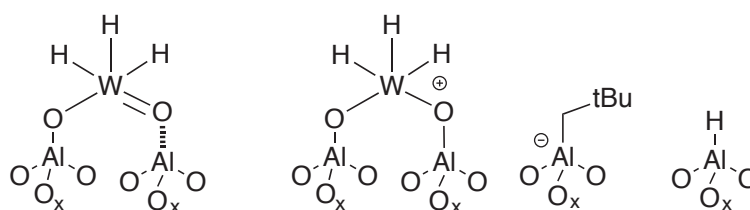
General conclusion

The aim of this thesis was to prepare new supported tungsten catalyst for the production of propylene. The grafting of $[W(\equiv C^tBu)(CH_2^tBu)_3]$, **1**, on $Al_2O_{3-(500)}$ (RP) leads to $1/Al_2O_{3-(500)}$ (RP), which surface exhibits a mixture of neutral and cationic species respectively **1a** and **1b** (Scheme 7.1). This later results from a transfer of a neopentyl ligand to an acidic aluminum atom. The structure of these species have been determined using IR spectroscopy, mass balance analysis of grafting and treatment under H_2 at $150^\circ C$, NMR spectroscopy. The formation of the cationic species, **1b**, is in agreement with the reactivity of group IV, group V and actinides organometallic complexes on alumina but contradict theoretical calculations results of Joubert *et al.*¹



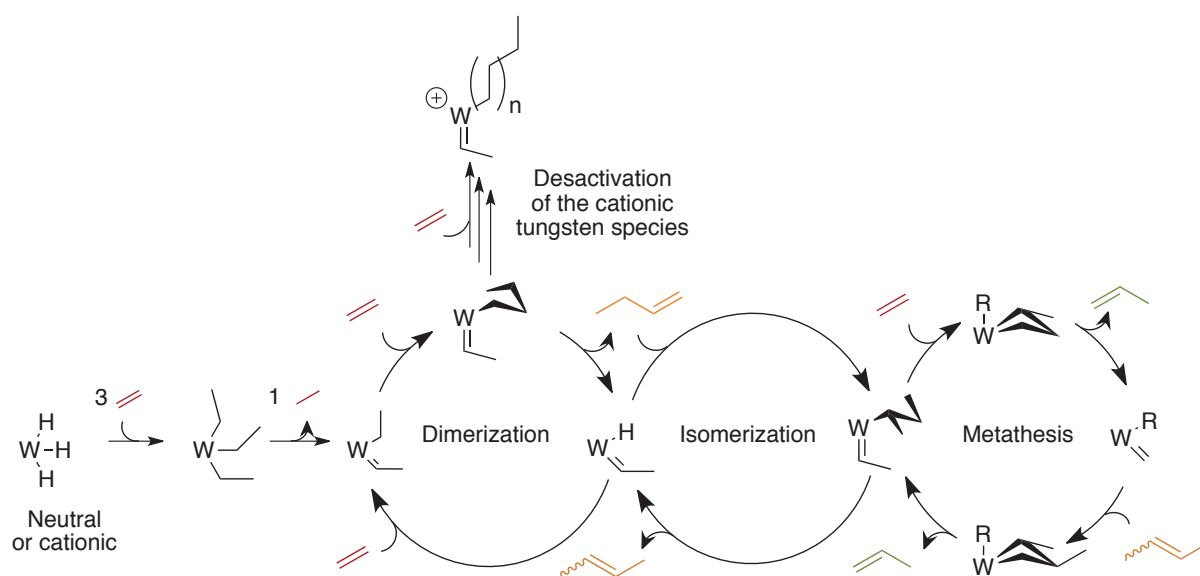
Scheme 7.1 Different surface species identified on $1/Al_2O_{3-(500)}$ (RP)

The treatment of $1/Al_2O_{3-(500)}$ (RP) under H_2 at $150^\circ C$ afford $WH/Al_2O_{3-(500)}$ (RP). The characterizations and theoretical calculations made on this product prove the presence of different surface species (Scheme 7.2). Indeed, a neutral tungsten oxo tris-hydride is formed from **1a**. The opening of strained aluminoxane bridges during the treatment at $150^\circ C$ or the activation of H_2 on default of alumina also creates surface $Al-H$. The cationic species **1b** is hydrogenated at $150^\circ C$ but its anionic $Al-CH_2^tBu$ counterparts is conserved during this treatment. The complexity of the system as not allowed a rigorous determination of the relative amount of each species. A complete study using DFT calculation is necessary to completely solve such a complex systems, the presence of a cationic species.



Scheme 7.2 Proposed surface species of $WH/Al_2O_{3-(500)}$ (RP)

The $\text{WH}/\text{Al}_2\text{O}_3-(500)$ catalyst exhibits an outstanding activity in the direct conversion of ethylene to propylene, which is the first example of isolated metal system affording this reaction. This reaction involves a threefold mechanism: dimerization, isomerization and cross-metathesis (Scheme 7.3). The different results have shown that the dimerization is the rate-determining step of this catalytic mechanism. The key intermediates in the mechanism is a tungsten carbene-hydride achieving: i) ethylene dimerization ii) butenes isomerisation and iii) olefin metathesis. Nevertheless, the most active cationic species is probably quickly deactivated by formation of a oligomeric species with a melting point of 116°C (Figure 7.1). A polymer with a melting point of 135°C is also observed. Unfortunately, after deactivation treatment under H_2 do not retrieves the active species.



Scheme 7.3 Proposed mechanism for the direct conversion of ethylene to propylene on $\text{WH}/\text{Al}_2\text{O}_3$

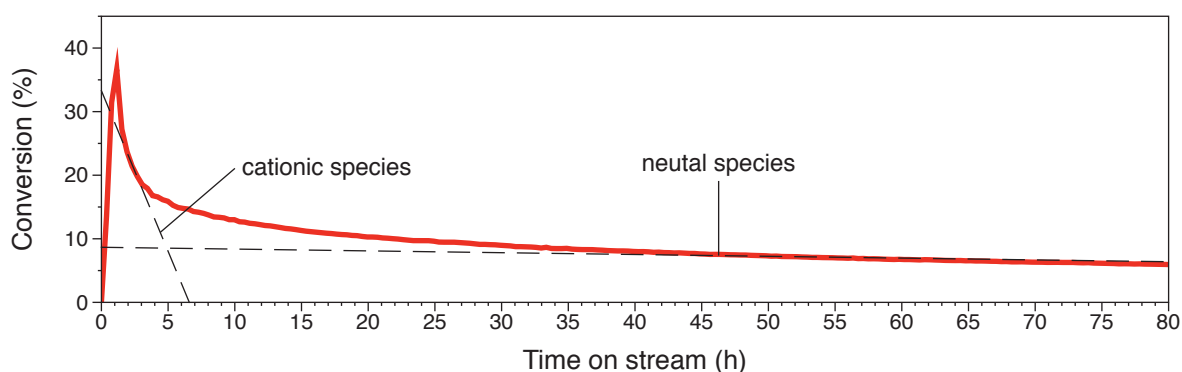


Figure 7.1 Conversion vs. time on stream for ethylene to propylene reaction on $\text{WH}/\text{Al}_2\text{O}_3$

In order to observe the role of alkyl aluminum and aluminum hydride present at the surface of $\text{WH}/\text{Al}_2\text{O}_3$, isolated alkyl aluminum, $2/\text{Al}_2\text{O}_3-(500)$, and isolated aluminum hydride, $\text{AlH}/\text{Al}_2\text{O}_3-(500)$, supported on alumina have been prepared.

Supported aluminum alkyl, **2/Al₂O₃₋₍₅₀₀₎**, was prepared by reaction between Al(*i*Bu)₃ and the surface of Al₂O₃₋₍₅₀₀₎. The isobutyl fragment is located on all types of surface aluminum, *i.e.* tetra- penta- and hexa- coordinated. **2/Al₂O₃₋₍₅₀₀₎** has shown an activity in ethylene polymerization in continuous flow reactor at 150°C.

Treatment of **2/Al₂O₃₋₍₅₀₀₎** under hydrogen afford the corresponding aluminum hydrides, **AlH/Al₂O₃₋₍₅₀₀₎**. These species are formed by heterolytic splitting of H₂ on Al-C bond of alkyl aluminum. The use of High field NMR spectroscopy (800 MHz), and particularly ²⁷Al-¹H J-HMQC sequence, has proved the presence of aluminum hydride on all types of surface aluminum, with a large scalar coupling constant ¹J_{Al-H} of 380 Hz and a ¹H chemical shift of 3.3 ppm.

As **2/Al₂O₃₋₍₅₀₀₎**, **AlH/Al₂O₃₋₍₅₀₀₎** has shown an activity in ethylene polymerization in continuous flow reactor in the same conditions that direct conversion of ethylene to propylene. The resulting polymers have a melting point of 135°C, whereas two melting point, *i.e.* 116 and 135°C, are observed for the polymers formed on **WH/Al₂O₃₋₍₅₀₀₎** during the ethylene to propylene conversion. These results prove that alkyl aluminum and aluminum hydride are involved in the deactivation of **WH/Al₂O₃₋₍₅₀₀₎** during direct conversion of ethylene to propylene, and that cationic tungsten species may promote the formation of the polymers with a melting point of 116°C.

AlH/Al₂O₃₋₍₅₀₀₎ have been tested for ethylene polymerization at 35 bar with a maximum activity of 21.9 kg_{PE}.mol⁻¹_(AlH).h⁻¹ at 100°C (Table 7.1). Moreover, it has been found that **AlH/Al₂O₃₋₍₅₀₀₎** was able to perform catalytically ethylene hydrogenation by double bond insertion in Al-H followed of H₂ heterolytic splitting over Al-C at high temperature (400°C).

Table 7.1 Ethylene polymerization results for **AlH/Al₂O₃₋₍₅₀₀₎**

Run ^[a]	T (°C)	Polymerization time (h)	Yield (mg _{PE})	Activity ^[b]	M _n ^[c]	M _w /M _n	T _m (°C)	Cristalinity (%)
1	50	0.5	660	11.0	8.9	2.6	135	45
2	50	1	1155	9.6	8.3	2.6	134	53
3	50	4	3270	7.7	8.7	2.6	135	56
4	100	0.5	1314	21.9	8.7	2.7	136	53
5	150	0.5	953	15.8	7.4	3.0	137	53

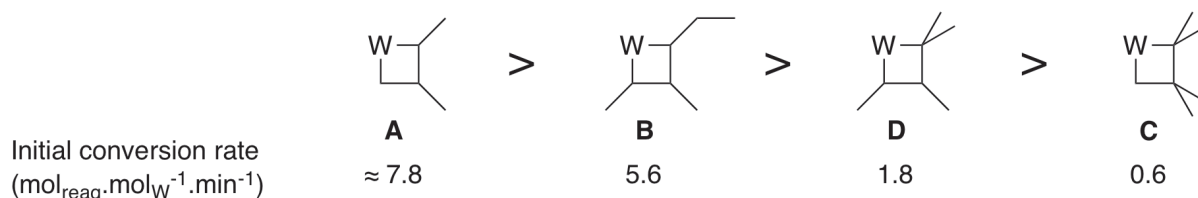
[a] All polymerization experiments were conducted under 35 bar of ethylene, using 100 mg of **AlH/Al₂O₃₋₍₅₀₀₎** (1200 μmol_(AlH).g⁻¹) in 20 mL of toluene; [b] Average activity in kg_{PE}.mol⁻¹_(AlH).h⁻¹ calculated over the whole polymerization time. [c] Average molecular weight (x 10⁵ g.mol⁻¹) determined by HTSEC in 1,2,4-trichlorobenzene at 150 °C, measured with a relative calibration based on standard polystyrene. [d] Determined by DSC (second heating).

As the regeneration of $\text{WH}/\text{Al}_2\text{O}_3$ after ethylene to propylene conversion was not possible, new routes to produce propylene has been developed. A study of the propylene metathesis has confirmed the ability of the tungsten hydride to perform olefin metathesis with high activities. Different routes allowing the production of propylene were then investigated. The results are summarized in Table 7.2.

Table 7.2 Productivity of the different routes to propylene

Reaction	Propylene selectivity (%)	Productivity at 20h on stream ($\text{mmol}_{\text{C}_3=\text{g}_{\text{cata}}^{-1}\cdot\text{h}^{-1}}$)
1-butene conversion	42.5	28.1
Trans-2-butene conversion	52.1	26.9
1-butene/trans-2-butene cross-metathesis	49.9	36.0
Isobutene/trans-2-butene cross-metathesis	40.0	10.5
Ethylene/trans-2-butene cross-metathesis (45% ethylene)	97.7	115.9
Ethylene/trans-2-butene cross-metathesis (35% ethylene)	96.4	142.8

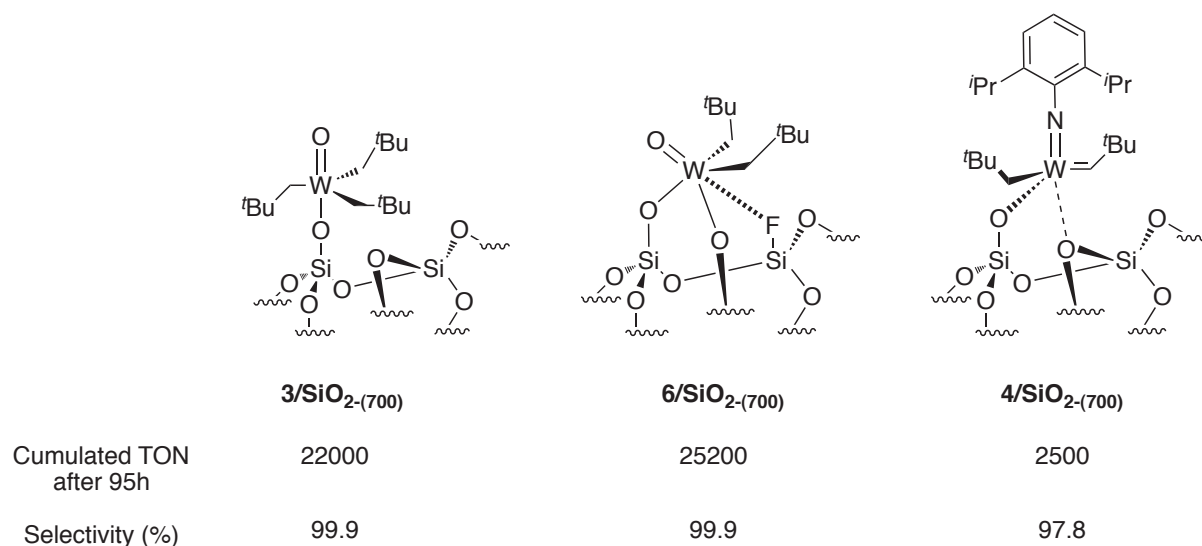
Using $\text{WH}/\text{Al}_2\text{O}_3\text{-(500)}$, the best route, in term of selectivity and productivity in propylene, is ethylene/trans-2-butene cross-metathesis, with a low deactivation rate (ca. $0.11\% \cdot \text{h}^{-1}$). Moreover, during this study, it has been observed, for metathesis reaction involving a stoichiometric ratio of reagent, that the number of substituent of the less thermodynamically favored metallacyclobutane governs the conversion rate of metathesis reaction (Scheme 7.4). The different reaction can thus be classified from higher to lower activity: i) Propylene self-metathesis or ethylene/trans-2-butene cross-metathesis where **A** is the less thermodynamically favored intermediate, ii) 1-butene/trans-2-butene cross-metathesis (metallacyclobutane **B**), iii) isobutene/trans-2-butene cross-metathesis (metallacyclobutane **D**) and iv) isobutene self-metathesis (metallacyclobutane **C**).



Scheme 7.4 Influence of the substituent of the metallacyclobutane on the conversion rate of metathesis reactions.

The characterizations of $\text{WH}/\text{Al}_2\text{O}_3$ have shown that cationic and neutral surface species are present at the surface. Moreover, oxo ligand has been evidenced on the tungsten site. In order to have a better understanding of structure of the $\text{WH}/\text{Al}_2\text{O}_3$ active site, but also of the WO_3/SiO_2 active site, single site tungsten-oxo complexes supported on ox-

ides have been prepared. Therefore, three novel tungsten complexes, *i.e.* $[W=O(CH_2^tBu)_4]$ (**3**), $[W=N(C_6H_5)(CH_2^tBu)_3F]$ (**5**) and $[W=O(CH_2^tBu)_3F]$ (**6**), have been successfully synthesized. Their reactivity toward partially dehydroxylated oxides have been investigated.



Scheme 7.5 Propylene metathesis catalyst precursors and their performances in continuous flow reactor (Selectivity in ethylene and 2-butenes, 80°C, 20 mL.min⁻¹)

The grafting of **3** on alumina has not afford single site species, while the grafting of these species on SiO₂₋₍₇₀₀₎ have afforded new, well-defined, oxo alkyl tungsten surface species **3c** and **6c**. The new supported complexes, **3**/SiO₂₋₍₇₀₀₎ and **6**/SiO₂₋₍₇₀₀₎, present a very high activity in propylene metathesis, under mild conditions and without need of a co-catalyst (Scheme 7.5). These systems shows a sustained conversion ad high selectivity in ethylene and 2-butenes, in contrast to the parent imido-derived material, **4**/SiO₂₋₍₇₀₀₎ (Figure 7.2).

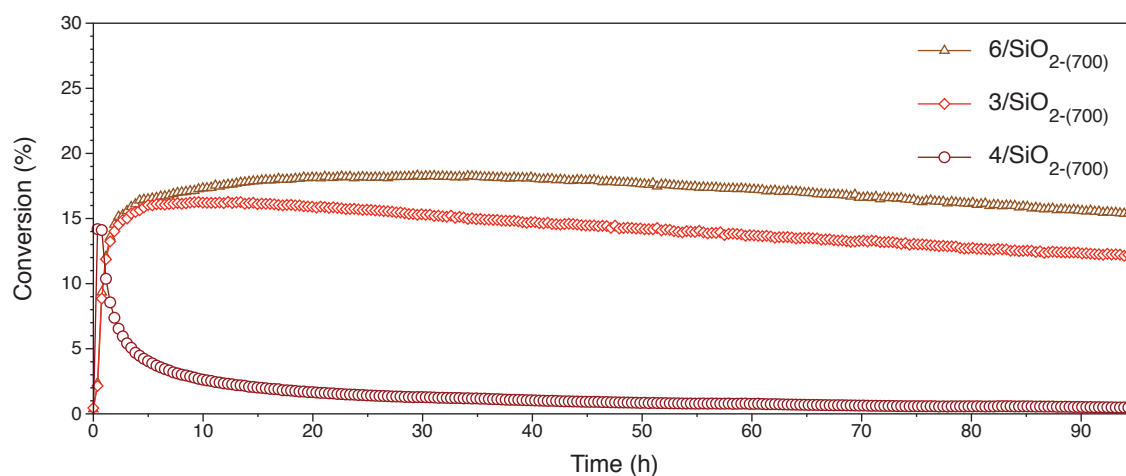
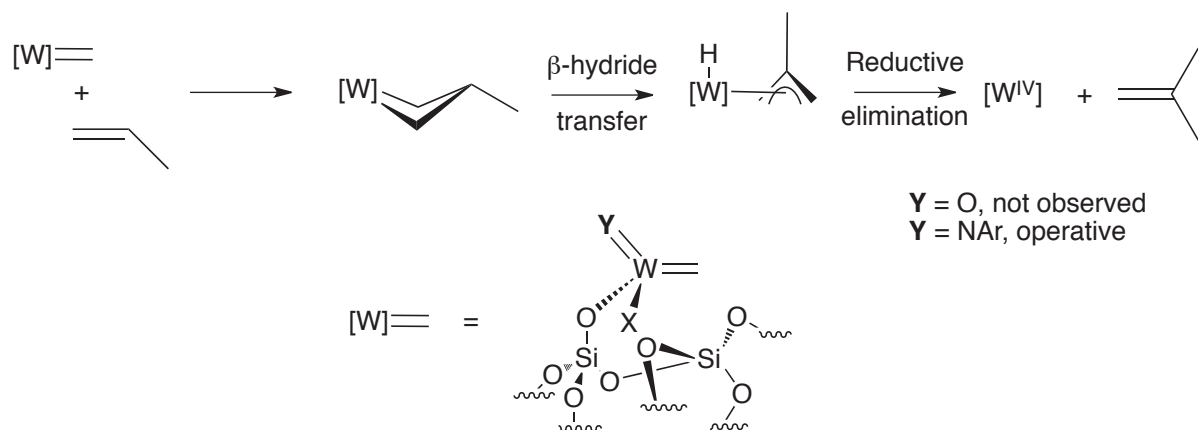


Figure 7.2 Conversion vs. time for **3**/SiO₂₋₍₇₀₀₎, **4**/SiO₂₋₍₇₀₀₎, **6**/SiO₂₋₍₇₀₀₎ in propylene metathesis (80°C, 20 mL.min⁻¹)

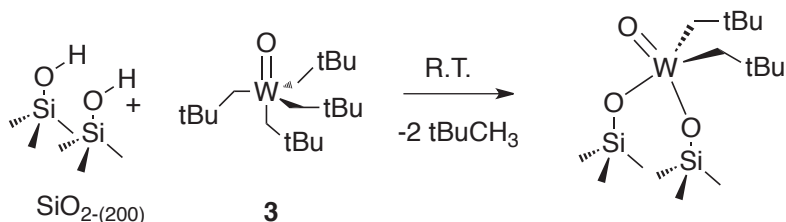
This imido species deactivate by reduction of the tungsten centre by decomposition of the metallacyclobutane and formation of isobutene, whereas this mechanism do not occurs for the oxo species (Scheme 7.6). This represents a significant step toward the understanding of the WO_3/SiO_2 system, as that isolated organometallic metal oxo fragments give rise to high performance in propene metathesis.



Scheme 7.6 Catalyst deactivation by β -H transfer in the metallacyclobutane

All this work has opened several outlooks. First, the investigation of group VI metals can be widened to the molybdenum. The preparation of supported molybdenum hydrides can be studied. Their catalytic activity should then be tested in all the reaction studied for tungsten hydride. A study of mechanism and deactivation pathway could broaden the understanding of metal hydride chemistry.

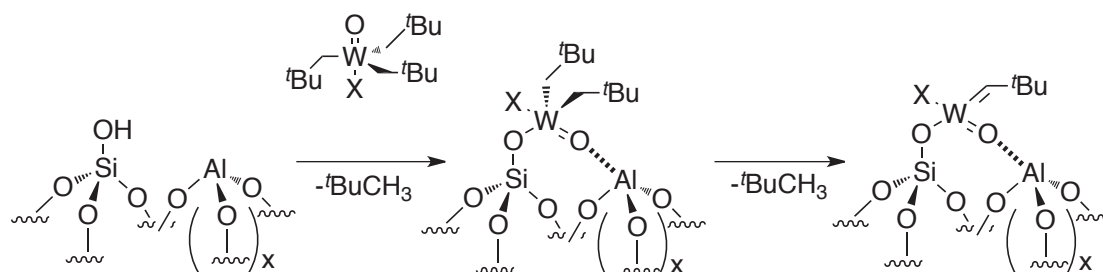
The synthesis of $[\text{W}=\text{O}(\text{CH}_2^t\text{Bu})_4]$ (**3**), which is quite tedious, should be revisited, *e.g.* using commercial $[\text{W}=\text{OCl}_4]$ as starting material with a selected alkylation agent. Its grafting has been extensively studied on $\text{SiO}_{2-(700)}$ leading to a monopodal species, the use of $\text{SiO}_{2-(200)}$ should be investigated in order to form bipodal species, very close from WO_3/SiO_2 active site (Scheme 7.7).



Scheme 7.7 Expected reactivity of $[\text{W}=\text{O}(\text{CH}_2^t\text{Bu})_4]$ (**3**) with $\text{SiO}_{2-(200)}$

The coordination of Lewis acid, such as AlBr_3 , on the oxo ligand of the newly prepared complexes should be examined following the work of Kress and Osborn.² The resulting oxo complexes coordinated to Lewis acid may have singular reactivity toward

grafting on oxide supports. Furthermore, the grafting of the oxo complexes described on this thesis on silica-alumina should lead to active catalyst as surface aluminum can coordinate to the oxo ligand of the tungsten increasing the electrophilic character of the tungsten centre. Moreover this coordination may favor the α -H abstraction to form a tungsten carbene (Scheme 7.8).



Scheme 7.8 Expected reactivity of $[W=O(CH_2^tBu)_3X]$ with silica-alumina

Finally, to complete the study of group VI oxo complexes, the synthesis of molybdenum-oxo species has to be investigated. In light of the result obtained with tungsten, and regarding high activity of molybdenum complexes supported on silica,³ this study looks very promising. The reactivity of supported molybdenum-oxo complexes has to be examined and compared to their tungsten homologues and notably the deactivation pathway of imido vs. oxo.

References

- (1) Joubert, J.; Delbecq, F.; Sautet, P.; Roux, E. L.; Taoufik, M.; Thieuleux, C.; Blanc, F.; Copéret, C.; Thivolle-Cazat, J.; and Basset, J. M. *J. Am. Chem. Soc.* 2006, 128, 9157-9169.
- (2) Fischer, J.; Kress, J.; Osborn, J. A.; Ricard, L.; and Wesolek, M. *Polyhedron*. 1987, 6, 1839-1842.
- (3) Rendón, N.; Blanc, F.; and Copéret, C. *Coordination Chemistry Reviews*. 2009, 253, 2015-2020.

Appendix A: Characterizations tungsten hydride grafting of the different supports and activity in ethylene/2-butene cross-metathesis

1. Characterizations of the different supports

1.1. Aluminas

On these materials, BET, XRD and Elemental analysis have been performed. The results of these characterizations are summarized in Table A.1.

Table A.1 Characteristics of Alumina RP, D and UOP A-E

Batch	Phase	BET surface area (m ² .g ⁻¹)	Pore Volume (mL.g ⁻¹)	Pore Diameter (Å)	Other Elements	Density (g.mL ⁻¹)
Evonik <i>AEROXIDE</i> [®] <i>Alu C (D)</i>	$\gamma + \delta$	115	-	-	74 ppm Fe <50 ppm Cu 372 ppm Cr	0.55
Rhône-Poulenc E7102 (RP)	γ	200	-	-	27 ppm Fe	0.56
33423-94A Alumina (UOP A) ^[a]	γ	213	0.486	91	n.a.	0.71
33423-94B Alumina (UOP B) ^[a]	γ	210	0.601	115	n.a.	0.56
33423-94C Alumina (UOP C) ^[a]	$\gamma + \alpha$	217	0.566	104	0.11% _{wt} Sn	0.6
33423-94D Alumina (UOP D) ^[a]	γ	199	0.485	98	0.19% _{wt} Ge	0.78
33423-94E Alumina (UOP E) ^[a]	α	ca. 10	n.a.	n.a.	n.a.	1.72

[a] Data provided by UOP

Except for Al₂O₃ (D), the pretreatment procedure was similar. Al₂O₃ (D) is a fumed alumina. As it is a very pulverulent compound, it was essential to compact it before use in order to facilitate its handling. The compacting procedure was the following: Al₂O₃ (D) was mixed with distilled water to obtain a kind of slurry. This slurry was put in the oven at 120°C for 2 days. The resulting blocks were crushed in a mortar and sieved (40-60 mesh). Others alumina were received as extrudates. These extrudates were identically crushed and sieved (40-60 mesh).

The Al_2O_3 (RP) and the five alumina provided by UOP have also been characterized after calcination and dehydroxylation at 500°C . DRIFT of these materials was performed (Figure A.1). These spectra in the $\nu_{(\text{OH})}$ region of Al_2O_3 show the presence of three types of OH groups. Two absorption bands highest frequencies, in the region $3800\text{-}3775\text{ cm}^{-1}$, correspond to terminal groups (μ_1) attached to Al_{IV} and Al_{VI} . Bands in the region $3730\text{-}3745\text{ cm}^{-1}$ are attributed to a (μ_2) OH coordinated to Al_{V} and Al_{IV} . Bands in the region $3710\text{-}3690\text{ cm}^{-1}$ correspond to a (μ_3) OH attached to three Al sites. The three types of OH groups are present on each Al_2O_3 except on Al_2O_3 UOP E. On the Al_2O_3 UOP D other stretching bands remain at lower frequencies ($<3600\text{ cm}^{-1}$) corresponding to H-bonded OH groups. This spectrum also shows absorption bands at 3550 cm^{-1} and in the $\nu_{(\text{CH})}$ region $<3000\text{ cm}^{-1}$. After the calcinations and dehydroxylation process, bonded OH and alkyl group may have disappeared. These fragments may be remains of the Ge doping method of this Alumina.

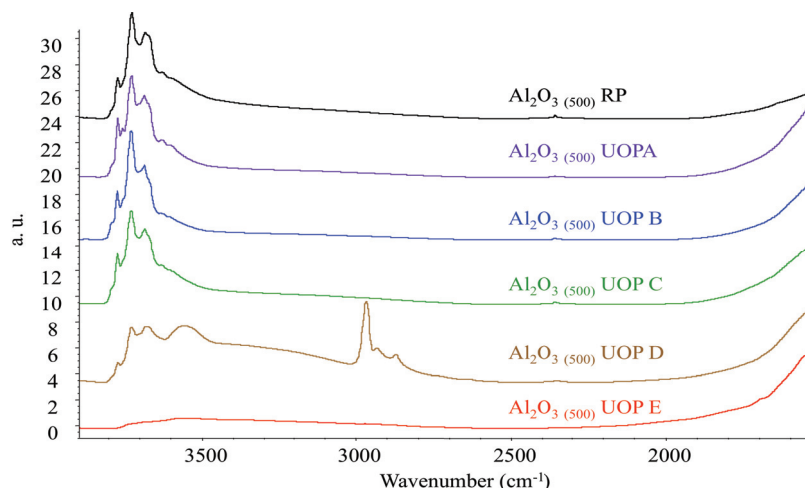


Figure A.1 DRIFT spectra of Alumina RP and UOP A-E dehydroxylated at 500°C

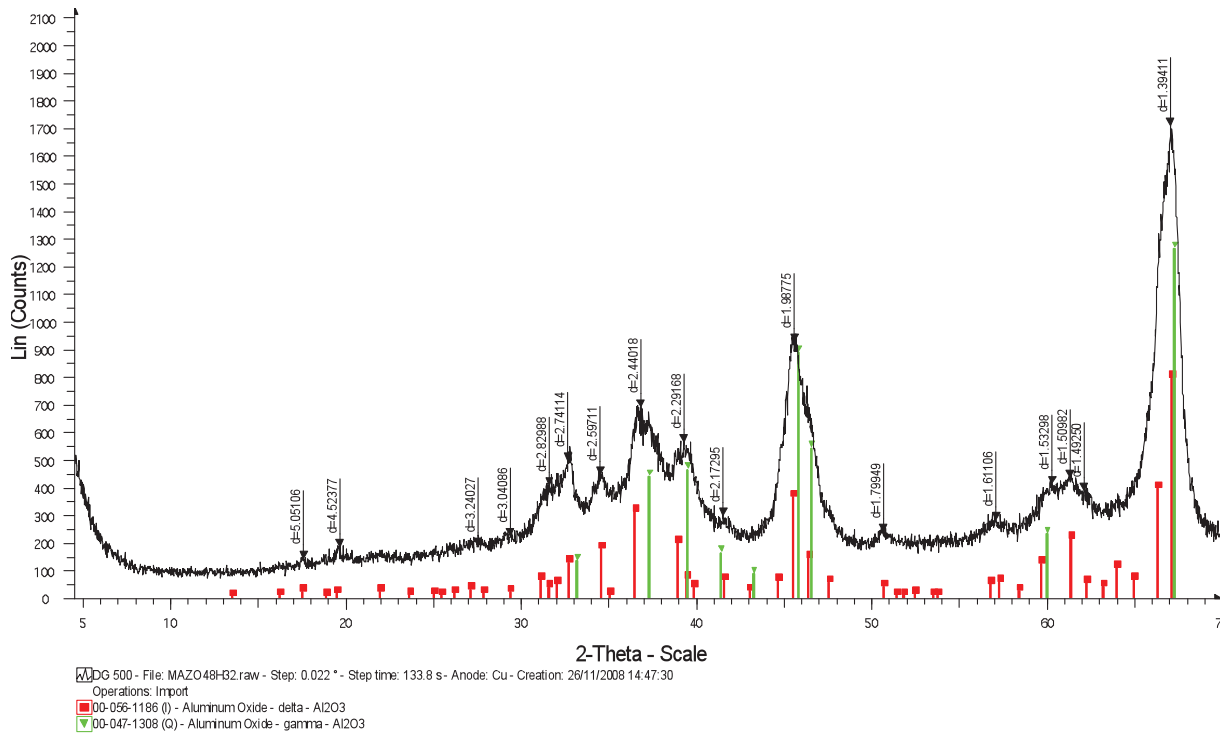


Figure A.2 DRX spectrum of Al₂O₃-(500) (D)

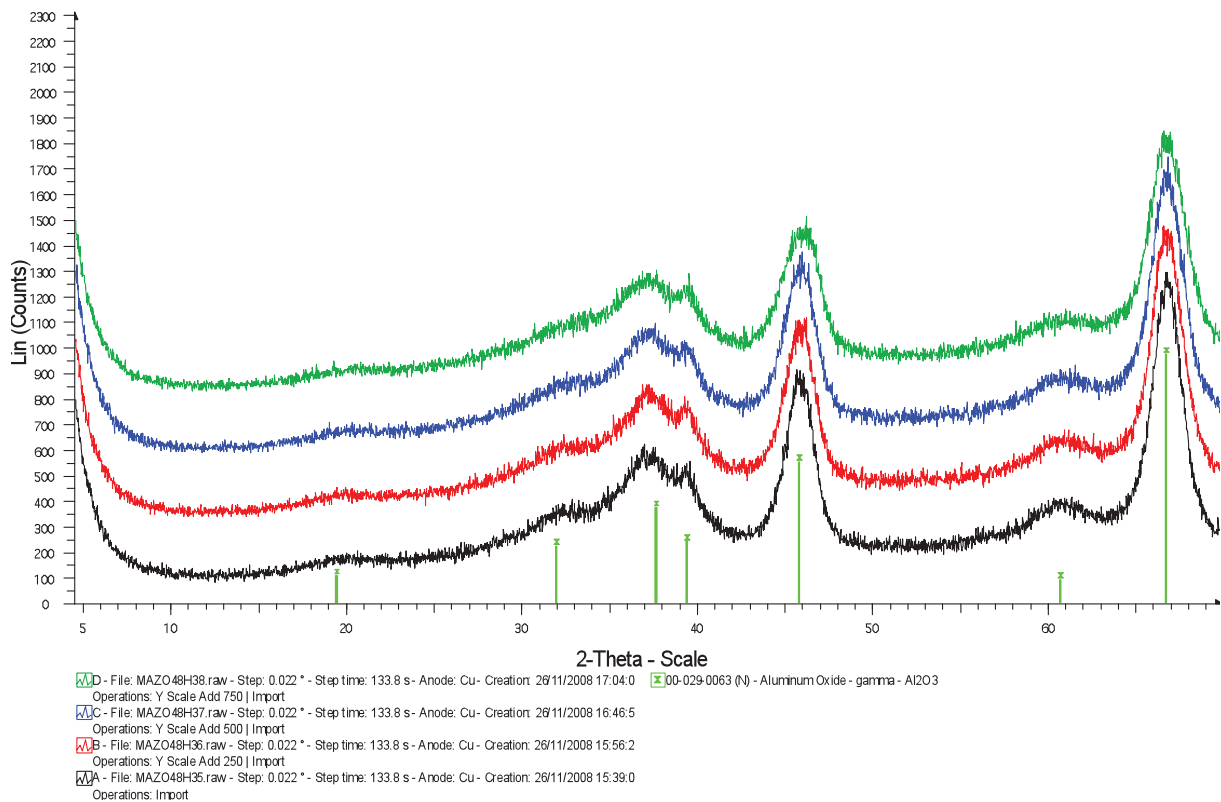


Figure A.3 DRX spectrum of Al₂O₃-(500) UOP (A), (B), (C) and (D) (top to bottom)

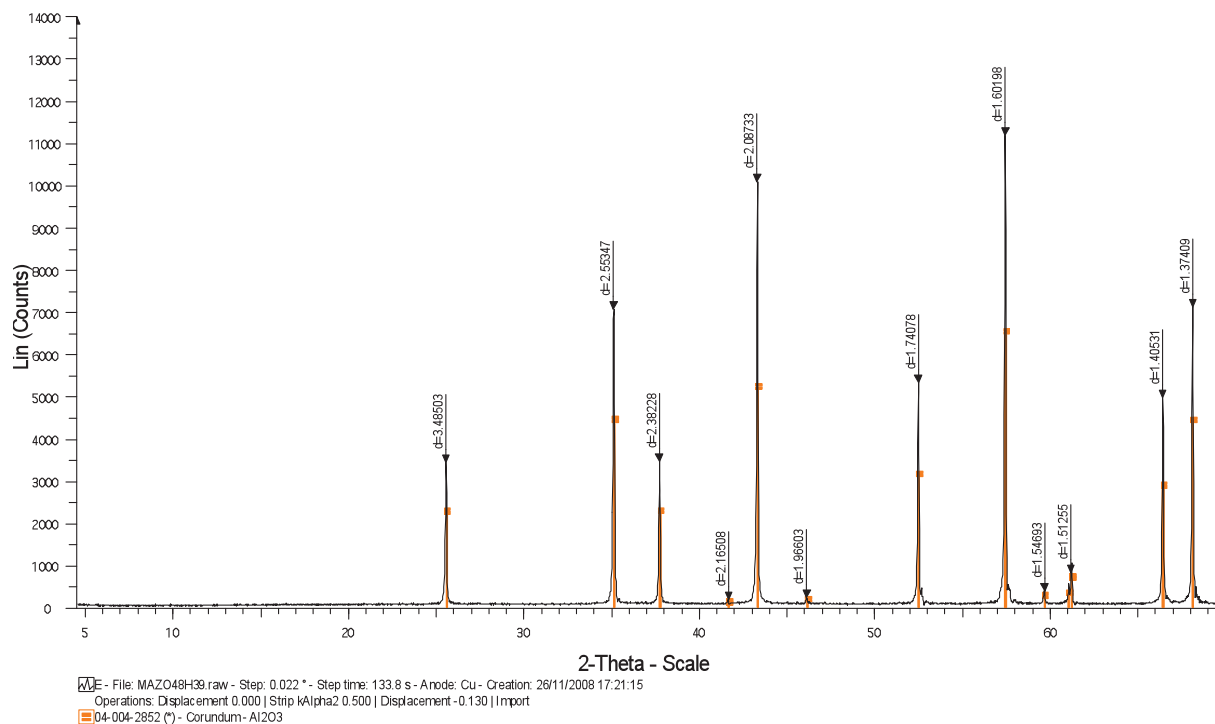


Figure A.4 DRX spectrum of $\text{Al}_2\text{O}_{3-(500)}$ UOP (E)

1.2. Silica-alumina and Aluminum Magnesium Hydroxyde

The tungsten hydride was prepared on Silica-Alumina (SiAl) and Aluminum Magnesium Hydroxyde (Pural) (see properties in Table A.2) and compared to Al_2O_3 . SiAl and Pural have been chosen for their difference of acidity compared to Alumina.

Table A.2 Properties of the different supports

Support	Supplier	Reference	BET surface area ($\text{m}^2 \cdot \text{g}^{-1}$)	Composition
Silica-Alumina (SiAl)	Akzo Nobel	HA-S-HPV	390	Si/Al = 3
Aluminum Magnesium Hydroxyde (Pural)	Sasol	Pural [®] MG50 595050	150	MgO/ Al_2O_3 = 1

The major surface hydroxyl groups on the SiAl are ($\equiv\text{Si-OH}$), while ($\text{Al}_s\text{-OH}$) surface species have not been observed (Figure A.5).¹⁻³ Note that the silica-alumina bulk is mainly constituted of ($\equiv\text{Si-O-Si}\equiv$)_n along with ($\equiv\text{Si-O-Al}_s$)_n moieties since the low Al content (25%) makes the presence of ($\text{Al}_s\text{-O-Al}_s$)_n moieties unlikely. Lastly, temperature programmed desorption of ammonia as shown that SiAl is more acidic than alumina.⁴ In con-

trast, Pural, due to its MgO sites, is reported to be more alkaline than Alumina.^{4,5} The drift spectra of these materials are presented in Figure A.7

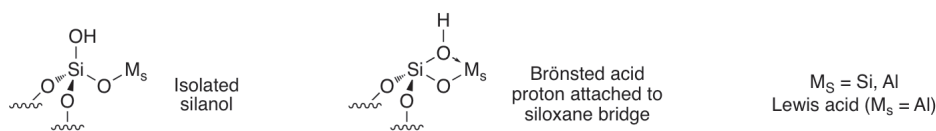


Figure A.5 Nature of the surface sites of the Silica-Alumina

2. Characterizations of the hydrides

The tungsten molecular precursor, i.e., $[\text{W}(\equiv\text{C}^t\text{Bu})(\text{CH}_2^t\text{Bu})_3]$ has been grafted and hydrogenolysed following the standard procedure. Table A.3 presents the tungsten loading of these prepared tungsten hydride.

Table A.3 Tungsten loading of the prepared catalysts

Support	Tungsten loading (% _{wt} W)
RP	5.5*
UOP A	6.0
UOP B	5.2
UOP C	5.0
UOP D	3.7
UOP E	Traces

All these resulting supported tungsten species were analyzed by DRIFT spectroscopy (Figure A.6). Except Al_2O_3 UOP E, all the spectra show a $\nu_{(\text{WH})}$ around 1900 cm^{-1} . Alpha alumina has not enough specific surface to graft the tungsten molecular precursor and form the corresponding hydride.

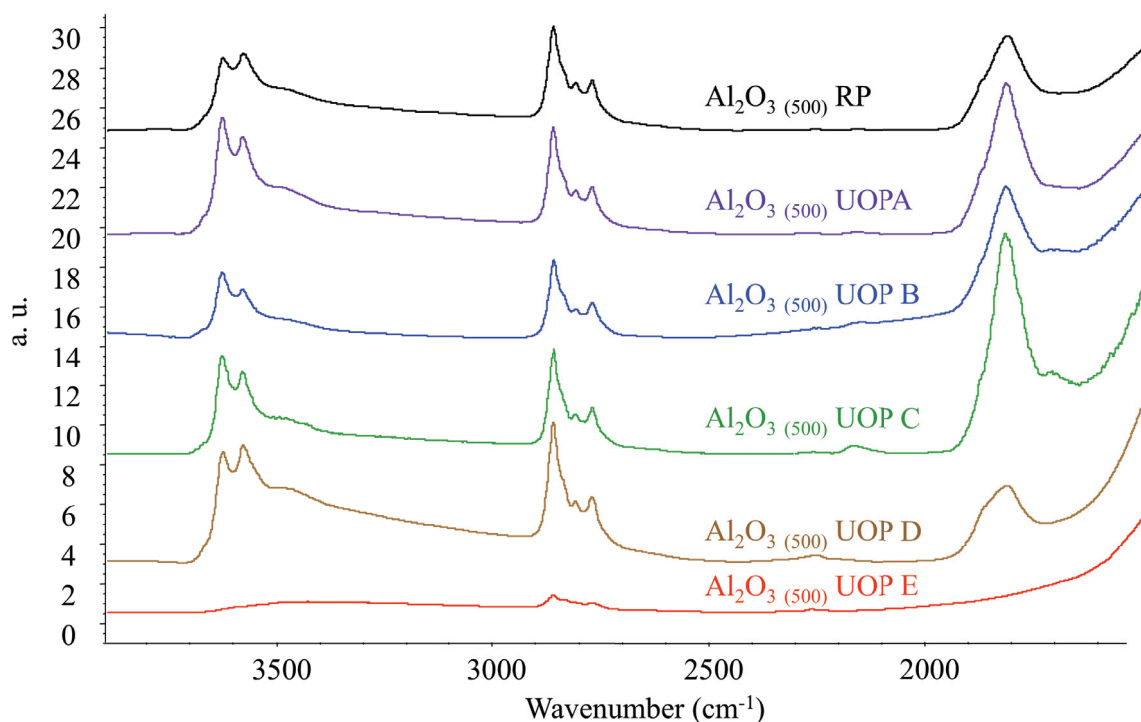


Figure A.6 DRIFT spectra of hydrogenolysed species resulting from the grafting of $[W(\equiv C^tBu)(CH_2^tBu)_3]$ on $Al_2O_3(500)$ RP and UOP A-E

Morover, the $[W(\equiv CtBu)(CH_2tBu)_3]$ complex was grafted on Silica-Alumina (SiAl) and Aluminum Magnesium Hydroxyde (Pural) partially dehydroxylated at $500^\circ C$. The grafting was performed by mechanical mixture at $66^\circ C$, using the same methodology described in the past report. The resulting species were treated at $150^\circ C$ under hydrogen to form tungsten hydrides. At each steps, the resulting materials were characterized by DRIFT and mass balance analysis. Figure A.7 presents the DRIFT spectra of each (*i.e.* SiAl and Pural) partially dehydroxylated support and of the grafted tungsten hydride. These spectra confirm the formation of an hydride on each supports with a band at 1953 cm^{-1} for SiAl and a broad band at 1868 cm^{-1} for Pural.

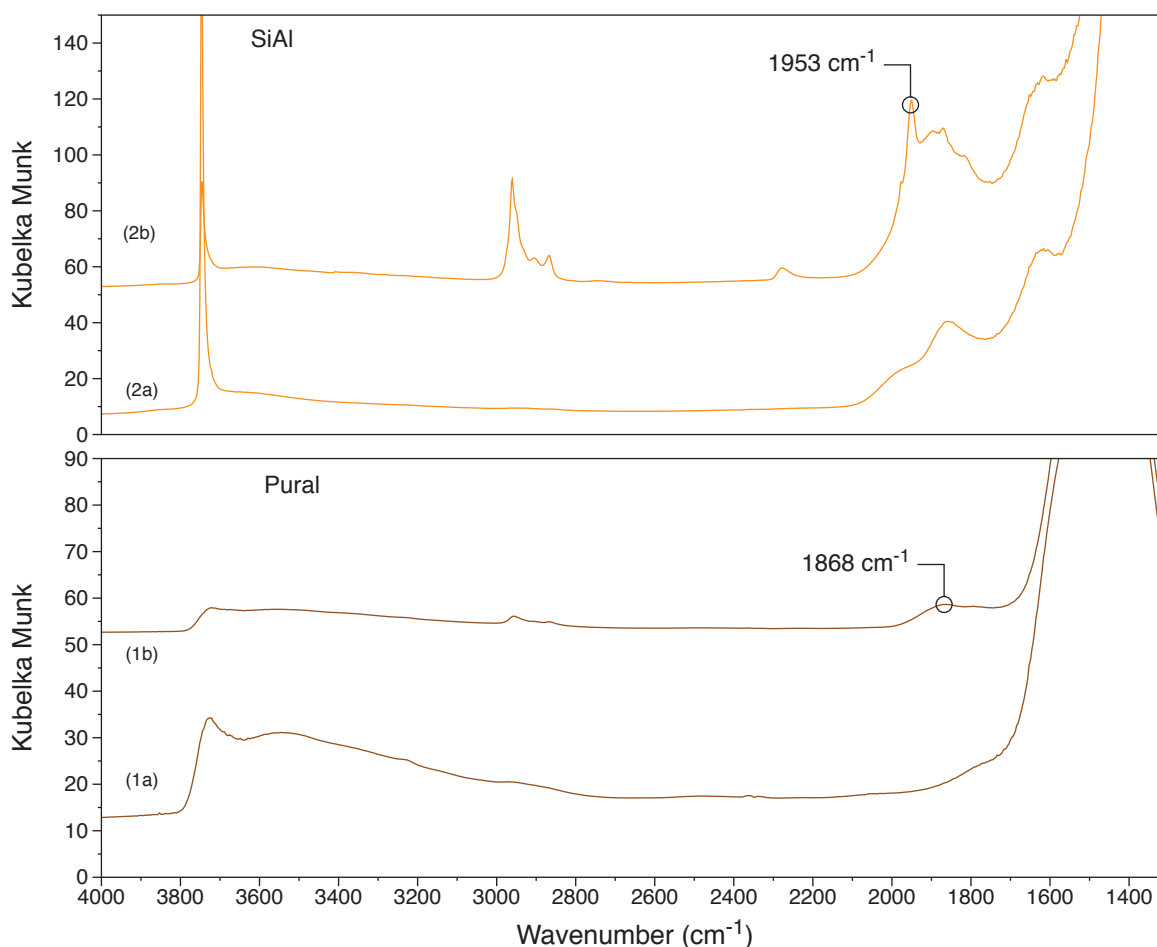


Figure A.7 DRIFT spectra of Pural₍₅₀₀₎ (1a) and SiAl₍₅₀₀₎ (1b) of hydrogenolysed species resulting from the grafting of $[W(\equiv C^tBu)(CH_2^tBu)_3]$: **WH/Pural₍₅₀₀₎** (1b) and **WH/SiAl₍₅₀₀₎** (2b)

3. Catalytic tests for ethylene/trans-2-butene cross-metathesis

Tungsten hydrides complexes grafted on Al₂O₃ (500) UOP A, UOP B UOP C, UOP D and UOP E have been tested in ethylene/trans-but-2-ene cross metathesis and compared to Al₂O₃ (500) RP. All experiments have been carried with 135 mg of catalyst whatever the tungsten loading. Thus the VHSV⁻¹ is constant for all experiments. Both gas were feed at 10 NmL.min⁻¹

Table 4 Experimental conditions *Calculated from chromatograms (both gas are feed at 10 mL.min⁻¹)

Total flow rate (NmL.min ⁻¹)	20
Mass of catalyst (mg)	135
Temperature (°C)	150
Ethylene/but-2-ene ratio	40 %*

All the catalyst tested have the same deactivation profile. The quantification of this deactivation have been established by linearisation of the plot between 10 and 20 hours on

stream. These results are reported on Table 5. As the catalyst prepared with Al_2O_3 (500) UOP E was not active, its deactivation was not modeled.

Table 5 Empirical equation of deactivation for each supported catalyst

Support	Equation (t in h, conversion in %)
RP	Conv = $-0.13 t + 31.6$
UOP A	Conv = $-0.17 t + 28,7$
UOP B	Conv = $-0.22 t + 30.2$
UOP C	Conv = $-0.12 t + 22.0$
UOP D	Conv = $-0.21 t + 31.4$
UOP E	n/a

All the deactivation rates are between 0.12 and $0.22 \text{ \%}\cdot\text{h}^{-1}$. The Al_2O_3 (500) UOP C seems to be the support with the lowest deactivation rate; despite it has the lowest starting conversion.

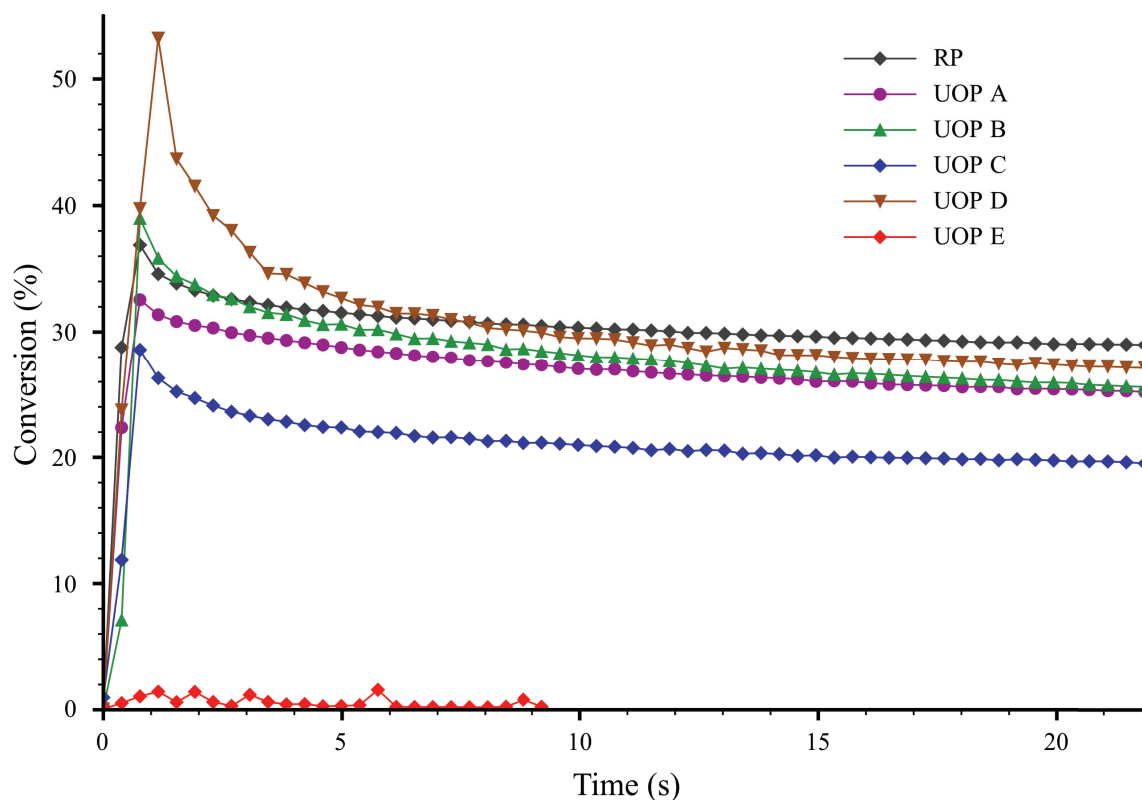


Figure A.8 Conversion in product vs. time on stream for ethylene/but-2-ene metathesis on $\text{WH}/\text{Al}_2\text{O}_3$ (500) RP, UOP A, UOP B, UOP C, UOP D and UOP E

The catalyst grafted on Al_2O_3 (500) UOP D, support doped with 0,19%wt of Ge, displays a higher activity than the other in the 5 first hours of catalysis. This catalyst is also very selective (Figure A.9). The Ge seems to have a positive effect on the catalyst activity compared to Sn. Indeed, the difference of conversion between Al_2O_3 UOP C (5.3%wt W, 0.11%wt Sn) and Al_2O_3 UOP D (4.0%wt W, 0.19%wt Ge) is high. This is confirmed by

the cumulated T.O.N. at 20h reported on Table 6 Cumulated T.O.N. for all the experiments.

Table 6 Cumulated T.O.N. for all the experiments

Support	Cumulated T.O.N. at 20h
RP	7380
UOP A	6036
UOP B	7536
UOP C	5313
UOP D	11119
UOP E	n/a

The selectivity in propylene of all these systems is very high, between 96.3 and 97.8%. For all these tests, with the same amount of catalyst, Al_2O_3 (500) RP exhibit the highest activity and selectivity and the lowest deactivation rate.

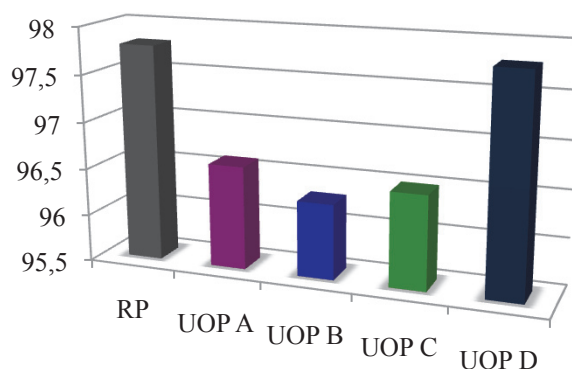
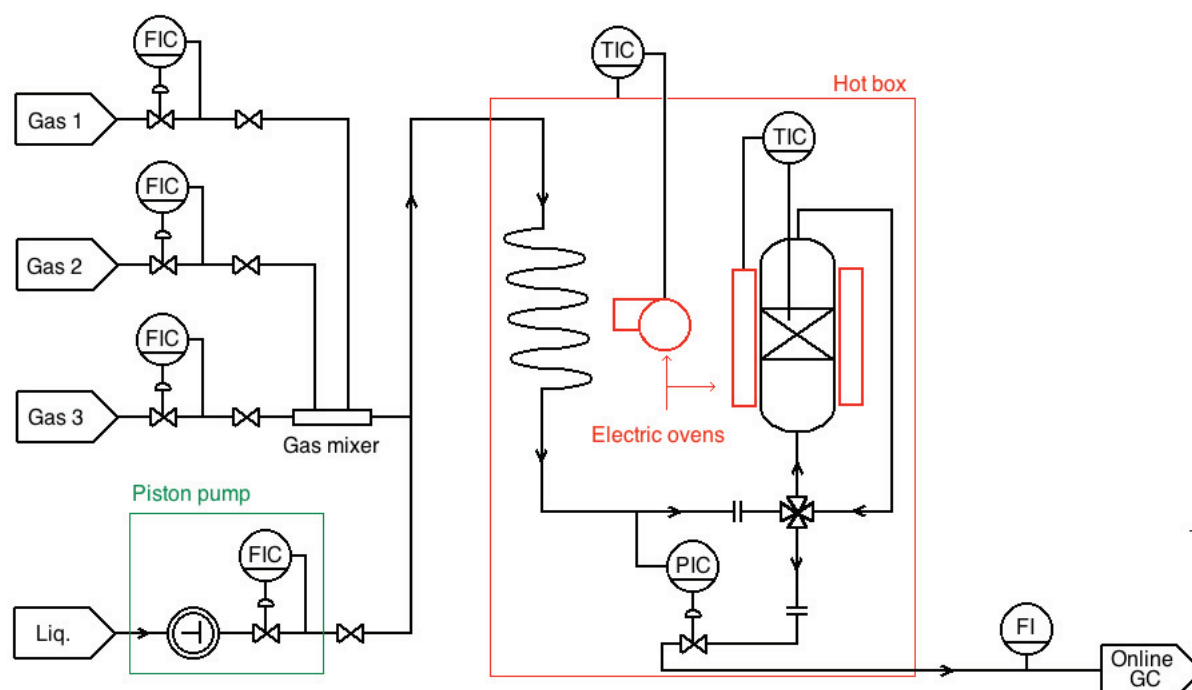


Figure A.9 Selectivity in propylene for ethylene/but-2-ene metathesis on $\text{WH}/\text{Al}_2\text{O}_3$ (500) RP, UOP A, UOP B, UOP C and UOP D

4. References

- (1) Peri, J. B. *Journal of Catalysis* 1976, 41, 227-239.
- (2) Baltusis, L.; Frye, J. S.; Maciel, G. E. *Journal of the American Chemical Society* 1987, 109, 40-46.
- (3) Bronnimann, C. E.; Chuang, I. S.; Hawkins, B. L.; Maciel, G. E. *Journal of the American Chemical Society* 1987, 109, 1562-1564.
- (4) M. Verhaak, A. J. van Dillen, J. W. Geus, *Applied catalysis. A, General* 105, 1993, 251-269.
- (5) <http://www.sasoltechdata.com/tds/PURAL-MG.pdf>

Appendix B: Simplified diagram of the continuous flow reactor used in this thesis



Scheme B.1 Simplified diagram of the continuous flow reactor

Appendix C: Additional characterizations of $\text{AlH}/\text{Al}_2\text{O}_3\text{-(500)}$

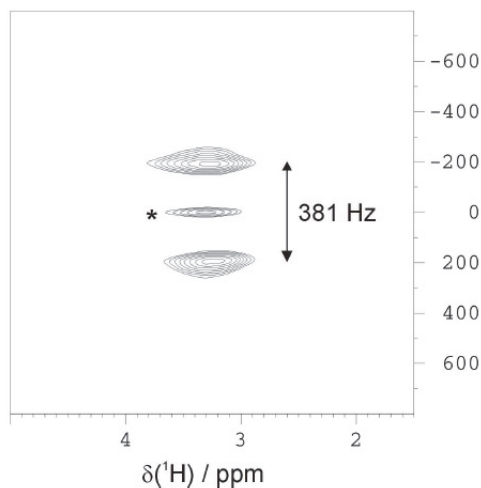


Figure C.1 ^1H J-resolved 2D spectrum (recycling delay of 1.6 s; 128 added transients; t_1 increment of 400 msec) obtained with J-HMQC pre-filtering (recoupling delay of 1 msec) and ^{27}Al RA-MP decoupling (decoupling pulse of 6 msec, interleave delay of 500 msec). Central peak (*) results from the incomplete inversion produced by the ^{27}Al π pulse leading to refocusing of the heteronuclear scalar coupling.

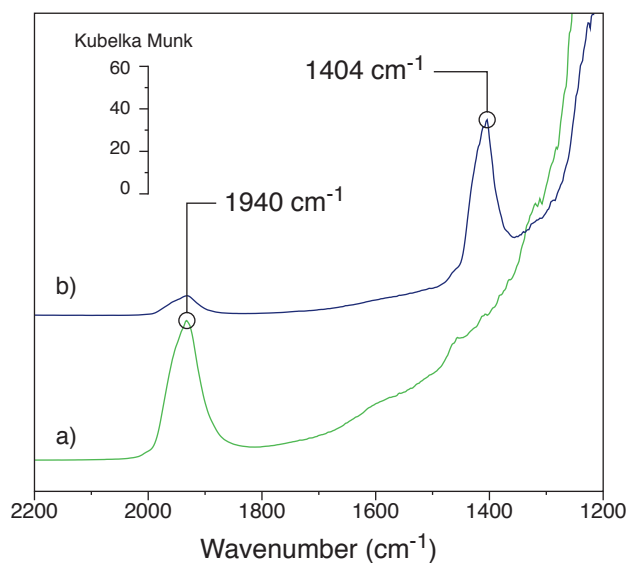


Figure C.2 Diffuse reflectance infrared spectra of a) $\text{AlH}/\text{Al}_2\text{O}_3\text{-(500)}$ and b) $\text{AlD}/\text{Al}_2\text{O}_3\text{-(500)}$ prepared following same procedure as $\text{AlH}/\text{Al}_2\text{O}_3\text{-(500)}$ but replacing H_2 by D_2 .

RESUME en français

La préparation de nouveaux catalyseurs à base de tungstène par la voie Chimie Organométallique de Surface a été abordée dans cette thèse pour la production du propylène à partir de l'éthylène et/ou de butènes. Deux types de systèmes catalytiques ont été développés. Des hydrures de tungstène supportés, obtenus par réaction de surface entre un complexe de tungstène $[W(=C^tBu)(CH_2^tBu)_3]$ et la γ -alumine suivi d'un traitement sous H_2 à $150^\circ C$ ont été préparés. Les caractérisations par différentes techniques spectroscopiques (IR, RMN solide, Raman et EXAFS) et réactivité stoechiométrique ainsi que les modélisations par calculs théoriques (DFT) ont montré la présence à la surface de deux espèces trishydrures : neutre et cationique. Ce catalyseur s'est révélé particulièrement actif pour la conversion directe de l'éthylène en propylène à $150^\circ C$ selon un mécanisme trifonctionnel (dimérisation, isomérisation et métathèse croisée). L'accent a été mis sur la détermination du mode de désactivation par oligomérisation de l'éthylène, due principalement à la présence en surface d'espèce cationique. Pour palier à ce problème, d'autres réactions permettant la production de propylène avec de meilleures activités ont été développées (conversion des butènes, métathèse croisée éthylène/2-butène, 2-butène/isobutène). La conversion directe de 2-butène en propylène, inconnue jusqu'à lors, a notamment été étudiée. Enfin, un second type de systèmes catalytiques, modèles du site actif de l'hydrures de tungstène supporté et du catalyseur industriel WO_3/SiO_2 , a été préparé et caractérisé. Ces nouveaux catalyseurs, portant un ligand oxo, se sont montrés bien plus actifs en métathèse des oléfines que leurs homologues portant un ligand imido. Ces derniers se désactivent rapidement par décomposition de metallacyclobutane entraînant une réduction du tungstène non observée dans le cas des systèmes oxo.

TITRE en anglais

Novel generation of tungsten-based catalysts grafted on oxides for propylene production.

RESUME en anglais

The preparation of new tungsten based catalyst using Surface Organometallic Chemistry is described in this thesis. These catalysts have been prepared for the production of propylene from ethylene and/or butenes. Two types of catalyst have been developed. Supported tungsten hydrides, resulting from the surface reaction of $[W(=C^tBu)(CH_2^tBu)_3]$ with γ -alumina followed by a treatment under H_2 at $150^\circ C$ have been prepared. The characterizations by several spectroscopic techniques (IR, SSNMR, Raman and EXAFS) and stoichiometric reactivity combined by with theoretical calculations (DFT) have demonstrated the presence of two tungsten hydride surface species: a neutral and a cationic. This catalyst have shown outstanding reactivity for the direct conversion of ethylene to propylene $150^\circ C$ following a tri-functional mechanism (dimerization, isomerization and cross-metathesis). The deactivation pathway has been attributes to ethylene oligomerization mainly due to the presence of cationic surface species. To circumvent this deactivation, other reactions affording propylene have been developed (butenes conversion, ethylene/2-butene and isobutene/2-butene cross metathesis). The conversion of 2-butene to propylene, until then unreported, has been notably studied. Finally, a second type of catalyst, models of the active site of supported tungsten hydrides and of WO_3/SiO_2 catalyst, has been prepared and characterized. These new catalysts, bearing an oxide ligand, have been shown to be more active than their imido counterparts. These later deactivates quickly by metallacyclobutane decomposition leading to the reduction of the tungsten non observed in the case of oxo systems.

DISCIPLINE

Chimie

MOTS-CLES

Propylène, tungstène, hydrures, oxydes, aluminium, métathèse, éthylène, butènes, oxo.

INTITULE ET ADRESSE DE L'U.F.R. OU DU LABORATOIRE :

Laboratoire de Chimie Organométallique de Surface ; UMR 5265 : Chimie, Catalyse, Polymères et Procédés ; CNRS - UCBL - CPE Lyon ; 43 Bd du 11 Novembre 1918 ; B.P. 2077 ; 69616 VILLEURBANNE Cedex